KALININ-3 COOLANT TRANSIENT BENCHMARK – SWITCHING-OFF OF ONE OF THE FOUR OPERATING MAIN CIRCULATION PUMPS AT NOMINAL REACTOR POWER

SPECIFICATION- First Edition 2008

V. A. Tereshonok[1], S. P. Nikonov[2], M. P. Lizorkin[2]

K. Velkov[3], A. Pautz[3], K. Ivanov[4]

[1] VNIIAES, Russia

[2] RRC "Kurchatov Institute", Russia

[3] GRS mbH, Germany

[4] The Pennsylvania State University, USA

ORGANISATION FOR ECONOMIC CO-OPERATION AND DEVELOPMENT

Pursuant to Article 1 of the Convention signed in Paris on 14th December 1960, and which came into force on 30th September 1961, the Organisation for Economic Co-operation and Development (OECD) shall promote policies designed:

- to achieve the highest sustainable economic growth and employment and a rising standard of living in Member countries, while maintaining financial stability, and thus to contribute to the development of the world economy;
- to contribute to sound economic expansion in Member as well as non-member countries in the process of economic development; and
- to contribute to the expansion of world trade on a multilateral, non-discriminatory basis in accordance with international obligations.

The original Member countries of the OECD are Austria, Belgium, Canada, Denmark, France, Germany, Greece, Iceland, Ireland, Italy, Luxembourg, the Netherlands, Norway, Portugal, Spain, Sweden, Switzerland, Turkey, the United Kingdom and the United States. The following countries became Members subsequently through accession at the dates indicated hereafter: Japan (28th April 1964), Finland (28th January 1969), Australia (7th June 1971), New Zealand (29th May 1973), Mexico (18th May 1994), the Czech Republic (21st December 1995), Hungary (7th May 1996), Poland (22nd November 1996), Korea (12th December 1996) and the Slovak Republic (14 December 2000). The Commission of the European Communities takes part in the work of the OECD (Article 13 of the OECD Convention).

NUCLEAR ENERGY AGENCY

The OECD Nuclear Energy Agency (NEA) was established on 1st February 1958 under the name of the OEEC European Nuclear Energy Agency. It received its present designation on 20th April 1972, when Japan became its first non-European full Member. NEA membership today consists of 28 OECD Member countries: Australia, Austria, Belgium, Canada, Czech Republic, Denmark, Finland, France, Germany, Greece, Hungary, Iceland, Ireland, Italy, Japan, Luxembourg, Mexico, the Netherlands, Norway, Portugal, Republic of Korea, Slovak Republic, Spain, Sweden, Switzerland, Turkey, the United Kingdom and the United States. The Commission of the European Communities also takes part in the work of the Agency.

The mission of the NEA is:

- to assist its Member countries in maintaining and further developing, through international co-operation, the scientific, technological and legal bases required for a safe, environmentally friendly and economical use of nuclear energy for peaceful purposes, as well as
- to provide authoritative assessments and to forge common understandings on key issues, as input to government decisions on nuclear energy policy and to broader OECD policy analyses in areas such as energy and sustainable development.

Specific areas of competence of the NEA include safety and regulation of nuclear activities, radioactive waste management, radiological protection, nuclear science, economic and technical analyses of the nuclear fuel cycle, nuclear law and liability, and public information. The NEA Data Bank provides nuclear data and computer program services for participating countries.

In these and related tasks, the NEA works in close collaboration with the International Atomic Energy Agency in Vienna, with which it has a Co-operation Agreement, as well as with other international organisations in the nuclear field.

Foreword

During the last several years a considerable effort was devoted and progress has been made in various countries and organizations in incorporating full three-dimensional (3D) reactor core models into system transient codes. The coupled thermal-hydraulic (TH) and neutron kinetics (NK) code systems allow performing of a "best-estimate" calculation of interactions between the core behaviour and plant dynamics. Several benchmarks have been developed to verify and validate the capability of the coupled codes in order to analyze complex transients with coupled core-plant interactions for different types of reactors.

The Nuclear Energy Agency (NEA) of the Organization for Economic Cooperation and Development (OECD) has recently completed the VVER-1000 Coolant transient benchmark (V1000CT-1) and (V1000CT-2) for evaluating coupled TH system NK codes by simulating transients at the Bulgarian NPP Kozloduy Unit #6. The available real plant experimental data made these benchmark problems very valuable.

This benchmark is a continuation of the above activities and it defines a coupled code problem for further validation of thermal-hydraulics system codes for application to Russian-designed VVER-1000 reactors based on actual plant data from the Russian NPP Kalinin Unit #3 (Kalinin-3). The selected transient 'Switching-off of one Main Circulation Pump (MCP)' is performed at a nominal power and leads to asymmetric core conditions with broad ranges of the parameter changes. The experimental data is very well documented. Measurements were carried out with a quite high frequency and their uncertainties are known for almost all measured parameters. This fact allows applying the studied transient not only for validation purposes but also for uncertainty analysis as a part of the NEA/OECD LWR Uncertainty Analysis in Modelling (UAM) Benchmark.

This report provides the specifications for the international, coupled VVER-1000 Coolant Transient (KALININ-3) benchmark problem. The specification report has been prepared jointly by leading specialists of the All-Russian Research Institute Nuclear Power Plant Operation (VNIIAES), the Russian Research Centre "Kurchatov Institute"(KIAE), the Gesellschaft für Anlagen und Reaktor-sicherheit mbH (GRS) and the Pennsylvania State University (PSU).

The specification covers the four exercises: point kinetics model inputs, transient core calculations, transient coupled calculations, and uncertainty analysis In addition, a CD-ROM is also made available with the detailed data for the transient boundary conditions, decay heat values as a function of time, and cross-section libraries.

In December 2008 the NEA Nuclear Science Committee (NSC) Bureau has expressed support for the coupled Kalinin-3 benchmark problem in general to become an international standard problem for validation of the best-estimate safety codes. The Working Party on Scientific Issues of Reactor Systems (WPRS) discussed in its February 2009 meeting the proposal and endorsed it as it is of particular importance for the last phase of the Uncertainty Analysis in Modelling (UAM) activities.

Acknowledgements

This report is a sum of many efforts made by many people from different organizations and different countries.

The authors gratefully acknowledge and highly appreciate the outstanding support and help done by Dr. Siegfried Langenbuch from GRS mbH, Germany.

The authors wish to express their sincere appreciation for the support offered by Enrico Sartori, who not only provided efficient administration, organization and valuable technical recommendations, but most importantly provided friendly counsel and advice.

ABBREVIATIONS[1]

АЗ/RP	- reactor protection
АКНП /NFC	- neutron flux control system
АРМ/APC	- automatic reactor power controller
АЭС/NPP	- nuclear power plant
БРУ-СН/FASB-HL	- fast acting steam bypass valves for house loads
БПУ/MCR	- main control room
EFPD	- effective full power days
ВВЭР/WWER	- reactor WWER
ВД/HP	- high pressure
ВКВ/UES	- upper end switch
ВПЭН /AFWP	- auxiliary feed water pump
СЭК/SEC	- system of experimental control
ГПК /MSH	- main steam header
ГЦН /MCP	- main circulation pump
ДПЗ/SPND	- self powered neutron detector
D7/D7	- secondary side de-aerator D7
ИК/ICh	- ionization chamber
КГТН/CHTP	- condenser hydro-turbine pump
КД/PRZ	- pressurizer
КНДР/THC	- secondary side condenser
КСН/ISC	- internal house loads collector
КЭН-1(2)/СР-1(2)	- condenser pump of the first (second) stage
«Н»	- mode of APC to maintain reactor power
НД/LP	- low pressure
НКВ/LES	- low end switch
НС РЦ/SL-RH	- shift leader of the reactor hall
ОР/CR	- control rods
ПВД /HP-PH	- high pressure pre-heater
HZP	- hot zero power
HFP	- hot full power
ПД /PD	- start-up sub-range
ПГ /SG	- steam generator
ПЗ-1/PP-1	- pre-protection – 1-st stage
ПК/PC	- primary circuit
ПНД/LP-PH	- low pressure pre-heater
РД-1/OR-1	- first sub-range scale of NFC
РД-2/OR-2	- second sub-range scale of NFC
«Рег. N»/“Contr. N”	- mode of TEC to maintain the TG load
«Рег. Р»/“Contr. P”	- mode of TEC to maintain pressure in the MSH
РОМ/LRPC	- load-off and reactor power controller
РУ/RF	- reactor facility
СВБУ/UBLS	- upper level unit control system
СВРК /ICMS	- in-core monitoring system
ССБ/CT	- condensate tank

[1] For better traceability of the graphs’ captions, the abbreviations are given both in their original (Russian) spelling and as translated into English (RU/EN)

СПП/SSSH - steam separator and steam superheater
СУЗ/CPS - reactor control and protection system
СЭК/MMS - measurement-monitoring system
«Т» - APC mode to maintain pressure in MSH
ТВС/FA - fuel assembly
ТВСА/AFA - „alternative“ fuel assembly
ТГ/TG - turbine generator
ТП/TC - thermocouple
ТП1(2)/TC1(2) - the 1st (2nd) set of thermocouples
ТПН /TFWP - turbo-feed water pump
ТС/RT - resistance thermometer
ТЭН/TEH - tube electroheater (in PRZ)
ЦВД /HPTP - high pressure turbine part
ЦНД /LPTP - low pressure turbine part
ЭГСР/TEC - turbine electrohydraulic controller
$С_{бк}/С_{В}$ - concentration of boric acid in the coolant, g/kg
$G_{впэнj}$ /$G_{j\text{-}AFWP}$ - feed water flow rate at pressure side of $AFWP_j$, (j = 1, 2), m3/h, t/h
$G_{D7\text{-}j}$ /$G_{D7\text{-}j}$ - condensate flow rate of the j-th de-aerator (j = 1, 2), m3/h, t/h
$G_{пві}$/ $G_{i\text{-}SG}$ - feed water flow rate of SG_i, (i=1,2,3,4), m^3/h, t/h
$G_{HP\text{-}PH\ j}$/$G_{j\text{-}HP\text{-}PH}$ - feed water flow rate of HP-PH_j, (j = 1, 2), m^3/h, t/h
$G_{подп}$/$G_{PC\text{-}supply}$ - make-up flow rate in PC, m^3/h, t/h
$G_{прод}$/$G_{blowdown}$ - blow-down flow rate in PC, m^3/h, t/h
$G_{пті}$/$G_{loop\text{-}i}$ - coolant flow rate in the i-th loop of PC (i= 1,2,3,4), m^3/h, t/h
$G_{р}$/G_{r} - coolant flow rate through the reactor, m^3/h, t/h
$G_{спп}$/G_{SSSH} - flow rate of heating steam to SSSH, t/h
$G_{тпнj}$ /G_{TFWPj} - feed water flow rate at pressure side of $TFWP_j$, (j=1, 2), m3/h, t/h
H_i - insertion depth of the CR_i group of CPS, i = 1, 2, … , 10, cm, %
$К_q$ - FA relative power (core power radial peaking factor), rel. unit
$К_{q\ max}$ - max. value of the FA relative power, rel. unit
$К_v$ - core power peaking factor, rel. unit
$К_{v\ max}$ - max. core power peaking factor, rel. unit
$L_{д7\text{-}j}$ /$L_{D7\text{-}j}$ -condensate level in the j-th de-aerator (j = 1, 2), mm, cm
$L_{кд}$ /L_{PRZ} - coolant level in pressurizer, cm
L_{SGi} - SG_i water level (i = 1,2,3,4), mm, cm
$L_{пвд\text{-}j}$ /$L_{j\text{-}HP\text{-}PH}$ - HP-PH_j water level, (j = 1, 2), mm, cm
$L_{пнд\text{-}j}$ /$L_{j\text{-}LP\text{-}PH}$ - LP-PH_j water level, (j = 1,…, 5), mm, cm
L_{sd} - water level of the turbine condenser, mm
$N_{1к}$ /N_{PC} - reactor thermal power calculated on the basis of the coolant parameters in the primary circuit, MW, % N_{nom}
$N_{2к}$ /N_{SC} - reactor thermal power calculated on the basis of feed water parameters of the SGs, MW, % N_{nom}
$N_{акз}$/N_{core} - average reactor thermal power, MW, % N_{nom}
$N_{акнп}$ /N_{NFC} - reactor thermal power calculated on the basis of NFC records, MW, % N_n
$N_{гцні}$ /N_{MCPi} - electrical power consumed by the motor of MCP_i, (i = 1, 2, 3, 4), MW
$N_{ДПЗ}$/N_{DCS} - reactor thermal power calculated on the basis of SPND, MW, % N_{nom}
$N_{икі}$/N_{nfi} - reactor power calculated on the basis of data from the i-th measurement channel of the operational range of NFC (i=1,.., 6), MW, % N_{nom}
$N_{ном}$ /N_{nom} - nominal reactor power
$N_{пті}$/ $N_{PC\text{-}loop\text{-}i}$ - $loop_i$ power of primary circuit, (i=1, 2, 3, 4), MW
$N_{тек}$ /N_{actual} - actual reactor power, MW, % N_{nom}
$N_{эл}$ /N_{el} - TG electrical power (active), MW
N_i - reactor power according to the i-th measurement channel of OR-1 NFC
$n_{тпнj}$/n_{TFWPj} - rotation speed of $TFWP_j$, (j = 1,2), min^{-1}

$P_{1к}/P_{PC}$ - PC pressure, MPa

$P_{аз}/P_{core}$ - core outlet pressure, MPa

$P_{впэнj}/P_{AFWP}$ - feed water pressure at the pressure side of $AFWP_j$, (j = 1, 2), MPa

$P_{гпк}/P_{MSH}$ - MSH pressure, MPa

$P_{д7-j}/P_{D7-j}$ - $D7_j$ pressure, (j = 1, 2), MPa

$P_{кнсб}/P_{CC}$ - pressure in the condenser collector, MPa

$P_{ксн}/P_{ISC}$ - ISC pressure, MPa

$P_{кэн1-j}/P_{CP-1-j}$ - $CP\text{-}1_j$ pressure at pressure side, (j = 1, 2, 3), MPa

$P_{кэн2-j}/P_{CP-2-j}$ - $CP\text{-}2_j$ pressure at pressure side, (j = 1,.., 5), MPa

$P_{отбі}/P_{extr-i}$ - steam pressure at the j-th turbine stage outlet, (i = 1,…, 8), MPa

$P_{пві}/P_{SG-i}$ - feed water pressure at SG_i inlet, (i = 1,.., 4), MPa

$P_{пвдj}/P_{HPH-j}$ - feed water pressure at $HP\text{-}PH_j$ outlet, (j = 1, 2), MPa

$Pпг_i/P_{SGi}$ - SG_i steam pressure, (i = 1,.., 4), MPa

$P_{спп}/P_{SSSH}$ - SSSH outlet pressure, MPa

$P_{тпнj}/P_{TFWPj}$ - overpressure at pressure side of j-TFWP (j = 1, 2), MPa

P_{HPTPi}/P_{HPTP} - $HPTP_i$ outlet pressure, (i = 1,..,8), MPa

$S_{бру\text{-}снj}/S_{FASB\text{-}HL}$ - position of pressure control valve of $FASB\text{-}HL_j$, (j = 1, 2), %

$S_{основі}/S_{main-i}$ - position of the main water level control valve of SG_i, (i = 1,.., 4), %

$S_{пускі}/S_{start-i}$ - position of the start-up water level control valve of SG_i, (i = 1,.., 4), %

$S_{рк}/S_{cv}$ - control valve position, %

$S_{рк\ пнд\text{-}j}/S_{cv\ LP\text{-}PH\text{-}j}$ - position of the level control valve of $LP\text{-}PH_j$, (j= 3, 4, 5), %

$S_{ркі}/S_{CV-i}$ - position of high pressure control valve of TG_i, (i = 1,.., 4), %

$T_{1к}/T_{PC}$ - mean coolant temperature in the primary circuit, ^0C

$T_{вх}/T_{inlet}$ - mean (by four operating MCP) coolant temperature at core inlet, ^0C

$T_{гі}/T_{hot-i}$ - hot leg coolant temperature of the $loop_i$, (i = 1,..,4), ^0C

$T_{кнсб}/T_{cc}$ - temperature in the condenser collector, ^0C

$T_{пві}/T_{SG-i}$ - SG_i, inlet feed water temperature, (i = 1,.., 4), ^0C

$T_{пвдj}/T_{HP\text{-}PH\text{-}j}$ - $HP\text{-}PH_j$ downstream feed water temperature, (j = 1, 2), ^0C

$T_{пвдj\ вх}/T_{HP\text{-}PH\text{-}j\ in}$ - $HP\text{-}PH_j$ inlet feed water temperature, (j = 1, 2), ^0C

$T_{пвдj\ вых}/T_{HP\text{-}PH\text{-}j\ out}$ - $HP\text{-}PH_j$ outlet feed water temperature, (j = 1, 2), ^0C

$T_{спп}/T_{SSSH}$ - heating steam temperature upstream SSSH, ^0C

$T_{хі}/T_{ci}$ - cold leg coolant temperature of the $loop_i$, (i = 1,.., 4), ^0C

$T_{цв}/T_{HPTP}$ - water temperature at turbine condenser inlet, ^0C

$T_{цвj}/T_{HPTP-j}$ - outlet water temperature at the j-th turbine condenser, (j = 1, 2), ^0C

$T_{цвд}/T_{HPTP}$ - steam temperature at the outlet of HPTP, ^0C

$T_{эф}/T_{ef}$ - full power effective days of reactor operation, (eff. days)

$T_{iтсг}/T_{icth}$ - hot leg coolant temperature of the i-th loop, (i = 1,.., 4) on the basis of the resistance thermometer measurements, ^0C

$T_{iтсх}/T_{ictc}$ -cold leg coolant temperature of the i-th loop, (i = 1,.., 4) on the basis of the resistance thermometer measurements, ^0C

$T_{iтпг1\text{-}j}/T_{itch1\text{-}j}$ - hot leg coolant temperature of the i-th loop, (i = 1,.., 4) on the basis of the j-th thermocouple measurements of the first set, ^0C

$T_{iтпг2\text{-}j}/T_{itch2\text{-}j}$ - hot leg coolant temperature of the i-th loop, (i = 1,.., 4) on the basis of the j-th thermocouple measurements of the second set, ^0C

$T_{iтпх1\text{-}j}/T_{itcc1\text{-}j}$ - cold leg coolant temperature of the i-th loop, (i = 1,.., 4) on the basis of the j-th thermocouple measurements of the first set, ^0C

$T_{iтпх2\text{-}j}/T_{tcc2\text{-}j}$ - cold leg coolant temperature of the i-th loop, (i = 1,.., 4) on the basis of the j-th thermocouple measurements of the second set, ^0C

T_k - outlet coolant temperature of FA_k, ^0C

$\Delta P_{гцні}/\Delta P_{MCPi}$ - pressure difference of MCP_i, (i = 1,.., 4), MPa

$\Delta Pпг_i/\Delta P_{SGi}$ - pressure difference of SG_i, (i = 1,.., 4), MPa

$\Delta P_p/\Delta P_r$ - pressure difference of reactor, MPa

ΔT_k - coolant heat-up of FA_k, (k = 1,.., 95), ^0C

$\Delta T_{k\ max}$	- maximum coolant heat-up of FA, ^{0}C
$\Delta T_{пті}/\Delta T_{ilt}$	- coolant average heat-up in the i-th loop (i = 1,.., 4), ^{0}C
$\Delta T_{iтп1}/\Delta T_{itc1}$	- coolant heat-up in the i-th loop (i = 1,..,4), averaged on the basis of thermocouples' measurements of the first set, ^{0}C
$\Delta T_{iтп2}/\Delta T_{itc2}$	- coolant heat-up in the i-th loop (i = 1,..,4), averaged on the basis of thermocouples' measurements of the second set, ^{0}C
$\Delta T_{iтп1\text{-}j}/\Delta T_{itc1\text{-}j}$	- coolant heat-up in the i-th loop (i = 1,..,4), on the basis of j-the thermocouple measurement of the first set, ^{0}C
$\Delta T_{iтп2\text{-}j}/\Delta T_{itc2\text{-}j}$	- coolant heat-up in the i-th loop (i = 1,..,4), on the basis of j-the thermocouple measurement of the second set, ^{0}C
$\Delta T_{iтс}/\Delta T_{irt}$	- coolant heat-up in the i-th loop (i = 1,..,4), on the basis of measurement data of the resistance thermometers, ^{0}C
$\delta W_{аз}/\delta W_{core}$	- axial offset calculated on the basis of reconstructed power distribution in the core, %
$\delta W_{дпз}/\delta W_{dcs}$	- axial offset calculated on the bases of SPND readings, %
τ	- actual time, h, min, s
Δ	- change of a value

ABBREVIATIONS APPLIED IN Y-AXES OF THE FIGURES

МПа / MPa	- pressure, pressure difference
кПа / kPa	- pressure, pressure difference
МВт / MWt	- power
м3/ч / m3/h	- volumetric flow rate
т/ч / t/h	- mass flow rate

Chapter 1

1.1 INTRODUCTION

During the last years considerable efforts and progress have been made in various countries and organizations in incorporating full three-dimensional (3D) models of the reactor core into system transient codes. The coupled thermal-hydraulic (TH) and neutron kinetics (NK) code systems allow performing of a "best-estimate" calculation of interactions between the core behavior and plant dynamics.

Several benchmarks have been developed to verify and validate the capability of the coupled codes to analyze complex transients with coupled core-plant interactions for different types of reactors

The Nuclear Energy Agency (NEA) of the Organization for Economic Cooperation and Development (OECD) has recently completed the VVER-1000 Coolant transient benchmark (V1000CT-1) and (V1000CT-2) for evaluating coupled TH system NK codes by simulating transients at the Bulgarian NPP Kozloduy Unit #6. The available real plant experimental data made the benchmark problem very valuable.

This specification is a further continuation of the above activities and it defines a coupled code benchmark problem for further validation of thermal-hydraulics system codes for application to Russian-designed VVER-1000 reactors based on actual plant data from the Russian NPP Kalinin Unit #3 [1]. The selected transient 'Switching-off of one Main Circulation Pump (MCP)' is performed at a nominal power and leads to an asymmetric core conditions with broad ranges of the parameter changes. The experimental data is very well documented. It is being measured with a quite high frequency and the measurements errors are known for almost all parameters. This fact allows applying the studied transient not only for the validation purposes but also for uncertainty analysis as a part of the NEA/OECD Uncertainty Analysis in Modelling (UAM) Benchmark [2].

1.2 Background, Scope and Goals

Under the guidance of the NEA/OECD a lot of benchmarks have been performed concerning the application of coupled 3D TH/NK codes. Some of them have utilized code-to-code comparisons, other have compared code predictions with real measured data.

Most transients in a VVER reactor can be properly analyzed with a system thermal-hydraulics code like ATHLET, with simplified neutron kinetics models (point kinetics). A few specific transients require more advanced modeling for neutron kinetics for a proper description. A coupled thermal-hydraulics 3D neutron kinetics code would be the right tool for such tasks.

The proposed benchmark problem is being analyzed with the coupled system code ATHLET-BIPR-VVER [3, 4] and the results compared with the measurements. A lot of very interesting additional problems have to be solved in order to perform correctly the comparisons. This experience is incorporated by writing of the specification.

The reference problem chosen for simulation is MCP #1 switching off at nominal power when the other three main coolant pumps are in operation, which is a real transient of an operating VVER-1000 power plant. This event is characterized by rapid rearrangement of the coolant flow through the reactor pressure vessel resulting in a coolant temperature change, which is spatially dependent. This leads to insertion of spatially distributed positive reactivity due to the modeled feedback mechanisms and a non-symmetric power distribution. Simulation of the transient requires evaluation of core

response from a multi-dimensional perspective (coupled 3D neutronics/core thermal-hydraulics) supplemented by a one-dimensional (1D) simulation of the remainder of the reactor coolant system. The purpose of this benchmark is four-fold:

- To verify the capability of system codes to analyze complex transients with coupled core-plant interactions and complicated fluid mixing phenomena.
- To fully test the 3D neutronics/thermal-hydraulic coupling.
- To evaluate discrepancies between predictions of the coupled codes in best-estimate transient simulations with measured data.
- To perform uncertainty analysis having at disposal not only the measured values but also their accuracy

1.3 Definition of four benchmark exercises

The present benchmark is designed to provide the framework to assess the ability of modern coupled thermal-hydraulic/neutronic system codes to predict the transient response of a NPP in a best – estimate manner and to perform uncertainty analyses for coupled system codes.

This benchmark employs many of the characteristics of the OECD/NEA VVER-1000 Coolant Transient Benchmark (V1000CT-1) [5]. The current Specification is also based on it and on the experimental data description [1] officially delivered from the Russian institutions to the OECD/NEA.

The benchmark includes a set of input data for the NPP Kalinin-3 and consists of four exercises.

1.3.1 Exercise 1 – Point kinetics plant simulation

The purpose of this exercise is to test the primary and secondary system model responses. Provided are compatible point kinetics model inputs, which preserve the axial and radial power distribution, and CR #10 and #9 reactivity obtained using a 3D code neutronics model and a complete system description.

1.3.2 Exercise 2 – Coupled 3-D neutronics/core T-H response evaluation

The purpose of this exercise is to model the core and the vessel only. Inlet and outlet core transient boundary conditions are provided by the benchmark team on the basis of calculations performed with ATHLET-BIPR-VVER coupled code system or the participants can apply the measured data. HFP state (**Exercise #2a**) of the core is required for comparison.

1.3.3 Exercise 3 – Best-estimate coupled code plant transient modeling

This exercise combines elements of the first two exercises in this benchmark and is an analysis of the transient in its entirety. For participants that have already taken part in the Kozloduy-6 OECD/NEA Benchmark [5], it is suggested to start directly with this exercise. As a preface step for these participants is recommended to perform steady state core calculations at HZP state (**Exercise #3a**), HFP (**Exercise #3b**) and deliver results for comparisons. That will ensure a check for the correct application of the cross section libraries, the core loading and the core design geometry.

1.3.4 Exercise 4 – Performing of uncertainty analysis for the purpose of PHASE-III (System Phase) of OECD Benchmark for Uncertainty Analysis in Best –Estimate Modelling (UAM) for Design, Operation and Safety Analysis of LWRs [2].

The aim and the specification of this exercise will be described in a separate volume which will depict the state of the art of the results and requirements gained after performing of UAM Exercises I and II.

Chapter 2

2 NEUTRONICS CORE DATA

2.1 General

The geometrical and thermal-hydraulic data provided for Kozloduy-6 Benchmark in [5] completely defines the Kalinin-3 benchmark exercise concerning the equipment geometry, piping, valves interlocks etc. and the needed modelling of the NPP thermal-hydraulics. The reason for that is the fact that the NPP Kalinin-3 and NPP Kozloduy-6 have the same design. A Kozloduy NPP Unit 6 RELAP5 thermal-hydraulic skeleton input deck in above quoted Specification can be used in case that the participants have no experience with the V1000-CT benchmark; all other participants who have already participated in the OECD/NEA Benchmark [5] can apply directly the same thermal-hydraulic model of NPP Kozluduy-6 to simulate the Kalinin-3 NPP transient. Only the core design and loading are different thereby it will be described more detailed in this chapter.

2.2 Core geometry and fuel assembly geometry

The core and fuel assembly geometry are the same like in the Specification [5]. There are differences in the core loading pattern and the radial location of the different control rod groups.

Radially, the core is divided into hexagonal cells (see Annex B) with a pitch 23.6 cm, each corresponding to one fuel assembly (FA), plus a radial reflector of the same size. There are a total of 211 assemblies, 163 FA and 48 reflector assemblies. Axially, the reactor core is divided into 10 layers with a height (starting from the bottom) of 35.5 cm, adding up to a total active core height of 355 cm. Both upper and lower axial reflectors have a thickness of 35.5 cm. The axial nodalisation scheme accounts for material changes in the fuel design and for the exposure and moderator temperature (spectral history) variations. Zero flux boundary conditions are specified on outer reflector surface for both radial and axial reflectors. The mesh used for the calculation is up to the participant, and should be chosen according to the numerical capabilities of the code. Output should, however, give volume-averaged results on the specified mesh in the format described in Chapter 7.

The first fuel loading of the reactor core in Unit 3, NPP Kalinin consists of AFA developed by OKBM (experimental engineering bureau) in Nizhni Novgorod, with uranium-gadolinium fuel and without burnable absorbers. Until the burnup of 96 eff. days the core loading had five types of AFA:

- 48 FA with U_{235}-enrichment of 1.3 %;
- 42 FA with U_{235}-enrichment of 2.2 %;
- 37 FA with average U_{235}-enrichment of 2.98 % (303 fuel rods with 3 %-enrichment, 9 gadolinium fuel rods with 2.4 %-enrichment);
- 24 radial profiled FA with average U_{235}-enrichment of 3.9 % (243 fuel rods with 4 %-enrichment, 60 fuel rods with 3.6 %-enrichment, 9 gadolinium fuel rods with 3.3 %-enrichment);
- 12 radial profiled FA with average U_{235}-enrichment of 3.9 % (240 fuel rods with 4 %-enrichment, 66 fuel rods with 3.6 %-enrichment, 6 gadolinium fuel rods with 3.3 %-enrichment).

It should be mentioned that AFA have stiffening fins which like the leading tubes and spacers were made of zirconium alloy (E-635).

After the operation of this fuel load during 96 EFRD a defected FA with coordinates 07-32 (FA with initial U_{235}-enrichment of 2.2 % weight metal) was replaced by a “fresh” standard FA with U_{235}-enrichment of 1.6 % weight metal. The spacers and the leading tubes of this FA were made of stainless steel.

The fuel loading map in the reactor core of Unit 3 NPP Kalinin after the replacement of the defected AFA by a standard FA is shown in Annex B. The scheme in this Annex gives also information of the layout of CR CPS rods and their assignment in groups.

The scheme in Annex C shows the layout of ionizing chambers channels (in the biological shield of the reactor); CR of CPS and their assignment in groups; ICMS thermocouple sensors locations at FA outlets; assemblies with SPND sensors in the leading (central) FA tubes; primary circuit loop nozzles' locations.

The core layout in Annex D shows conditionally accepted division of FA locations in the reactor core into 6 sectors with a 60^0-symmetry together with layout of CR of CPS and their assignment in groups; ICMS thermocouples' locations (at FA-outlets) and SPND sensors' locations.

The schema in Annex E shows the locations of the casings of the temperature measurement devices in the main and the corresponding numbering of the temperature devices' casings located in the primary loops.

According to the measurement system established at the NPP the positions of CR of CPS are given with respect to the position of the lower end switches (LES). They are located 17.25 cm higher than the bottom of the reactor core. With the length of the reactor core of 355 cm and the distance between the lower and the upper end switches of 352 cm, it turns out that the CR of CPS when withdrawn from the reactor core (while H = 352 cm, then H = 100 %) are 14.25 cm higher than the upper end of the core. Thus, the upper end of the core corresponds to the positions of CR of CPS H = 337.75 cm = 96 % withdrawn.

The data of the power load timetable –operational history (applied to calculate the fuel burnup) for Unit 3 NPP Kalinin from the beginning of the first fuel cycle up to the day when the experiment with the switching off of one MCP took place, are provided separately on a digital medium. Additionally, tables are supplied with the daily averaged effective operation time of the reactor; boron concentration history; history of the position of the tenth group of CR of CPS; average thermal reactor power history and the electrical power history of the turbine generator.

The available gap width is 0.08 mm (distance between pellet surface and inside clad wall). For the neutronic problem, each of the FAs is considered to be homogeneous. The sixty-one assemblies which can be controlled, grouped into ten groups, are full-length control rods except group #5, which consists of part-length control rods. The part-length control rods have neutron absorber only in its lower half and they are used to damp the Xe oscillations. The full-length control rods contain a strong neutron absorber over a length that spans most of the active core region. The lower 30 sm of those CRs have dysprosium as absorber and the rest part - boron.

2.3 Neutron modelling and cross-section library

Two neutron energy groups and six decay groups for delayed neutrons are modelled. The energy release per fission for the two prompt neutron groups is 0.3213 × 10-10 and 0.3206 × 10-10 W-s/fission, and this energy release is considered to be independent of time and space. Time constants and the local fractions of effective delayed neutrons will be provided on the CD-ROM.

It is recommended that ANS-79 be used as a decay heat standard model (see [5]). For participants who are not capable of using the ANS-79 decay heat standard, a file of the decay heat evolution throughout the transient for the scenario will be provided on CD-ROM. The average value for each time step should be redistributed spatially according to the fission power spatial distribution at the initial hot power steady-state conditions. The effective decay heat energy fraction of the total thermal power (the relative contribution in the steady state) is equal to 0.07143.

The number of the assembly types with their unrodded and rodded compositions will be provided on CD-ROM together with the corresponding sets of cross-sections. The axial locations of compositions for each assembly will be delivered also on a CD-ROM.

A complete set of two neutron group diffusion macroscopic cross sections and kinetic parameters defined for each assembly (composition) will be provided in a NEMTAB-like format used for the OECD/NEA-CEA benchmark V1000-CT1 [5]. Two types of tables will be available – one for uncontrolled status (nemtab) and the other for controlled status for rodded numerical nodes (nemtabr).

For the assemblies which have been controlled (CR are moving) during the transient will be given two types of cross section data for controlled status (for dysprosium absorber and for boron absorber). Four reflector compositions are defined: upper reflector, bottom reflector, two radial reflectors. The approximation of nuclear data within the proposed table format will be done in a three dimensional space. Variables are the fuel temperature, the coolant moderator density and moderator temperature (four support points for each variable). The burn-up distribution will be account in the composition numbers in axial layers for each assembly type. Due to the fact that during the transient the boron concentration is not changing, the core macroscopic cross sections will be derived for C_b=660 ppm [3.6 g/kg$H_2$0]. Xe concentration is in equilibrium state and is taken into account by the cross section generation.

The assembly discontinuity factors (ADF), the group inverse neutron velocities and the delayed neutron parameters are also provided for each composition. For the first energy group are provided two diffusion coefficients – radial and axial.

All the data in the cross-section library is obtained using the TVS-M cross section generation code. Each composition is assigned to a cross section set containing separate tables for the diffusion coefficients and cross-sections, with each point in the table representing a possible core state. The expected range of the transient is covered by the selection of an adequate range for the independent variables as follows:

T_{fuel}: 540.0 K – 1700.0 K

ρ_{moder} : 660.0 [kg/m^3] – 790.0 [kg/m^3]

T_{mod}: 540.0 K – 600.0 K

A linear interpolation scheme is used to obtain the appropriate total cross sections from the tabulated ones based on the reactor conditions being modelled.

Table 1 shows the macroscopic cross section table structure for one cross-section set. The format of each library is as follows:

- The first line of data is used to show the number of data points used for the independent thermal-hydraulic parameters. These parameters include fuel temperature, moderator temperature and moderator density.
- Each cross-section set is in the order shown in Table 1. First, the values of the independent thermal-hydraulic parameters (fuel temperature, moderator temperature and moderator density) used to specify that particular set of cross-sections are listed, followed by the values of the cross sections and ADFs. Finally, the group inverse neutron velocities complete the data for a given cross-section set.
- As addition to the provided library for the reflector (radial, bottom and top) the reflector data generated in [5] can be used. In that case the reflector cross sections are also dependent on fuel temperature, moderator temperature and moderator density.

All cross-section data, along with a program for linear interpolation will be supplied in an electronic form.

Table 1 Structure and key of the macroscopic cross-section table

```
*****************************************************************************************
*       Nemtab and nemtabr  – Cross-Section Table Input
*       number of support points of:
* Fuel temperature      Rho        Moderator temperature
          4              4             4
*
*       Tf  - Doppler (fuel) temperature, (K)
*       ρm  -  moderator density (kg/m3)
*       Tm – moderator temperature, (K)
*
        Tf1     Tf2     Tf3     Tf4
        Tm1     Tm2     Tm3     Tm4
        ρm1     ρm2     ρm3     ρm4
*
********** X-Section Set #*************************************************************
* Group No. 1
********** Radial Diffusion Coefficient Table
*
D11 (Tf1, Tm1, ρm1)  D12(Tf2, Tm1,ρm1)  D13(Tf3, Tm1,ρm1)  D14(Tf4, Tm1, ρm1)  D15(Tf1, Tm2, ρm1)
D16 (Tf2, Tm2, ρm1)  D17 (Tf3,Tm2,ρm1)  D18 (Tf4, Tm2,ρm1) ……
…….. D163 (Tf3, Tm4, ρm4) D164 (Tf4, Tm4, ρm4)
*
********** Absorption X-Section Table
*
********** Scattering from Group 1 to 2 X-Section Table
*
********** Axial Diffusion Coefficient Table
*
********** Nu-Fission X-Section Table
*
********** Kappa X-Section Table
*
*****************************************************************************************
* Group No. 2
********** Diffusion Coefficient Table
*
********** Absorption X-Section Table
*
********** Nu-Fission X-Section Table
*
********** Kappa X-Section Table
*
*****************************************************************************************
* Additional parameters
********** ADF in radial direction Table
*
********** Inverse Neutron Velocities – 2 values
*
*Delayed  neutron parameters
********** Betta (6 values)
*
********** Lambda (6 values)
```

Chapter 3

3 THERMAL-HYDRAULIC DATA

3.1 Component specifications for the full thermal-hydraulic system model

The design of NPP Kalinin-3 is the same as the NPP Kozloduy-6 design. This fact allows using all available data in [5] for the component description needed for modelling the thermal-hydraulic system. That means that the tables and the description of main equipment (reactor vessel, reactor coolant system, steam generator, feed water system etc.) can be used as described in the Specification [5] of the NPP Kozloduy-6.

3.2 Definition of the core thermal-hydraulic boundary conditions model

By defining an inlet condition at the core bottom and outlet condition at the full Kalinin NPP Unit 3 thermal-hydraulic model can be converted to a core TH boundary condition model.

The boundary conditions (BC) for this model will be provided on the CD-ROM.

The BCs have been calculated using the ATHLET-BIPR-VVER [3, 4] best-estimate core plant system code. Core inlet radial distributions will be provided in all 163 assemblies which have been modelled as separate thermo-hydraulic channels. On the base of this mapping scheme there will be given all needed parameters with a time dependent histories (0-300 s) like: mass flow rate, inlet and/or outlet pressure, inlet coolant temperature, positions of the control rod groups.

3.3 Thermal-physical and heat-transfer specifications

The Doppler temperature (T_f) can be calculated via the relation:

$$T_f = 0.3T_{fc} + 0.7T_{fs}$$

where, T_{fc} is the fuel rod center temperature and T_{fs} – the fuel pellet surface temperature.

The UO_2 density is 10.6 [g/cm^3] (95% of the theoretical density) at a temperature of 293.15 K. The pellet dishing amounts to 1.956 %. The cladding material is Zr + 1% Nb with a density of 6.55 g/cm^3. All other necessary data (λ (W/m K), cp (J/kg K), etc.) can be taken from [5]. Expansion effects of fuel and cladding are not to be considered in this benchmark. The heat transfer coefficient between cladding and moderator has to be calculated using code specific correlations.

Chapter 4

4 NEUTRONIC/THERMAL-HYDRAULIC COUPLING

The transient calculations for Exercise #3 must be performed with coupled system codes which should take into account the following effects:

- Fluid mixing in the down comer, upper and bottom plenum. The measurements showed that the flow through the active core is more or less laminar and no flow mixing is observed in it.
- In order to predict correctly the measured coolant temperatures at 96 assembly outlets should be necessary to model the mixing of the fluid passing through the control rod guide tubes with the main assembly flow. If not possible, there will be given the pre-calculated with ATHLET-BIPR-VVER mixing coefficients [6, 7].
- The delay (inertia) terms of the measurements (mainly coolant temperature) should be modeled in order to be possible a correct comparison with the measured thermocouples' readings [8].
- By the simulation of the SPND predictions should be taken into account the real positions of the sensors which will be given on CD-ROM in a special file. It will be compared the relative SPND currents (simulated nodal relative power)

In case participants have difficulties to model the secondary circuit response it will be possible to apply the experimental data (see Annex A) as boundary conditions at SGs or will be also possible to require the ATHLET-BIPR-VVER simulated data from the benchmark team.

Each participant should use his own coupling TH/NC schema and methodology.

Chapter 5

5 REACTOR CONTROL SYSTEM AND MEASURING AND RECORDING DEVICES

5.1. Short description of the control system logic operating by this transient

The purpose of the experiment at Kalinin-3 which is selected for this benchmark is the complete testing of reliability of all power plant equipment, testing the reliability of the main regulators (ARC, Electro-Hydraulic Turbine Controller and the regulator of the level in the steam generator) and to check the expected neutron reactor power change in case of switching off of one MCP.

The ARC is a part of the Unit Power Control System and operates in coordination with the reactor power limitation controller and the TEC. The controller stabilizes the reactor power or makes it to follow the turbine power.

The ARC does not set any set point specification devices and stores the current values of neutron power or main steam header pressure as a set point at the time of switching off. In order to reset a set point, switching off and then switching on to the appropriate mode is needed. The ARC usually uses the control rod group #10 to operate. In this particular transient the control rod group #10 and group #9 are changing its position during the transient. The reactor power limiting controller - CPS is used to constrain the maximum thermal and neutron power to set points automatically chosen depending on the operational status of certain plant components such as MCP, FWP, SG and TG. The CPS inserts the control rod group #10 and #9 with normal operation speed of 2 cm/sec. Control signal is the neutron flux, measured by the neutron flux monitoring system. This signal is corrected once in every 50 seconds using the thermal power evaluated on the basis of the average temperature rise in the operating loops. When CPS is in operation, ARC is automatically disconnected and PP-1 signals are not used. Depending on the initiating event, the reactor power is lowered to and then kept at specified set points by CPS.

Control rod group #10 and #9 are changing its position during the transient. Analysis of the initial 3D relative power distribution showed that this insertion introduced axial neutronics asymmetry in the core. At the beginning of the transient there is also a thermal-hydraulic asymmetry coming from the asymmetric coolant change introduced in ¼ of the core when MCP #1 is switched off. This causes a spatial asymmetry in the reactivity feedback, which has been propagated through the transient.

5.2 Measuring and recording devices

Measuring and recording in this dynamic mode were conducted by standard devices i. e. by the upper block level system – (СВБУ/UBLS) and by the ICMS as well as by means of additional measurement equipment (a system of experimental control СЭК/SEC).

The list of parameters recorded by the UBLS, (with periodicity of 1 s) is given in CD-ROM. The aperture of recording for directly measured signals is 0.1 % of the sensor's scale maximal value.

The list of parameters recorded by ICMS with time step 1 s is given in CD-ROM. The signal recordings aperture is not available for them. It should be mentioned that the currents of the SPND were recorded taking into account of the background sensors currents, i. e. with the deduction of background sensors currents.

The list of parameters recorded by the SEC computer with frequency of 10 Hz is given in CD-ROM, the aperture of parameter recordings is missing. The signals have been taken from plant standard sensors and systems. The NFC system have recorded the reactor power only in the sub-range OR-1

which was determined by the signals of the ionization chambers (Type KNK-53M9), located in the lower part of the core.

All the data recorded by UBLS, ICMS and SEC is provided on the CD-ROM.

On CD-ROM can be found information for the CR of CPS positions recorded by the systems UBLS, ICMS and SEC in cm related to the position of the rigid end-stops which are located 10 cm lower than the lower end switches and 7.25 cm higher than the bottom of the reactor core.

Chapter 6

6. TRANSIENT DESCRIPTION

6.1 Initial steady-state conditions (HFP- Exercise #3b)

The reactor is at the middle of cycle (MOC) with average core exposure of 130.6 EFPD and boron concentration 3.6 [g/kgH_2O]. The definition of the initial steady state is given in Table 2 and is derived from the measurements.

Table 2 The main reactor parameters before and at the end of the transient

Parameters	Values	
	Initial state	Final state
Date	02.10.2005	02.10.2005
Time, h:min:s	20:30:00	20:34:42
$T_{eff.}$ eff. days	128.50	128.50
N_{core}, MW	2907	1946
N_{PC}, MW	2918	1926
N_{SC}, MW	2877	1938
N_{DCS}, MW	2887	1948
N_{NFC}, MW	2965	1996
N_{el}, MW	986	625
H_{1-8}, cm (%)	352 (100)	352 (100)
H_{10}, cm (%)	292 (82.95)	160 (45.45)
C_B, g/kgH_20	3.60	3.60
Tk_i, ^{0}C	288.14; 287.81; 287.69; 287.50	284.96; 287.40; 287.83; 284.80
$\Delta T_{loop\ i}$, ^{0}C	29.23; 28.87; 28.74; 29.26	-7.98; 23.86; 25.40; 17.88
T_{inlet}, ^{0}C	287.79	286.68
ΔT_{loop}, ^{0}C	29.03	22.38
P_{PC}, MPa	15.52	15.46
ΔP_r, MPa	0.38	0.21
$\Delta P_{MCP\ i}$, MPa	0.569; 0.564; 0.565; 0.562	0.153; 0.460; 0.448; 0.431
G_{loopi}, m3/h	22292; 22223; 21784; 21772	-7198; 24668; 24280; 24725
G_r, m3/h	88073	66475
L_{PRZ}, cm	860	780
L_{SGi}, cm	222; 220; 220; 222	229; 215; 216; 221
G_{i-SG}, t/h	1445; 1367; 1364; 1360	143; 1241; 1283; 937

T_{SG-i}, ^0C	215.70; 215.50; 216.40; 214.50	208.90; 201.70; 205.50; 201.10
P_{SGi}, MPa	6.27; 6.30; 6.25; 6.24	6.02; 6.27; 6.23; 6.16
P_{MSH}, MPa	6.02	5.99
δW_{DCS}, %	-6.06	-23.40
δW_{core}, %	-2.15	-20.70
$K_{q\ max}$/FA	1.27/08-25	1.29/12-21
$\Delta T_{c\ max}$, ^0C/FA	28.71/08-25	27.69/08-25
$K_{v\ max}$/FA/layer	1.50/10-31/2	1.81/10-31/2

Additional HZP state is defined for initialization of the 3D core neutronics model for Exercise #2 – Exercise #2a and for Exercise #3 – Exercise#3a (only for those participants that do not need to perform Exercise #1 and #2 because of availability of a system model for NPP-Kozloduy -6).

The HZP (Exercise #2a or Exercise #3a) conditions are defined as follows: the power level is 0.1% of the nominal power; the fuel and moderator temperature are 552.15 K and the moderator density is 767.1 [kg/m^3]. Only control rod group #10 is 82.95 % inserted from below. Boron concentration is 3.6 [g/kg$H_2$0].

6.2 Transient scenario

The transient scenario (recovered from the measured data histories) is listed shortly below. The detailed analysis and description of all primary and secondary loop parameters' histories supplied with the corresponding graphics are discussed in Annex A. The time interval of interest is 300 s.

- Manually switching off of MCP #1 at t=0s.
- After the signal 'one pump out of operation' which is generated after 1.41 s, rector limiting controller starts to decrease the power to a level of 67.2 %.
- The following sequence of actuations for rector limiting controller and automatic reactor power controller is recorded:

  - At t=1.41 s the reactor limiting controller starts to decrease the reactor power. CR #10 starts to move downwards. When the CR #10 reaches 50 % insertion depth (at about 60 s) the CR #9 starts also to enter the active core according to the control rod movement algorithm.

  - Protection system level #1 of automatic reactor power controller switches off from option 'T' (keeping the secondary loops' parameter constant) to option 'H' (keeping neutron power constant)

  - Control rod controller decouples from automatic reactor power controller.

- At t=71 s the reactor power load-off procedure is cancelled and power reaches a level of 67.2 % P_{nom}. At this moment the position of the CR #10 is at 43.4 % and remains till the end of the transient at this position. CR #9 is inserted into the core and reaches at 71 s the position of 93.1 % and keeps it till 180 s after which it returns back to 100 %. The automatic reactor power controller was again switched on to the control rod controller with option 'H' and it starts to keep the power level in the range of 66.2-67.3 % P_{nom}.

  With the reactor limiting controller the reactor power was decreased from 98.9 % P_{nom} to 67.2 % P_{nom} within 71 s. The speed of reactor power decrease (load-off) within the reactor limiting controller operations is 26.8 % /min. The change of the coolant heat-up in the core decreases from 29 ^{o}C to 23.3 ^{o}C.

- Due to reactor limiting controller operation and switching off of automatic reactor power controller, the electronic controller of the turbine generator electro-hydraulic automatic controller starts the

load-off operation of the turbine generator. At t=222 s the power of the turbine generator corresponds to the reactor power and stabilizes at 625.5 MW.

- The pressure in the main steam line changes from initial 6.01 MPa to a level of 5.86 - 6.02 MPa. At 300 s the pressure is stabilized at 6.02 MPa.
- Primary pressure changes from initial 15.52 MPa to 15.12 -15.56 MPa following the change of the mean primary coolant temperature.
- The temperature decrease of the affected loop #1 (within the time interval from 30 s to 140 s) leads to a decrease of the mean reactor coolant temperature and in its turn it leads to a decrease of the volume of the coolant in the primary loop. That affects (decreases) the pressurizer level which leads to a decrease of the primary loop pressure. At 94 s of the transient the pressure is stabilized at 15.13 MPa. Due to the pressurizer heaters operation starting from 140 s the pressure starts to increase and at 300 s it stabilizes at 15.47 MPa. As a result the pressurizer level changes from 858.5 cm at the beginning to 801.1 cm at the end of the transient.

During the transient the maximum coolant temperature measured at the assemblies' outlets is registered at 46 s and has a raise of approximately 3 ^{o}C. The maximum raise (2.8 ^{o}C) of the hot loop temperature is observed in loop #3. The cold loop coolant temperatures at the loops where the pumps remain in operation change as follows: loop #2 - 3.7 ^{o}C; loop #3 - 2.8 ^{o}C and loop #4 – 4.8 ^{o}C. It is observed that as a result of the switching off of MCP #1 the main part of the coolant with lower temperature of hot leg #1 moves into the hot leg #4. Therefore, the coolant flow with the lowest mean temperature reaches SG #4 and it has also the lowest outlet temperature.

6.3 Point kinetics model inputs (Exercise #1)

The point kinetics model is necessary only for Exercise #1 which should be performed in case that the participants have not taken part in the OECD/DOE/CEA V1000CT Benchmark [5] or have no a consistent model for VVER-1000. Point kinetics model inputs, which preserve axial and radial core power distributions obtained with 3D neutronics model BIPR-VVER are given in the CD-ROM. The following parameters for the point kinetics model can be found:

- Control Rod Group #10 and #9 worth;
- Axial power distribution;
- Moderator temperature coefficient;
- Moderator density coefficient;
- Doppler temperature coefficient;
- Other kinetics parameters (delay neutron parameters, etc.).

6.4 Transient core calculations (Exercise #2)

Exercise #2 is a boundary condition problem which aim is to test the correctness of participants' core loading, neutronic data and core thermal hydraulic without modelling the primary loops. The required thermal-hydraulic data will be recorded on the CD-ROM. It includes the time histories of the following parameters calculated with the coupled system code ATHLET-BIPR-VVER or they can be taken from the measurements:

- Core inlet assembly wise mass flow distribution ;
- Core inlet assembly wise coolant temperature distribution ;
- Core inlet/outlet pressure ;

- Position of the CR groups #9 and #10.

6.5 Transient coupled calculations (Exercise #3)

Exercise #3 is the final aim of the Benchmark - to predict the NPP response in a 'best estimate' manner with a coupled code system.

The main parameters' changes at the end of the transient can be seen in Table 1. MCP test plant data recorded with time interval of 1 s and the transient analysis are described in detail in Appendix A. The simulated results should be compared with the real measured data.

The neutronics and thermal-hydraulic information presented in Chapter 2 and 3, suffices for performing Exercises 1, 2, and 3.

Chapter 7

OUTPUT REQUESTED

The requested output is as near as possible to the same format and data quantity like in the Specification for the Kozloduy -6 Benchmark [5].

- The analysis results will be presented in a benchmark analysis report, which will be made available in both hard copy and electronic form.
- Results should be presented in digital form (format details are given in Section 7.3).
- All data should be in SI units (kg, m, sec).
- For time histories, data should be at 1.0-second intervals.
- Graphical comparison of calculated results and test data should be performed.

7.1 Initial steady-state results (HZP - Exercise#2a or HZP - Exercise#3a, HFP – Exercise#3b)

For the initial HZP (**Exercise #2a** or **Exercise #3a)** the following parameters will be compared:

- Keff;
- the power peaking factors Fxy, Fz;
- axial offset;
- scram rod worth (SRW), and control rod group #10 and #9 worth (CRW).
- Radial power distribution – 2D assembly NP distribution – axially averaged radial power distribution for 163 radial nodes (full core) normalized to core average power (relative radial power distribution).
- Axial power distribution – core average axial shape – radially averaged axial power distribution for 10 axial nodes (each 35.5 cm in length), normalized to core average power (relative axial power distribution).

For the initial HFP (**Exercise #3b)** state the same information as for the HZP state plus:

- 2D map of core inlet and outlet coolant temperature and density distribution
- 2D inlet flow rate distributions
- Power peaking factors – Fxy, Fz, and axial offset.
- Axial power and coolant temperature distribution in the following selected fuel assemblies (SFA):
    - From sector #1 (see Annex D)
      09-16 SFA-1 08-25 SFA-2 08-19 SFA-3 10-23 SFA-4
    - From sector #2
      12-25 SFA-5 14-31 SFA-6
    - From sector #3
      09-34 SFA-7 10-35 SFA-8
    - From sector #4
      05-34 SFA-9 07-34 SFA-10
    - From sector #5
      02-31 SFA-11 02-33 SFA-12
    - From sector #6
      04-23 SFA-13 06-27 SFA-14

The 14 SFA are selected because they have either thermocouples at assemblies' outlets or SPND at 7 axial levels or both of them.

The spatial distributions should follow the format of the radial and axial power distributions.

7.2 Transient results

Exercise 1

- Sequence of events.
- Transient core average results (time histories): total core power; fission power; RCS pressure – core average, loop #1 (loop #1 is associated with the switch off of MCP #1); core average coolant temperature; hot and cold leg coolant temperatures in all four loops (last cell before/after vessel); coolant heat-up temperature in all four loops; pressurizer water level; SG water levels; secondary side pressure; primary side flow rates; reactivity edits; and core average fuel temperature.

Exercise 2

- Snapshots at the 45th second after switching off MCP #1, and at the 300th second – the same data as for the HP steady-state except the total and fission power levels will be compared instead of Keff.
- Time histories (core volume averaged without the reflector region): total power, fission power; coolant density; and Doppler temperature. In addition, the maximum nodal Doppler temperature vs. time will be compared.

Exercise 3

- Sequence of events
- Transient average results (time histories): RCS pressure – core average, loop #1; core average coolant temperature; hot and cold leg coolant temperatures in all four loops (last cell before/after vessel); coolant heat-up temperature in all four loops; pressurizer water level; SG water levels; secondary side pressure; primary side flow rates; and reactivity edits.
- Time histories (core volume averaged without the reflector region): total power; fission power; coolant density; and Doppler temperature. In addition, the maximum nodal Doppler temperature vs. time will be compared.
- Time histories of radial and axial power peaking factors and axial offset
- Time histories of all assemblies' outlet coolant temperatures
- Snapshot at the 45th second (ATHLET-BIPR-VVER time of coolant temperature peak at core exit) after switching off MCP #1 and snapshot at the 300th second (end of the transient). Axial power and coolant temperature distributions in the following **selected fuel assemblies (SFA)**:
    - From sector #1 (see Annex D)
      09-16 SFA-1 08-25 SFA-2 08-19 SFA-3 10-23 SFA-4
    - From sector #2
      12-25 SFA-5 14-31 SFA-6
    - From sector #3
      09-34 SFA-7 10-35 SFA-8
    - From sector #4
      05-34 SFA-9 07-34 SFA-10
    - From sector #5
      02-31 SFA-11 02-33 SFA-12
    - From sector #6
      04-23 SFA-13 06-27 SFA-14
- Time histories of the relative neutron fluxes (nodal power) at 6 axial layers for SFA #2, 3, 5, 6, 7, 9, 10, 12, 14 where SPND sensors are located (see Annex D and the key tables of the SPND numbering and locations which is included in the CD-ROM).

7.3 Output format

Templates in Excel format will be prepared and delivered to the participants. They should be filled in with maximum data required.

Remarks:

- Time histories start at -30 seconds (i. e. 30 s zero transient), up to 300s with a step of 1 s like by the experiments.
- Please provide the units on the first line of each time history.
- A plot of time histories would be appreciated for a first comparison of the transient results.
- The plots of calculated results and experiment results should be compared on the same graph.
- Radial and axial profiles should be given according to the form shown in the output sample points B2 and B3
- Please do not use tabs in the data files.

Output sample:

A) VVER-1000 Kalinin-3 BENCHMARK

Hot Full Power

RESULTS FROM CODE “XXXXXXXX”

EXERCISE #2

B) STEADY STATE RESULTS -HFP

B1) Keff = 1.0000

B2) Radial power distribution (full core) – start each line in column one, leave a blank space in between each number, and use a total of six spaces per number):

0.9999 0.9999 0.9999 0.9999 0.9999 0.9999

0.9999 0.9999 0.9999 0.99990.9999 0.9999 0.9999 0.9999 0.9999

0.9999 0.9999 0.9999 0.9999 0.9999 0.9999 0.9999 0.9999 0.9999 0.9999

0.9999 0.9999 0.9999 0.9999 0.9999 0.9999 0.9999 0.9999 0.9999 0.9999 0.9999

0.9999 0.9999 0.9999 0.9999 0.9999 0.9999 0.9999 0.9999 0.9999 0.9999 0.9999 0.9999

0.9999 0.9999 0.9999 0.9999 0.9999 0.9999 0.9999 0.9999 0.9999 0.9999 0.9999 0.9999 0.9999

0.9999 0.9999 0.9999 0.9999 0.9999 0.9999 0.9999 0.9999 0.9999 0.9999 0.9999 0.9999 0.9999 0.9999

0.9999 0.9999 0.9999 0.9999 0.9999 0.9999 0.9999 0.9999 0.9999 0.9999 0.9999 0.9999 0.9999

0.9999 0.9999 0.9999 0.9999 0.9999 0.9999 0.9999 0.9999 0.9999 0.9999 0.9999 0.9999 0.9999 0.9999

0.9999 0.9999 0.9999 0.9999 0.9999 0.9999 0.9999 0.9999 0.9999 0.9999 0.9999 0.9999 0.9999

0.9999 0.9999 0.9999 0.9999 0.9999 0.9999 0.9999 0.9999 0.9999 0.9999 0.9999 0.9999

0.9999 0.9999 0.9999 0.9999 0.9999 0.9999 0.9999 0.9999 0.9999 0.9999 0.9999

0.9999 0.9999 0.9999 0.9999 0.9999 0.9999 0.9999 0.9999 0.9999 0.9999

0.9999 0.9999 0.9999 0.9999 0.9999 0.9999 0.9999 0.9999 0.9999

0.9999 0.9999 0.9999 0.9999 0.9999 0.9999

B3) Axial power distribution – place all data starting in column one, leave a blank in between each number, and use a total of six spaces per number:

0.9999 0.9999 0.9999 0.9999 0.9999 0.9999 0.9999 0.9999 0.9999 0.9999

B4) Scram rod worth: 1.000 % dk/k

Control rod group #10 worth: 1.000 % dk/k

Control rod group #9 worth: 1.000 % dk/k

B5) Calculated steady state conditions compared to those in the measurements.

Steady state calculation should be compared to the steady state measured parameters according to Table 1.

C) SEQUENCE OF EVENTS

The template will have as a first column the time, starting from -30s and ending at 300s with a time step 1s. The time scale from -30s to 0 is required to be seen if before the transient start a stable values of the parameters are reached.

D) TRANSIENT CORE AVERAGED RESULTS (TIME HISTORIES) of following parameters:

fission power [W], total power [W], coolant temperature (core average, hot and cold legs) [K], pressure (core average, loop #1-4) [Pa], total core reactivity [dk/k] (or rector period) and reactivity components (contributions from changes in moderator density, fuel temperature and neutron flux distribution – optional), core average fuel temperature [K]; time histories of all assemblies' outlet coolant temperatures;

time histories of the relative neutron fluxes (nodal power) at 7 axial layers for SFA #2, 3, 5, 6, 7, 9, 10, 12 and 14.

E) SNAPSHOTS:

− At 0 s

− At the time of maximum power after switching off MCP #1

− At the end of the transient (300 seconds).

- Axial power and coolant temperature distributions in the SFA:
    - From sector #1
      09-16 SFA-1 08-25 SFA-2 08-19 SFA-3 10-23 SFA-4
    - From sector #2
      12-25 SFA-5 14-31 SFA-6
    - From sector #3
      09-34 SFA-7 10-35 SFA-8
    - From sector #4
      05-34 SFA-9 07-34 SFA-10
    - From sector #5
      02-31 SFA-11 02-33 SFA-12
    - From sector #6
      04-23 SFA-13 06-27 SFA-14

F) Radial power distribution (full core) – start each line in column one, leave a blank space in between each number, and use a total of six spaces per number):

0.9999 0.9999 0.9999 0.9999 0.9999 0.9999
0.9999 0.9999 0.9999 0.99990.9999 0.9999 0.9999 0.9999 0.9999
0.9999 0.9999 0.9999 0.9999 0.9999 0.9999 0.9999 0.9999 0.9999 0.9999
0.9999 0.9999 0.9999 0.9999 0.9999 0.9999 0.9999 0.9999 0.9999 0.9999 0.9999
0.9999 0.9999 0.9999 0.9999 0.9999 0.9999 0.9999 0.9999 0.9999 0.9999 0.9999 0.9999
0.9999 0.9999 0.9999 0.9999 0.9999 0.9999 0.9999 0.9999 0.9999 0.9999 0.9999 0.9999 0.9999
0.9999 0.9999 0.9999 0.9999 0.9999 0.9999 0.9999 0.9999 0.9999 0.9999 0.9999 0.9999 0.9999 0.9999
0.9999 0.9999 0.9999 0.9999 0.9999 0.9999 0.9999 0.9999 0.9999 0.9999 0.9999 0.9999 0.9999
0.9999 0.9999 0.9999 0.9999 0.9999 0.9999 0.9999 0.9999 0.9999 0.9999 0.9999 0.9999 0.9999 0.9999
0.9999 0.9999 0.9999 0.9999 0.9999 0.9999 0.9999 0.9999 0.9999 0.9999 0.9999 0.9999 0.9999
0.9999 0.9999 0.9999 0.9999 0.9999 0.9999 0.9999 0.9999 0.9999 0.9999 0.9999 0.9999
0.9999 0.9999 0.9999 0.9999 0.9999 0.9999 0.9999 0.9999 0.9999 0.9999 0.9999
0.9999 0.9999 0.9999 0.9999 0.9999 0.9999 0.9999 0.9999 0.9999 0.9999
0.9999 0.9999 0.9999 0.9999 0.9999 0.9999 0.9999 0.9999 0.9999
0.9999 0.9999 0.9999 0.9999 0.9999 0.9999

G) Axial power distribution – place all data starting in column one, leave a blank in between each number, and use a total of six spaces per number:

0.9999 0.9999 0.9999 0.9999 0.9999 0.9999 0.9999 0.9999 0.9999 0.9999

REFERENCES

[1] V. A. Tereshonok, V. S. Stepanov, V. V. Ivchenkov, V. A. Pitilimov (VNIIAES), S. P. Nikonov (RRC "Kurchatov Institute"), Description of a Transient Caused by the Switching-off of One of the Four Operating MCP at Nominal Reactor Power at NPP Kalinin Unit 3, OECD/NEA, July, 2008.

[2] K. Ivanov, M. Avramova, I. Kodeli, E. Sartori, "Benchmark for Uncertainty Analysis in Modelling (UAM) for Design, Operation and Safety Analysis of LWRs. Volume 1 – Specification and Supporting Data for the Neutronics Cases (Phase I) Version 1.0", NEA/NSC/DOC(2007)23.

[3] Lizorkin M.P., Nikonov S.P., Langenbuch S., Velkov K., Development and Application of the Coupled Thermal-Hydraulics and Neutron-Kinetics Code ATHLET/BIPR-VVER for Safety Analysis, EUROSAFE -2006, Paris, 13-14 , Nov., 2006.

[4] Langenbuch S., Nikonov S.P., Lizorkin M.P., Velkov K., ATHLET/BIPR-VVER – an Advanced Coupled Code System for VVER Safety Analysis, PHYSOR-2008, Interlaken, Switzerland, Sep. 14-19, 2008.

[5] Boyan Ivanov, Kostadin Ivanov, Pavlin Groudev, Malinka Pavlova, Vasil Hadjiev, VVER-1000 Coolant Transient Benchmark, PHASE 1 (V1000CT-1), Vol.I: MAIN Coolant Pump (MCP) Switching On – Final Specifications, NEA/NSC/DOC (2002) 6, 2002.

[6] S. Nikonov , M. Lizorkin , S. Langenbuch, K. Velkov, Modelling of Thermocouples' Measurements at Core Exit of Reactor VVER-1000 with the Coupled Code ATHLET/BIBR-VVER, 17th Symposium of AER, Yalta, Crimea, Ukraine, Sept. 24-29, 2007.

[7] S. Nikonov , M. Lizorkin , S. Langenbuch, K. Velkov, Advanced Analysis of the CEA-OECD/NEA VVER-1000 Coolant Transient Benchmark with the Coupled system Code ATHLET/BIPR-VVER, 17th Symposium of AER, Yalta, Crimea, Ukraine, Sept. 24-29, 2007.

[8] S. Nikonov, K. Velkov, Accounting for the Inertia of the Thermocouples' measurements by Modelling of a NPP Kalinin-3 Transient with the Coupled System Code ATHLET-BIPR-VVER, 18th Symposium of AER, Eger, Hungary, Oct. 6-10, 2008.

ANNEX A

ANALYSIS OF THE TRANSIENT AND MEASURED DATA

(Prepared on the basis of Ref. [1])

Initial steady state reactor parameters are shown in Table 2 (Chapter 6), in column "Initial state" (data from ICMS, with exception of C_B which are determined through laboratory analysis). Values of FA relative power and heat-up of the coolant in FA are shown in the core schema of Fig. 1 and 2 (line-"initial state"). The operational state of the loop equipment and control systems are unchanged, as designed. The reactor was Xe_{135} poisoned. The boron concentration in the coolant of the primary circuit, pressurizer and de-aerator of the feed water was balanced. The APC was operating in mode "T" and, respectively, TEC was in mode «Control N".

At 20:30:02 on 02.10.2005 (time recorded by UBLS), the shift leader of the reactor manually switched off MCP-1 (YD10D01 - one of the four operated) from the control room.

The time histories ("0" on the time scale corresponds to the time 20:30:02) of the main parameters of the PC and SC are presented in the following Figures:

- Fig. 3 – 81 parameters recorded on ICMS and UBLS;
- Fig. 82 – 100 data recorded on of the additional SEC.

Parameters recorded at the end of the transient caused by the switching off of MCP-1 are shown in Table 1 (the column "end state") and on the core map of Fig. 1, 2 (the line "end state").

After 1.41 s (here and below from the moment of the switching off of MCP-1) and upon the signal "load off #2 switch off ¼ MCP PP-1 1KO" the LRPC load-off algorithm started with the insertion at first, the CR group #10 (from the initial position H_{10} = 82.95 %) and after that by reaching H_{10} = 50 % - both CR groups #10 and #9 (from the upper end switches-UES).

Upon actuation of PP-1, the APC switched from mode "T" into mode "H" and so eliminated the control role of CPS. At the same time TEC switched on from mode "Control N" into "Control R".

At the 73rd s of the transient, by N_{ifco} = 67.2 % N_{nom} (recorded by ICMS), LRPC stopped the reactor load-off process. After completing of LRPC procedure, the automatic power control (APC) switched on to CPS in mode "N" and then maintained the "neutron" power of the reactor in the range from 66.2 % to 67.0 % N_{nom} (Fig. 5, 6).

During the reactor load-off the CR group #10 was inserted from 82.95 % to 43.18 %, whereas the group #9^t up to 92.61 % (from the BES). The reactor power recorded by NFC was reduced from 98.83 to 67.2 % N_{nom} , with the average reduction gradient of $dN_{nfc}/d\tau$ = -0.452 % N_{nom}/s = -27.1 % N_{nom}/min. The lower gradient of load reduction in the time interval from the 42nd s to the 73rd s is apparently due to termination of the temperature increase at core inlet (see Fig. 18 – 23), and so terminating the impact of the negative feedback of the coolant temperature, that increased (up to the 42nd s of the transient) the gradient of power reduction due to the increase of T_{inlet}. The decrease of T_{inlet} after 42 s of the process caused an insertion of additional positive reactivity into the core $\Delta\rho = (\partial\rho/\partial T)\cdot\Delta T_{inlet}$, which interfered reactor power reduction from LRPC.

According to Fig. 4, the reactor power recorded by the measurement channel #2 of OR-2 of NFC in the time period from 14th to 35th s of the process exceeded the power identified by other measurement channels. This is due to the fact, that the channel #2 (see Annex D) is situated at the side of core sector #2 where streams mainly cooled-down the coolant from the cold leg of loop #2 (see Fig. 45, 16, 17), which causes higher power generation in this sector due to negative temperature feedbacks.

During the TG load-off the HP control valves changed their position as shown in Fig. 50 (recorded by the UBLS, with aperture of recording) and in Fig. 95 (data of SEC, without aperture of recording). El-power of TG reduced from the initial value of 983 MW during the time from the 10th to the 18th s of the transient to 967 MW. The control valves (Fig. 95) partly closed from the initial positions 47.6, 29.4, 36.5 and 34.3 % to respectively 47.6, 28.6, 35.5 and 33.6 % at the 15th s. By the

30^{th} s of the process, N_{el} reduced rapidly to 828 MW due to the partial closure of the control vales till the 29^{th} s respectively to 33.7, 21.6, 27.3 and 27.3 %. As a result of pressure decrease in the main steam collector (Fig. 85) the control valves opened at the 39^{th} s respectively to 36.4, 23.2, 29.0 and 29.0 %, which caused the increase of N_{el} by the 40^{th} s up to 845 MW. Then the control valves have been closing partially until approximately the 222^{nd} s of the transient, and their positions reached respectively 26.6, 16.6, 21.2 and 22.6 %. For that time N_{el} decreased till the 222^{nd} s to 622 MW. Then, approximately by the 235^{th} s, control valves partly re-opened up to 26.7, 16.7, 21.5 and 22.8 %, which caused an increase of the electrical power up to 627 MW and stabilized at this level.

Fig. 3 denotes the electrical power consumption history of MCP 1-4. It can be seen that the reduction of N_{MCP1} to 0 took place within 1 s. After switching off of MCP-1 a slight drop of N_{MCP2}, N_{MCP3} and N_{MCP4} is observed due to the reduction of the hydraulic resistance of the PC as a result of the coolant flow reduction.

The time-dependent changes of pressure differences of MCP1-4 and in the reactor are presented in Fig. 7, 83. Figure 83 shows that particularly at the 70^{th} s the values ΔP_{MCPi} (i = 1, 2, 3, 4) and ΔP_p have reached their minimal (for this mode) values and after that have stabilized. The pressure differences of MCP1-4 and of the reactor before and after switching off of MCP-1 are listed in Table 1.

The change of the flow direction in the loop 1 began approximately at the 25^{th} s after the switching off of MCP-1 at ΔP_{MCP-1} approximately equal to 0.29 MPa (see e. g., Fig. 16, 17, 45).

Time histories of the coolant flow rate in the 4 PC loops and in the reactor are shown in Fig. 9 (ICMS data). It should be mentioned that the values G_{PC} and G_R are not very reliable up to the 70^{th} s of the transient and especially for the time moment of the run out mode of the MCP after its switching off because the ICMS has not a calculation model for this condition. An increase in the flow rate of loops #2, 3, 4 with running MCP is caused by the reduction of the hydraulic resistance in PC (most of all in the core) due to the reduction of the flow rate.

Fig. 8 shows the time histories of loops' thermal power and reactor power, calculated on the bases of PC coolant measured data. It should be mentioned, that in the interval approximately up to the 150^{th} s the values $N_{PC\text{-}loop\text{-}i}$ (i = 1, 2, 3, 4) and $N_{1к}$ are not reliable.

Time histories of the reactor power calculated in various ways (N_{PC}, N_{SC}, N_{DCS}, N_{core}), also the reactor power recorded by NFC (N_{NFC}) and the TG electrical power (N_{el}.) are shown in Fig. 4. The exact definition of N_{PC}, N_{SC} and indirect also N_{core} under the conditions of fast changing parameters (for all, that of flow rates and temperatures) without consideration of the coolant transportation time (delay time) as it is done in the ICMS, is generally impossible. In that sense, the values N_{PC}, N_{SC} and N_{core} in the interval approximately up to the 150^{th} s of the transient are not reliable. The strong lapse in the $N_{SC}(\tau)$ evolution at the time interval approximately from the 44^{th} to the 49^{th} s of the process is due to the disturbance in the recording of the SG-1feedwater flow rate caused by its abrupt decrease (Fig. 61).

In that way, the reactor power can only be evaluated on the basis of the data recorded by NFC and DCS till the 150^{th} s of the transient.

PC pressure histories are presented in Fig. 10, 11, 84 and $P_{PC}(\tau)$ history in Fig. 84 (data without recording aperture). Analysing the results in Fig. 84, it can be seen that the initial PC pressure of 15.52 MPa, grew insignificantly by the 10^{th} s (up to 15.55 MPa) due the coolant heat-up in the core caused by the reduced flow rate. From the time period after the 30^{th} to the 90^{th} s it dropped from 15.54 to 15.12 MPa due to the PC coolant temperature decrease caused by the reactor power load reduction controlled through LRPC. For this period the coolant flow rates in all loops and through the core are practically stabilized, and the steam pressure reduction in SGs with operating MCP remained also practically constant up to the 137^{th} s (with minor reduction of T_{PC} and with all heaters of the pressurizer in operation). Later on the pressure in the PC began to increase and reached 15.47 MPa by the 300^{th} s with practically constant temperature of the coolant (due to the operation of the electroheaters in the pressurizer).

The coolant level in PRZ recorded by the UBLS (Fig. 10) increased from the initial value 841.6 cm approximately by the 10^{th} s up to 844.7 cm, and then from the 30^{th} s to the 136^{th} s of the transient it has decreased to 751.5 cm; later on, starting from the 215^{th} s of the process it began to grow smoothly reaching 763 cm by the 288^{th} s. L_{PRZ} (recorded by MMS) insignificantly increased (Fig. 84) from the

initial value of 859 cm to 866 cm till the 22nd s, and then, by the 136th s it reduced to 790 cm, later on increased smoothly and stabilized at the 260th s at a level of 800 cm. The difference in the values of L_{PRZ} (recorded by the upper level control measurements and the MMS) are due to the fact, that the UBLS data considers the corrections for the coolant temperature in the pressurizer whereas the MMS data do not take that into account.

According to the UBLS records (Fig. 12) after the load-off of process was completed and reactor parameters stabilized, the make-up flow rate insignificantly increased whereas the blow-down flow rate insignificantly decreased. On the other hand, it can be seen in Fig. 13 that the position of valve TK32S02 changed from approximately 34 % in the initial state to approximately 40 % in the final state, whereas the changes occurred mostly in the interval from the 86th to the 150th s.

Figure 51 (UBLS records), Fig. 85 and Fig. 86 (MMS records) show the time history of SG vapour pressure. It should be mentioned that P_{SGi} (i = 1, 2, 3, 4) recorded by UBLS (Fig. 51) are by (0.02 – 0.04) MPa higher than the analogous records of MMS (Fig. 85). It is due to the fact that the pressure measuring sensors are located not in the SG but in the fresh steam pipes. MMS records the values of just these sensors whereas UBLS records considered (though, hard to say how precisely) the corrections for pressure losses in the region length from SGs to the places of the sensors' locations. Further the SC pressure histories recorded by MMS (Fig. 85 and 86) are analysed, and then are added some corrections on the basis of data recorded by UBLS.

According to Fig. 85 the steam pressure in SG-1 decreased sharply from initially 6.21 MPa to 5.8 MPa by the 25th s (due to the loop-1 power reduction), and then, from the 29th s to the 31st s it dropped to 5.77 MPa. After the coolant flow reverse in the loop-1 took place, the pressure increased to 5.92 MPa in the interval from the 36th to 47th s and later on it was changing like $P_{MSH}(\tau)$. It should be mentioned that in the time interval from the 20th to the 129th s the SG-1 pressure was lower than the steam pressure in MSH. The SG2-4 pressure, which initially were 6.22, 6.24 and 6.26 MPa, unevenly and insignificantly decreased in relation to the initial values in the intervals (17 – 24 s), (16 – 27 s) and (19 – 26 s) due to the reduction of P_{MSH} caused by the reactor power reduction parallel to a minor reduction of N_{el}. Then it increased respectively to 6.37, 6.32 and 6.30 MPa by the 39th, 37th and the 40th s (due to the power increase in loops #2-4 caused by the increase of the coolant flow rate and temperature and to the increase of P_{MSH} as a result of the decrease of N_{el}). Later on the pressure decreased respectively up to the 129th, 135th and 131st s (whereas mostly intensively by the 89th – 90th s due to the reactor power reduction by LRPC, thus reaching the minimum values of 6.13, 6.09 and 6.02 MPa, whereupon practically stable reactor power was reached and $P_{MSH}(\tau)$ could be determined. The fact that the pressure in SG-4 reduced most sharply from the 38th s, becoming at the end lower than P_{SG2} and P_{SG3}, is due to the power reduction in loop #4 as a results of flow mixing of the already cooled down coolant from the "hot" leg of loop #1 into loop #4.

Steam pressure in MSH (Fig. 85) reduced from the initial value 6.01 MPa to 5.87 MPa by the 21st s (due to the reactor power reduction, and, but by a minor load-off of TG), and then increased up to 6.014 MPa by the 37th s (due to the sharp reduction of N_{el} by the 30th s as it is can be seen in Fig. 50 and 51), and then reduced to 5.89 MPa by the 65th s (due to the reactor power reduction and slow load-off of TG). After completion of reactor load-off , due to insufficient load-off of TG, the pressure P_{MSH} reached 5.86 MPa by the 130th s, after that it started to increase smoothly (due to the smooth closure of control valves) becoming practically stable by 300th s at a value of 6.0 MPa.

According to ICMS records (Fig. 51) steam pressure in SG-2, 3 and 4 with initial values 6.29, 6.24 and 6.24 MPa, reached maximal values 6.41, 6.35 and 6.35 MPa, by the 35th – 37th s and dropped to minimal values 6.15, 6.12 and 6.04 MPa by the 131st s.

Figure 56 (UBLS records) shows the time history of steam pressure in the house loads collector and the valve position of FASB-HL. Figure 100 denotes the time history of P_{ISC} recorded by MMS. According to Fig. 100 the steam pressure in ISC decreased from the initial value 1.186 MPa to 0.737 MPa by the 120th s and then (due to the opening of valves in the 1st and 2nd device of FASB-HL – Fig. 56) it increased and reached 1.072 MPa by the 248th s. In the initial phase the valves of the 1st and 2nd device of FASB-HL were closed (Fig. 56). Starting from the 36th s, the valve of the 1st device of FASB-HL began to open and reached 57 % by the 133rd s. At the 65th s the valve of the 2nd device of

FASB-HL began to open and reached the position of 44 % by the 132nd s. Afterwards the position of FASB-HL's valves did not change.

The water level evolutions in SGs are shown in:

– Figures 57, 89, 90 – recorded on the basis of the measurements of the 2-chamber level measurement devices;

– Figures 58, 91, 92 – recorded on the basis of the measurements of the 1-chamber level measurement devices.

According to Fig. 89, 90 (data without recording aperture) L_{SG1} from the initial value of 165 mm, changed by +14 mm by the 13th s and then decreased by the 30th s with -73 mm (apparently due to the steam increase in SG-1 after the sharp reduction of P_{SG1}), and later it increased to +191 mm by the 76th s (due to the sharp power reduction of loop #1 after the flow reverse), and after that began to decrease (most fast till the 180th s) becoming practically stable at the 390th s thus a different of +10mm resulted compared with the initial value. There, the main feed water control valve of SG-1 began to close from the 35th s and closed practically completely at the 52nd s (Fig. 62). The starter valve of the feed water controller partly closed to 49 % in the interval from the 44th to 51st s, then opened up to 55 % by the 55th s, and later on partly dropped to 24 % by the 72nd s changing after that its position (mostly to open) maintaining the water level in SG-1.

Water levels in SG2-4 (Fig. 89 and 90) related to the initial values respectively 185, 165 and 161 mm increased by +7, +25 and +36 mm at the 22nd, 25th and 23rd s respectively (possibly due to reduction of heat transfer in SG-2-4 at the beginning of the flow rate reduction and the coolant speed in loops #2-4), then they began relatively sharply to increase (due to power increase in loops #2, 3 and 4 and thus leading to increase of flow rates and coolant heat-up in the loops). Maximum deviations from the initial values of minus 174, minus 126 and minus 134 mm were reached at 63, 67 and 60 s and then, due to additional opening of the main and the starting feed water valve of SG-2-4 as well as due to the power reduction of loops #2, #3 and #4 and also the integral reactor power, they increased to values different from the initial ones by minus 44, minus 1 and minus 3 mm at 132, 171 and 132 s respectively. Then, due to the closure of the starting control valves to the initial positions as well as due to the closure and the following smoothly partial opening of the main feedwater valves of SG-2 -3 -4, (Fig. 62) they began to stabilize. Relatively quickly has stabilized the level L_{SG4} (Fig. 90), beginning approximately from the 340th s it returned to initial value very fast. The water level in SG-2 at 270 s reached a level change of -85 mm, and after that it began to increase and at 420 s it stabilized at a slightly different value from the initial one. The water level in SG-3 decreased during the stabilisation to -65 mm (at the 364th s) and then it began to grow, reaching practically the initial value at 465s. After the SG water levels drop by more than 100 mm at the 48th s, the both AFWP were actuated (Fig. 94).

The main feed control valves of SG-2-4 with initial positions of 59, 71 and 58 %, opened during the transient respectively to 84 % (at the 64th s), to 100 % (at the 79th s) and to 66 % (at the 49th s), and closed to respectively 50 % (at the 138th s), to 68 % (at 168th s) and to 30 % (at the130th s).

The records of one-chamber level measurement devices denoted the following (Fig. 91 and 92):

– L_{SG1} with initial value of 2218 mm reduced by the 21st s to minus 142 mm, and increased by +205 mm by the 53rd s, then it smoothly reduced and stabilized practically by the 450th s with a difference of +25 mm in comparison with the initial state;

– L_{SG2}, L_{SG3} and L_{SG4} with initial values of 2203, 2196 and 2214 mm increased by the 13th, 18th and 15th s respectively by +13, +23 and +22 mm, and then the water levels reduced respectively by the 69th, 72nd and 48th s to minus 114, minus 90 and minus 126 mm. After that they increased by the 122nd, 170th and 129th s respectively to minus 44, +4 and +3 mm and finally their stabilisation began and completed respectively by the 480th, 465th and 360th s at values different from the initial ones by respectively minus 39, minus 12 and +2 mm.

SGs feedwater flow rates evolutions are shown in Fig. 61 (records of the ICMS) and in Fig. 87 (records of MMS). According to the MMS records, the SG-1 feed water flow rate volume increased from the initial value of 1463 m^3/h by the 29th s to 1577 m^3/h (apparently due to the reduction of P_{SG1}), and then, by the 50th s it reduced to 152 m^3/h (closure of the feed water main control valve of SG-1), and approximately by the 75th s it reduced practically to zero (partial closure of the feedwater starting control

valve of SG-1 – Fig. 62). Later, G_{SG1} began to increase approximately from the 175th s (reduction of L_{SG1} and step-by-step partial opening of the feed water starting valve of SG-1). Concerning the data from ICMS (Fig. 61), during the measurement time interval of about (33 – 38) s there has been a device malfunction of recording $G_{fw1}(\tau)$. The minimal value of G_{fw1}, recorded approximately at the 120th s denotes 109 t/h. After the 145th s G_{SG1} has began slowly to increase ant at the 300th s reached the value of 154 t/h. At first the SG-2, 3, 4 feedwater flow rates reduced slightly (at the (30 – 37)th s) and then increased by the (52nd – 54th) s; later decreased according to the heat sinking through SG-2-4.

SG feed water pressure histories are shown in Fig. 63, 88. The changes of Pfw_i (i = 1, 2, 3, 4) during the transient have been determined by feed water flow rates (Fig. 61, 87) and pressure in SG (Fig. 51, 85).

The TFWP #1, #2 rotational speed histories and the feed water flow rates at the pressure side as recorded by UBLS are shown in Fig. 59. Apart from the feed water flow rates at the pressure side of TFWP #1, #2, Fig.60 denotes also the FW-pressure at the pressure sides (recorded by UBLS). Fig. 93 shows the rotational speed change during the transient of TFWP #1, #2 recorded by MMS. According to Fig. 93, n_{TFWP1} and n_{TFWP2} with initial values of respectively 3068 and 3053 r/min decreased from the 20th s to the 37th and 34th s respectively to 3041 and 3027 r/min (insignificant partial closure of the feed water main control valves of SG and a pressure reduction in SG), and then increased respectively by the 52nd and 53rd s up to 3097 and 3083 r/min (partial opening of the feed water main control valves to SG-2-4 and an increase of P_{SG2}, P_{SG3} and P_{SG4}). Then they began to decrease according to the thermal power of the reactor relieved mostly into SG-2, 3, 4 (partial closure of the feed water control valves of SG and a pressure reduction in SG). During the time interval from the 112th to 153rd s there was an increase of the rotational speed of TFWP-2 (maximum of 2990 r/min during τ = 142 s), whereas the rotation speed of TFWP-1 reduced. The flow rates at the pressure site of TFWP-1, 2 in principle were following their rotational speed (Fig. 59).

Figure 67 shows the time-dependences of the feed water flow rates in the lines of HP-PH as recorded by the in-core monitoring system and Fig. 68 shows the analogous dependences of flow rates, as well as the pressure values in the lines of HP-PH recorded by UBLS. The form of the curves of $G_{HP-PH\ 1}(\tau)$ and $G_{HP-PH\ 2}(\tau)$ are close to the average flow rates dependences at the pressure sides of TFWP (Fig. 59). A minor increase of pressure in the lines of HP-PH in the time interval from the 40th to approximately the 58th s (Fig. 67) is apparently a result of the cut-off of the steam line connection of HP-PH (s., e. g. Fig. 69 and 65).

According to Fig. 69 (recorded by UBLS) it follows:

– the levels in HP-PH #6- 1, 2 increased from the 55th to the 50th s respectively to 3156 and 2954 mm; as a result of the water level growth, the HP-PH were approximately at the 45th and 60th s switched off, at first group "B" and after that, the group "A";

– the level control valves of HP-PH #6-1, 2 with a water discharge line into THC opened from approximately 47 % in the intervals (125 – 145) and (145 – 157) s to approximately 99 %;

– the level control valves in HP-PH #6-1, 2 with water discharge line into D7 in the intervals (133 – 145) and (146 – 157) s from the position 45 % closed respectively to zero and to 10 %;

– the level control valves in HP-PH #7-1 in the interval (133 – 156) s partially opened from 21 to 29 %, and the respective the valve HP-PH #7-2 in the interval (146 – 158) s partially opened from the position 41 % to the position 30 %.

The feed water temperature evolution at HP-PH inlets and outlets is shown in Fig.65. It should be mentioned that the water temperature sensors downstream HP-PH are installed upstream the water inlets of CHTP.

The inlet SG feed water histories are shown in Fig.64. It can be seen that the main decrease of T_{fw2} and T_{fw4} occurred by the 380th s, whereas that of Tfw_3 took place by the 407th s.

Figure 66 denotes the water temperature evolution at the pressure side of CHTP. According to the figure this temperature increased starting from the initial value 262.9 ^{0}C at the 123rd s to the 133rd to 264.8 ^{0}C, and then, from the 292nd to the 300th s it decreased, reaching practically the initial value (to 263 ^{0}C).

Figure 52 shows the time history of the heating steam flow rate to SSSH and the position of the control valve in the line of steam flow to the SSSH. According to this figure Scv did not change. The flow rate of the heating steam to the SSSH reduced from the initial value 496 t/h to 459 t/h by the 21st s (steam generation reduction in SG), and then, by the 33rd s, it increased up to 505 t/h (due to the partial closure of the control valves ТГ – Fig. 95), after that, by the 57th s it increased relatively quickly to 447 t/h (steam reduction in SG), and later the flow rate followed the change of the thermal power transferred to the secondary circuit and it was changing in counter-phase to the sequential change of TG control valves positions.

Figure 53 shows the temperature and the pressure time-dependences of the heating steam upstream SSSH and in the condensate collector. According to the figure, the heating steam temperature upstream SSSH and in the condensate collector did not change (within the recording aperture) and had respectively 274.2 and 272.3 ^{0}C. The heating steam pressure upstream SSSH and in the condensate collector dropped (within the recording aperture) from the initial values of respectively 5.727 and 5.652 MPa in the time intervals from the 6th to the 17th s of the process and from the 9th to the 20th s of the process respectively to 5.689 and 5.570 MPa, then it increased in the intervals from respectively the 43rd to the 55th s and from the 32nd to the 42nd s to respectively 5.730 and 5.628 MPa; later it began to increase again from the 162nd and 150th s respectively and reached 5.872 and 5.800 MPa at the 295th and 278th s.

Figure 54 shows the time histories of the steam temperature downstream SSSH #1-4 (low pressure) and at the outlet of the high pressure part. According to the figure, the steam temperature at the outlet of the high pressure part began to decrease from the initial value of 153.5 ^{0}C at 47th s and reached 144.2 ^{0}C at the 277th s. The steam temperature at the downstream of SSSH #1-4 (low pressure part) increased, starting from the initial values 255.3, 255.3, 254.8 and 255.1 ^{0}C at the 103rd, 123rd, 127th and 109th s and reached at the 291st, 232nd, 294th and 204th s respectively 261.0, 259.0, 259.8 and 258.5 ^{0}C, afterwards remaining practically the same.

Figure 55 depicts the time histories of the steam pressure at the in-takes #1-3 of the turbine and at the HPTP #1-4 (recorded by UBLS). The changes of the steam pressure at turbine in-takes #1-8 recorded by MMS are shown in Fig. 97 – 99. It should be mentioned that the pressure measurement channels in the 6th (Fig. 98) and the 7th (Fig. 99) intakes were out of order.

The D #7-1, 2 changes of the water flow rate and the changes in the positions of the main and starting water level control valves of the of D7-1, 2 are shown in Fig.70. The figure proves that for the time period of the transient the flow rates in D7 recorded by UBLS in the interval from the 13th to the 214th s reduced from the initial values of 3000 m^3/h (D7-1) and respectively 3052 m^3/h (D7-2) to 1788 and 1765 m^3/h, and then, by the 300th s they slightly increased to 1956 and 1986 m^3/h. In the interval from the 161st to the 174th s an increase of the condenser flow rates in D7-1, 2 took place (approximately by 300 m^3/h in each one). The position of the starting control valve in D7-1, 2 practically did not change and stayed opened at about 49 %. The position of the main control valve of the water level in D7-1,2 sharply changed to 63 % from an initial position of 45 % in the time interval 15 – 40 s, and then, in the interval from the 53rd to the 57th s it changed sharply from 62 to 49 %; later, in the interval (171 – 181) s it changed from 17 % to zero. Beginning from the 203rd s the main control valve of the water level began to open and reached the position of 24 % at the 300th s.

During the transient the water level in the de-aerators (Fig. 71) changed from the initial value of 2509 mm within the limits of 2488 to 2598 mm.

Figure 72 shows D7-1, 2 pressure histories and the change of the control valves' positions of in heating steam supply into the de-aerator columns. According to the figure, the pressure in the de-aerator D7-1 and D7-2 reduced to 0.582 and 0.581 MPa from the initial values of 0.596 and 0.598 MPa respectively starting from the 23rd to the (128th – 131st) s, and then, from the 178th to respectively the 224th and the 234th s it increased to 0.611 and 0.615 MPa, later, from the 256th to the 295th s it reduced to 0.594 and 0.593 MPa. The positions of control valves at heating steam supply into the de-aerator columns practically did not change till the 30th s and has the values respectively 21.6 and 22.6 %, and then, by the 178th s they increased to 37.4 and 39.4 % (due to the steam pressure reduction in the secondary circuit and the water level increase in D7-1, 2), after that, by the 242nd s they dropped to respectively 31.1 and 32.4 % (the increase of the water level in D7-1,2 was stopped).

Figure73 shows graphs of time histories of the condensate water levels in LP-PH #3-5 and the positions of the level control valves in the same LP-PH. The figure denotes that $L_{LP\text{-}PH\text{-}3}$ increased to 550 mm from the initial value of 330 mm starting at approximately the 21st s and continuing to the 99th s and then it dropped to 25 mm approximately by the 200th s, changing then insignificantly till the 289th s and it increased again to 100 mm by the 293rd s. The condensate level in LP-PH-4 changed insignificantly: in the initial state it denoted 327 mm, and by the 39th s it raised to 334 mm, and then it dropped to 276 mm by the 165th s, and till the 300th s it raised again till 345 mm. The water level of $L_{LP\text{-}PH\text{-}5}$ practically did not change till the 30th s staying at 34 mm, and then it sharply increased to 575 mm by the 65th s changing till the 100th s within the range of (575 – 592) mm, then, sharply dropped to 25 mm by the 119th s, and later it raised again from 32 to 421 mm in the interval from the 131st to 285th s. The position of the level control valve of LP-PH #3 did not change till the 149th s and was open to 75 %, then, by the 169th s it changed to 40 %. The position of the level control valve of LP-PH #4 was 68 % till the 140th s and then it reduced to 60 % by the 154th s.

Figure 75 denotes the condensate level history of LP-PH #2 recorded by level measurement devices based on 1000 and 1600 mm, and also the time history of the positions of the main and starting water level control valves of LP-PH #2. It can be seen that $L_{LPH\text{-}2}$ measured by the level measurement device with a basis of 1000 mm increased from the initial value of 742 mm to 889 mm starting at the 180th to 235th s, and then by the 300th s it dropped to 647 mm. The condensate level recorded by the measurement device with a basis of 1600 mm, which has initially a value of 221 mm, was changing approximately till the 258th s in the range of (200 – 313) mm, and then it dropped to 140 mm by the 292nd s. The position of the water level main control valve of LP-PH #2 did not change till the 211th s staying at 63 %, then it reduced to approximately 20 % by the 224th s, and then it increased to 36 % in the time period from the 287th to 300th s. The position of the starting control valve for the level control of LP-PH #2 practically did not change.

Figure 76 shows the condensate levels history of LP-PH #1 (shown by two separate level measurement devices), and the average water level history of LP-PH #1. According to this figure the condensate level $L_{LP\text{-}PH1\text{-}1}$ increased from the initial value 62 mm in the time interval from the 63rd to the 198th s from 74 to 288 mm and changed later insignificantly. The condensate level in $L_{LP\text{-}PH1\text{-}2}$, which was 31 mm in the initial state practically did not change till the 126th s and then raised to127 mm by the 228th s and began to decrease smoothly starting from the 285th s thus becoming 108 mm by the 300th s.

Figure 74 denotes the coolant temperature histories in various measurement points from the suction area of CP #1 to the outlet of LP-PH #5. According to this figure the LP-PH#5 temperature at the outlet began to decrease approximately from the 46th s. As a result of this, the coolant temperature decreased by the 273rd s from 150 to 141 ^{0}C, which is due to the steam pressure decrease in the turbine in-takes of LP-PH (see Fig. 98, 99).

Figure 78 shows the pressure histories at the pressure side of CP-1 #1 and #3 (CP-1 #2 is in hot stand-by mode). Figure 77 shows the pressure histories at the pressure side of CP-2(#1 - #5). The pressure drop at the pressure sides of CP-2 in the interval from the 15th to 44th s is due to the additional partial opening of the main level control valve of D7 (Fig. 70). In principle, the pressure change at the pressure sides of CP-2 was in counter-phase to the change of the position of the level control valve of D7.

Condensate level histories of the first (SD11,12) and the second (SD13,14) groups of the turbine condensers are given in Fig. 79. The figure shows that in the interval from the 46th to the (276 – 278)th s the condensate level raised from 1017 mm to 1210 mm. The local minimum of $L_{sd11,12}(\tau)$ at τ = 57 s and the maximum value of $L_{sd13,14}(\tau)$ with τ = 59 s (pitches) are, in our opinion, due to the disturbances in the recording.

The pressure time history of the first (SD11,12) and the second (SD13,14) groups of the turbine condensers are depicted in Fig. 80 (recorded by UBLS) and in Fig. 96 (recorded by MMS). As MMS records show, the pressure in the turbine condenser at the 240th s (after the completion of the dynamic mode connected with the reduction of the reactor power from approximately 98.8 to 64.7 % N_{nom} (recorded by NFC)) reduced in relation to the initial values by approximately0.7 kPa.

Figure 81 shows the circuit water temperature history at the inlet and outlet of the first and the second group of the turbine condensers. The figure denotes that the circuit water temperature at the

outlet of the first group of condensers related to the interval from the 84th to the 271st s decreased by 1.6 ^{0}C, and at the outlet of the second group in the interval from the 80th to the 297th s it decreased by 2.1 ^{0}C.

The transient results of the loop temperature control by ICMS are shown in Fig. 14-43. These figures use the following notations:

– T_{ictc}, T_{icth}, T_{ict} – cold and hot leg coolant temperatures and the coolant temperature difference between the hot and the cold legs of the $loop_i$ (i = 1, 2, 3, 4) of the primary circuit recorded by the resistance thermometers (RT);

– $T_{itcc1\text{-}j}$, $T_{itcc2\text{-}j}$ and $\Delta T_{itc1\text{-}j}$ - cold and hot leg coolant temperatures and the coolant temperature difference between the hot and the cold legs of the $loop_i$ (i = 1, 2, 3, 4) of the primary circuit recorded by the j-th thermocouples (j = A,B,C) of the first set (TC-1);

– $T_{itcc2\text{-}j}$, $T_{itcc2\text{-}j}$ and $\Delta T_{itc2\text{-}j}$ - cold and hot leg coolant temperatures and the coolant temperature difference between the hot and the cold legs of the $loop_i$ (i = 1, 2, 3, 4) of the primary circuit recorded by the j-th thermocouples (j = A, B, C) of the second set (TC-2);

– ΔT_{itcc1} and ΔT_{itch2} – coolant temperature difference between the cold and hot legs of the coolant temperature in the $loop_i$ (i = 1, 2, 3, 4) of the primary circuit, averaged on all thermocouple measurements of the first (TC-1) and the second (TC-2) sets;

– T_{ci}, T_{hi} and ΔT_{ilt} – the average value of coolant temperature of all thermocouples (TC-1 and TC-2) and resistance thermometers (RT) for the cold and hot legs; the difference of the coolant temperature between the cold and hot legs of the $loop_i$ (i = 1, 2, 3, 4) in the primary circuit.

The locations of the temperature monitoring casings in the primary loops (for all cold and hot legs) at Unit 3, NPP Kalinin are given in Annex E.

The measured data of some of the cold leg thermocouples in the PC-loops as: $T_{1tcc1\text{-}1}$ (Fig. 16), $T_{1tcc2\text{-}1}$ (Fig. 17), $T_{2tcc2\text{-}1}$ (Fig. 19), $T_{3tcc1\text{-}2}$ (Fig. 20), T_{3tcc} and T_{3tcc} (Fig. 21), T_{4tcc} and $T_{4tcc1\text{-}3}$ (Fig. 22) and $T_{4tcc2\text{-}3}$ (Fig. 23), are not taken into account by the analysis because these thermo-couples did not have the required direct contact area with the coolant. Due to the same reasons the hot leg temperature measurement of $T_{2rSG1\text{-}3}$ (Fig. 28) was also not considered by the analysis.

It should be mentioned that by determining the average (measured by TC-1, TC-2 and RT) coolant temperature of the cold legs (Fig. 14), the average coolant temperature of the hot legs (Fig. 24) and the coolant average temperature differences between the hot and cold legs (Fig. 43) of PC-loops, the above listed thermocouple measurements are excluded for the calculations.

According to Fig. 16 the hot leg #1 coolant temperature recorded by TC-1, $T_{1tcc1\text{-}2}$ and $T_{1tcc1\text{-}3}$ began sharply to decrease from the initial values respectively 288.2 and 288.0 ^{0}C starting from the 7th s (due to increased cooling of SG-1 because of the flow rate and coolant flow speed reduction in loop #1) thus reaching at the 27th and 30th s the minimum values respectively 282.1 and 282.0 ^{0}C, and then sharply increasing (caused by the flow reverse in loop #1, which consists of flow parts from cold legs #4 and #2, but mostly that of cold leg #4) and after that reaching at the 45th s maximum values 289.8 and 289.6 ^{0}C. Later it began to decrease practically parallel to the coolant changes in the cold leg #4 and completed the decrease by the 150th s at values 284.1 and 283.9 ^{0}C, afterwards (due to the increase in T_{c4}) raised and stabilized practically at approximately the 276th s at values 285.0 and 284.9 ^{0}C.

As recorded by TC-2 (Fig. 17), the coolant temperature $T_{1tcc2\text{-}2}$ and $T_{1tcc2\text{-}3}$ decreased to 282.0 and 282.1 ^{0}C (initial value 288.2 ^{0}C) in the time period from 7 s to 28 s and to 30 s respectively, and then increased to 289.9 and 289.7 ^{0}C by the 46th s, later dropped to (284.0 – 284.1) ^{0}C by the 150th s, and after that increased to 285.1 ^{0}C by the 276th s becoming then practically stable.

The coolant temperature of cold leg 2 recorded by TC-1 (Fig. 18) increased from the initial value (287.8 – 287.9) ^{0}C in the interval from the 8th to the 44th s up to (290.3 – 290.4) ^{0}C (caused by the loop power increase due to: the increase coolant heat-up in the reactor, the decrease of flow rate in the reactor and the increase of the coolant flow rate in the loop as well as due to the steam pressure rise in SG-2 as a results of the partial closure of the control valves). Then, by the 139th s it decreased to 284.4 ^{0}C (most intensive decrease occurring up to the 94th s) due to the decrease of the loop power caused by the reactor load-off mode of LRPC (also due to a partial mixing of a cooled-up coolant into

the hot leg of this loop coming from the hot leg of loop #1) and, due to the pressure decrease in SG2, later it slowly raised following the changes of $P_{SG2}(\tau)$ and getting practically stable by the 276th s at a value of 287.4 ^{0}C.

Recorded by TC2 (Fig. 19) the coolant temperature $T_{2tcc2-2}$ and $T_{2tcc2-3}$ from the initial value 287.9 ^{0}C grew from the 9th to 44th s up to 290.4 ^{0}C, and then, by the 145th s it decreased to 286.4 ^{0}C (having most significant decrease till the 94th s), and began to grow slowly, thus getting stable by the 276th s at value 287.4 ^{0}C.

The cold leg #3 coolant temperature recorded by TC-1 $T_{3tcc1-1}$ and $T_{3tcc1-3}$ (Fig. 20) increased from the initial values 287.9 and 287.6 ^{0}C in the time interval from the 10th to (42nd – 44th) s up to 290.3 and 289.9 ^{0}C (caused by the loop power increase due to the coolant heat-up in the reactor and the decreased flow rate through the reactor and the increased flow rate of the coolant in the loop as well as the steam pressure increase in SG-3 as a result of a relatively sharp partial closure of TG control valves by the 29th s). Later on, the coolant temperature decreased to 286.7 ^{0}C approximately by the 141st s (with most sharp decrease till the 94th s) due to the reactor power decrease, which continued till the 73rd s with still LRPC being in operation and due to the steam pressure decrease in SG-3 caused by some delay of TG load-off, after which it increased according to the change in $P_{SG3}(\tau)$ and stabilizing at the 276th s at a level (287.7 – 287.8) ^{0}C.

According to Fig. 21 recorded by TC-2 the coolant temperature $T_{3tcc2-3}$ raised from the initial value 287.8 ^{0}C at the 10th to the 43rd s to 290.1 ^{0}C, and then, by the 148th s it dropped to 286.9 ^{0}C (reducing mostly fast up to the 94th s of the process), and then began to increase reaching stabilization at the 276th s at a value of 287.9 ^{0}C.

The cold leg #4 coolant temperature $T_{4tcc1-1}$ recorded by TC-1 (Fig. 22) increased from the initial value 287.4 ^{0}C in the interval from the 7th to the 41st s to 289.9 ^{0}C (due to the loop power rise caused by the coolant flow rate and steam pressure increase in SG-4), and then, by the 142nd s it reduced to 283.7 ^{0}C (the strong reduction was taking place till the 90th s) due to the reactor power reduction by LRPC till the 74th s and due to the mixing of a cooled-up coolant into the hot leg of this loop coming from the hot leg of loop #1, as well as due to the pressure reduction in SG-4. Then the temperature $T_{4tcc1-1}$ began to increase (following the rise of P_{SG4}) and it stabilized at the 276th s at 284.8 ^{0}C.

The cold leg #4 coolant temperature recorded by TC-2 (see time-dependences $T_{4tcc2-1}$ and $T_{4tcc2-2}$ in Fig.23) with initial value 287.5 ^{0}C began to increase and in the interval from the 9th to the 41st it became (289.9 – 290.0) ^{0}C, then by the 150th s it reduced to 283.8 ^{0}C, and later on it started to increase and stabilized by the 276th s at (284.8 – 284.9) ^{0}C.

The cold leg coolant temperature recorded by the resistance thermometers shows that (Fig. 15):

– The leg #1 temperature (initial value 288.0 ^{0}C) reduced to 283.0 ^{0}C from the 10th to the 33rd s, and then it increased to 288.5 ^{0}C by the 50th s, later on, it decreased by the 149th s to 284.0 ^{0}C, followed by an increase to 284.9 ^{0}C by the 294th s after that reached practically a stable level;

– The leg #2, #3 and #4 temperatures (initial values 287.8, 287.6 and 287.5 ^{0}C) increased from the 11th to the 51st, 54th and the 46th s up to 289.9, 289.3 and 289.4 ^{0}C, then decreased by the 150th s to 286.5, 287.0 and 283.7 ^{0}C, and later on, by the 294th s, they increased to 287.3, 287.7 and 284.8 ^{0}C and practically reached a stable level.

The fact that the cold leg #4 coolant temperature at the end of the transient caused by the switching off of MCP-1, stabilized at a lower level than the analogue coolant temperature of loops #2 and #3, is due to the lower power of this loop caused by the mixing of coolant flow coming from the cooled-up hot leg of loop #1 into hot leg#4.

The hot leg #1 coolant temperature:

– according to Fig. 26 (as recorded by TC-1) the coolant temperature $T_{1тSG1-2}$ and $T_{1тSG1-3}$ had initial values of 317.3 ^{0}C which have been changing insignificantly till the 32nd s (due to - till the moment of reverse flow in the loop took place which was caused by the cooled-up coolant entering into the core from this loop, and later on, right after the flow reverse disappeared due to the penetration of that coolant through the thermosensors which practically have not passed through the SG until the moment of reverse flow have taken place). After that the coolant temperatures began sharply to decrease

(due to coolant reverse flow development and its cooling down in the SG-1) and reached maximum values 269.7 and 271.6 ^{0}C at the 58th and 61st s, after which it increased relatively fast (by the 90th s) to 275.5 ^{0}C (practically, the coolant temperature began to reduce in the cold leg of this loop and formed a stable reverse flow in this loop), then it slightly changed (following the steam pressure change in SG-1) and became stable at the 270th s at values 276.9 and 276.6 ^{0}C;

– the coolant temperature $T_{1тSG2-1}$, $T_{1тSG2-2}$ and $T_{1тSG2-3}$ recorded by TC-2 (Fig. 27) (initial values 317.5, 317.0 and 317.1 ^{0}C) changed insignificantly by the first 32 s and denoted 317.1, 316.4 and 316.4 ^{0}C; by the 59th s they reduced to 271.3, 269.5 and 269.5 ^{0}C, and then, mostly by the 90th s, they increased and stabilized approximately at the 290th s at 276.7, 276.8 and 276.5 ^{0}C.

The hot leg #2 coolant temperature $T_{2тSG1-1}$ and $T_{2тSG1-2}$ (Fig. 28) recorded by TC-1 (initial values 316.4 and 317.1 ^{0}C) increased in the interval 5 -35 s to (319.7 – 319.8) ^{0}C (due to heat-up of the coolant in the reactor caused by the reduction of flow rate), and then, mostly by the 90th s, they decreased (due to the reactor power reduction by LRPC with stable coolant flow through the reactor, partially mixing of cooled-down flow from the hot leg #1, and also due to the reduction of P_{SG2} caused by the slow down TG load-off in this interval). Approximately at the 167th s, the temperatures reached the minimum value (310.8 – 310.9) ^{0}C, and then they began slowly to increase (due to the coolant temperature growth at the core inlet) and approximately at the 70th s they stabilized at values (311.5-311.6) ^{0}C.

The hot leg #2 coolant temperature $T_{2tch2-1}$, $T_{2tch2-2}$ and $T_{2tch2-3}$ (Fig. 29) recorded by TC-2 (initial 316.9, 317.3 and 317.3 ^{0}C) increased approximately from the 5th to the 33rd, 37th and 36th s up to 319.9, 319.7 and 319.4 ^{0}C, and then, by the 150th s they decreased to 310.9, 310.7 and 310.5 ^{0}C (having the most significant coolant temperature reduction till the 90th s), after that they began to rise slowly and approximately by the 270th s stabilized at values 311.8, 311.6 and 311.4 ^{0}C.

It should be mentioned that bending points on the coolant temperature time-dependent curves (Fig. 28, 29) at τ = (15 – 16) s are caused by the specifics of the coolant temperature histories measured with the thermocouples at FA outlets in sector 2 (Fig. 45). These thermocouples were affected by the cooled-down flow of the cold leg #1 (till the change of the flow direction in this loop). It should be mentioned that the coolant flow swirling after FA outlet till the hot leg nozzles take place counterclockwise.

The hot leg #3 coolant temperature:

– according to Fig. 30, the recorded by TC-1 coolant temperature $T_{3тSG1-1}$, $T_{3тSG1-2}$ and $T_{3тSG1-3}$ increased from the initial values 316.6, 316.6 and 316.3 ^{0}C up to 319.2, 319.6 and 319.4 ^{0}C in the interval from the 6th the 42nd s, and then they decreased to 312.3, 312.9 and 312.5 ^{0}C by the 150th s (with most significant reduction till the 90th s), later on they increase slowly stabilized at values 313.3, 313.7 and 313.4 ^{0}C by the 270th s;

– according to Fig. 31 recorded by TC-2 the coolant temperature $T_{3тSG2-1}$, $T_{3тSG2-2}$ and $T_{3тSG2-3}$ (initial values 316.5 ^{0}C, up to 319.2, 319.6 and 319.4 ^{0}C) increased in the interval from the 6th to 43rd s, and then they decreased to 312.6, 312.9 and 312.6 ^{0}C by the 150th s (with most significant reduction till the 90th s). Later on, they slightly increased and stabilized at values 313.3, 313.7 and 314.4 ^{0}C by the 270th s.

The reasons for the rise and the reduction of the hot leg #3 coolant temperature during the transient are the same as for the hot leg #2. The only one difference is that in this case there was no mixing of a cooled-down flow from the hot leg #1 into the hot leg #3.

The coolant temperature change of the hot leg #4 (Fig. 32 and 33) was less significant from the beginning of the process up to the 35^{t} s than that in other hot legs where the MCP were in operation. That is due to the impact of the cooled-down coolant of the neighbouring hot leg #1 (s. Fig. 16 and 17) entering the core for the time period before the reverse flow appeared in this leg.

According to the records by TC-1 (Fig. 32), the coolant temperature $T_{4tch1-1}$, $T_{4tch1-2}$ and $T_{4tch1-3}$ (with initial values 317.3, 317.1 and 317.2 ^{0}C) reached at the 35th s values 318.1, 317.5 and 317.6 ^{0}C. The temperature $T_{4тSG1-1}$ increased by the 19th s up to 318.3 ^{0}C, and then, by the 27th s it decreased to 317.8 ^{0}C. By the 35th s it raised again to the above mentioned value. During the transient $T_{4тSG1-2}$ and $T_{4тSG1-3}$ changed insignificantly until the 27th s but nevertheless they had the local minimum at the 27th s.

The existence of the local minimum on the coolant temperature evolution in the hot leg #4 is due to the flow reverse in loop #1. Starting from the 35th to the 150th s the coolant temperature $T_{4тSG1-1}$, $T_{4тSG1-2}$ and $T_{4тSG1-3}$ decreased to 302.0, 302.8 and 304.0 ^{0}C (with most significant reduction till the 75th s), and then they slowly increased and approximately by the 270th s they stabilized at values 303.0, 304.1 and 305.1 ^{0}C. It should be mentioned that approximately from the 35th s the coolant temperature of the hot leg #4 was influenced by the flow mixing of the cooled-down coolant coming from the hot leg #1.

The coolant temperature change of hot leg #4 as recorded by TC-2 (Fig. 33) was analogous to the change as recorded by TC-1 (Fig. 32). According to Fig. 33, $T_{4тSG2-1}$, $T_{4тSG2-2}$ and $T_{4тSG2-3}$ changed starting from the initial values 317.1, 317.4 and 317.2 ^{0}C till the 35th s to values 317.5, 317.8 and 317.6 ^{0}C; and then, by the 150th s they reduced to 303.5, 302.7 and 303.7 ^{0}C, after which they insignificantly increased and became practically stable at the 270th s at values 304.9, 303.9 and 304.9 ^{0}C.

The coolant temperature in the hot legs as recorded by the resistance thermometers (Fig. 25), have the following evolutions:

– Loop #1: Starting from the initial value 317.4 ^{0}C the temperature increased up to 318.2 ^{0}C in the interval from the 9th to the 20th s, and by the 33rd s it decreased to the initial value and dropped sharply to 278.4 ^{0}C by the 74th s after which it practically did not change and reduced to 277.4 ^{0}C by the 150th s. Later on it increased insignificantly and stabilized at 277.7 ^{0}C by the 270th s. The fact that $T_{1тcr}$ at τ approximately equal to 60 s did not have the local minimum (see also Fig. 26, 27), is apparently due to the different azimuthal location of the resistance thermometers on the pipe with a diameter of 850 which is higher from the low pipe edge area where TC-1 and TC-2 are located (Annex E), and also due to a higher delay measuring time (measurement inertia) by the resistance thermometer;

– Loops #2 and #3: Starting from the initial values 314.5 and 316.1 ^{0}C the temperature increased respectively to 316.5 and 318.5 ^{0}C in the time interval from the 6th and 9th s to respectively the 41st and the 35th s, and then they reduced from 309.3 and 311.9 ^{0}C by the 150th s (with most fast reduction till the 104th s at temperatures respectively 310.1 and 312.5 ^{0}C). Later on they increased insignificantly and stabilized at values 309.9 and 312.5 ^{0}C at the 270th s. The $T_{2тcr}(\tau)$ evolution has at τ = 24 s a bending point caused by the same reasons as the similar points on the time histories of the thermocouples (Fig. 28 and 29);

– Loop #4: Starting from the initial value 314.0 ^{0}C it increased from the 15th to the 37th s up to 317.0 ^{0}C, and then, by the 104th s it decreased to 299.0 ^{0}C and reached 298.8 ^{0}C by 150th s, after which it slightly increased and reached 299.1 ^{0}C at the 270th s.

Let's summarize shortly the analysis of the time histories of the coolant temperature differences between the hot and cold legs of the PC-loops during the transient, without taking into account the measured values (thermocouples records were not exact) for the following parameters: $\Delta T_{1TC1-1}(\tau)$ (Fig. 34), $\Delta T_{1TC2-1}(\tau)$ (Fig. 35), $\Delta T_{2TC1-3}(\tau)$ (Fig. 36), $\Delta T_{2TC2-1}(\tau)$ (Fig. 37), $\Delta T_{3TC1-2}(\tau)$ (Fig. 38), $\Delta T_{3TC2-1}(\tau)$ and $\Delta T_{3TC2-2}(\tau)$ (Fig. 39), $\Delta T_{4TC1-2}(\tau)$ and $\Delta T_{4TC1-3}(\tau)$ (Fig. 40) and $\Delta T_{4TC2-3}(\tau)$ (Fig. 41).

The coolant temperature differences between the hot and cold legs considered below do not have much physical sense because by their calculation (carried out by the in-core monitoring system) the coolant temperature in the hot and cold legs are taken at the same time under the conditions of constantly changing parameters (flow rates and temperature in the PC). When performing the calculations of the studied differences it is necessary to take into account "transportation" characteristics (delay time) of the coolant in the PC-legs but there was not a consistent model applied for such consideration. However, the analysis of the temperature changes between the hot and cold legs of PC-loops, without considering the delay time during the transient, is though approximate, still useful.

The coolant temperature differences between the hot and cold legs of loop #1 of the primary circuit as recorded by TC-1 - $\Delta T_{1TC1-2}(\tau)$ and $\Delta T_{1TC1-3}(\tau)$ (Fig. 34) (initial values 28.9 and 29.3 ^{0}C) increased in the interval from 7 to 29 s up to 34.5 and 34.7 ^{0}C (due to the heat-up of the coolant in the reactor caused by the decrease of the flow rate), and then, by the 58th s they dropped to minus 14.7 and minus 15.0 ^{0}C (caused by the cool-down of the coolant in SG-1 after the flow reversed in the loop). By the 90th s they increased to minus 9.1 ^{0}C (due to the completion of the reactor load-off by LRPC, thus slowing down the decrease of the coolant temperature in the cold leg of loop #4, mostly influencing T_{x1},

and leading to the stabilization of the flow rate in loop #1 and the heat exchange in SG-1). At the 180th s the temperature change stabilized at 8.3 ^{0}C.

As recorded by TC-2 (Fig. 35), the coolant temperature differences ΔT_{1TC2-2} and ΔT_{1TC2-3} (with initial value 29.0 ^{0}C) at first, beginning from the 7th to the 29th s, increased to 34.6 ^{0}C, and then, by the 58th s they decreased to minus 17.7 ^{0}C. By the 90th s they increased to minus 9.1 and minus 9.5 ^{0}C, and at the 180th s they stabilized at minus 8.5 ^{0}C.

The coolant temperature differences between the hot and cold legs of loop #2 in the primary circuit ΔT_{2TC1-1} and ΔT_{2TC1-2} , as recorded by TC-1 (Fig. 36), increased from the initial values 28.5 and 29.3 ^{0}C up to 30.0 and 30.2 ^{0}C in the interval from the 5th to the 14th s, and then, by the 19th s they slightly decreased to 29.8 and 30.1 ^{0}C. In the time interval 29 – 30 s they increased to 30.4 and 30.5 ^{0}C, after which they decreased to 24.7 ^{0}C by the 90th s, later on, followed a smooth decrease till the 210th s when and the temperature change reached 24.1 ^{0}C.

According to Fig. 37, the coolant temperature differences ΔT_{2TC2-2} and ΔT_{2TC2-3} as recorded by TC-2 increased from the initial value 29.4 ^{0}C in the time interval 5 - 13 s respectively up to 30.3 and 30.0 ^{0}C, and then, by the 19th s they decreased to 30.1 and 29.7 ^{0}C. By the 29th s a new rise took place, respectively to 30.5 and 30.3 ^{0}C, and then, by the 82nd s they decreased sharply to 24.7 and 24.5 ^{0}C, followed by a smooth decrease and stabilization at 24.0 and 23.9 ^{0}C by the 210th s.

The specifics of the coolant temperature differences changes between the hot and the cold legs of loop #2 are related mostly to the specifics of the coolant temperature changes in the hot leg of this loop which were described before. The existence of local minimum points on the time histories of the above mentioned differences at τ = (12 – 15) s is caused by the cooled-down coolant flow coming from the neighbouring to the loop #1 cold leg, which has reached the core inlet before the flow has reversed and the cessation of these impacts when the flow stagnated and turned to the primary direction.

The coolant temperature differences between the hot and the cold legs of loop #3 ΔT_{3TC1-1} and ΔT_{3TC1-3} as recorded by TC-1 (Fig. 38), increased from the initial value 28.7 ^{0}C approximately from the 3rd to the 29th s to approximately 30.0 and 30.4 ^{0}C (due to the increase of the coolant heat-up in the reactor caused by the decrease of the flow rate), and then, by the 90th s they decreased to 26.2 and 26.4 ^{0}C (due to the continued reactor load-off mode of LRPC with small change of the coolant flow rate through the core), then they changed slightly and stabilized at the 240th s at values 25.3 and 25.7 ^{0}C.

As recorded by TC-2, the coolant temperature difference in loop #3 ΔT_{3TC2-3} (Fig. 39) (with initial value 28.7 ^{0}C) increased to 30.3 ^{0}C in the time interval 5 - 29 s, then, by the 90th s it decreased to 26.1 ^{0}C, and stabilized at 25.5 ^{0}C approximately in the time period 220 – 240 s.

As recorded by TC-1, the coolant temperature difference between the hot and the cold legs of loop #4 ΔT_{4TC1-1} (Fig. 40) increased from the initial value 29.9 ^{0}C to 30.2 ^{0}C in the time interval 6-15 s, and then, by the 34th s it decreased to 29.0 ^{0}C, and approximately by the 75th s it sharply reduced to 18.9 ^{0}C, after which it smoothly changed and reached 18.4 ^{0}C at the 240th s.

As recorded by TC-2, the coolant temperature differences between ΔT_{4TC2-1} and ΔT_{4TC2-2} (Fig. 41) increased from the initial values 29.6 and 29.9 ^{0}C to 29.8 and 30.3 ^{0}C in the time interval 4-8 s, and then, by the 34th s, they reduced to 28.3 and 28.7 ^{0}C. By the 75th s, differences sharply reduced to 20.3 and 19.8 ^{0}C, and later remained practically unchanged reaching 20.0 and 19.1 ^{0}C at the 240th s.

The specific behaviour of time histories of the coolant temperature difference between the hot and cold legs of loop #4 were mostly caused by the specifics of the coolant temperature change in the hot leg of this loop (see the above mentioned remarks). The reduction of the temperature difference by the (34 – 35)th s was caused by the coolant temperature increase in the cold leg of that loop (mostly due to the increase of P_{SG4}) and small change of the coolant temperature in the hot leg of the corresponding loop (due to entering into the core a cooled-down coolant flow from the cold leg #1 till the moment of flow reverse in the loop).

As recorded by the resistance thermometers, the difference of the coolant temperature between the hot and the cold legs (Fig. 42) is as follows:

– Loop #1: Starting from the initial value 29.4 ^{0}C the difference increased to 34.4 ^{0}C from the 10th to 33rd s, and then, by the 67th s, it sharply decreased to minus 7.9 ^{0}C, later by the 90th s it increased to minus 6.4 ^{0}C, after which it smoothly decreased and stabilized at minus 7.0 ^{0}C at the 240th s;

– Loop 2: Starting from the initial value 26.5 ^{0}C it raised to 27.5 ^{0}C from the 7th to the 19th s practically without changing till the 40th s, and then, by the 90th s it decreased to 23.2 ^{0}C, after which it continued slightly to decrease and stabilized at 22.7 ^{0}C at the 160th s;

– Loop 3: Starting from the initial value 28.5 ^{0}C it raised to 30.1 ^{0}C from the 9th to the 34th s, and then, by the 90th s it decreased to 25.4 ^{0}C, after which it practically stabilized at the 210th s to 25.0 ^{0}C;

– Loop 4: Starting from the initial value 26.4 ^{0}C, it raised to 28.3 ^{0}C from the 15th to the 37th s, and then, by the 56th s it decreased to 23.1 ^{0}C. Later on, after some slowing down of the reduction it started again to decrease faster and at the 90th s it reached $\Delta T_{4тс}$ = 15.2 ^{0}C. After that, the temperature difference practically did not increase, but oscillated about the average value 15.2 ^{0}C.

The "stepwise" decrease of $\Delta T_{4тс}$ was caused by the similar change of $T_{4тсг}$ =(τ) (Fig. 25), which is due to the relatively strong influence of the flow mixing of the cooled-down coolant from the hot leg #1 into the hot leg #4 during the development and stabilisation of the reverse flow in the loop #1, and after that (when the loops and reactor flows reached stabilization), it is due to the load-off operation mode by LRPC.

Figure 44 – 49 show time histories of the coolant temperature at the FA outlet respectively in sectors 1-6 recorded by the ICMS (see also Annex D). These figures denote that the coolant temperature increased at the FA outlets with respect to the initial values by the following values:

– in sector #1 (Fig. 44) by (2.2 – 3.9) ^{0}C at the (42nd – 46th) s;

– in sector #2 (Fig. 45) by (2.3 – 3.9) ^{0}C at the (41st – 45th) s;

– in sector #3 (Fig. 46) by (2.3 – 4.1) ^{0}C at the (41st – 48th) s;

– in sector #4 (Fig. 47) by (2.3 – 4.0) ^{0}C at the (43rd – 47th) s;

– in sector #5 (Fig. 48) by (2.3 – 3.9) ^{0}C at the (42nd – 47th) s;

– in sector #6 (Fig. 49) by (2.9 – 3.9) ^{0}C at the (42nd – 46th) s.

Some local minima (small pitches) on the $T_к(\tau)$ curves of some FAs of sector 2 (Fig. 45) in the interval 18 – 22 s have been caused by the impacts of the cooled-down coolant coming from the cold leg #1 and entering into the inlet region of these FA before the flow reverse in this loop has taken place. After reaching the maximal values during the transient, the FA outlet coolant temperature decreased mainly by the 150th s. The most rapid reduction of T_c occurred up to the 90th s. The temperature reduction was caused by two reasons: 1) operation in power reduction mode of LRPC; 2) core inlet coolant temperature reduction (as a result of the cold legs #2, #3, #4 flow redistribution) due to the steam pressure decrease in the secondary circuit. Later the coolant temperature at the outlet for most of the FA increased (due to the cold legs' coolant temperature rise in the loops with operating MCP) and began to stabilize from the 270th s.

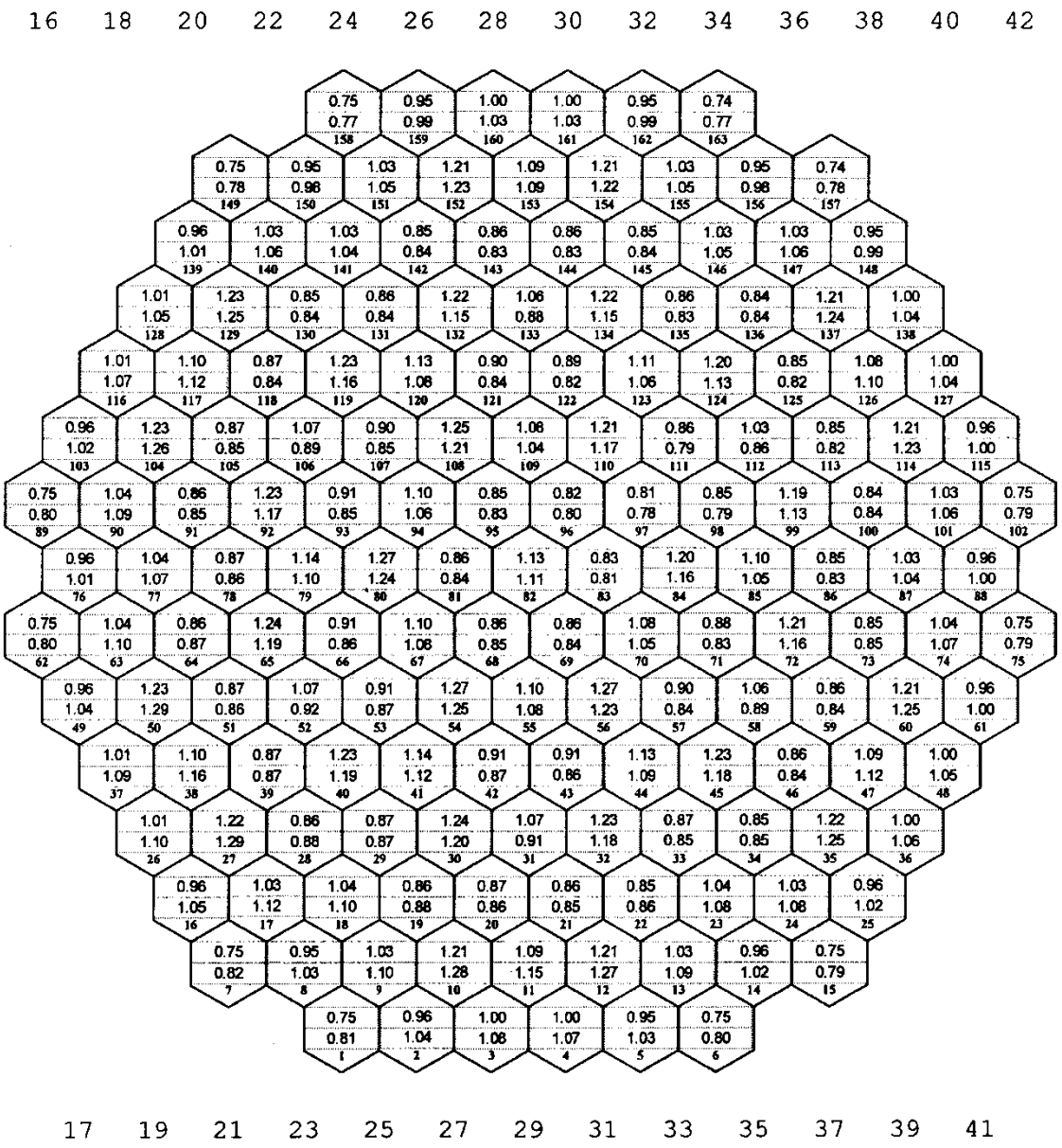

Fig. 1 – Relative power generation in FA

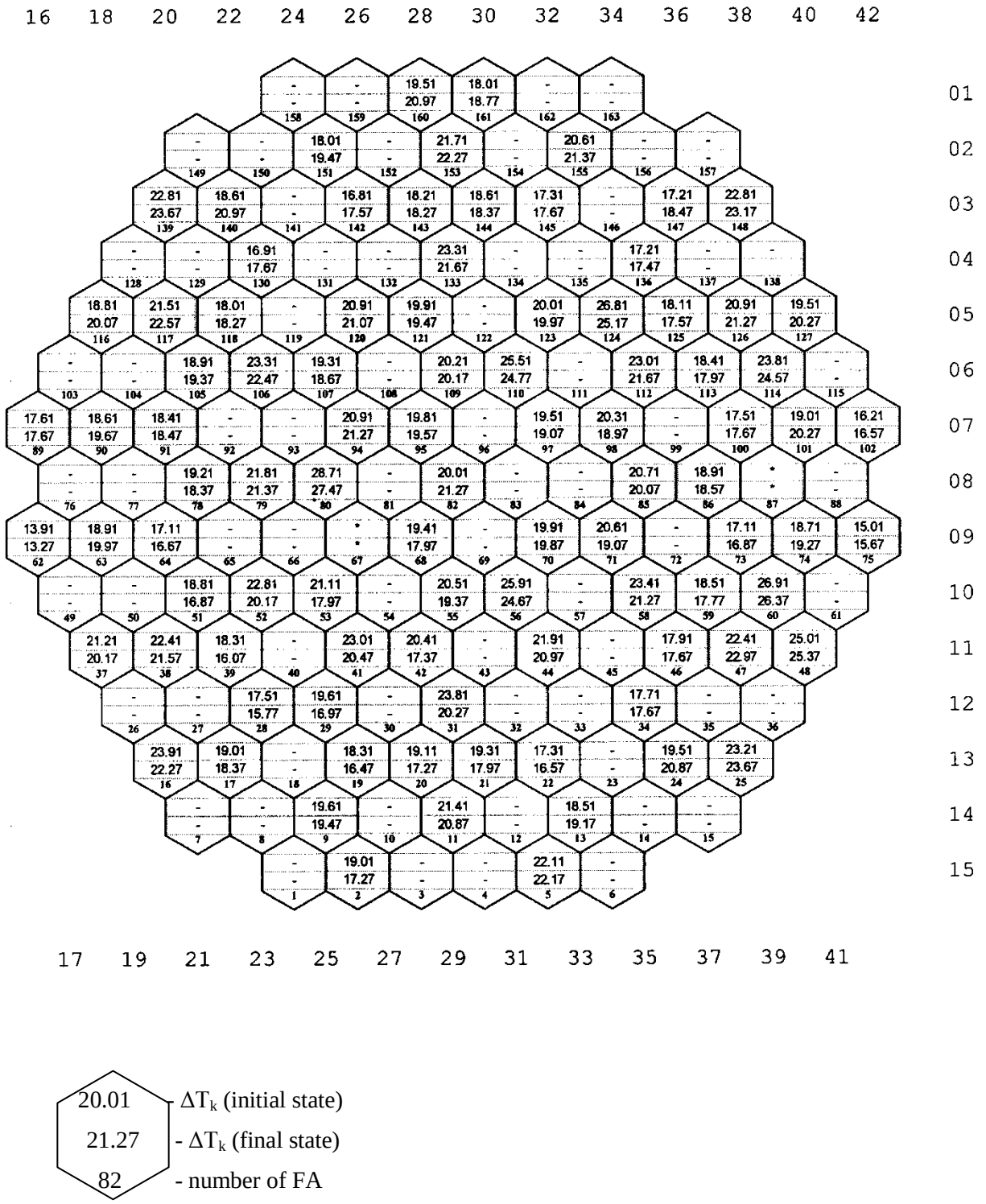

Fig. 2 – Coolant heat-up in FA recorded by the ICMS

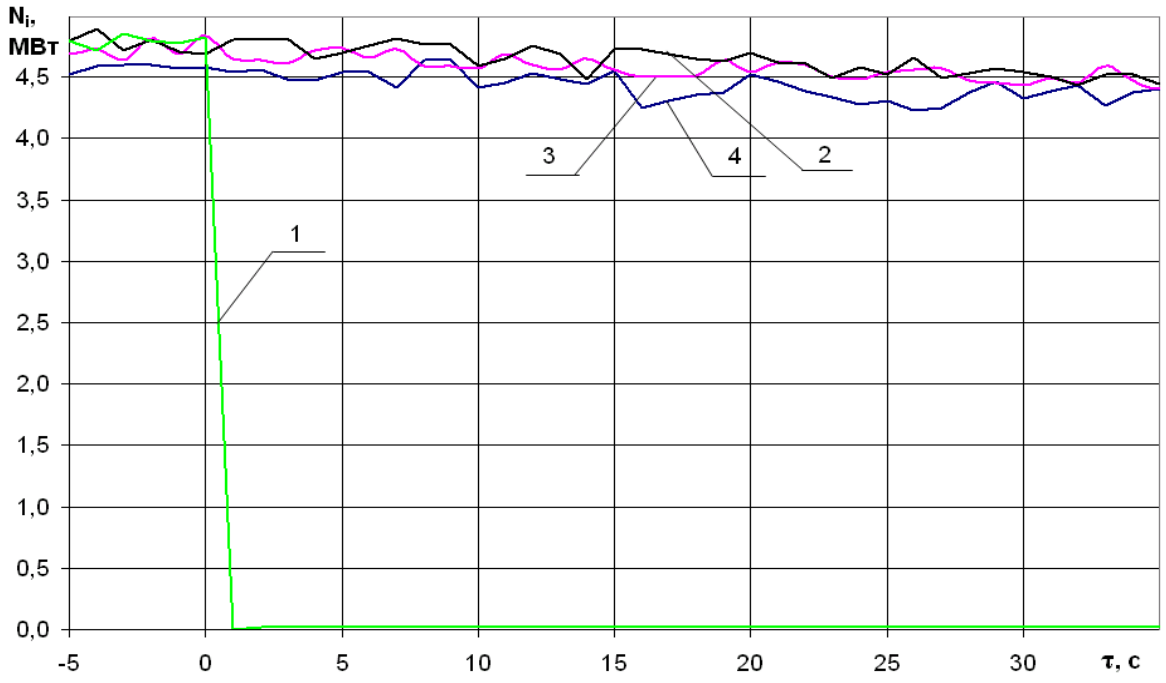

1 - N_{MCP1}; 2 - N_{MCP2}; 3 - N_{MCP3}; 4 - N_{MCP4}

Fig. 3 – Power change of MCPs recorded by the ICMS during the transient caused by the switching off of MCP #1

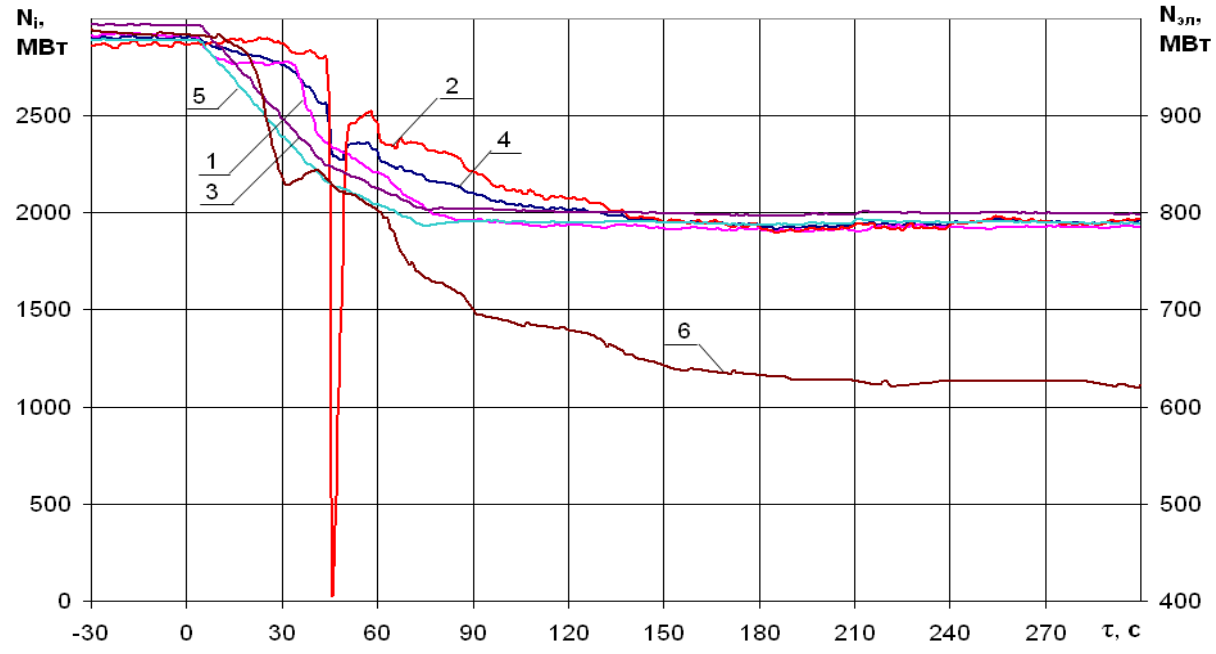

1 – N_{PC}; 2 – N_{SC}; 3 – N_{NFC}; 4 – N_{core}; 5 – N_{DCS}; 6 – N_{el}

Fig. 4 – Time histories if integral reactor power, integral reactor power recorded by the NFC and electrical power of TG recorded by the UBLS

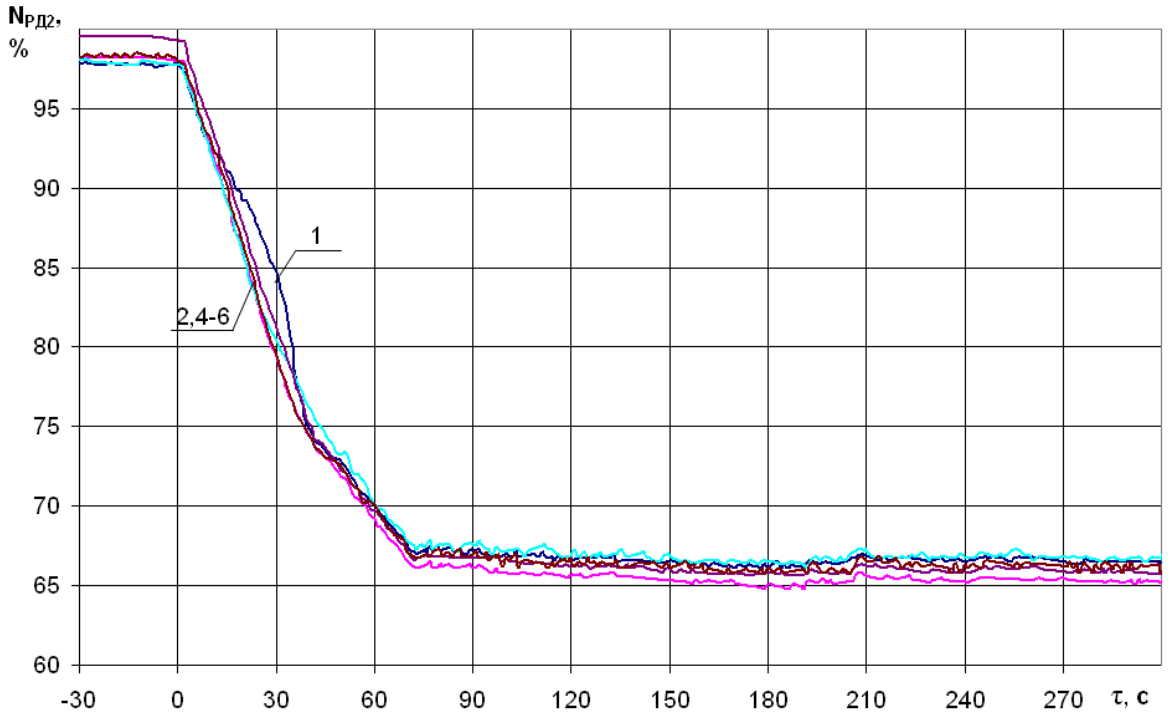

1–N_2; 2–N_{12}; 3–N_{22}; 4–N_7; 5–N_{17}; 6–N_{27}

Fig. 5 – Reactor power change recorded by the different measurement channels OR-2 of NFC recorded by the UBLS

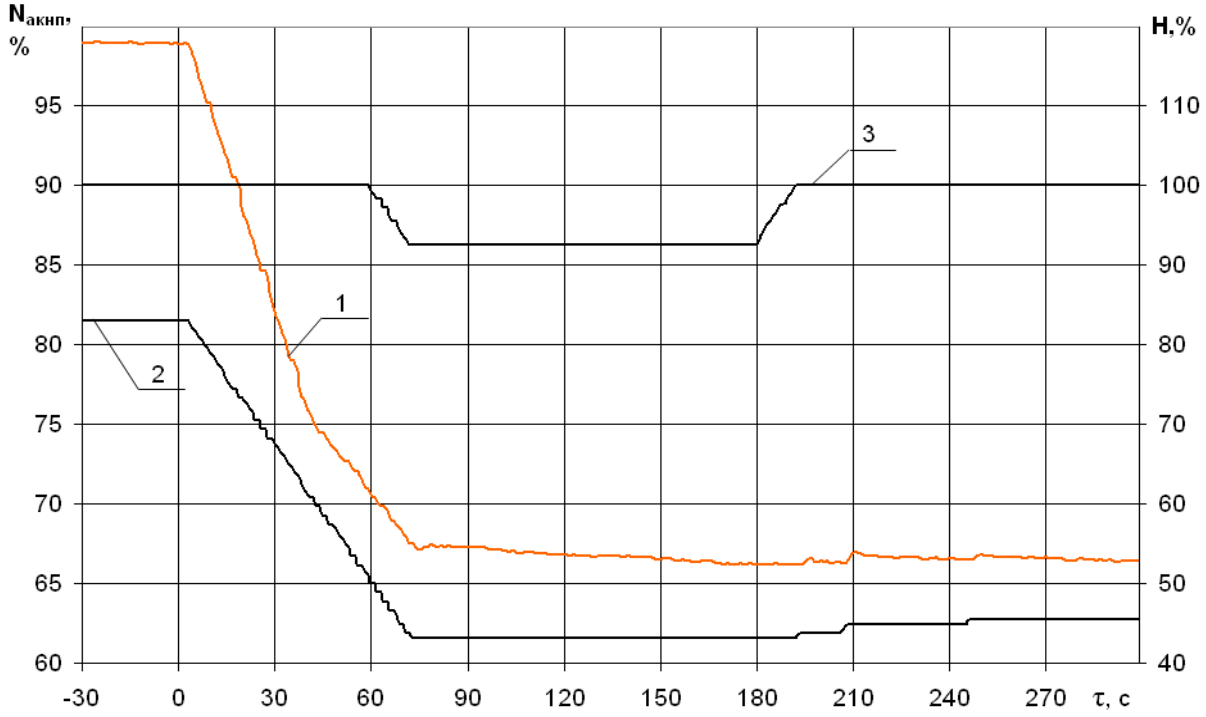

1– N_{NFC}; 2–H_{10}; 3–H_9;

Fig. 6 – Change of CPS-group #10 and #9 positions and reactor power on the basis of NFC recorded by ICMS

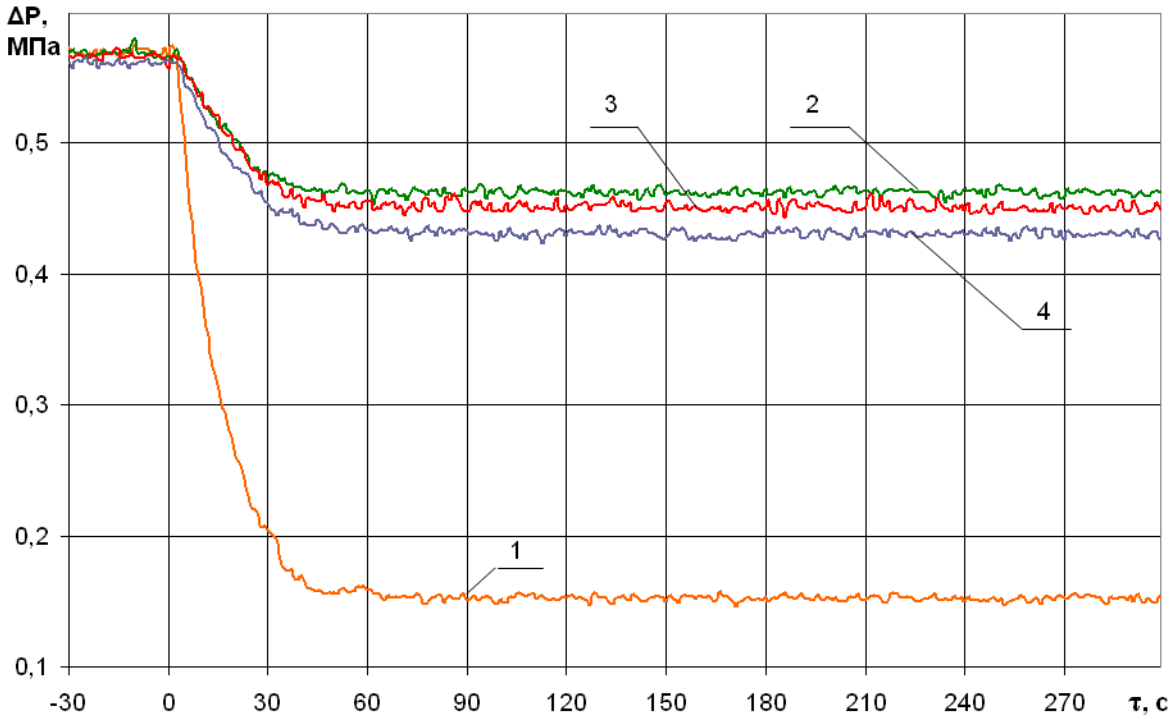

1 – $\Delta P_{МСР1}$; 2 – $\Delta P_{МСР2}$; 3 – $\Delta P_{МСР3}$; 4 – $\Delta P_{МСР4}$

Fig. 7 – Change of the pressure differences of MCP-1–4 recorded by the ICMS

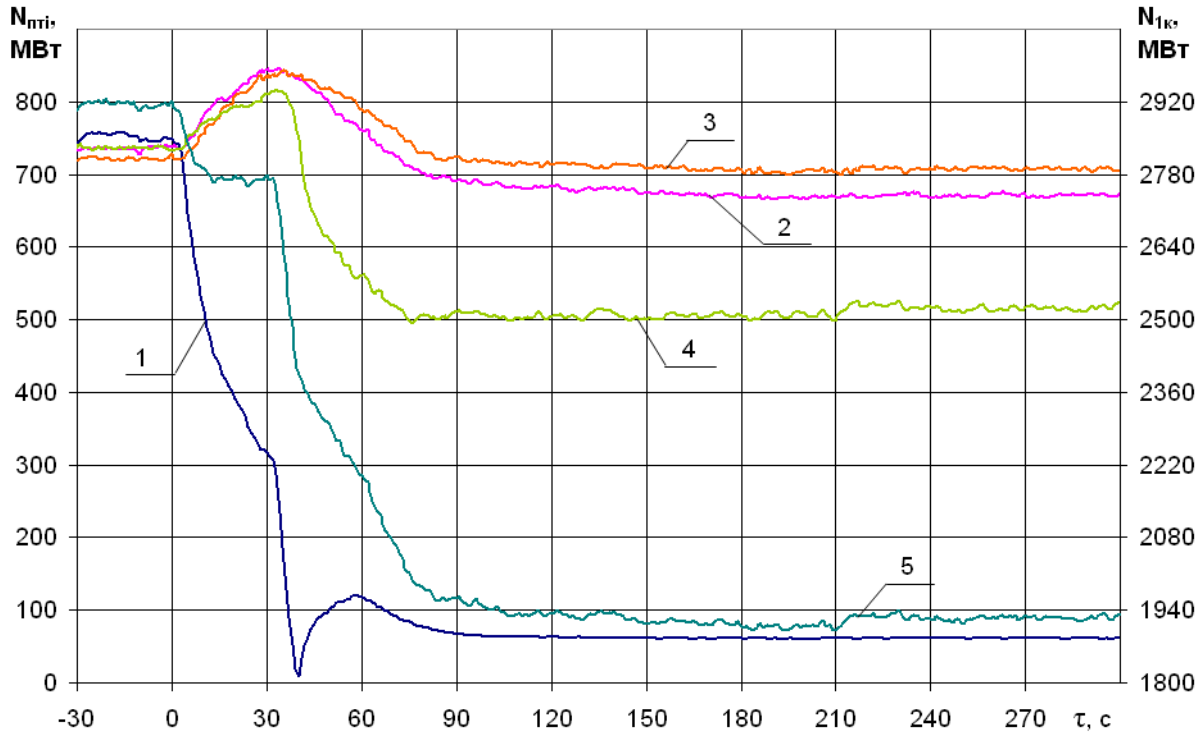

1 – $N_{пт1}$; 2 – $N_{пт2}$; 3 – $N_{пт3}$; 4 – $N_{пт4}$; 5 – $N_{1к}$

Fig. 8 – Thermal power histories of the primary loops and the integral reactor thermal power recorded by the ICMS

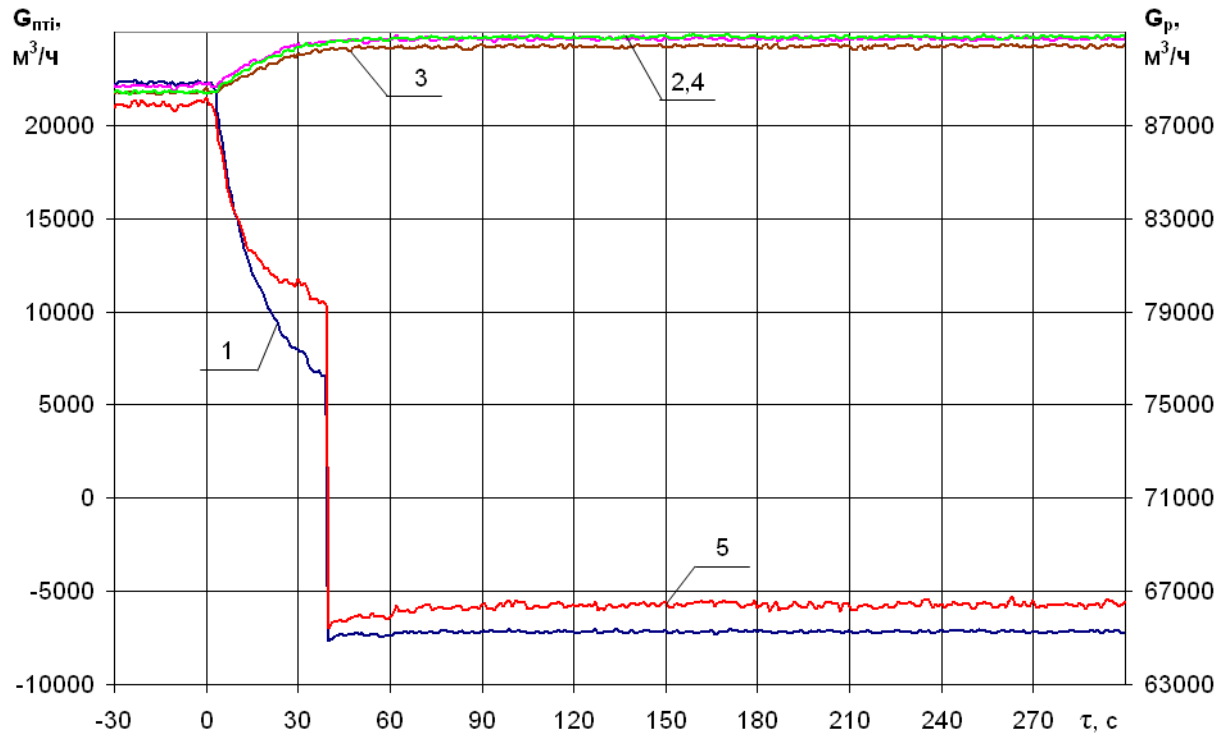

1 – $G_{пт1}$; 2 – $G_{пт2}$; 3 – $G_{пт3}$; 4 – $G_{пт4}$; 5 – $G_{р}$

Fig. 9 – Coolant flow rates time histories of the primary loops and the reactor mass flow rate recorded by the ICMS

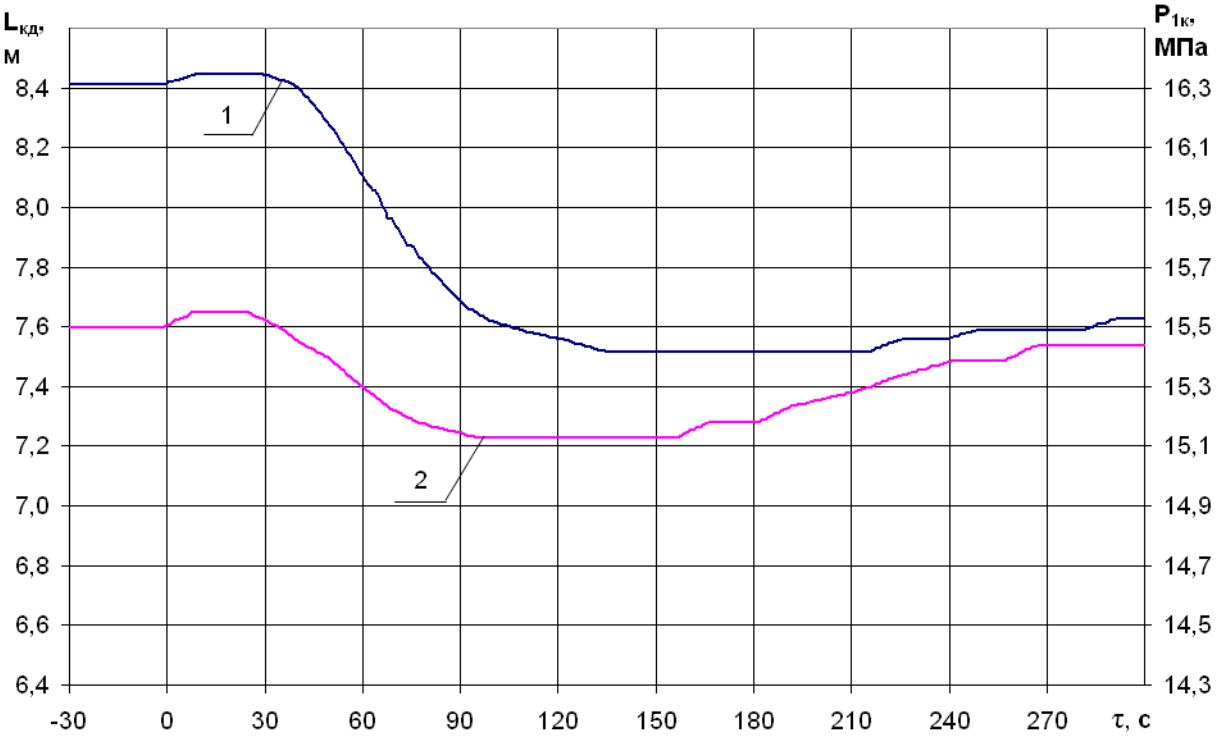

1 – L_{PRZ}; 2 – P_{PC}

Fig. 10 – PRZ water level and PC-pressure change recorded by the UBLS

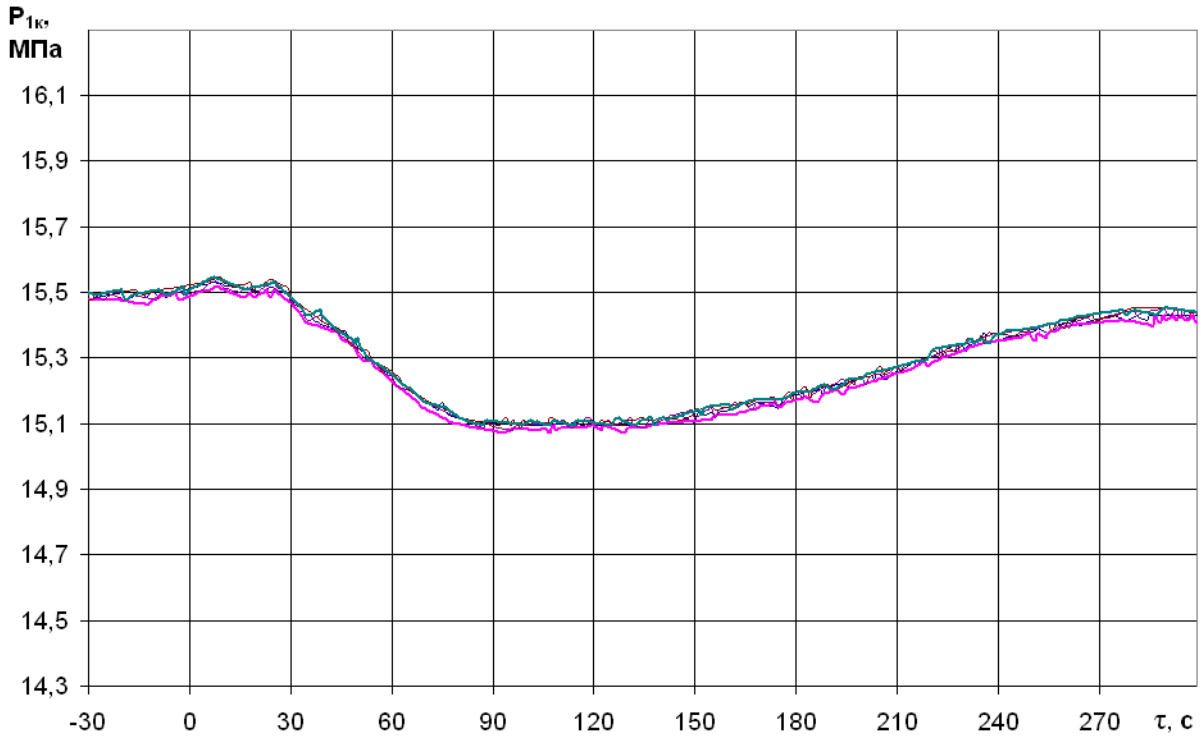

Fig. 11 – PC-pressure change by the reactor protection system (6 sensors) recorded by the UBLS

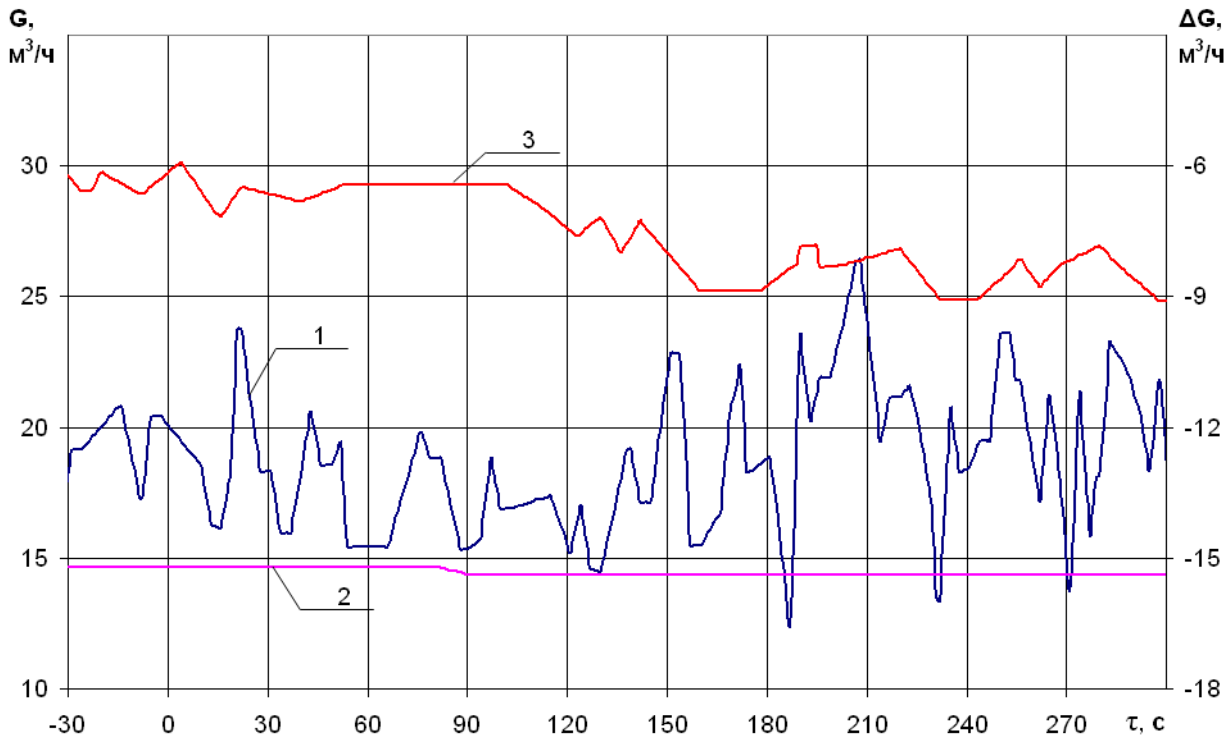

1 – $G_{подп}$; 2 – $G_{прод}$; 3 – $\Delta G_{прод-под}$

Fig. 12 - (controlling for power level 100% N_{nom}) Mass flow rate of make-up and blow-down systems and the difference between the blowdown and the make-up flow rate recorded by the UBLS

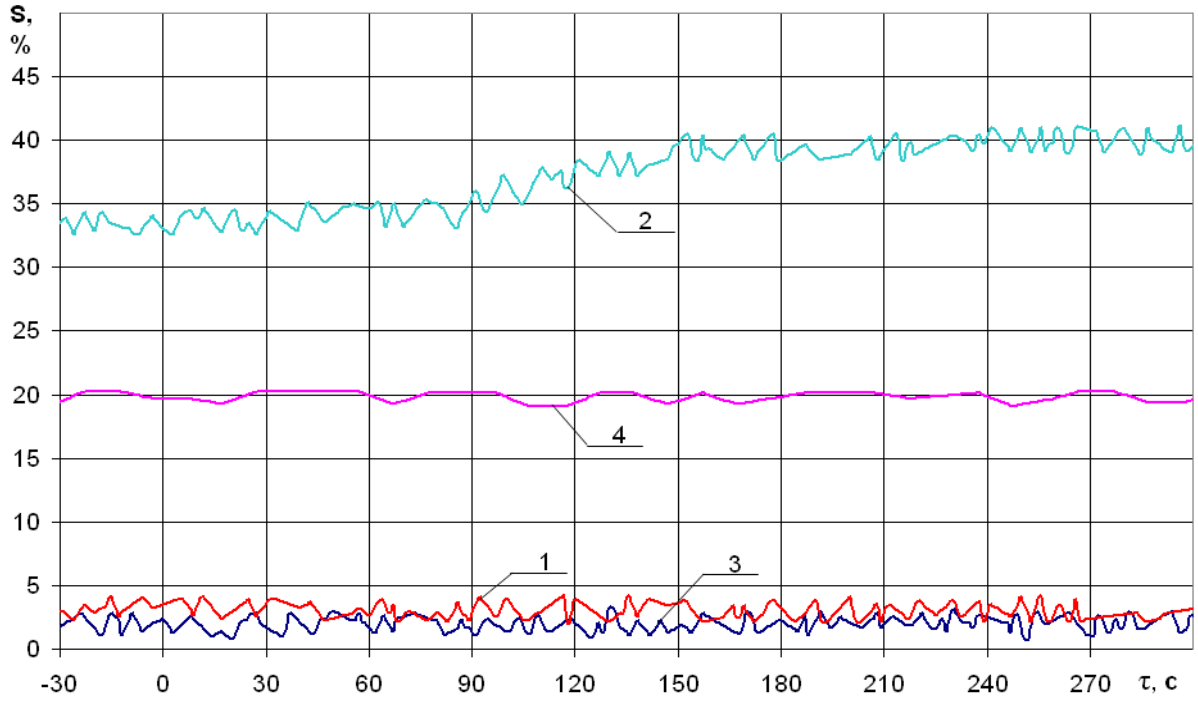

1– $S_{TK31S02}$; 2 – $S_{TK32S02}$; 3 – $S_{TK81S02}$; 4 – $S_{TK82S02}$

Fig. 13 – Change of the position of the make-up system valves (TK31,32S02) and of the blow-down system valves (TK81,82S02) recorded by the UBLS

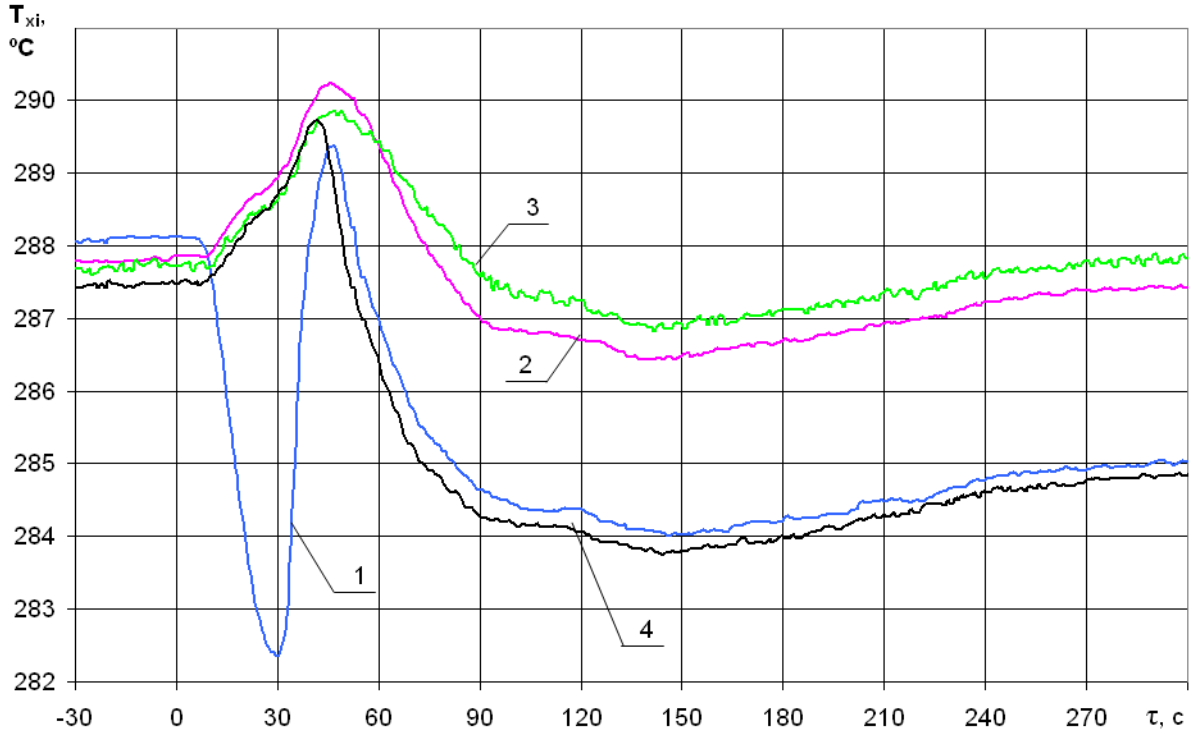

1 – T_{x1}; 2 – T_{x2}; 3 – T_{x3}; 4 – T_{x4}

Fig. 14 – Mean coolant temperature histories of the cold legs of PC-loops recorded by the ICMS

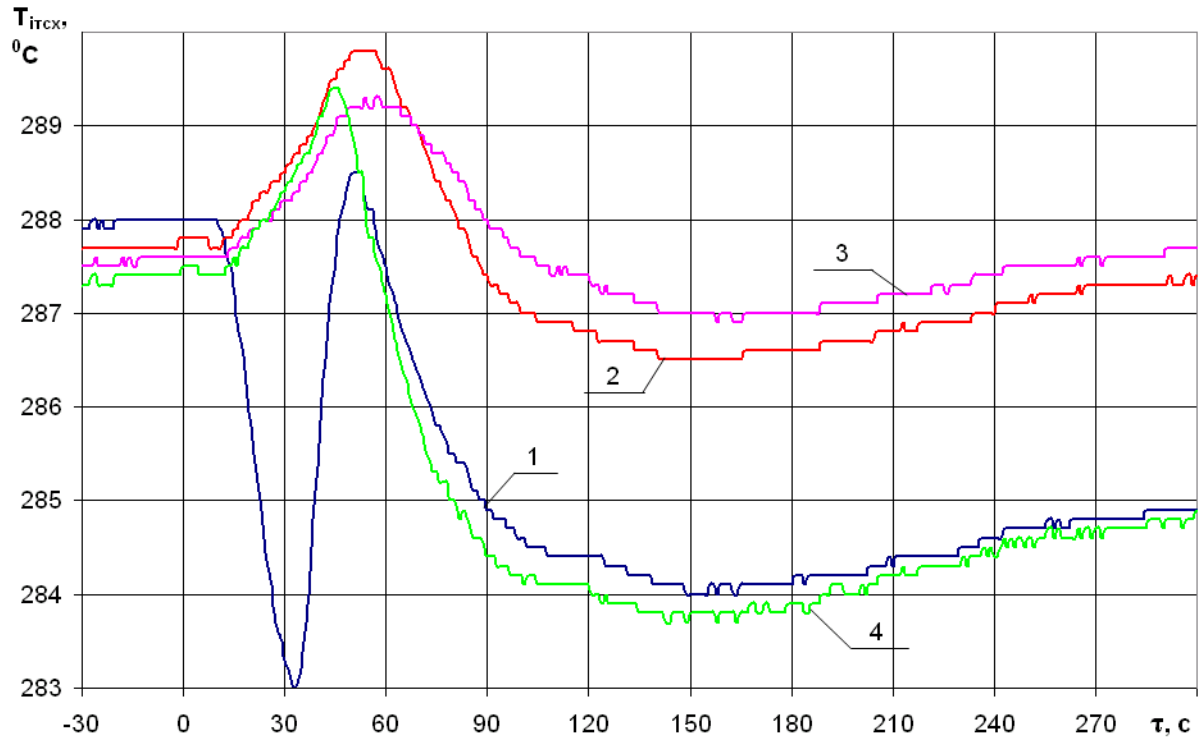

1 – $T_{1тсх}$; 2 – $T_{2тсх}$; 3 – $T_{3тсх}$; 4 – $T_{4тсх}$

Fig. 15 – Mean coolant temperature histories of the cold legs of PC-loops recorded by the thermoresistors

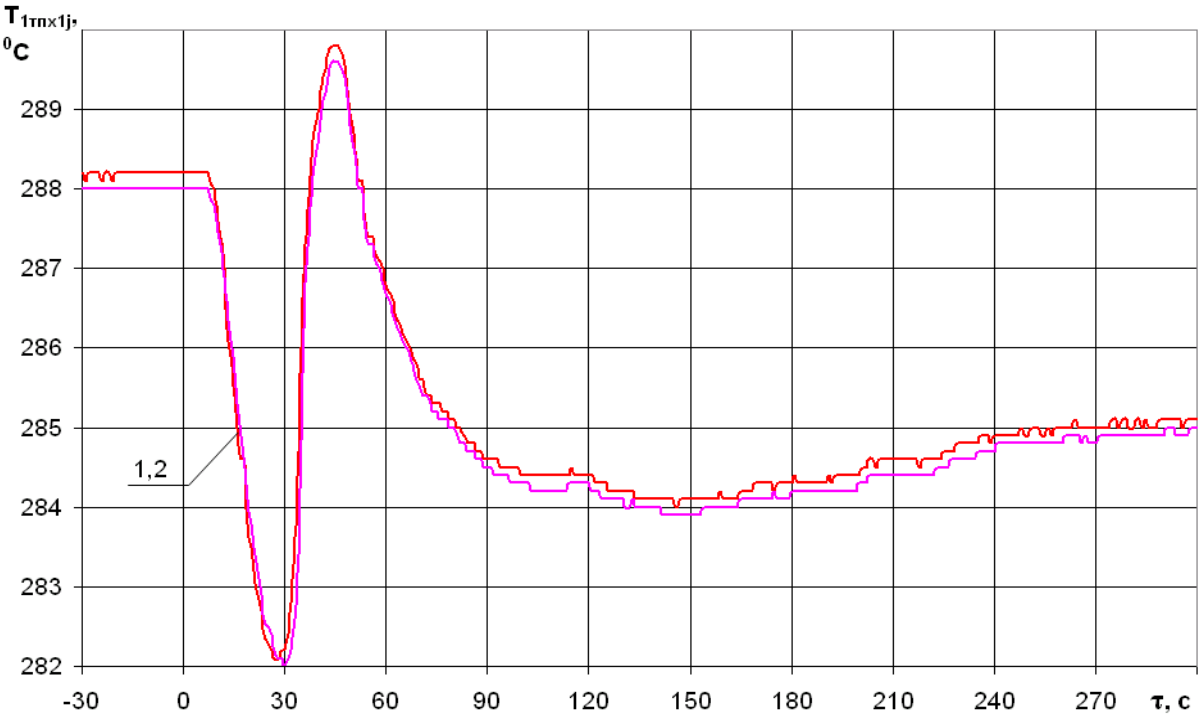

1 – $T_{1тсс1\text{-}2}$; 2 – $T_{1тсс1\text{-}3}$

Fig. 16 – Cold leg #1 mean coolant temperature history recorded by the first set of thermocouples

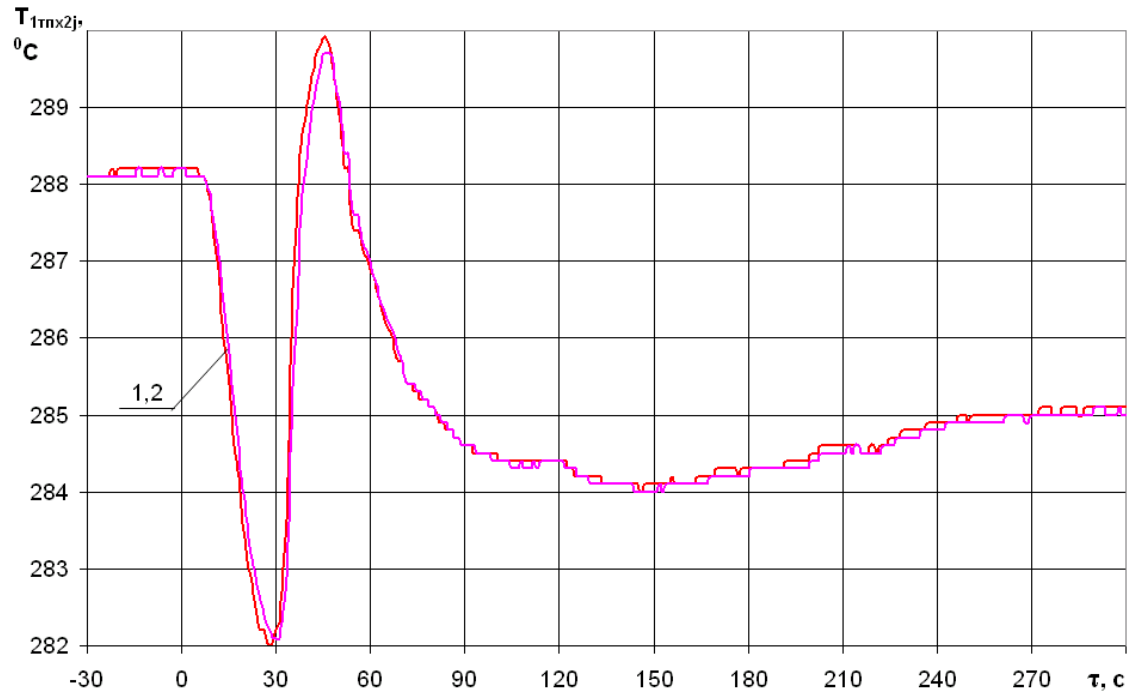

$1 - T_{1tpc2\text{-}2}$; $2 - T_{1tpc2\text{-}3}$

Fig. 17 – Cold leg #1 mean coolant temperature history recorded by the second set of thermocouples

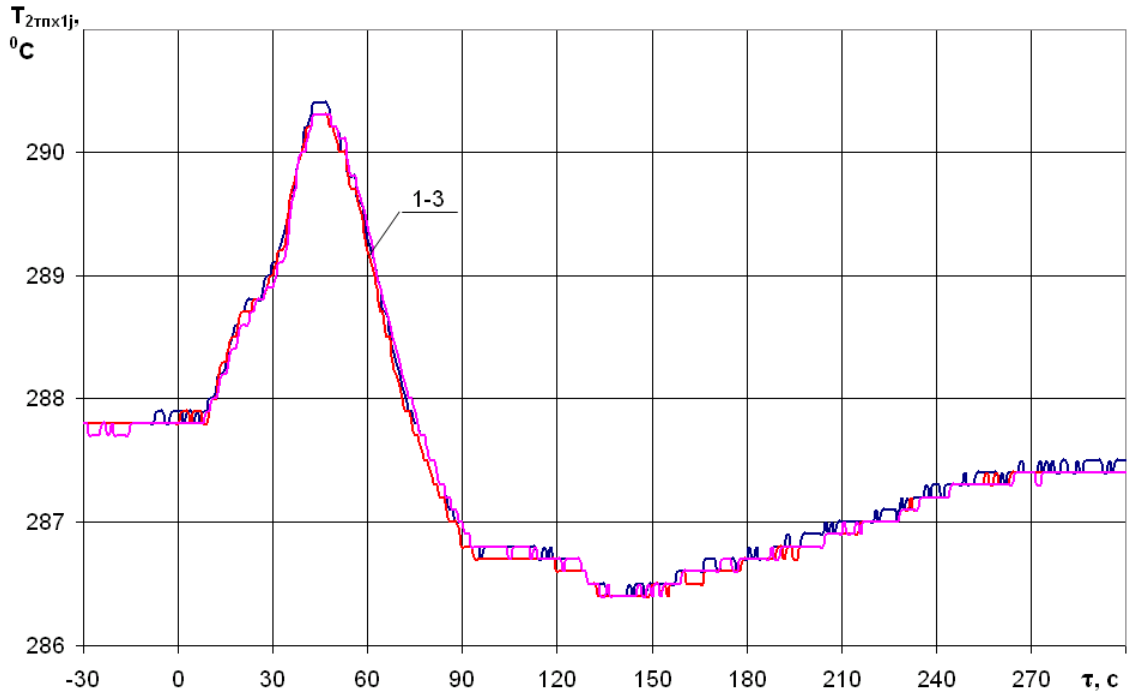

$1 - T_{2tcc1\text{-}1}$; $2 - T_{2tcc1\text{-}2}$; $3 - T_{2tcc1\text{-}3}$

Fig. 18 – Cold leg #2 mean coolant temperature history recorded by the first set of thermocouples

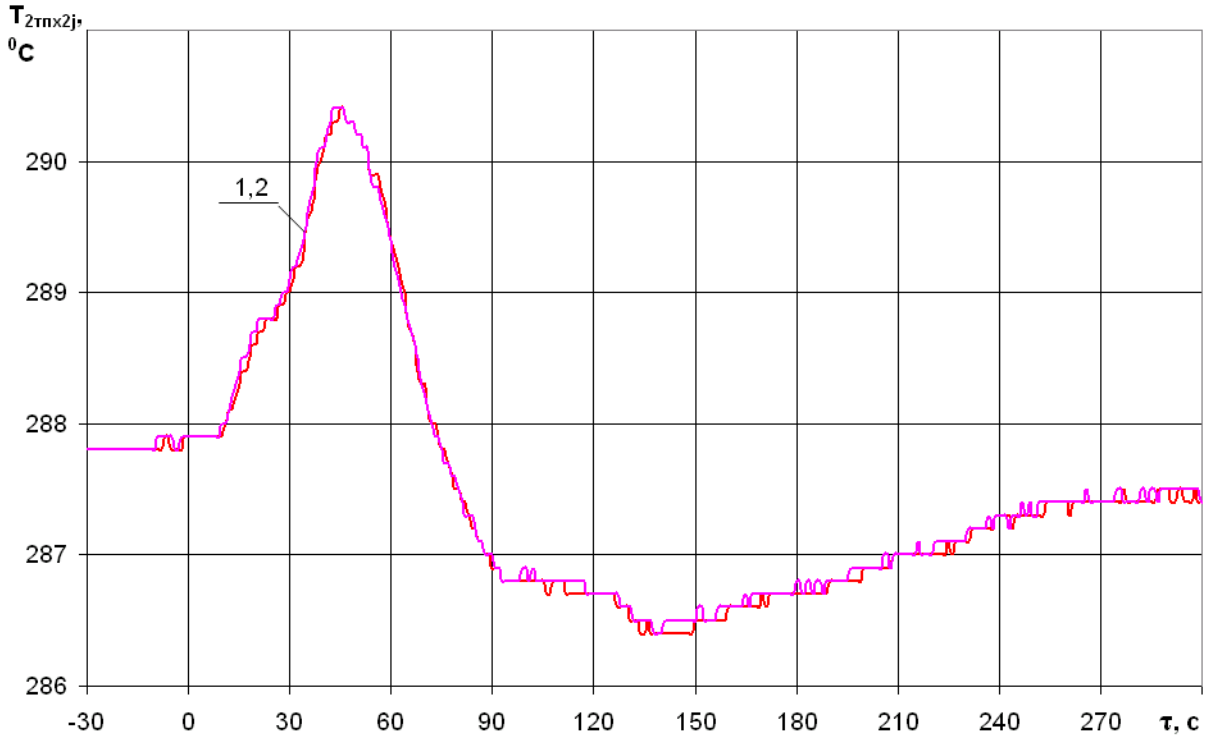

$1 - T_{2tcc2\text{-}2}$; $2 - T_{2tccx2\text{-}3}$

Fig. 19 – Cold leg #2 mean coolant temperature history recorded by the second set of thermocouples

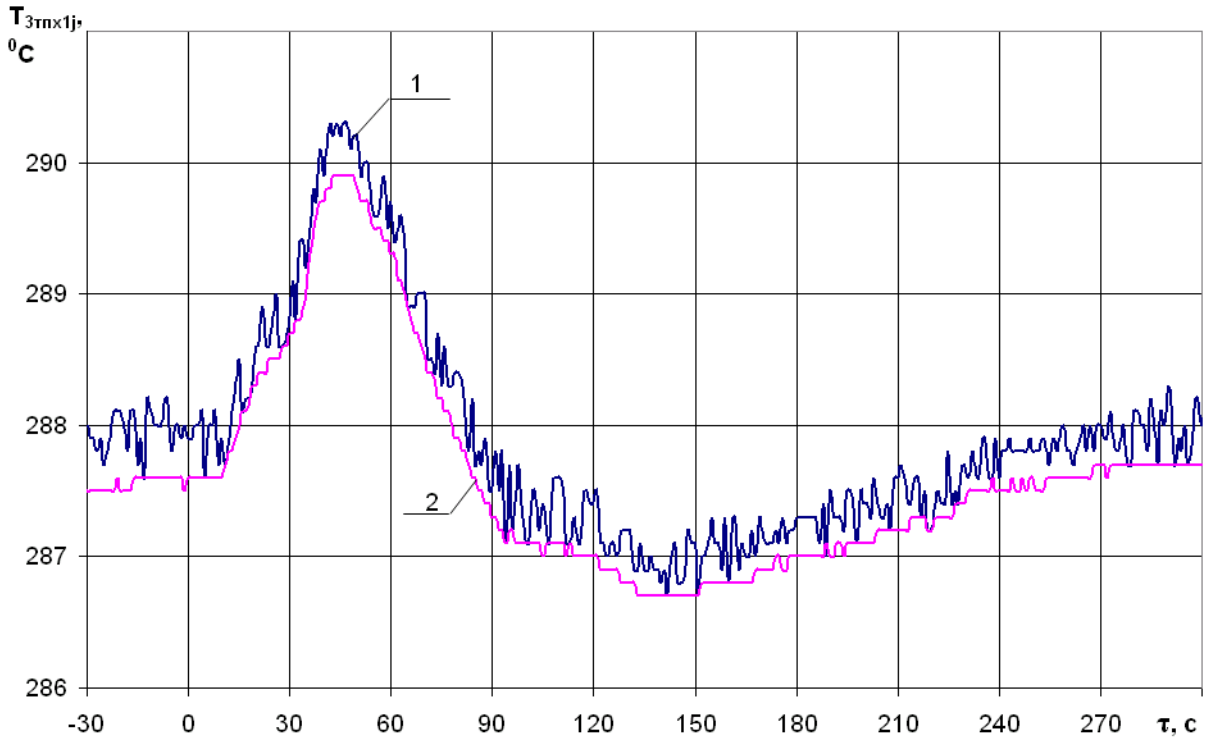

$1 - T_{3tcc1\text{-}1}$; $3 - T_{3tcc1\text{-}3}$

Fig. 20 – Cold leg #3 mean coolant temperature history recorded by the first set of thermocouples

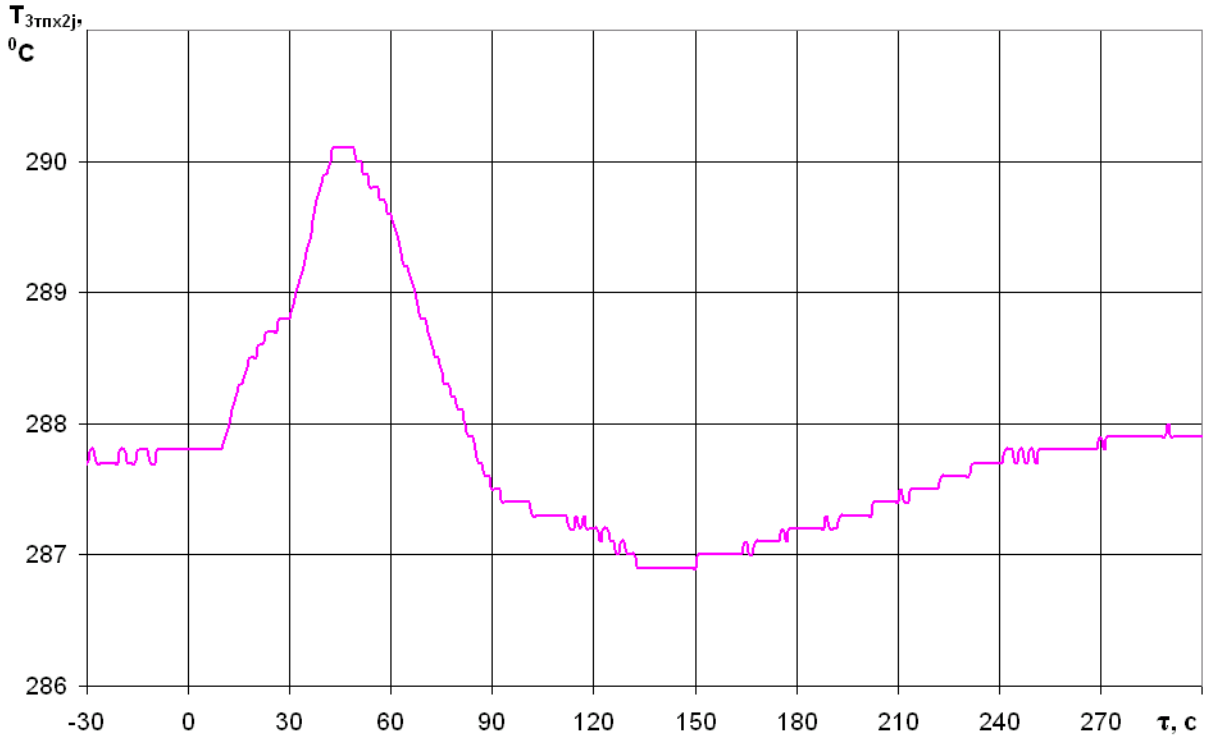

Fig. 21 – Cold leg #3 mean coolant temperature history recorded by the second set of thermocouples

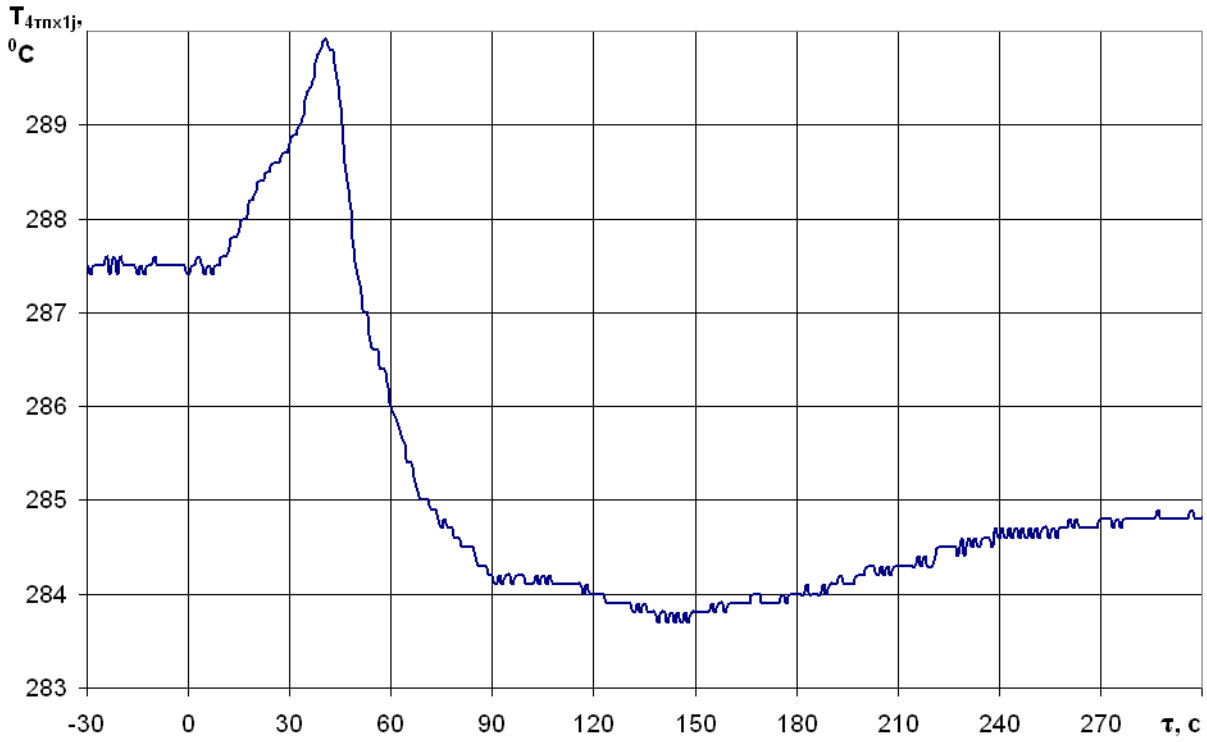

Fig. 22 – Cold leg #4 mean coolant temperature history recorded by the first set of thermocouples

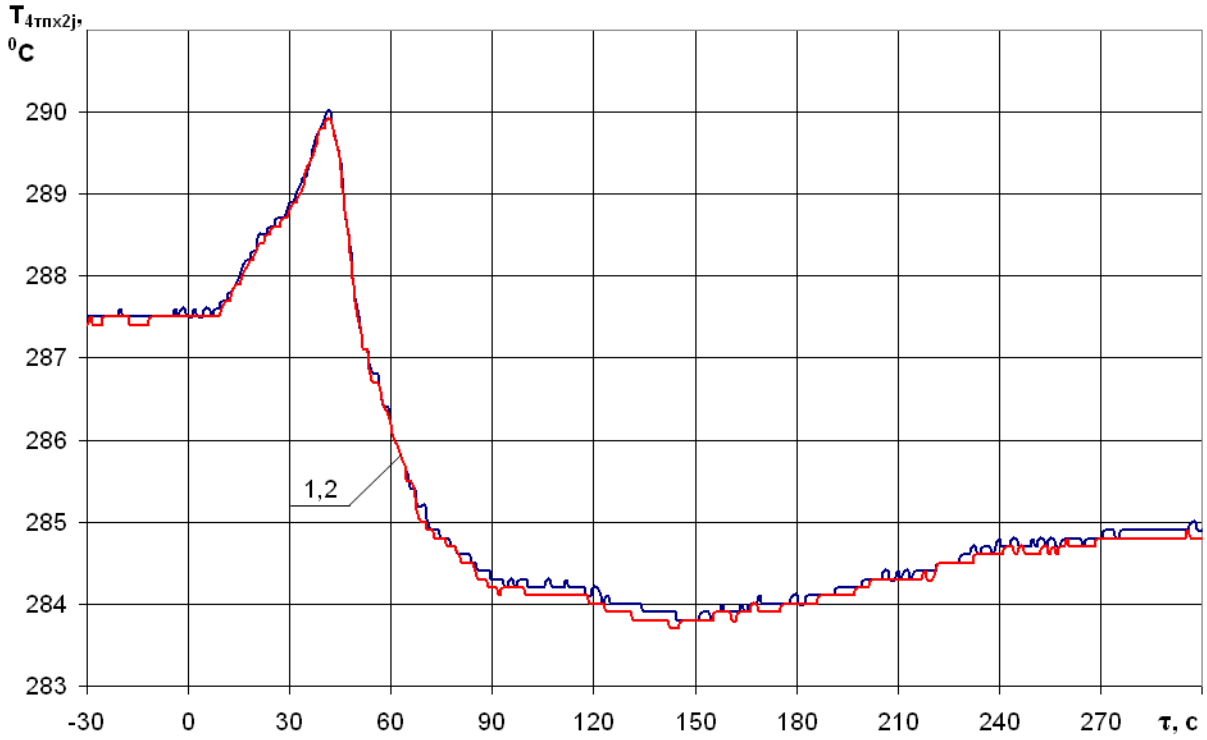

1 – $T_{4tcc2\text{-}1}$; 2 – $T_{4tcc2\text{-}2}$

Fig. 23 – Cold leg #4 mean coolant temperature history recorded by the second set of thermocouples

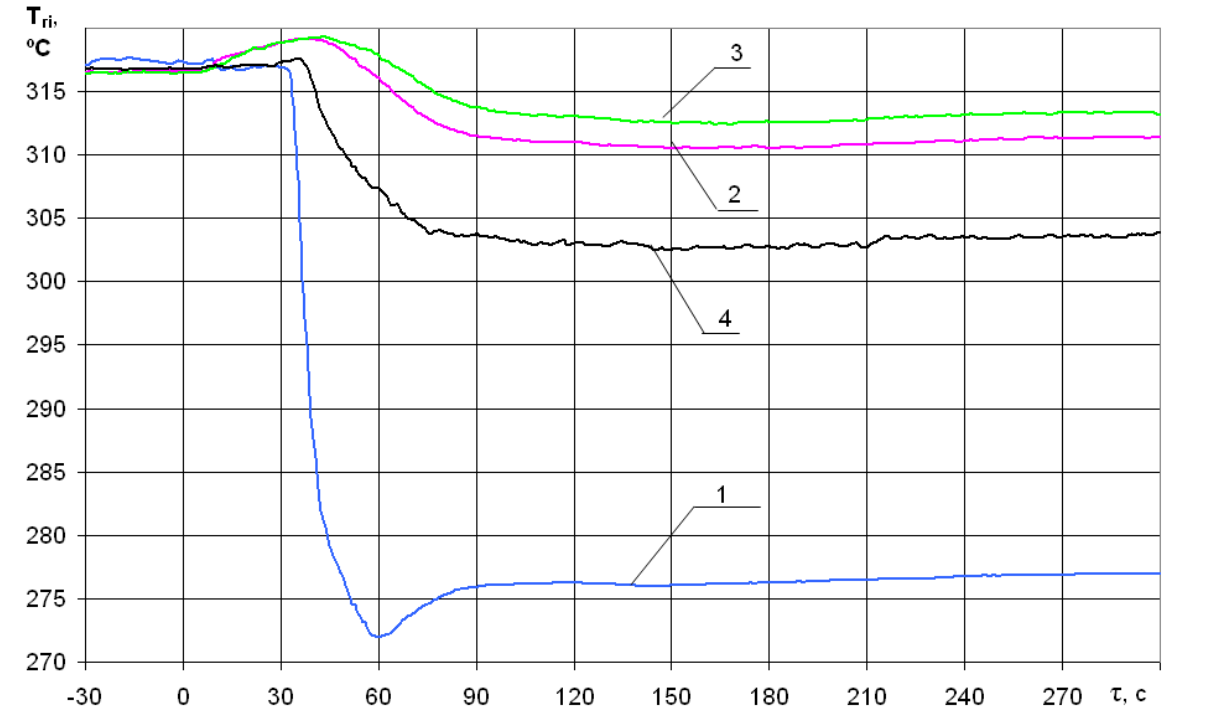

1 – T_{r1}; 2 – T_{r2}; 3 – T_{r3}; 4 – T_{r4}

Fig. 24 – Mean coolant temperature histories of the hot legs of PC-loops recorded by the ICMS

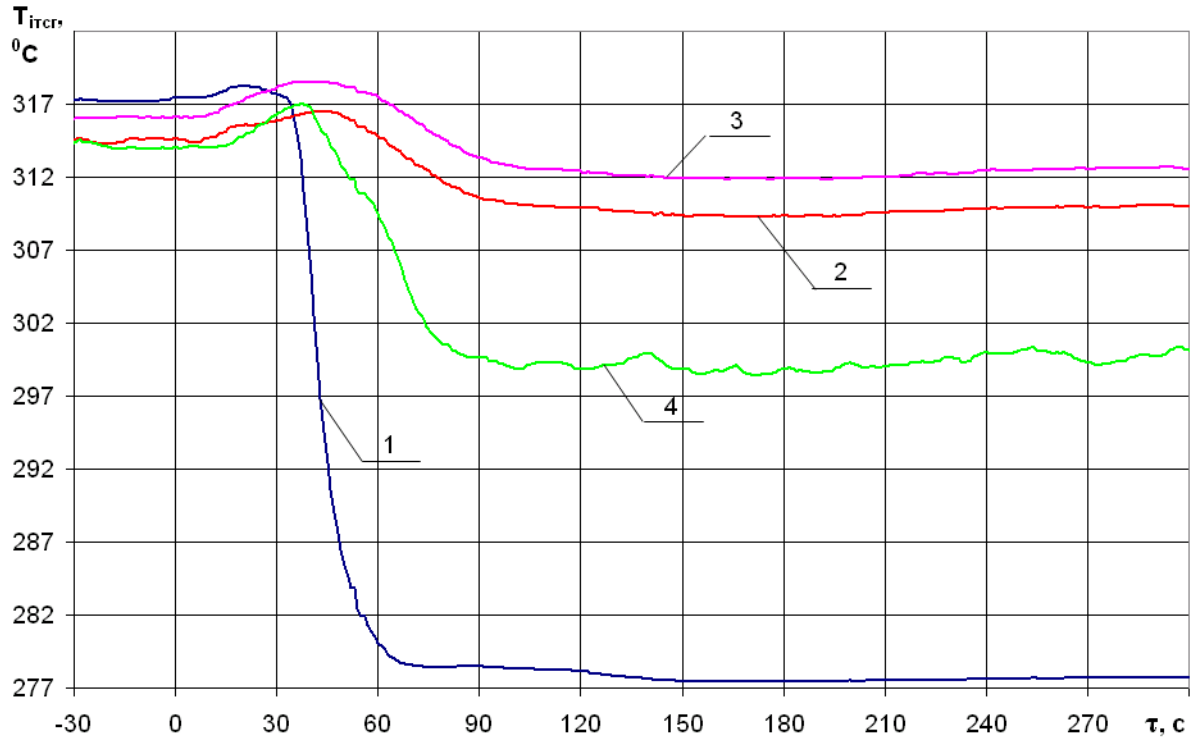

$1 - T_{1\tau cr}$; $2 - T_{2\tau cr}$; $3 - T_{3\tau cr}$; $4 - T_{4\tau cr}$

Fig. 25 – Mean coolant temperature histories of the hot legs of PC-loops recorded by the thermal resistors

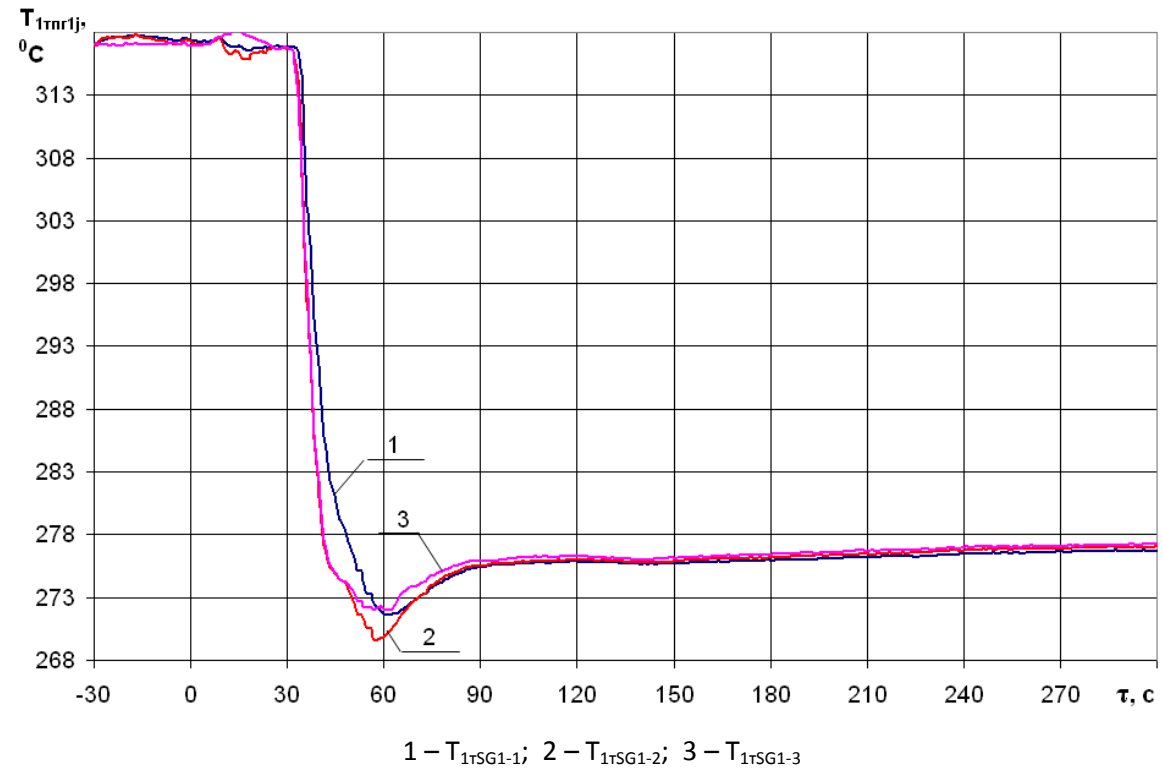

$1 - T_{1\tau SG1\text{-}1}$; $2 - T_{1\tau SG1\text{-}2}$; $3 - T_{1\tau SG1\text{-}3}$

Fig. 26 – Hot leg #1 mean coolant temperature history recorded by the first set of thermocouples

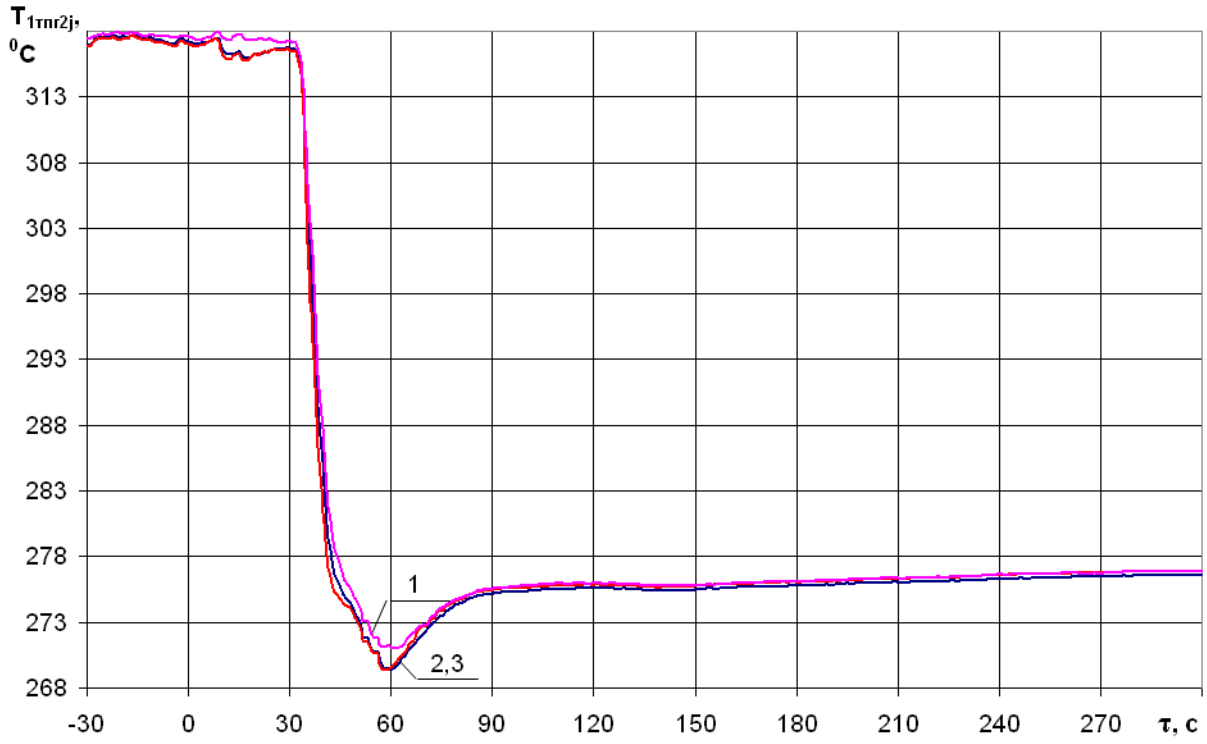

$1 - T_{1\tau SG2\text{-}1}$; $2 - T_{1\tau SG2\text{-}2}$; $3 - T_{1\tau SG2\text{-}3}$

Fig. 27 – Hot leg #1 mean coolant temperature history recorded by the second set of thermocouples

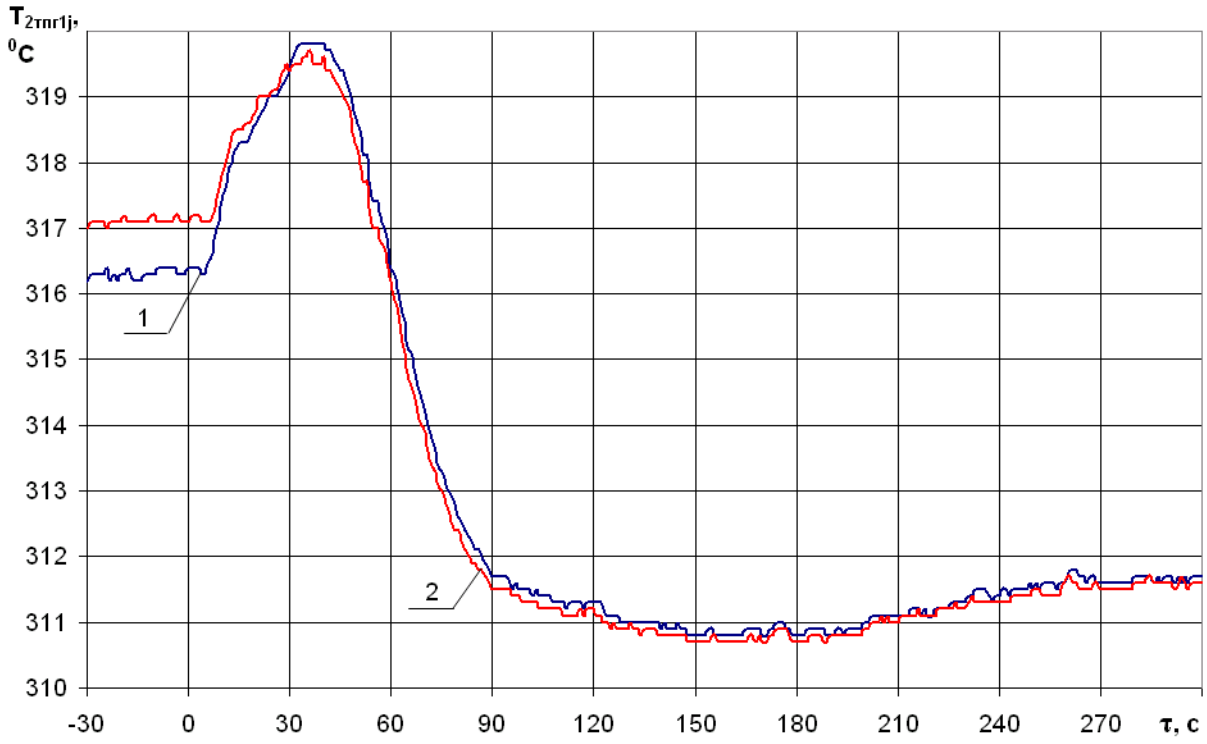

$1 - T_{2\tau SG1\text{-}1}$; $2 - T_{2\tau SG1\text{-}2}$

Fig. 28 – Hot leg #2 mean coolant temperature history recorded by the first set of thermocouples

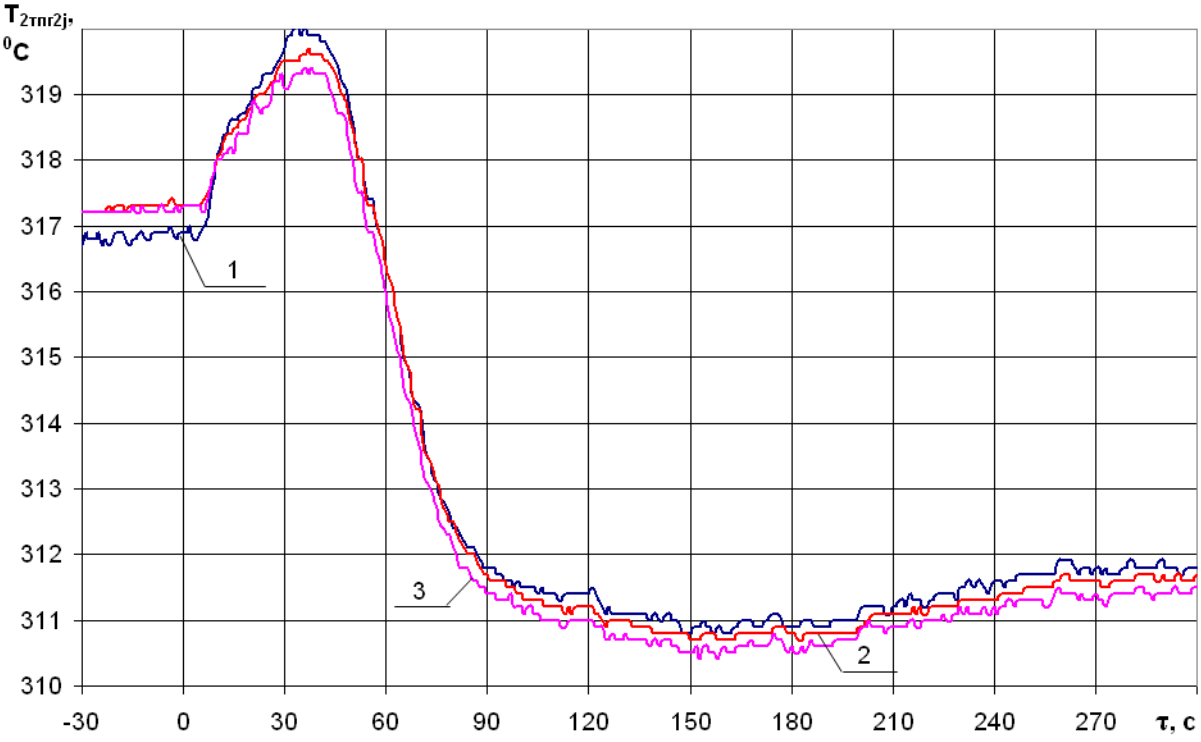

1 – $T_{2тSG2\text{-}1}$; 2 – $T_{2тSG2\text{-}2}$; 3 – $T_{2тSG2\text{-}3}$

Fig. 29 – Hot leg #2 mean coolant temperature history recorded by the second set of thermocouples

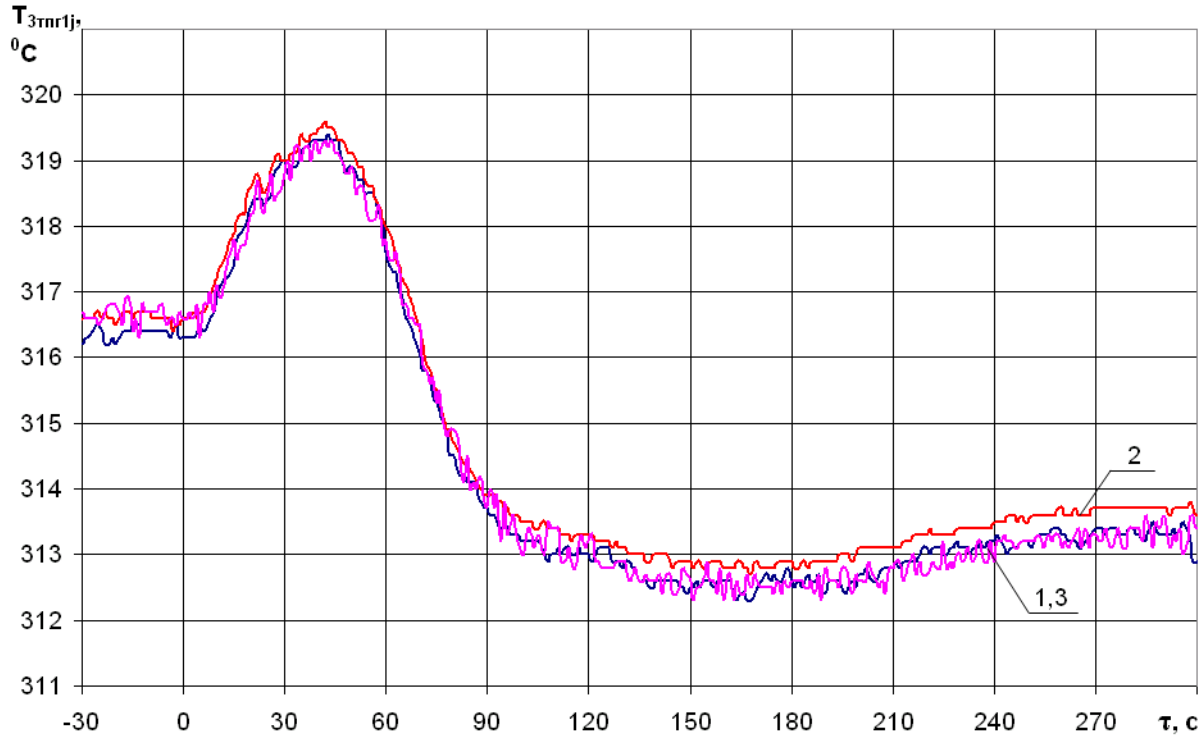

1- $T_{3тSG1\text{-}1}$; 2 – $T_{3тSG1\text{-}2}$; 3 – $T_{3тSG1\text{-}3}$

Fig. 30 – Hot leg #3 mean coolant temperature history recorded by the first set of thermocouples

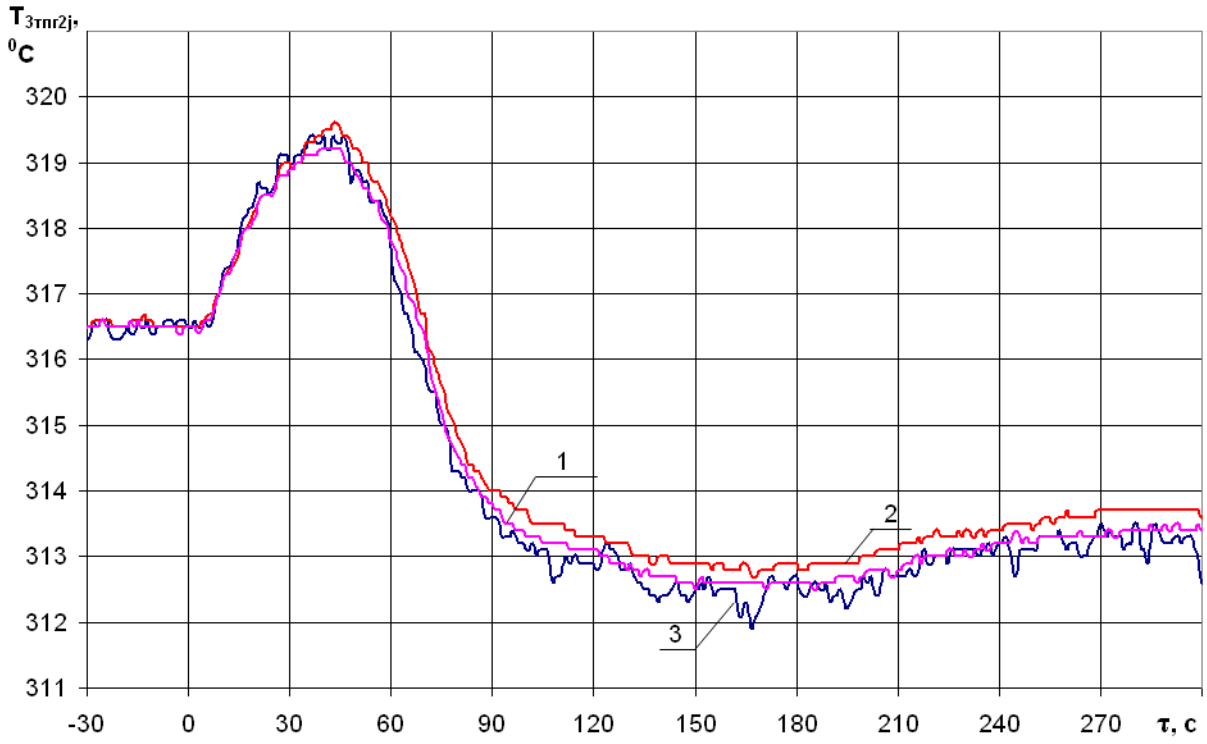

1 – $T_{3тSG2-1}$; 2 – $T_{3тSG2-2}$; 3 – $T_{3тгп2-3}$

Fig. 31 – Hot leg #3 mean coolant temperature history recorded by the second set of thermocouples

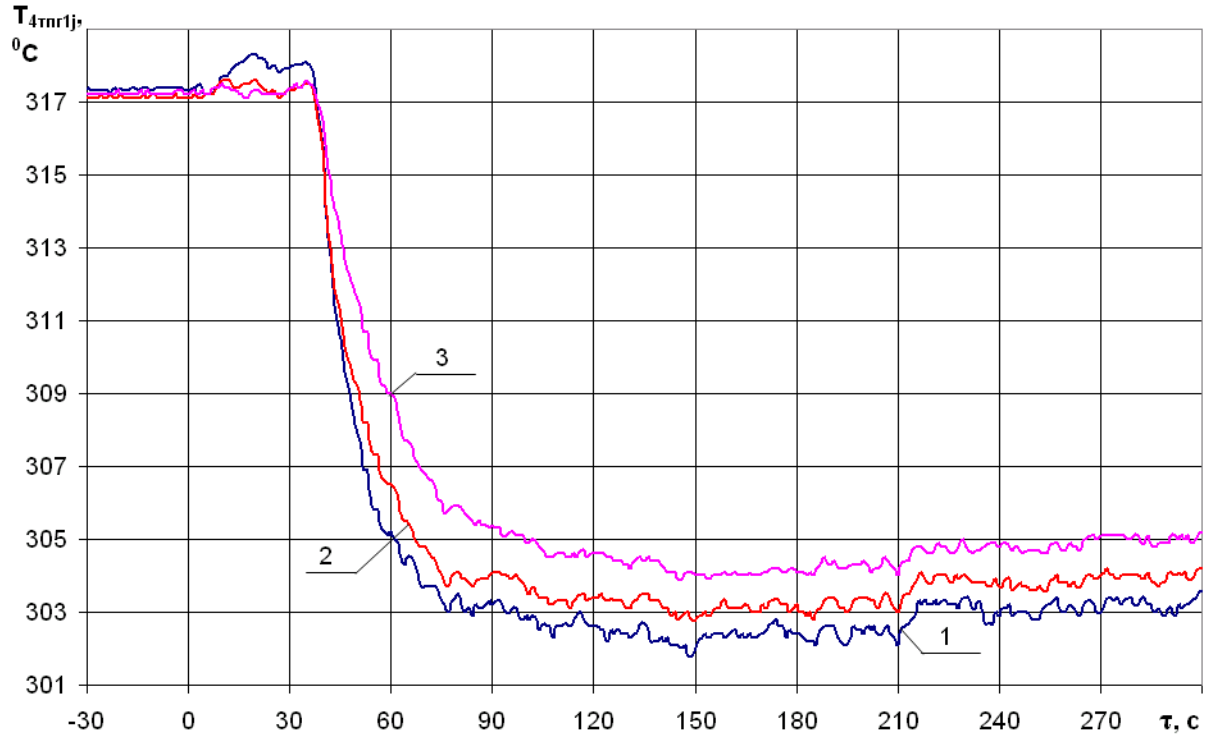

1– $T_{4тSG1-1}$; 2 – $T_{4тгп1-2}$; 3 – $T_{4тSG1-3}$

Fig. 32 – Hot leg #4 mean coolant temperature history recorded by the first set of thermocouples

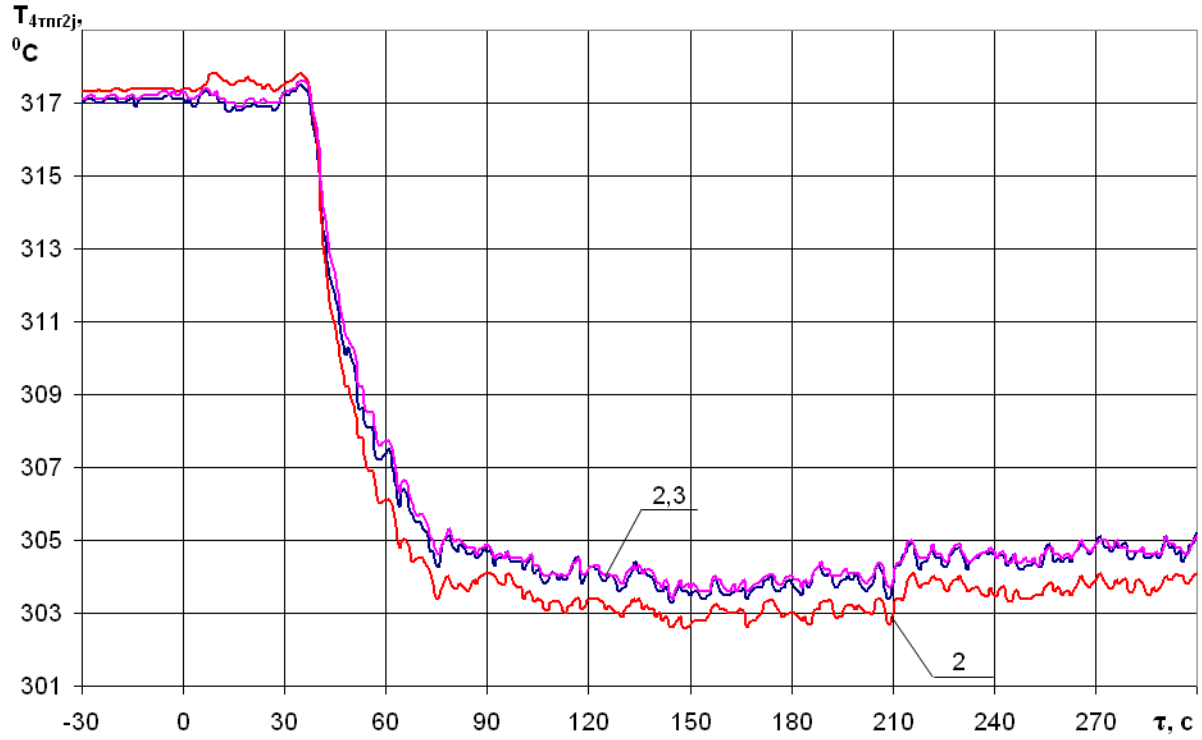

1 – $T_{4тSG2-1}$; 2 – $T_{4тSG2-2}$; 3 – $T_{4тSG2-3}$

Fig. 33 – Hot leg #4 mean coolant temperature history recorded by the second set of thermocouples

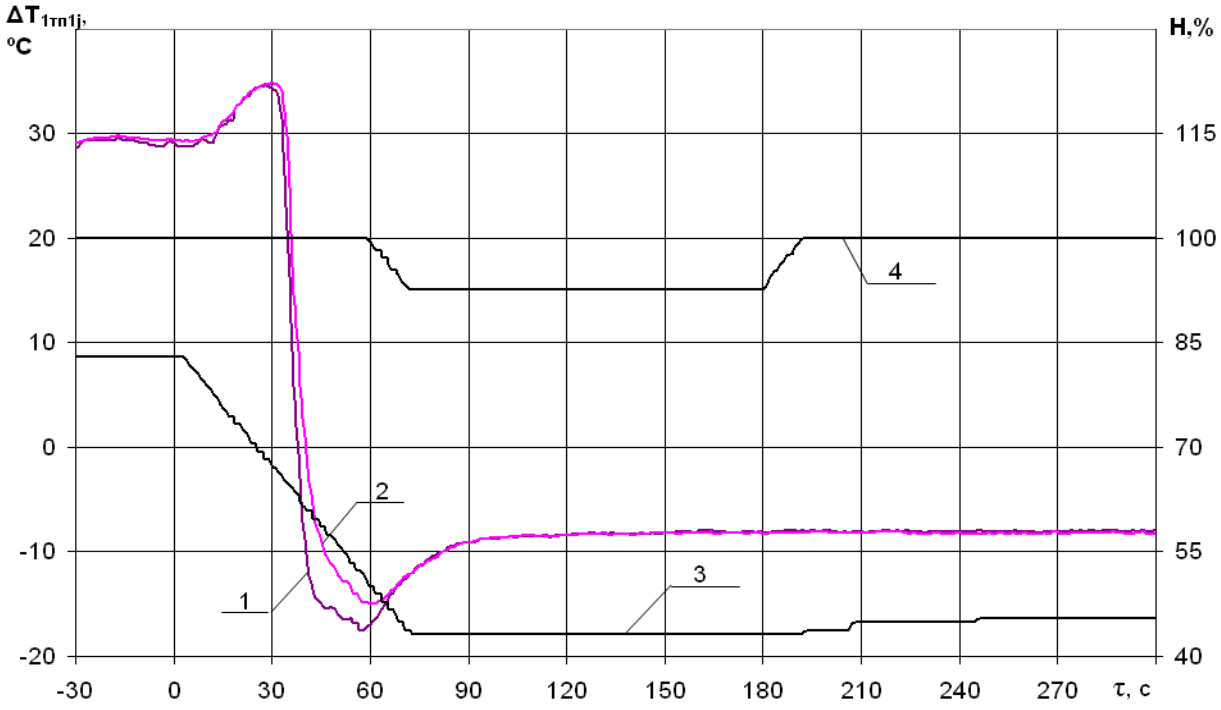

1 – ΔT_{1TC1-2}; 2 – ΔT_{1TC1-3}; 3 – H_{10}; 4 – H_9

Fig. 34 – Change of CPS-group #10 and #9 positions and the coolant heat-up of loop #1 recorded by the first set of thermocouples

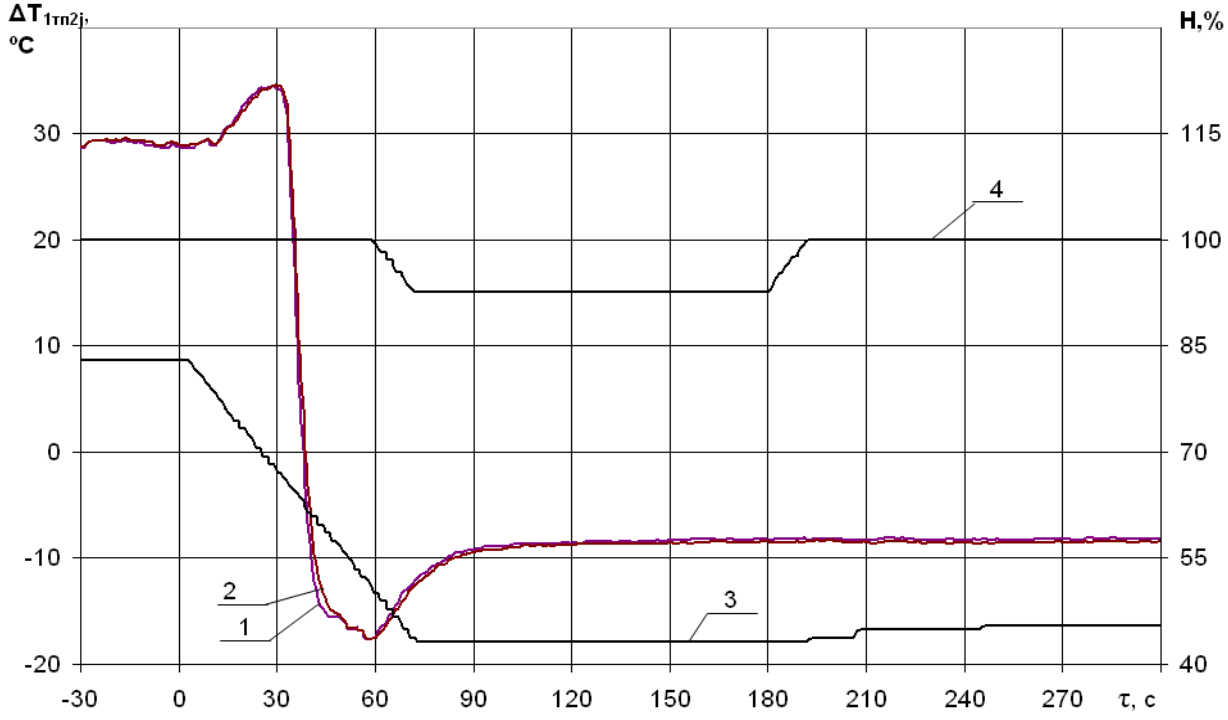

1 – $\Delta T_{1TC2\text{-}2}$; 2 – $\Delta T_{1TC2\text{-}3}$; 3 – H_{10}; 4 – H_9

Fig. 35 – Change of CPS-group #10 and #9 positions and the coolant heat-up of loop #1 recorded by the second set of thermocouples

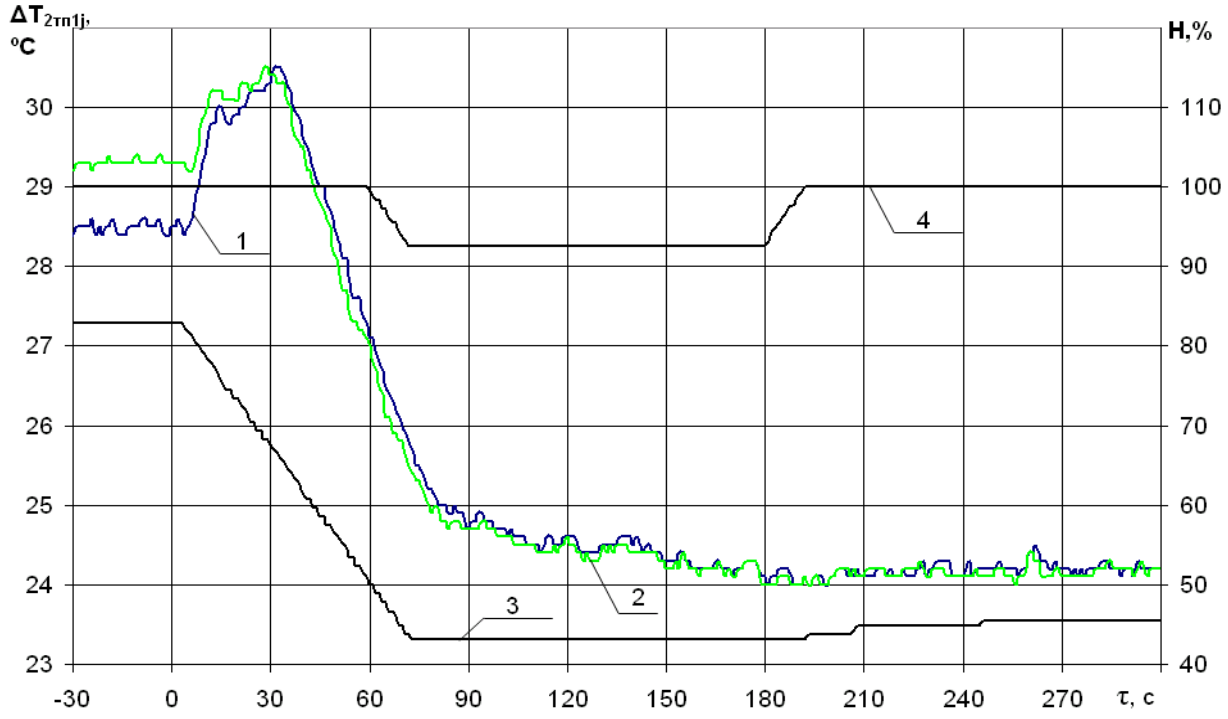

1 – $\Delta T_{2TC1\text{-}1}$; 2 – $\Delta T_{2TC1\text{-}2}$; 3 – H_{10}; 4 – H_9

Fig. 36 – Change of CPS-group #10 and #9 positions and the coolant heat-up of loop #2 recorded by the first set of thermocouples

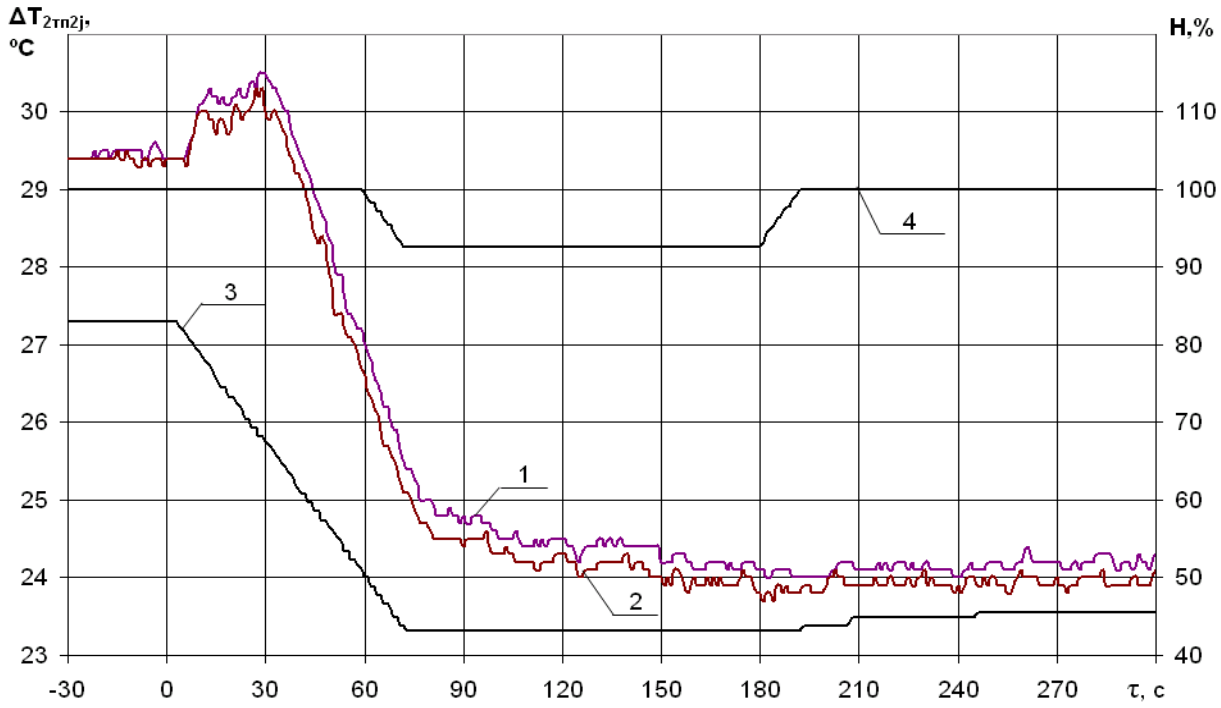

1 – $\Delta T_{2TC2\text{-}2}$; 2 – $\Delta T_{2TC2\text{-}3}$; 3 – H_{10}; 4 – H_9

Fig. 37 – Change of CPS-group #10 and #9 positions and the coolant heat-up of loop #2 recorded by the second set of thermocouples

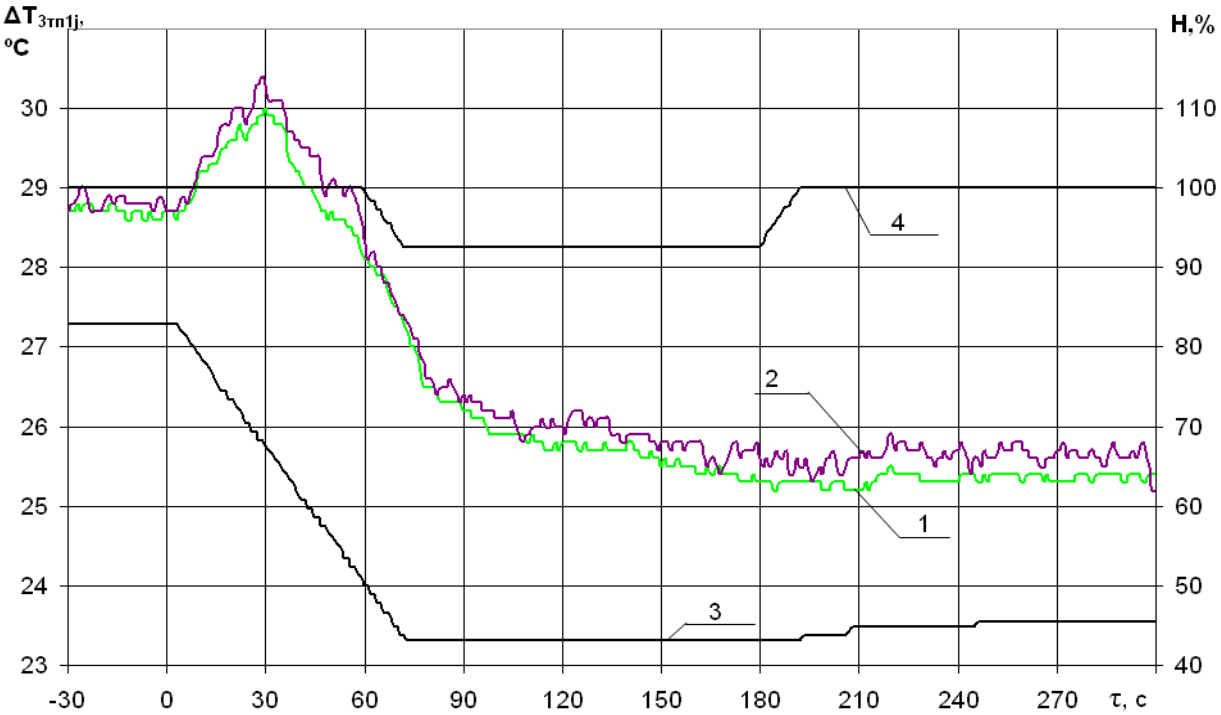

1 – $\Delta T_{3TC1\text{-}1}$; 2 – $\Delta T_{3TC1\text{-}3}$; 3 – H_{10}; 4 – H_9

Fig. 38 – Change of CPS-group #10 and #9 positions and the coolant heat-up of loop #3 recorded by the first set of thermocouples

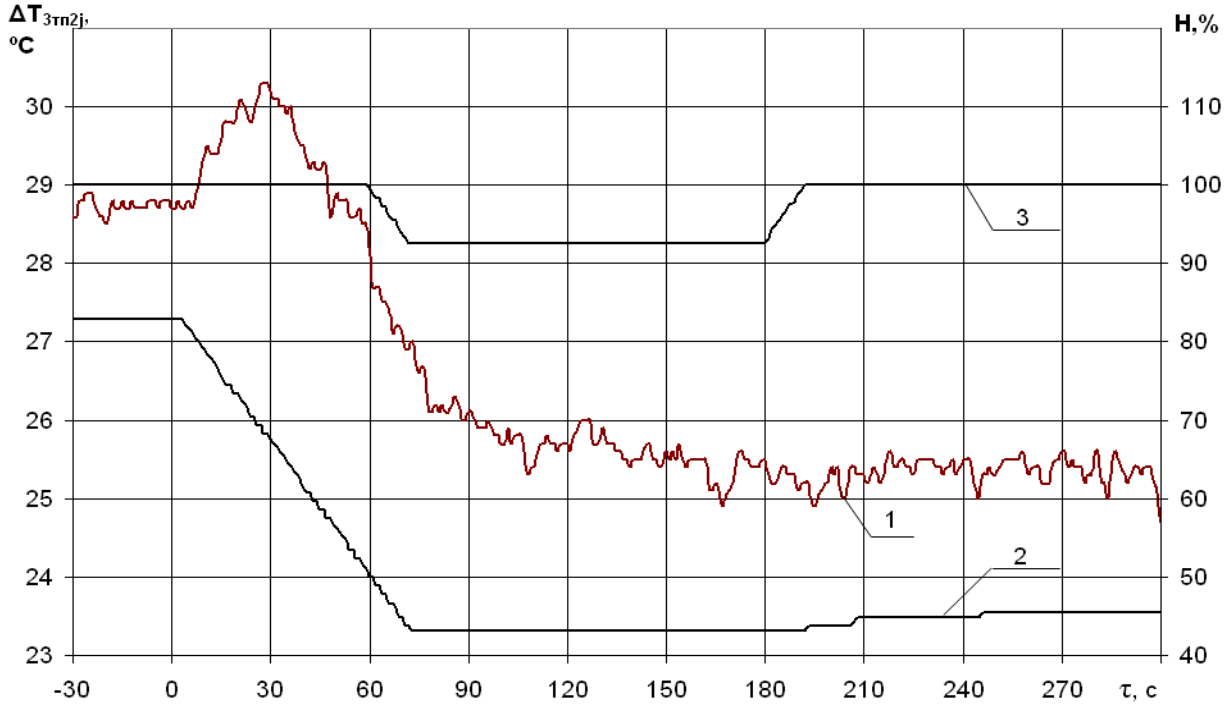

1 – $\Delta T_{3TC2\text{-}3}$; 2 – H_{10}; 3 – H_9

Fig. 39 – Change of CPS-group #10 and #9 positions and the coolant heat-up of loop #3 recorded by the second set of thermocouples

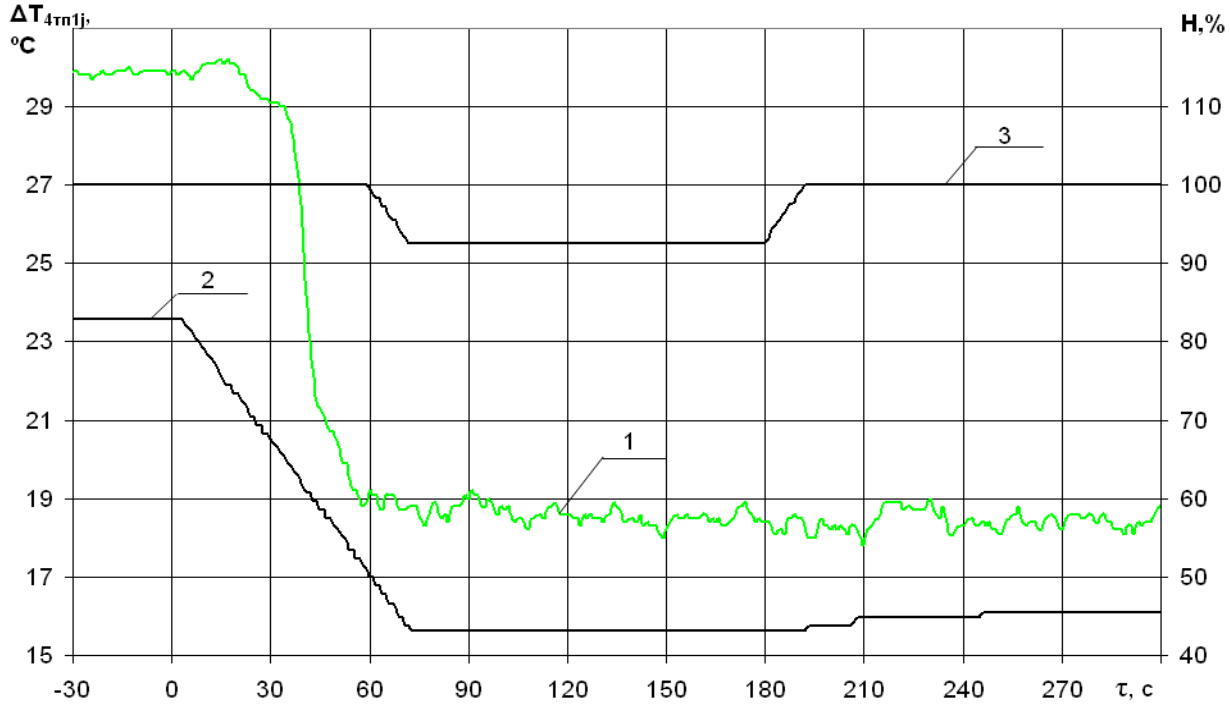

1 – $\Delta T_{4TC1\text{-}1}$; 2 – H_{10}; 3 – H_9

Fig. 40 – Change of CPS-group #10 and #9 positions and the coolant heat-up of loop #4 recorded by the first set of thermocouples

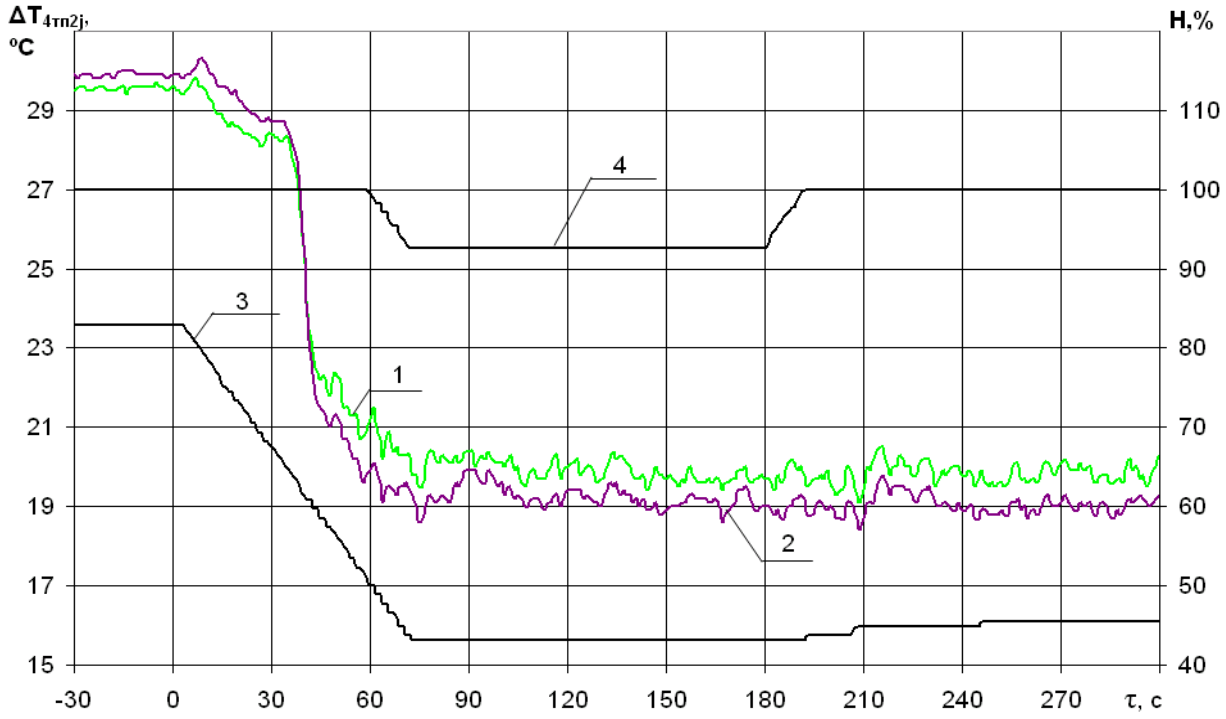

1 – $\Delta T_{4TC2\text{-}1}$; 2 – $\Delta T_{4TC2\text{-}2}$; 3 – H_{10}; 4 – H_9

Fig. 41 – Change of CPS-group #10 and #9 positions and the coolant heat-up of loop #4 recorded by the second set of thermocouples

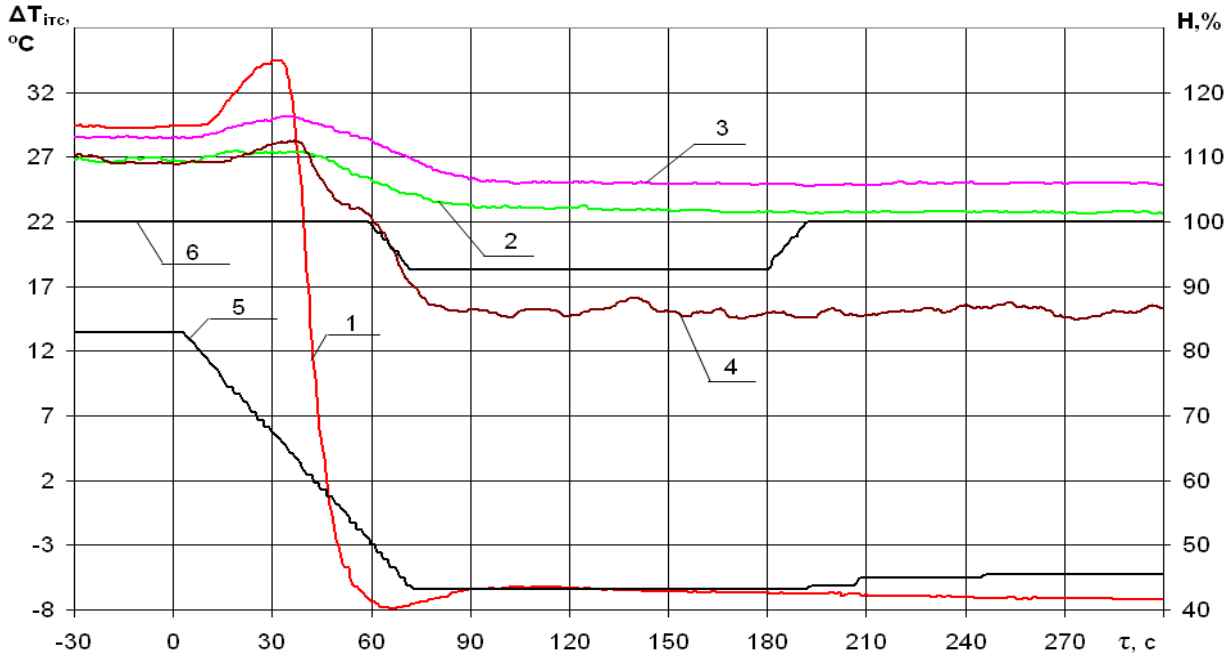

1-$\Delta T_{1тс}$; 2 – $\Delta T_{2тс}$; 3 – $\Delta T_{3тс}$; 4 – $\Delta T_{4тс}$; 5 – H_{10}; 6 – H_9

Fig. 42 – Change of CPS-group #10 and #9 positions and the coolant heat-up of all loops of PC recorded by the thermoresistors

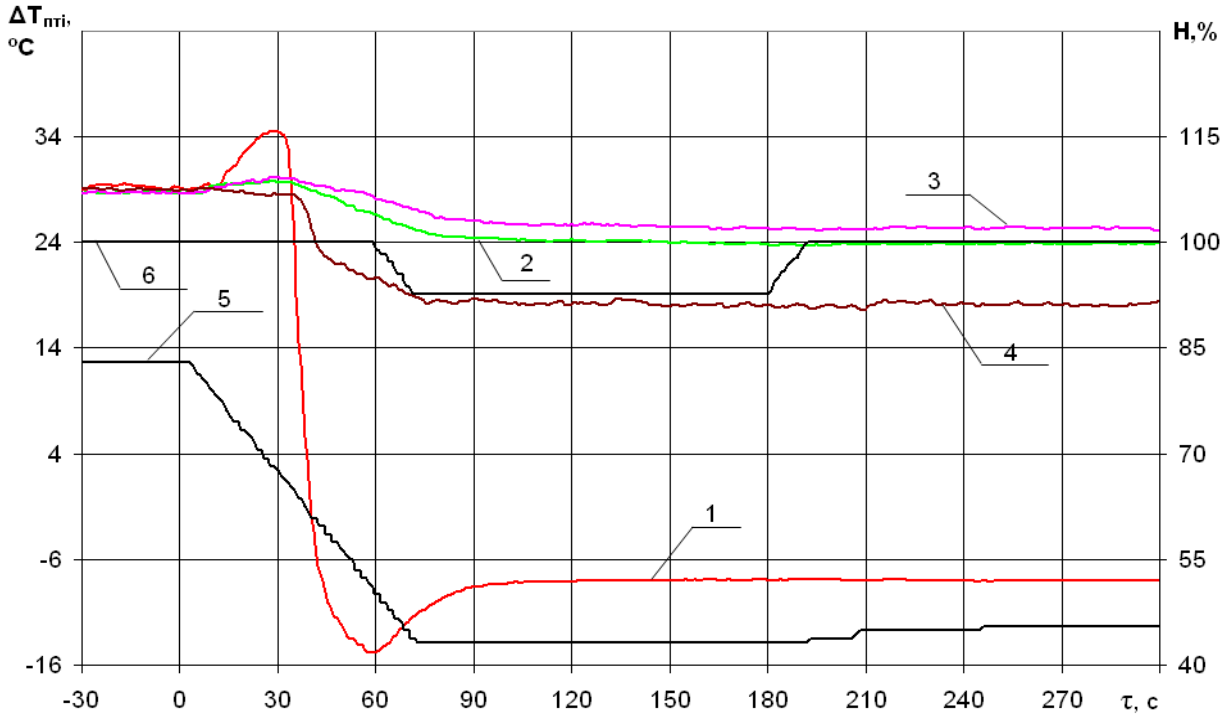

1 – $\Delta T_{пт1}$; 2 – $\Delta T_{пт2}$; 3 – $\Delta T_{пт3}$; 4 – $\Delta T_{пт4}$; 5 – H_{10}; 6 – H_9

Fig. 43 – Change of CPS-group #10 and #9 positions and the coolant heat-up of all loops of PC recorded by the ICMS

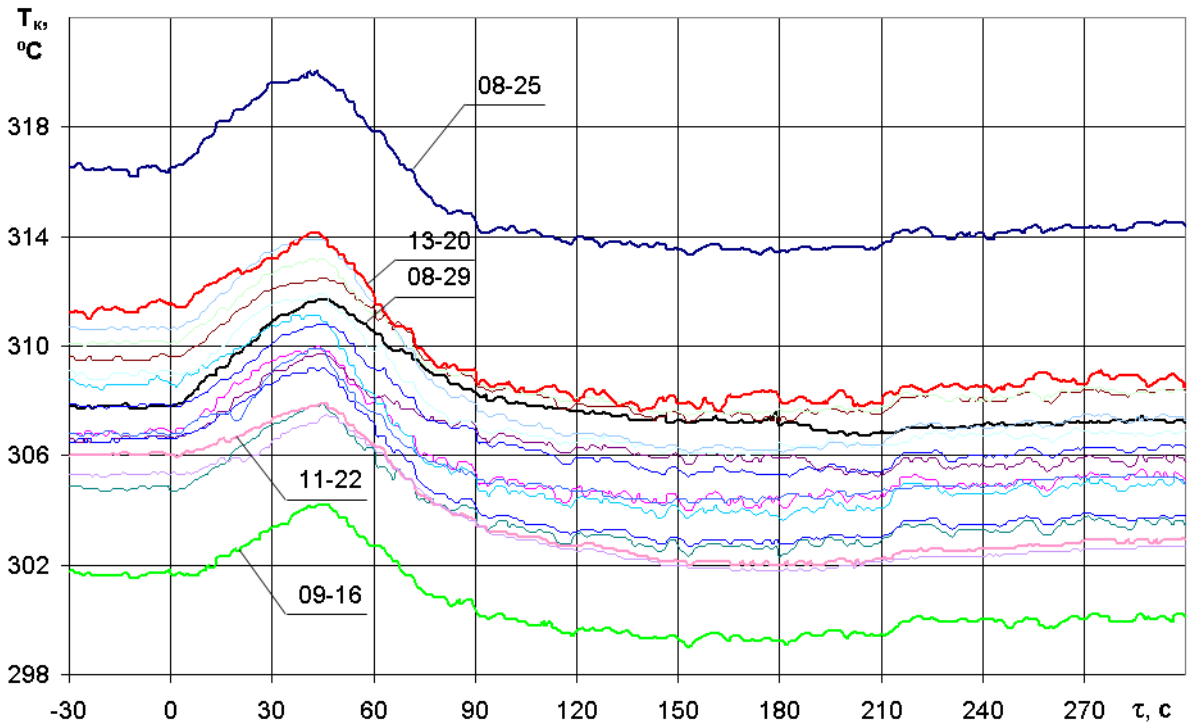

T_k in FA: 08-25; 08-21; 08-29; 09-16; 09-18; 08-23;09-20;10-21;10-25; 11-18; 11-20; 09-26; 10-23;11-22; 12-23; 13-20; 13-22

Fig. 44 – FA outlet coolant temperature histories of sector #1 recorded by the ICMS

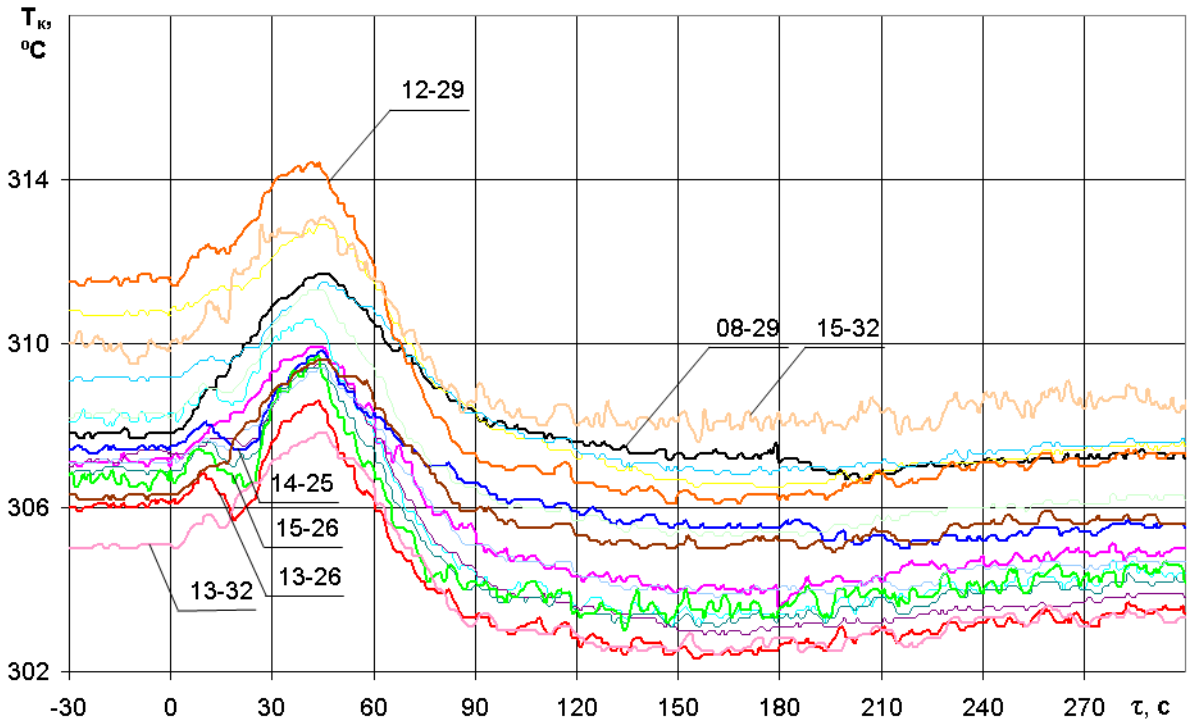

T_k in FA: 08-29; 09-28; 11-26; 11-28; 12-25; 13-26; 13-28; 4-25; 14-29; 15-26; 10-29; 12-29; 13-30; 13-32; 14-33; 15-32

Fig. 45 – FA outlet coolant temperature histories of sector #2 recorded by the ICMS

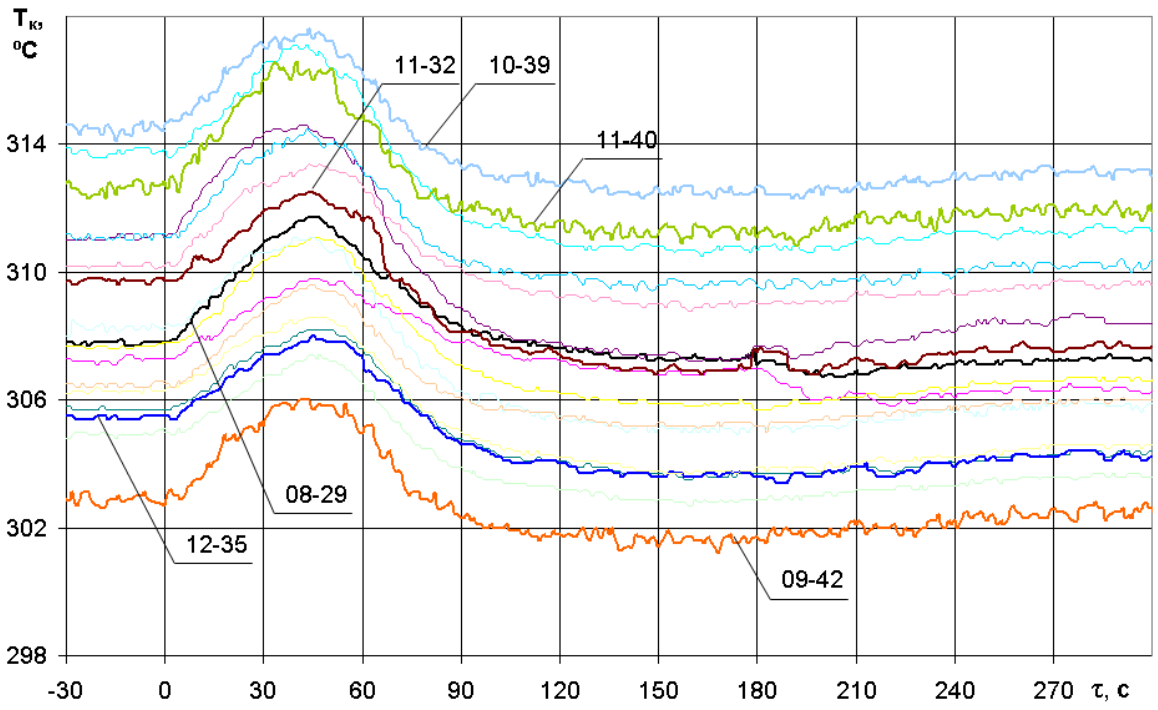

T_k in FA: 08-29; 13-36; 09-32; 10-31; 10-35;11-32;11-36; 12-35; 13-38; 09-34; 09-38; 10-37; 10-39; 11-38; 11-40; 09-40; 09-42

Fig. 46 – FA outlet coolant temperature histories of sector #3 recorded by the ICMS

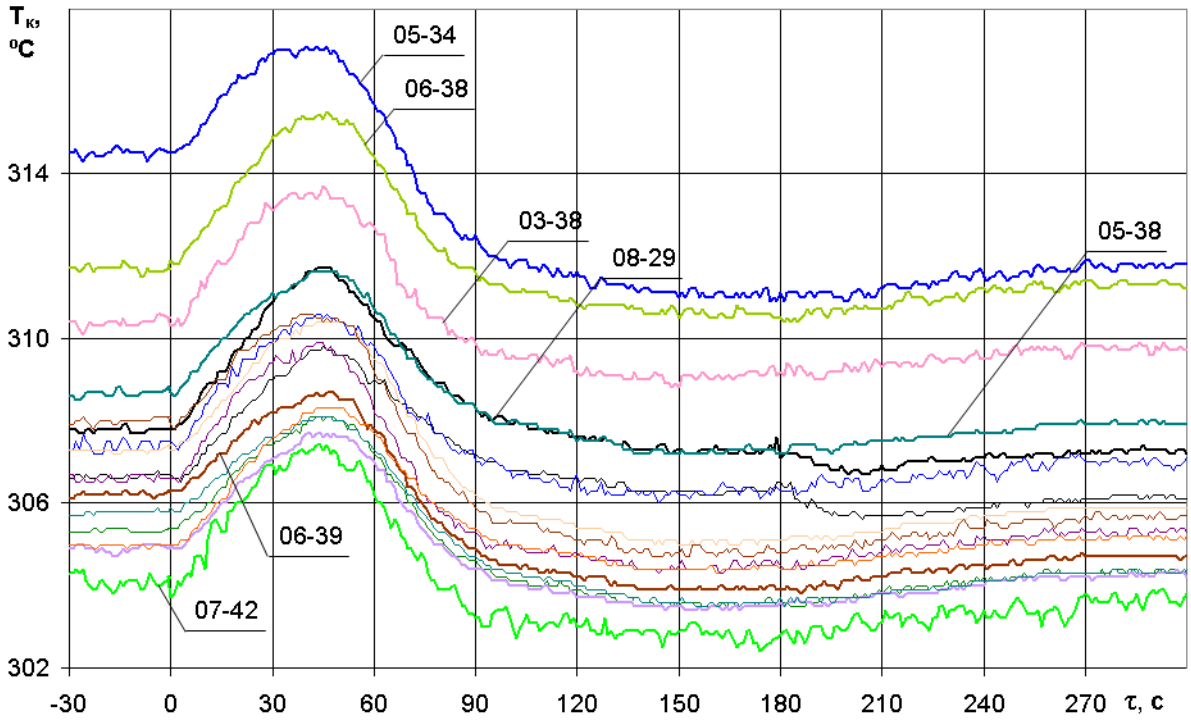

T_k in FA: 08-29; 08-35; 07-40; 07-42; 08-37; 08-39; 05-38; 05-40; 06-39; 06-38; 07-32; 07-34; 07-38; 03-38; 04-35; 05-34;05-36; 03-36

Fig. 47 – FA outlet coolant temperature histories of sector #4 recorded by the ICMS

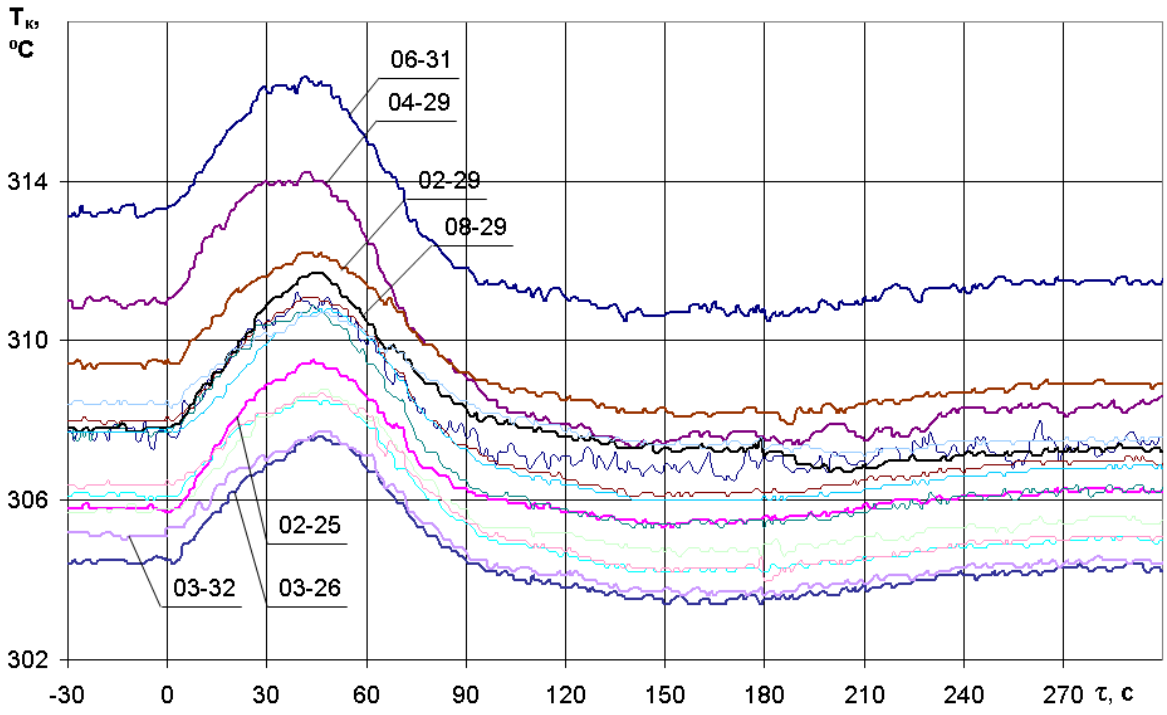

T_k in FA: 01-28; 02-25; 03-36; 03-28; 04-29; 06-29; 05-28; 08-29; 05-32; 06-31; 01-30; 02-29; 02-33; 03-30; 03-32

Fig. 48 – FA outlet coolant temperature histories of sector #5 recorded by the ICMS

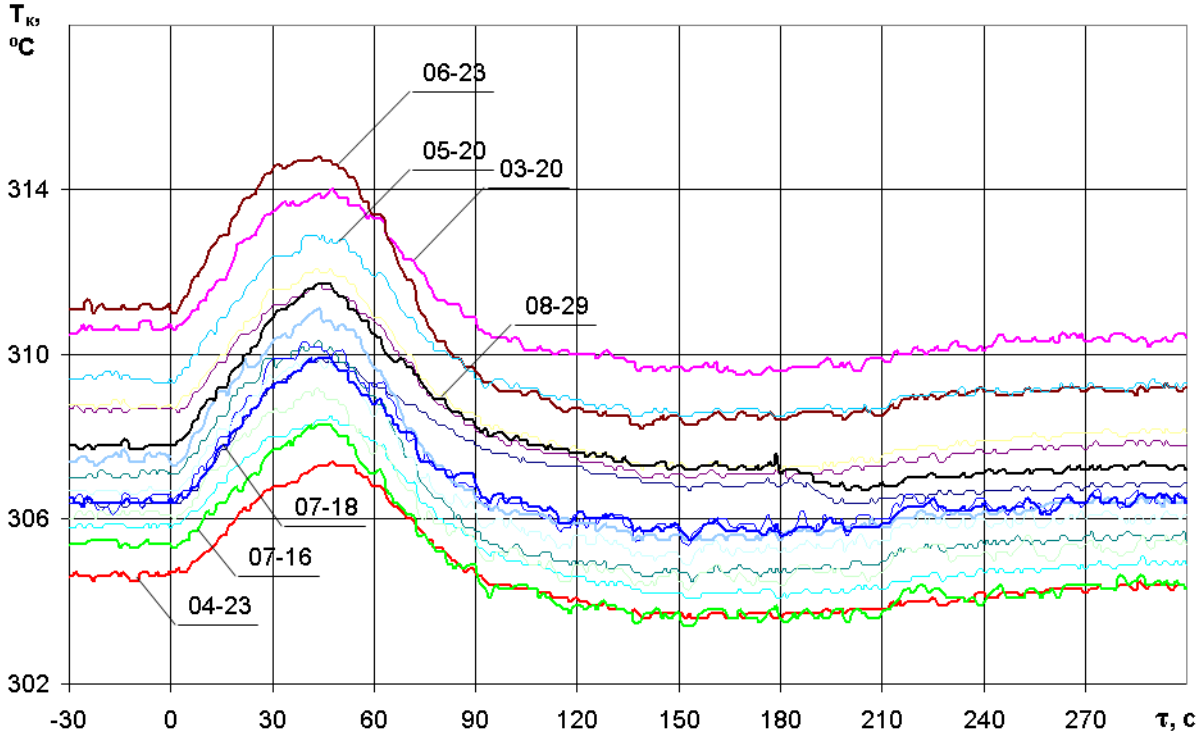

T_k in FA: 03-32; 03-20; 04-23;05-22;05-26; 06-23; 06-25; 05-18; 05-20; 06-21; 07-20; 07-26; 07-28; 07-16; 07-18; 08-29

Fig. 49 – FA outlet coolant temperature histories of sector #6 recorded by the ICMS

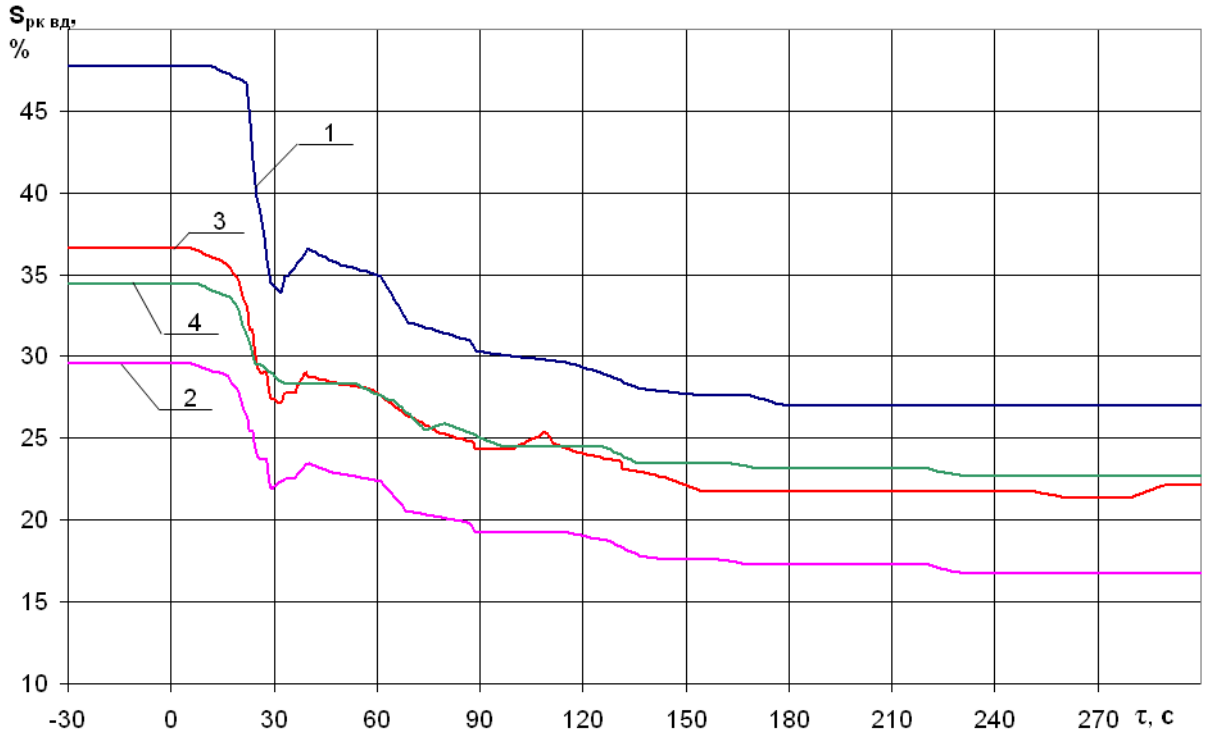

1– S_{RV1}; 2 – S_{RV2}; 3 – S_{RV3}; 4 – S_{RV4}

Fig. 50 – Change of the HP regulating valves' positions recorded by UBLS

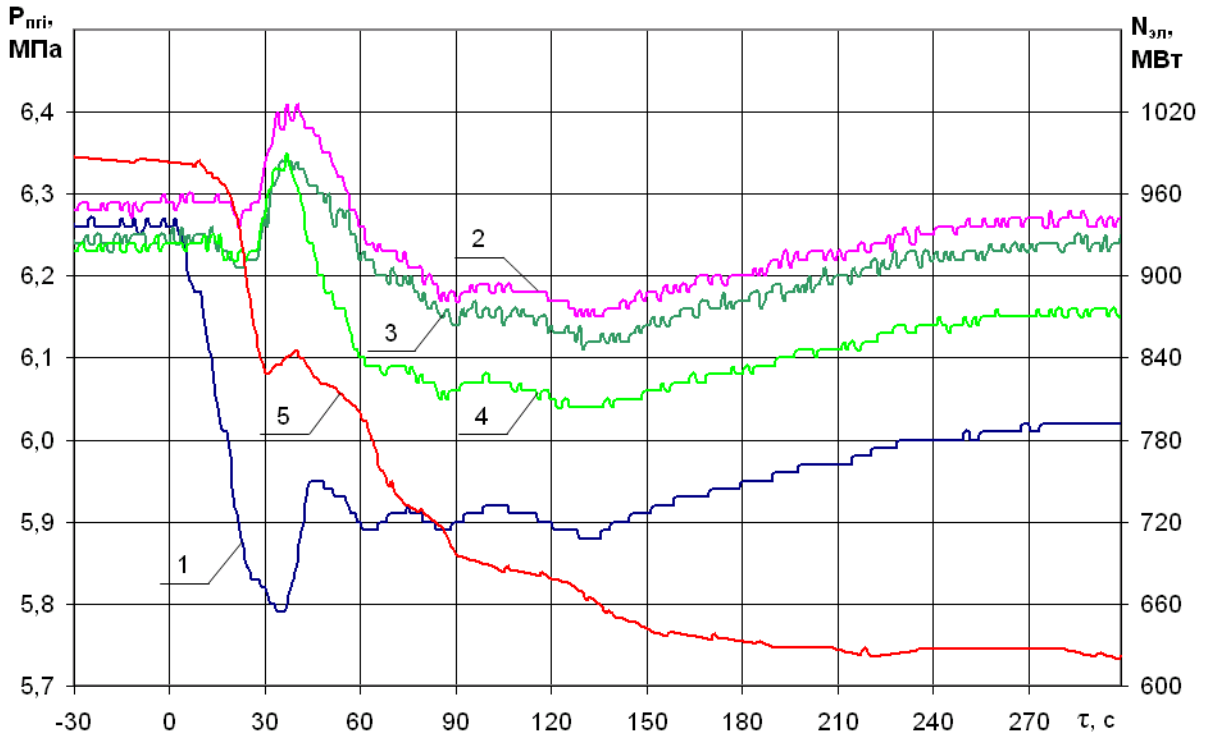

1 – P_{SG1}; 2 – P_{SG2}; 3 – P_{SG3}; 4 – P_{SG4}; 5 – $N_{эл}$

Fig. 51 – SG-#1–4 pressure histories and the electrical power history of TG recorded by the ICMS

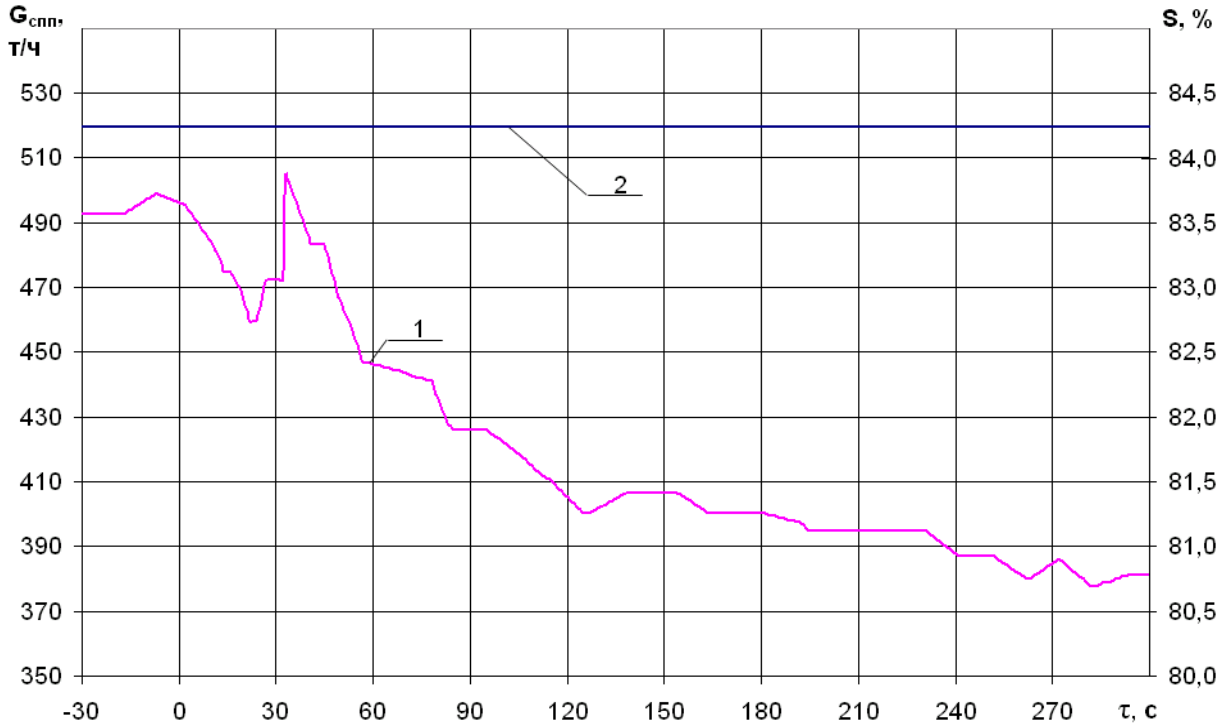

1 – G_{SSSH}; 2 – S_{RV}

Fig. 52 – SSSH heating steam flow rate histories and the time history of the RV position on the steam supply line of the SSSH

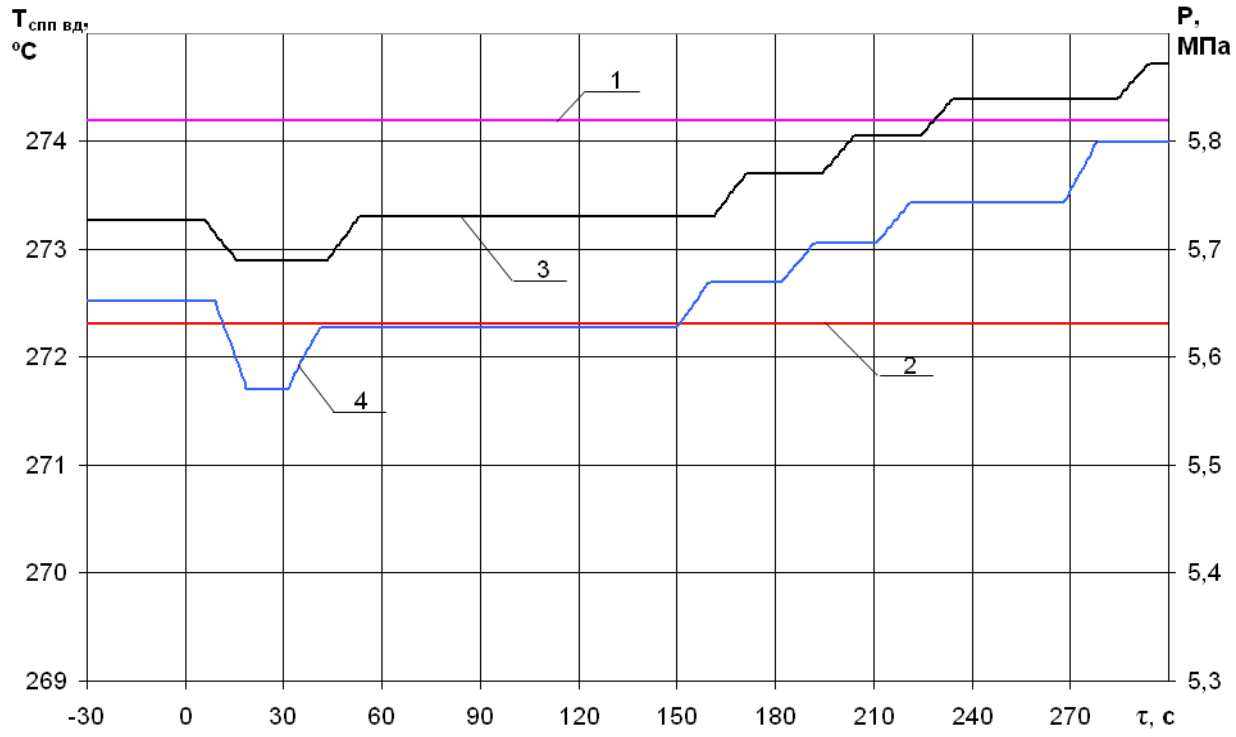

1 – T_{SSSH}; 2 – $T_{кнсб}$; 3 – P_{SSSH}; 4 – $RV_{нсб}$

Fig. 53 – Temperature and pressure histories of the heating steam upstream the SSSH and in the condensate collector recorded by the UBLS

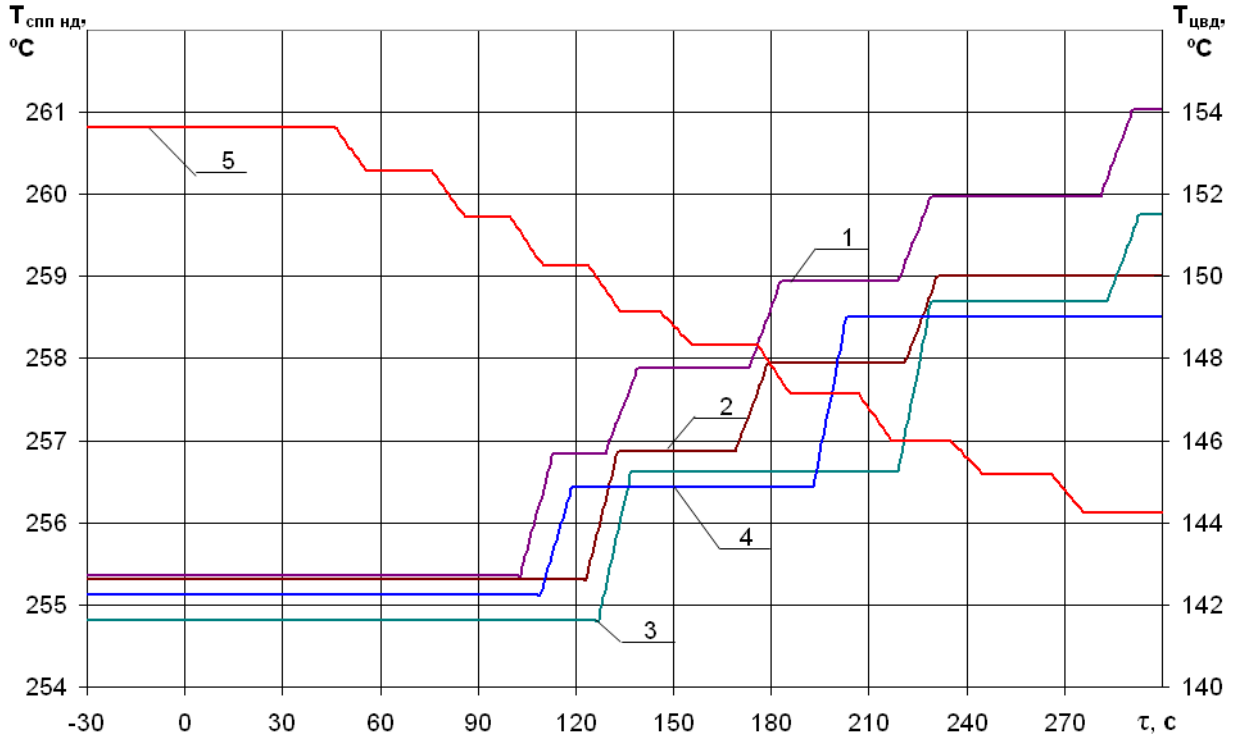

1 – $T_{SSSH\ нд1}$; 2 – $T_{SSSH\ нд2}$; 3 – $T_{SSSH\ нд3}$; 4 – $T_{SSSH\ нд4}$; 5 – $T_{НРТР}$

Fig. 54 – Steam temperature histories at the outlet of the HPTP and downstream of the low pressure SSSH1-4 recorded by UBLS

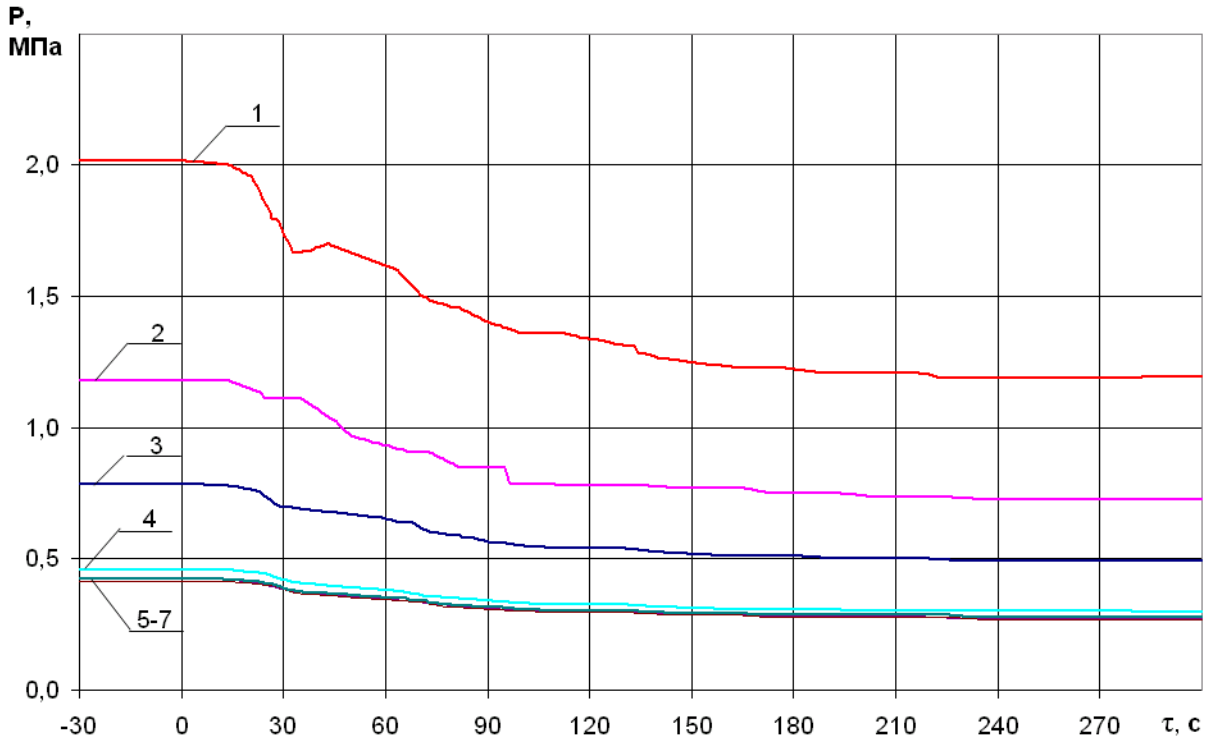

1 – $P_{отб1}$; 2 – $P_{отб2}$; 3 – $P_{отб3}$; 4 – $P_{НРТР1}$; 5 – $P_{НРТР2}$; 6 – $P_{НРТР3}$; 7 – $P_{НРТР4}$

Fig. 55 – Steam pressure histories of the intakes #1-3 and at the outlet from HPTP #1-4 recorded by UBLS during

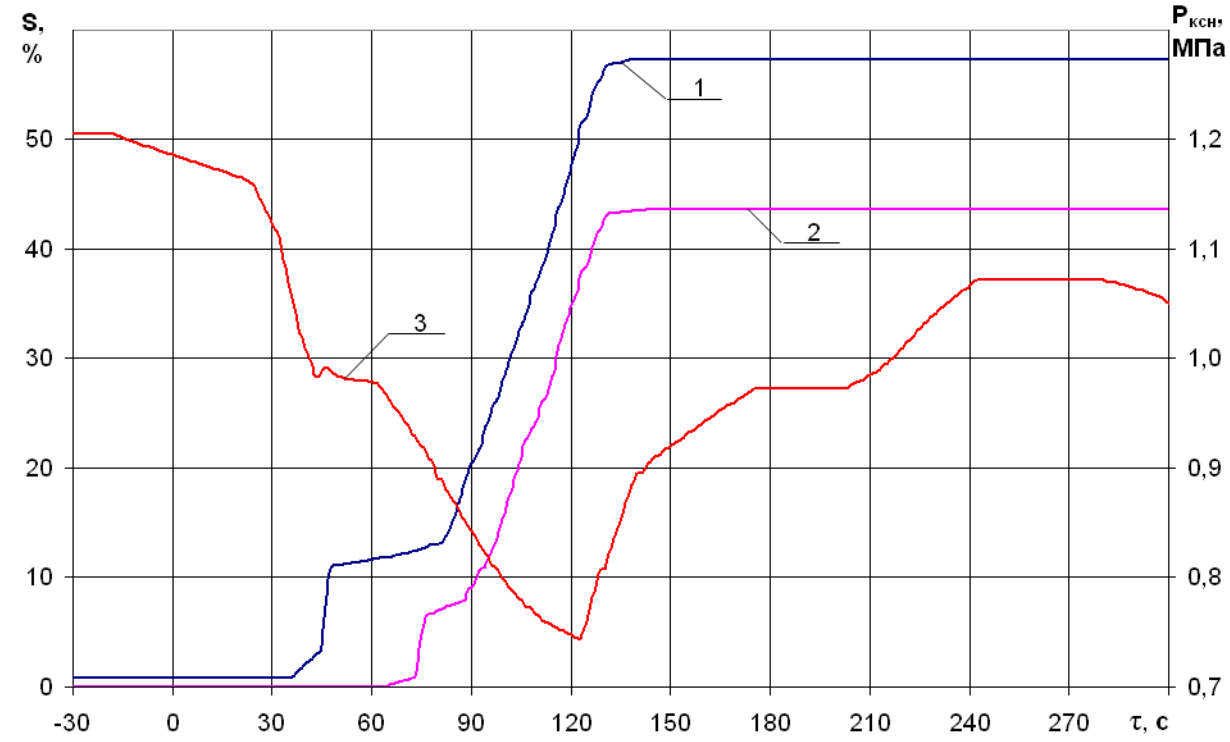

1– $S_{БРУ-СН1}$; 2 – $S_{БРУ-СН2}$; 3 – $RV_{СН}$

Fig. 56 – Change of the FASB-HL valve position and the pressure histories of ISC recorded by UBLS

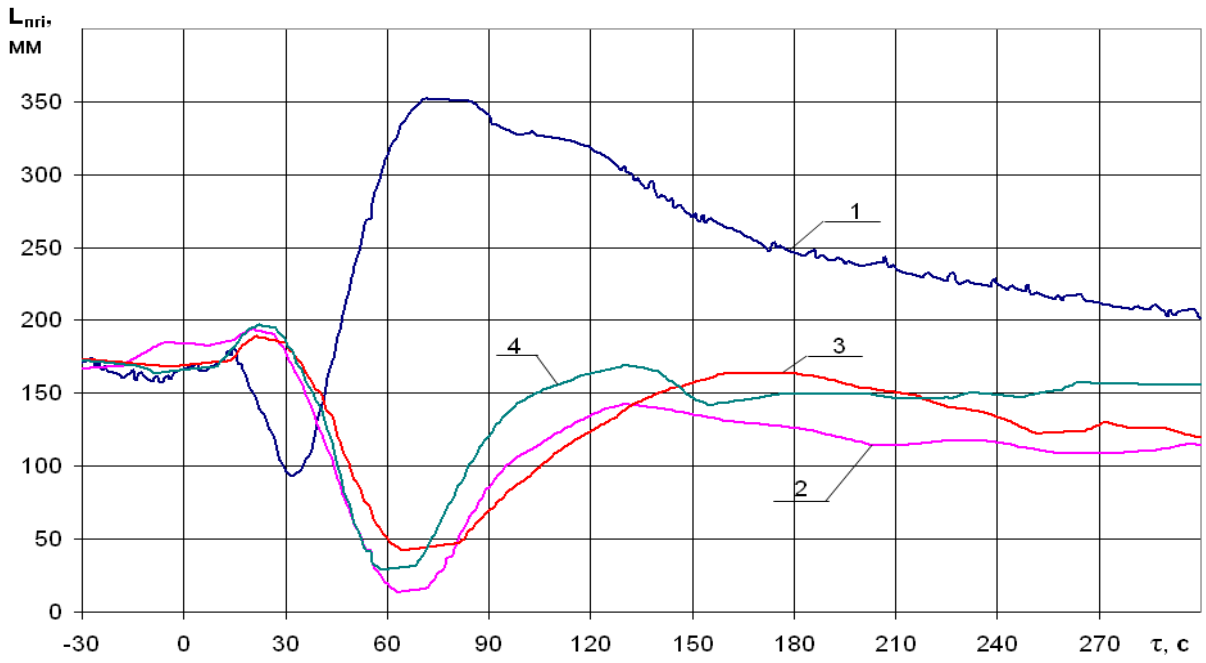

1 – L_{SG1}; 2 – L_{SG2}; 3 – L_{SG3}; 4 – L_{SG4}

Fig. 57 – SG water level histories (measurements on “small” basis) by UBLS

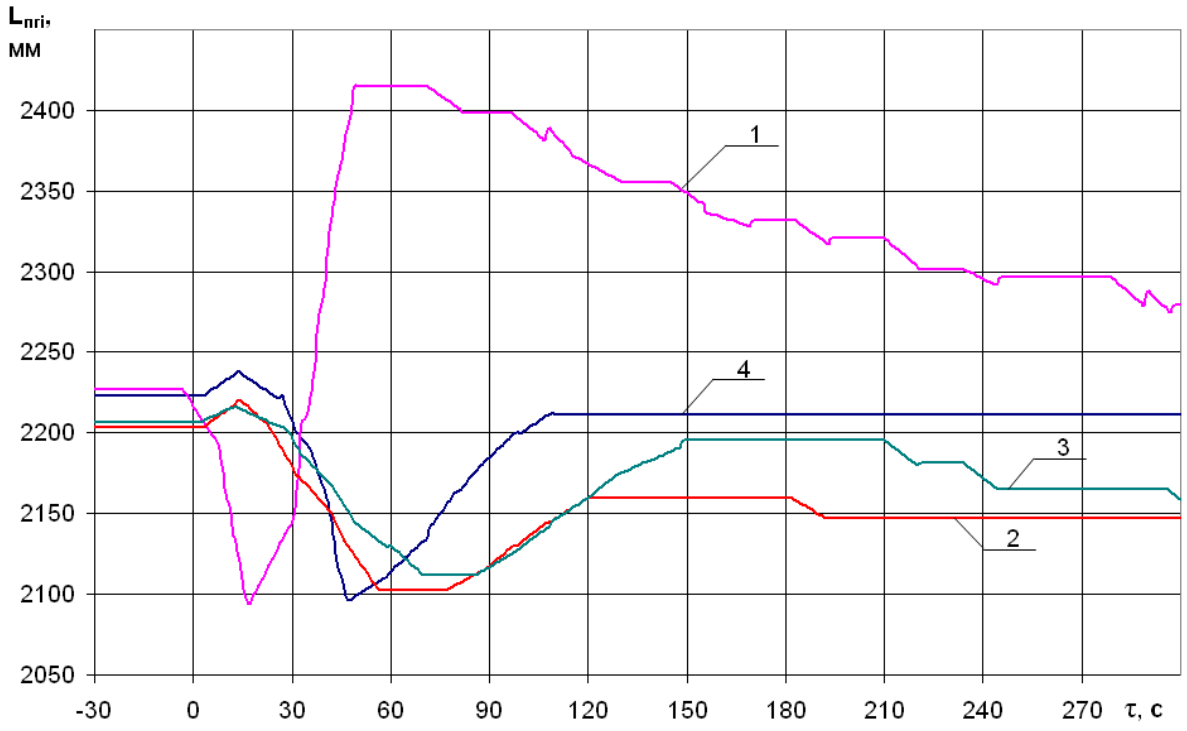

1 – L_{SG1}; 2 – L_{SG2}; 3 – L_{SG3}; 4 – L_{SG4}

Fig. 58 – SG water level histories (measurements on “large” basis) by UBLS

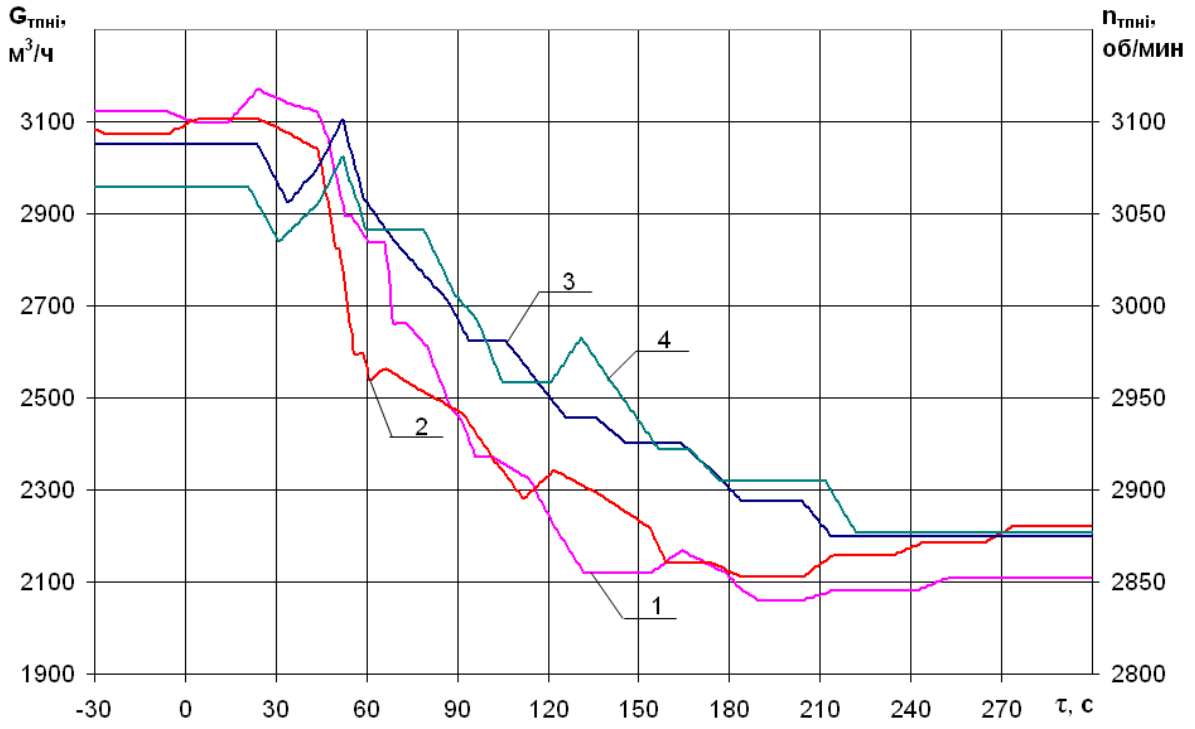

1 – G_{TFWP1}; 2 – G_{TFWP2}; 3– n_{TFWP1}; 4– n_{TFWP2}

Fig. 59 – Change in flow rates of the feedwater at pressure side and the rotation speed of the turbine feedwater pumps recorded by the UBLS

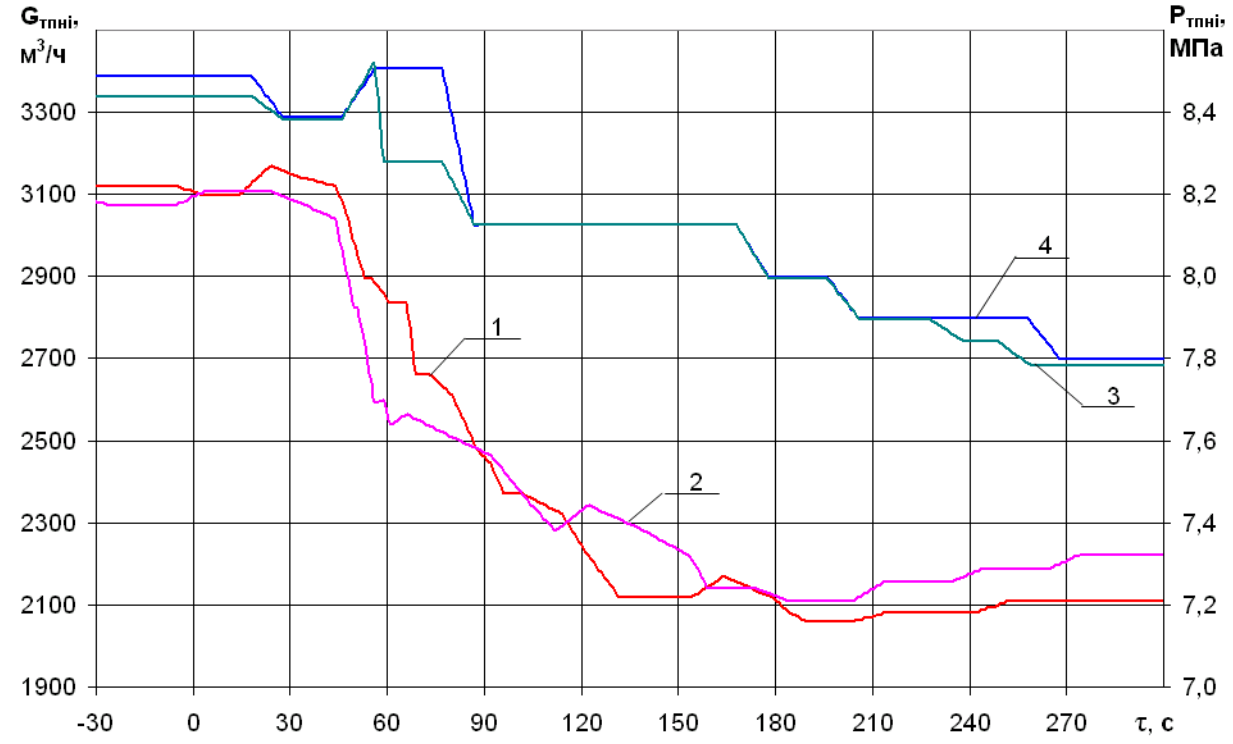

1– G_{TFWP1}; 2 – G_{TFWP2}; 3– P_{TFWP1}; 4– P_{TFWP2}

Fig. 60 – Feedwater flow rate histories and pressure at the pressure side of the TFWP-#1-2 recorded by UBLS

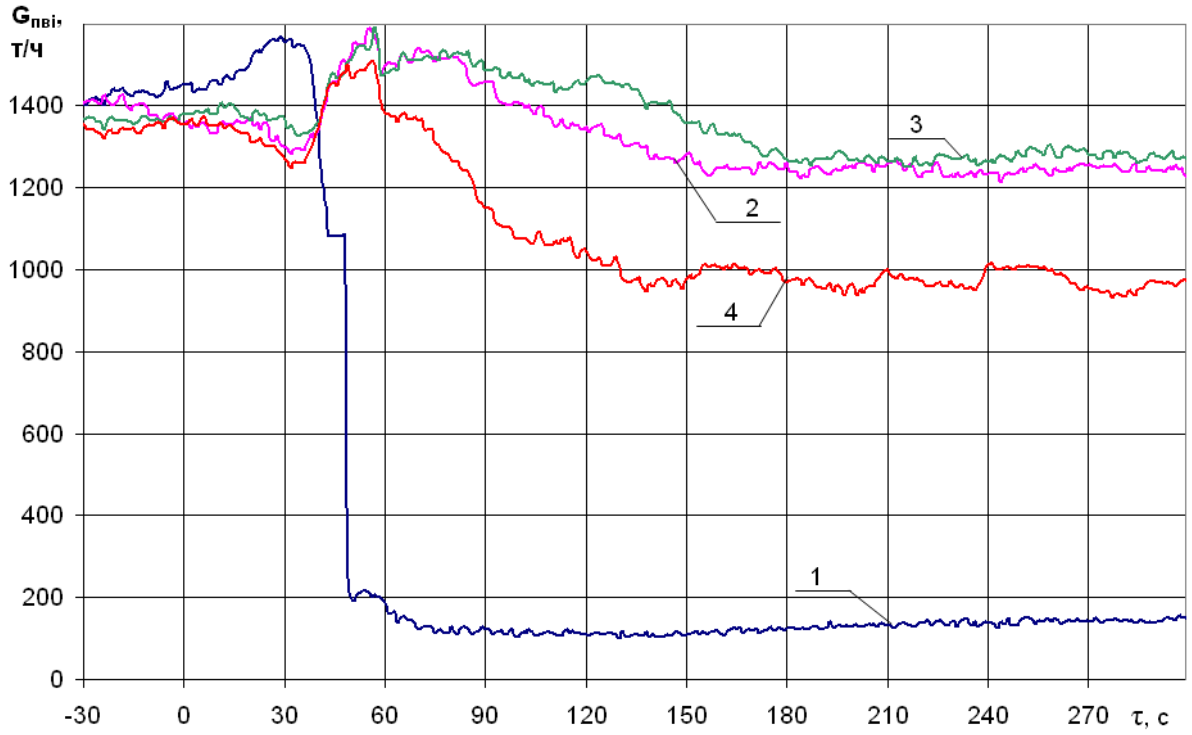

1 – $G_{пв1}$; 2 – $G_{пв2}$; 3 – $G_{пв3}$; 4 – $G_{пв4}$

Fig. 61 – SG-1–4 feedwater flow rate histories recorded by ICMS

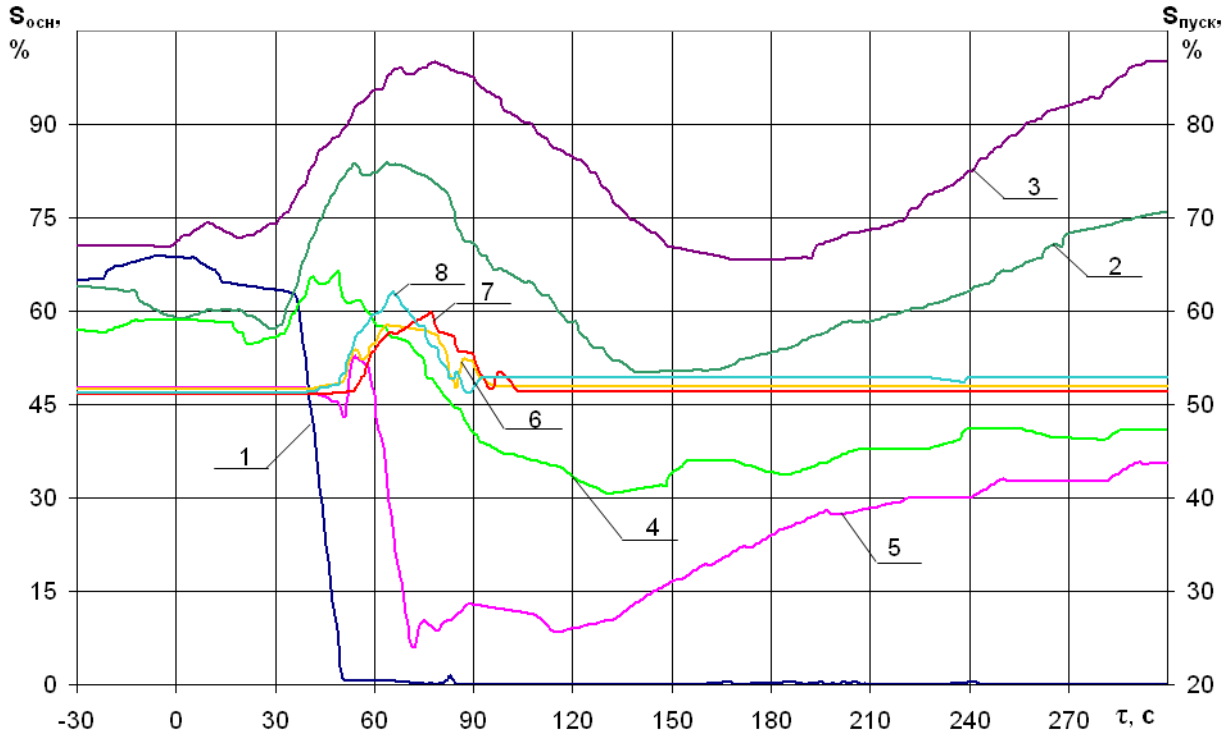

1 – $S_{осн1}$; 2 – $S_{осн2}$; 3 – $S_{осн3}$; 4 – $S_{осн4}$; 5– $S_{пуск1}$; 6 – $S_{пуск2}$; 7 – $S_{пуск3}$; 8 – $S_{пуск4}$

Fig. 62 – Degree of opening of the SG-1–4 feedwater main and starting valves recorded by the UBLS

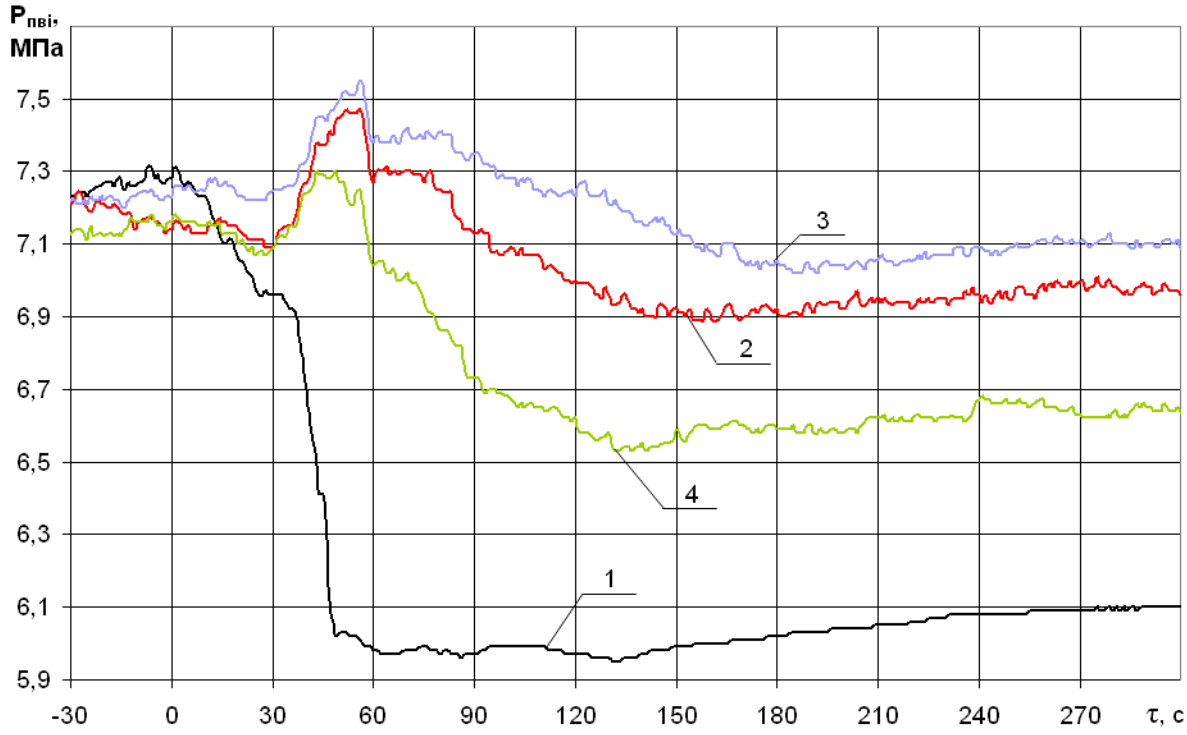

1 – $P_{пв1}$; 2 – $P_{пв2}$; 3 – $P_{пв3}$; 4 – $P_{пв4}$

Fig. 63 – SG-1–4 feedwater pressure histories recorded by the ICMS

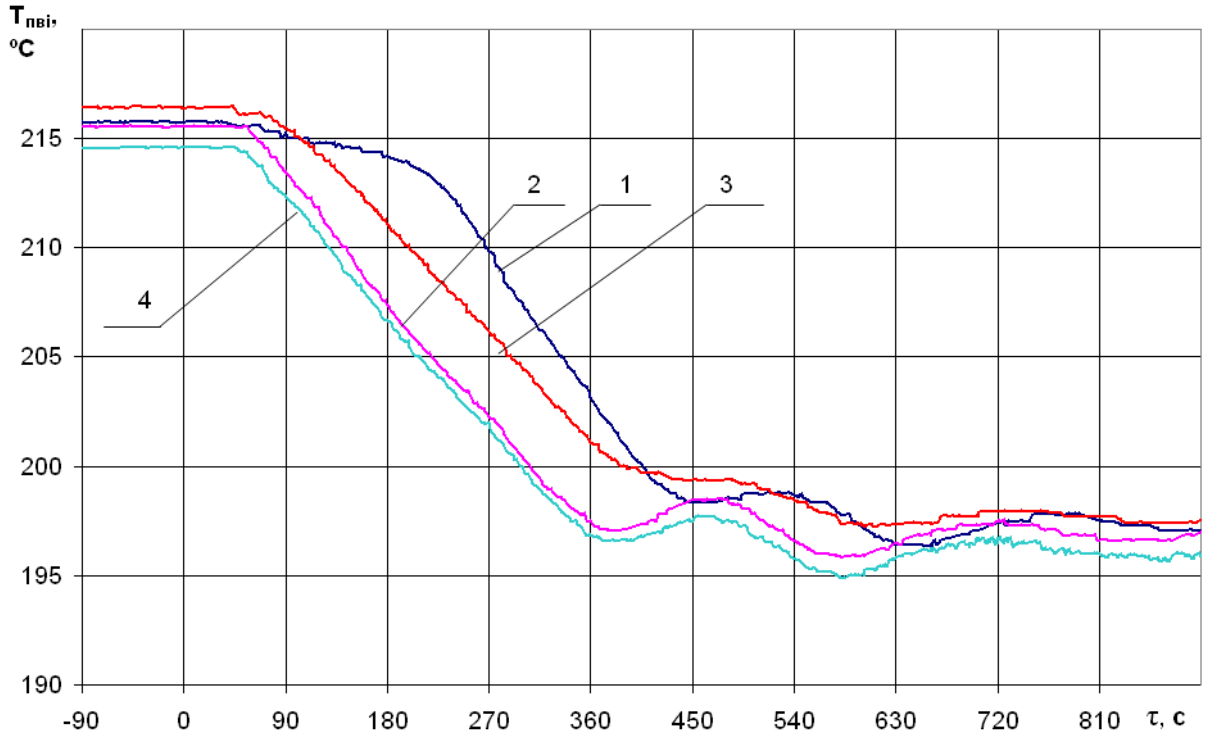

1 – $T_{пв1}$; 2 – $T_{пв2}$; 3 – $T_{пв3}$; 4 – $T_{пв4}$

Fig. 64 – SG-1–4 feedwater temperature histories recorded by the ICMS

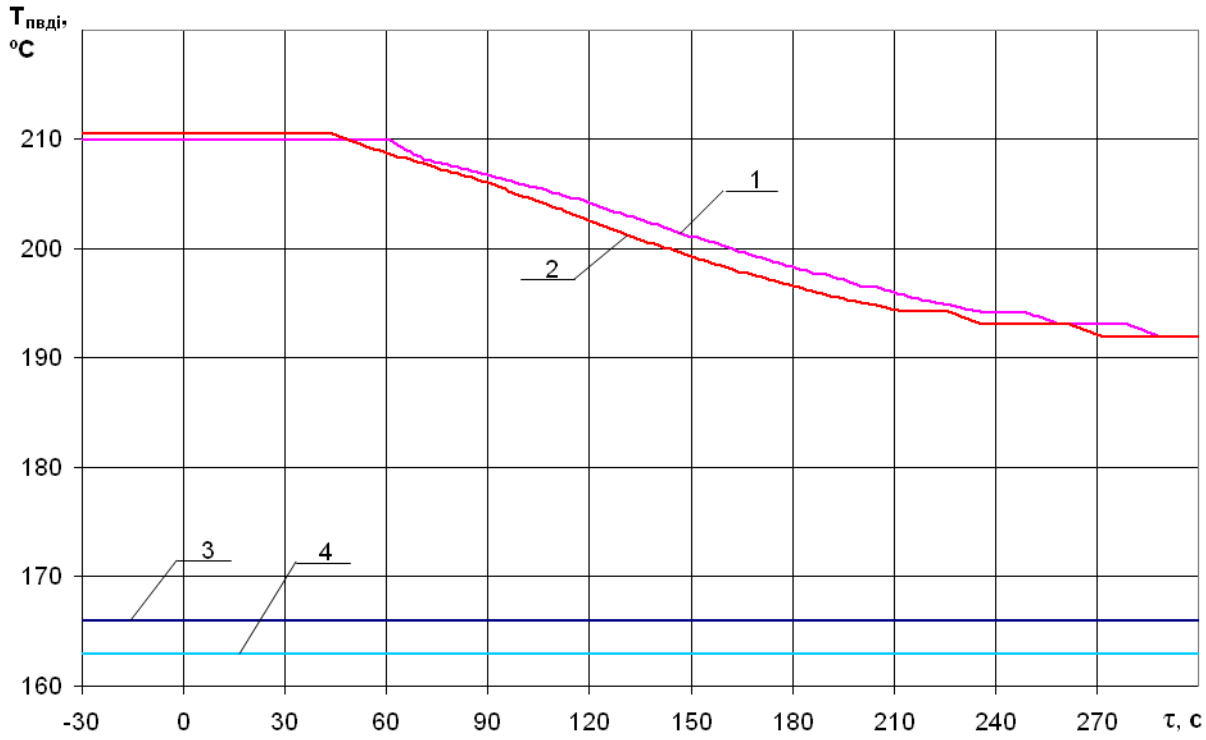

1 – $T_{НР\text{-}РН\ 1\ вых}$; 2 – $T_{НР\text{-}РН\ 2\ вых}$; 3 – $T_{НР\text{-}РН\ 1\ вх}$; 4 – $T_{НР\text{-}РН\ 2\ вх}$

Fig. 65 – Inlet and outlet feedwater temperature histories of the HP-PH recorded by UBLS

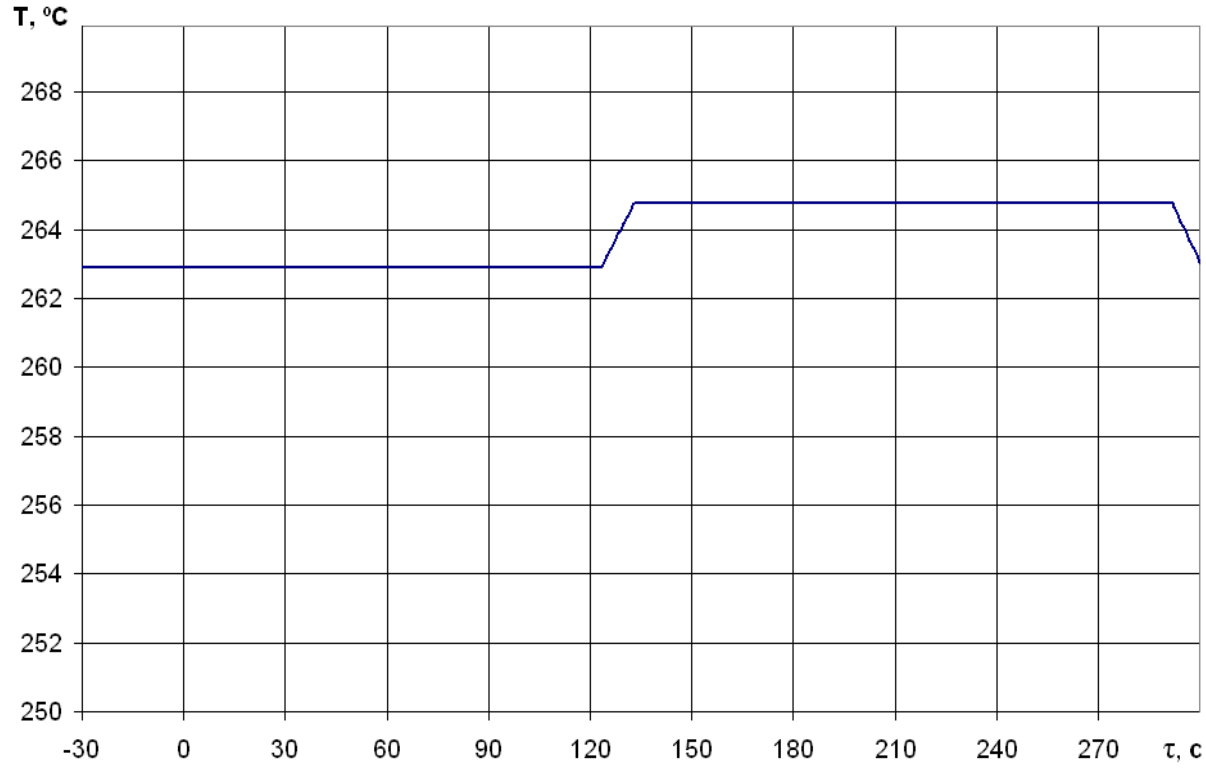

Fig. 66 – Feedwater temperature history at the pressure side of the condenser hydro-turbine pump recorded by UBLS

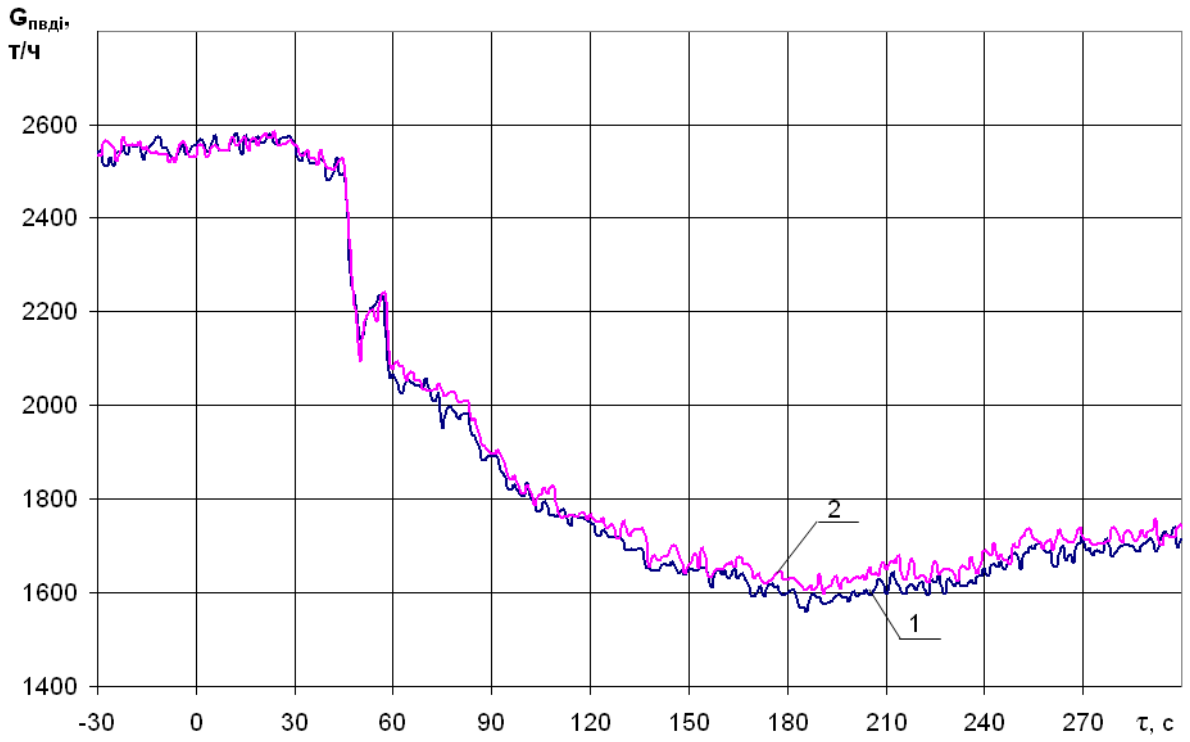

1 – $G_{HP\text{-}PH\ 1}$; 2 – $G_{HP\text{-}PH\ 2}$

Fig. 67 – Feedwater flow rates of HP-PH lines recorded by the ICMS

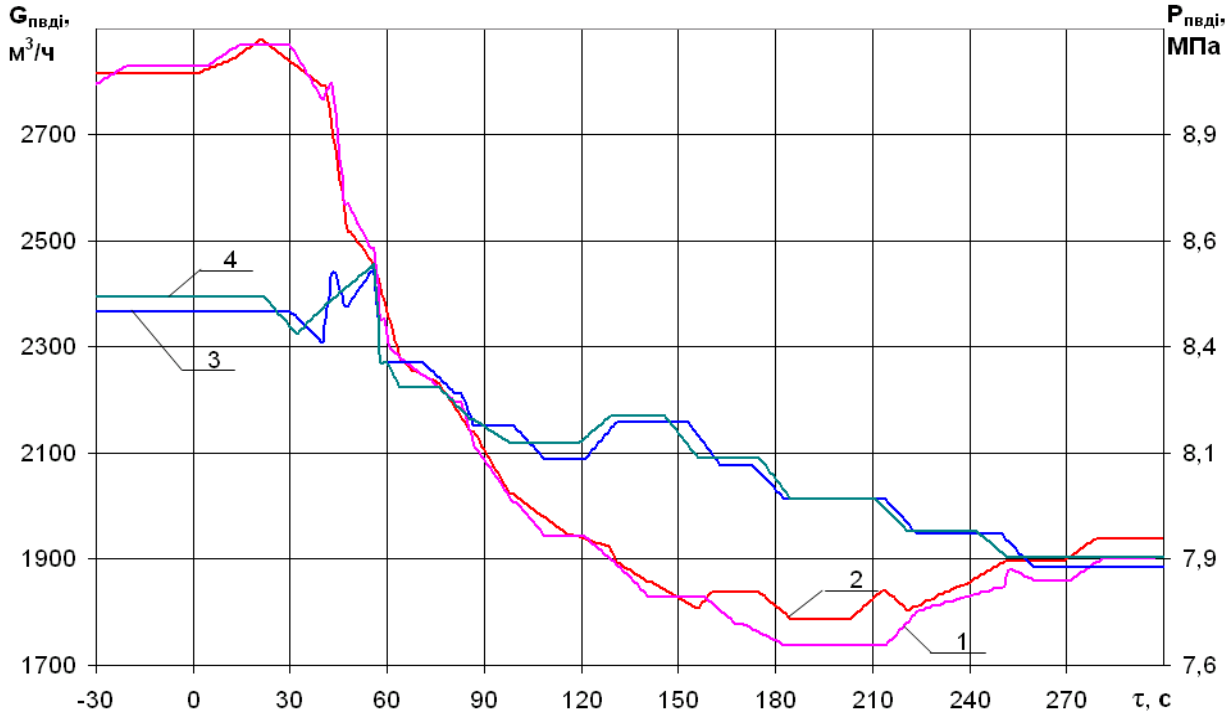

1 – $G_{HP\text{-}PH\ 1}$; 2 – $G_{HP\text{-}PH\ 2}$; 3 – $P_{HP\text{-}PH\ 1}$; 4 – $P_{HP\text{-}PH\ 2}$

Fig. 68 – Feedwater flow rates of the HP-PH lines recorded by the UBLS

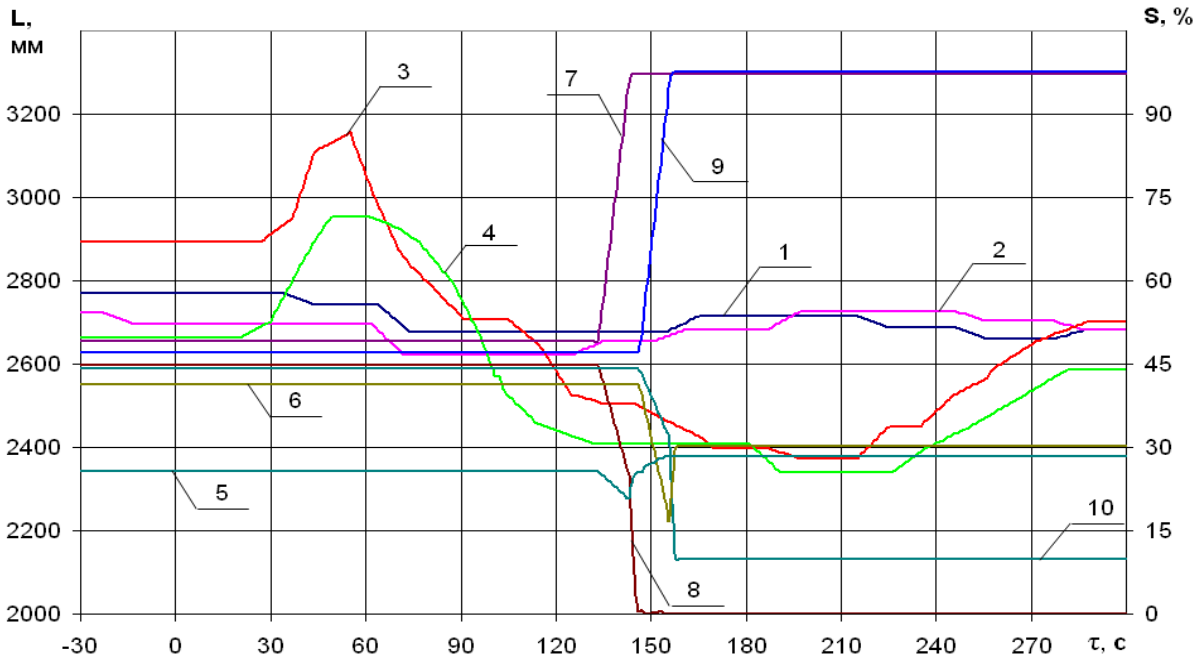

1 – $L_{HP\text{-}PH7\text{–}1}$; 2 – $L_{HP\text{-}PH7\text{–}2}$; 3 – $L_{HP\text{-}PH\ 6\text{–}1}$; 4 – $L_{HP\text{-}PH\ 6\text{–}2}$; 5 – $S_{RV\ ур7\text{-}1}$; 6 – $S_{RV\ ур7\text{-}2}$; 7 – $S_{RV\ ур6\text{-}1\ КНДР}$; 8 – $S_{RV\ ур6\text{-}1\ D7}$; 9 – $S_{RV\ ур6\text{-}2\ КНДР}$; 10 – $S_{RV\ ур6\text{-}2\ D7}$;

Fig. 69 – HP-PH #6,7 water level histories, position of the level regulator of the HP-PH #7-1,2, position of the level regulator of the of HP-PH #6-1,2 with the discharge of the condensate into THC and de-aerator D-7 recorded by UBLS

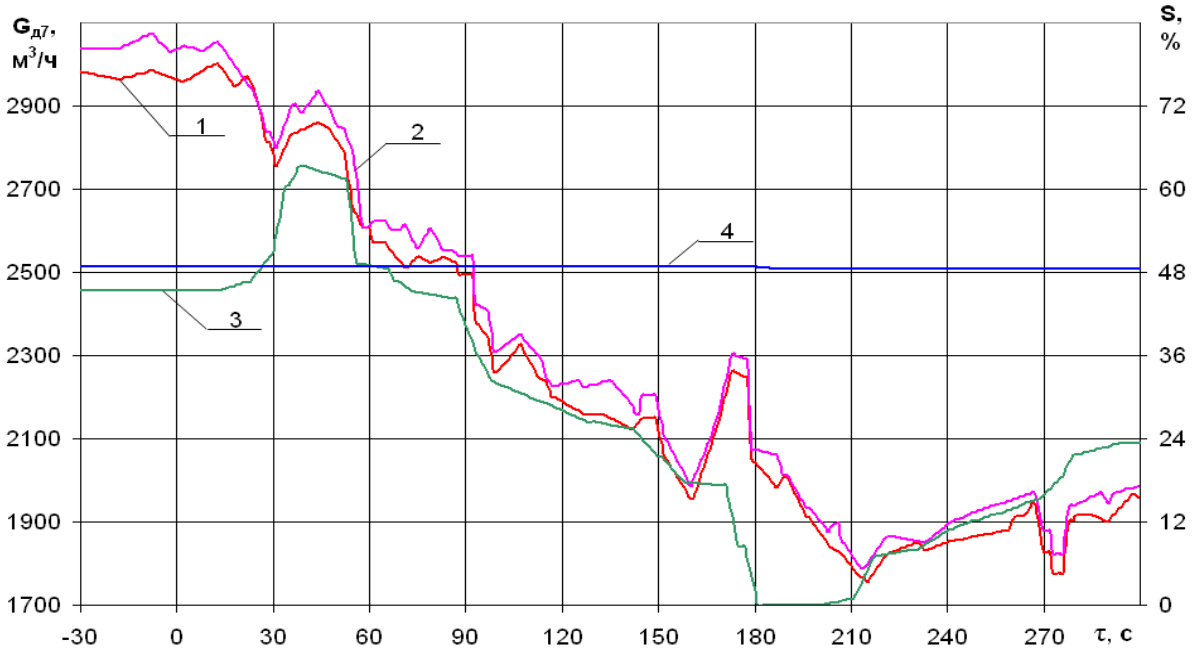

1 – $G_{D7\text{–}1}$; 2 – $G_{D7\text{–}2}$; 3 – $S_{осн}$; 4 – $S_{пуск}$

Fig. 70 – De-aerator (D7) flow rate history and the positions of the main and starting level regulators recorded by UBLS

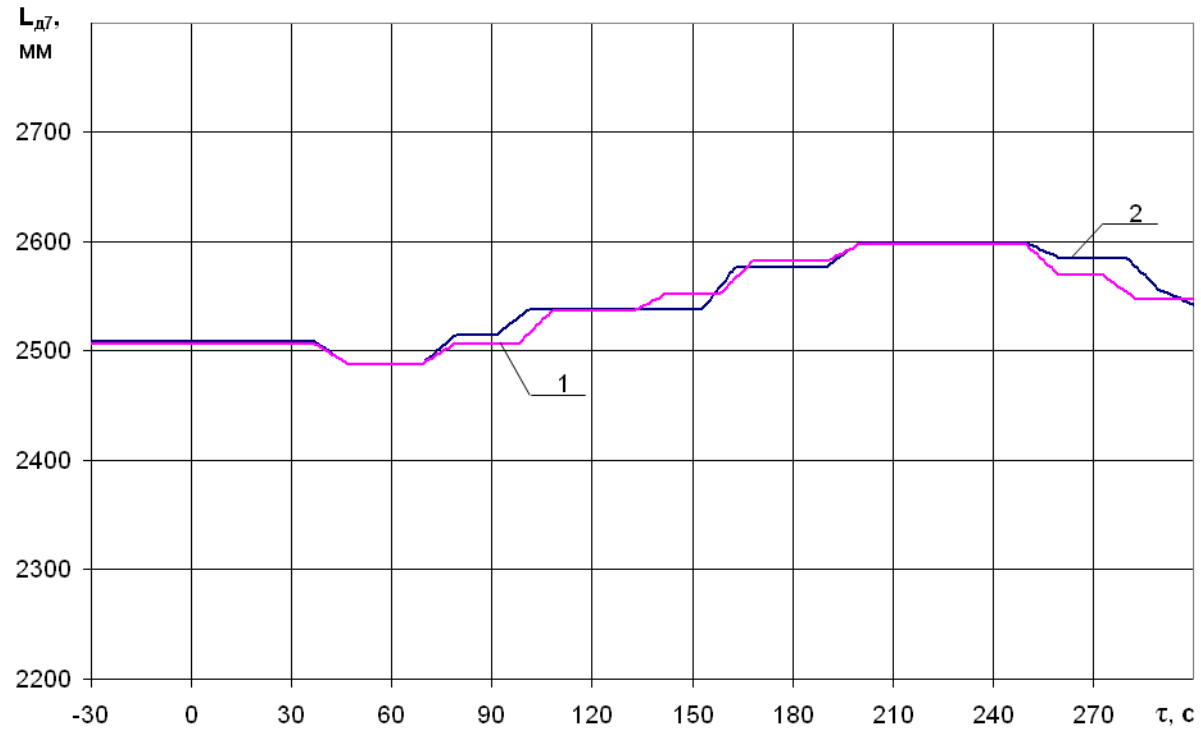

1 – L_{D7-1}; 2 – L_{D7-2}

Fig. 71 – De-aerator (D7) water level histories recorded by the UBLS

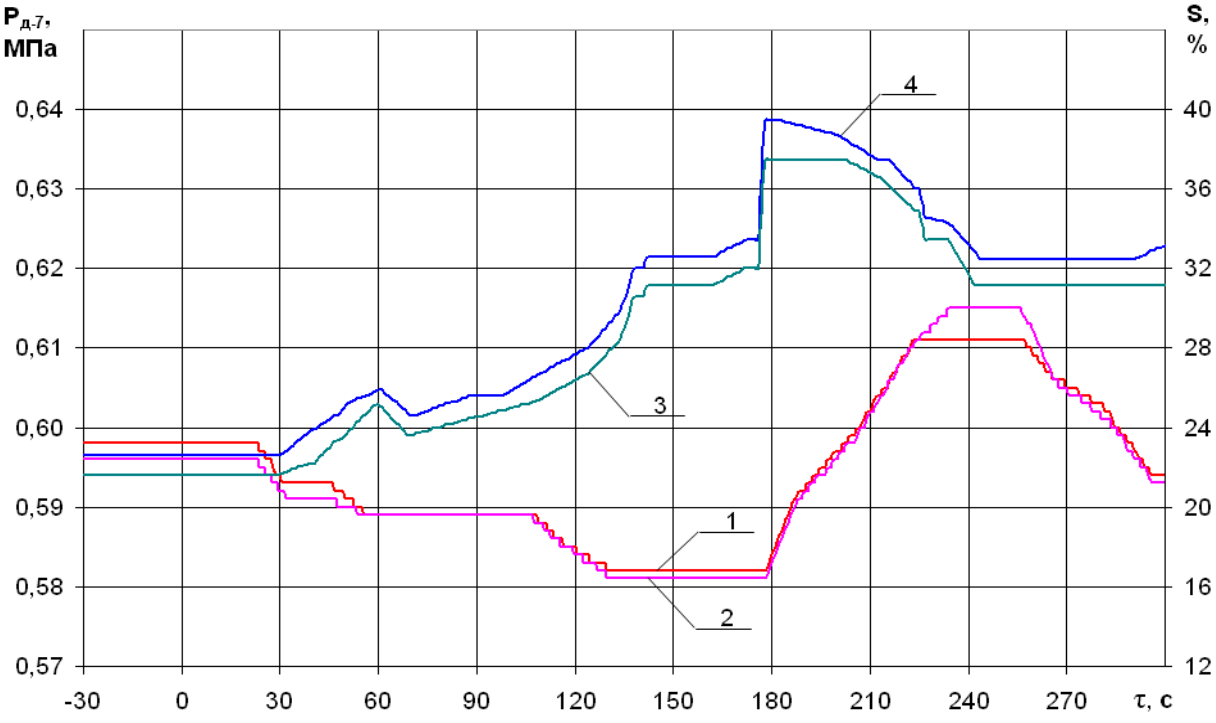

1 – P_{D7-1}; 2 – P_{D7-2}; 3 – $S_{30RQR21S08}$; 4 – $S_{30RQR22S08}$

Fig. 72 – De-aerator (D7) pressure histories and the positions of the control valves of the heating steam supply into de-aerator columns recorded by the UBLS

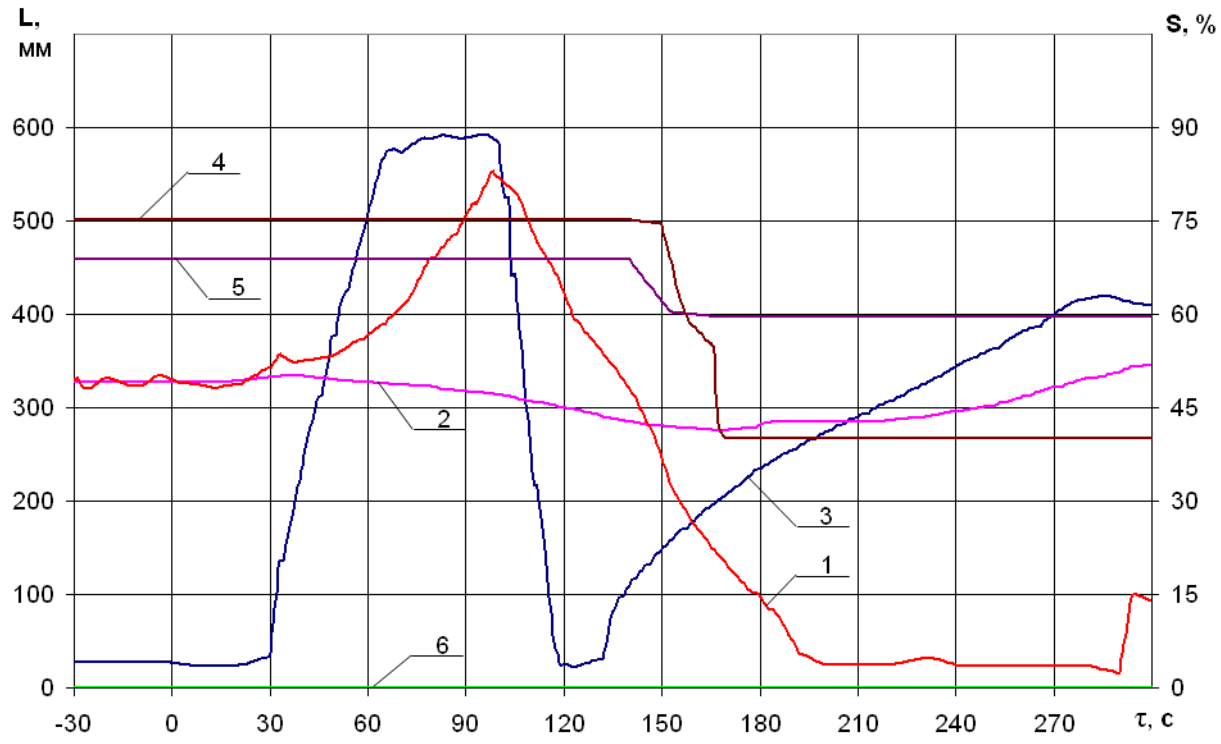

1 – $L_{LP\text{-}PH\text{–}3}$; 2 – $L_{LP\text{-}PH\text{–}4}$; 3 – $L_{LP\text{-}PH\text{–}5}$; 4 – $S_{RV\ LP\text{-}PH\text{-}3}$; 5 – $S_{RV\ LP\text{-}PH\text{-}4}$; 6 – $S_{RV\ LP\text{-}PH\text{-}5}$

Fig. 73 – Condensate level time-histories and the positions of the level regulators of LP-PH-3-5 recorded by the UBLS

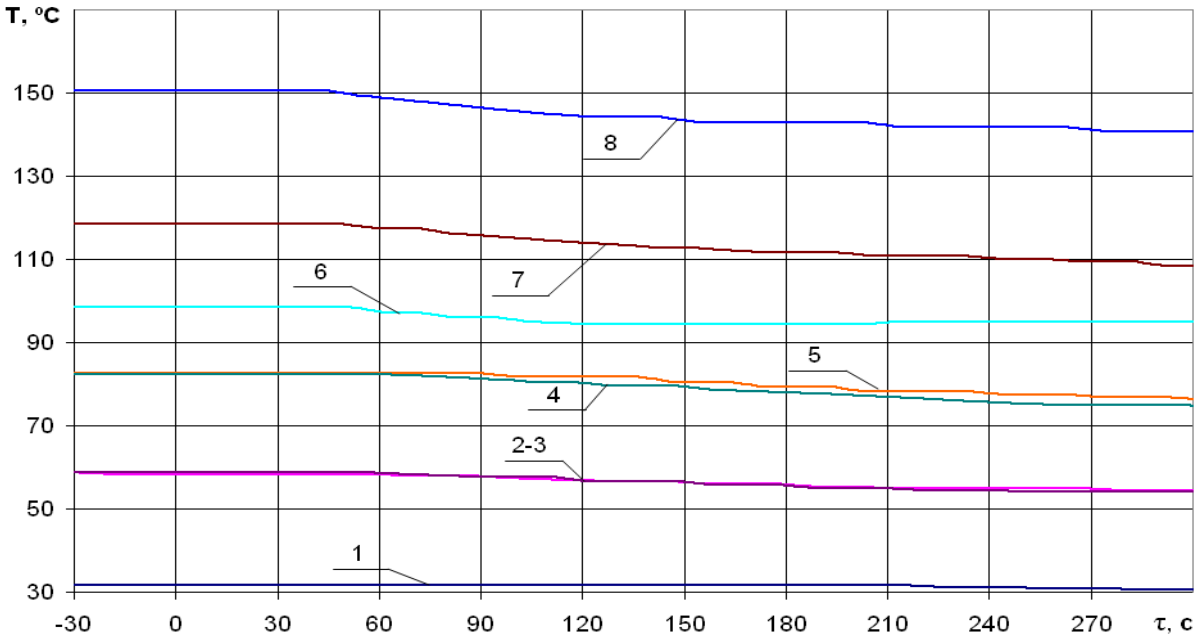

1 – $T_{всас\ CP\text{-}1}$; 2 – $TFWP_{д1\text{–}1}$; 3 – $TFWP_{д1\text{–}2}$; 4 – $T_{всас\ CP\text{-}2}$; 5 – $TFWP_{д\text{–}3\ вх}$; 6 – $TFWP_{д\text{–}3\ вых}$; 7 – $TFWP_{д\text{–}4\ вых}$; 8 – $TFWP_{д\text{–}5\ вых}$

Fig. 74 – Temperature histories measured at the condensate line starting from the CP-1 till the inlet of LP-PH -#5 recorded by the UBLS

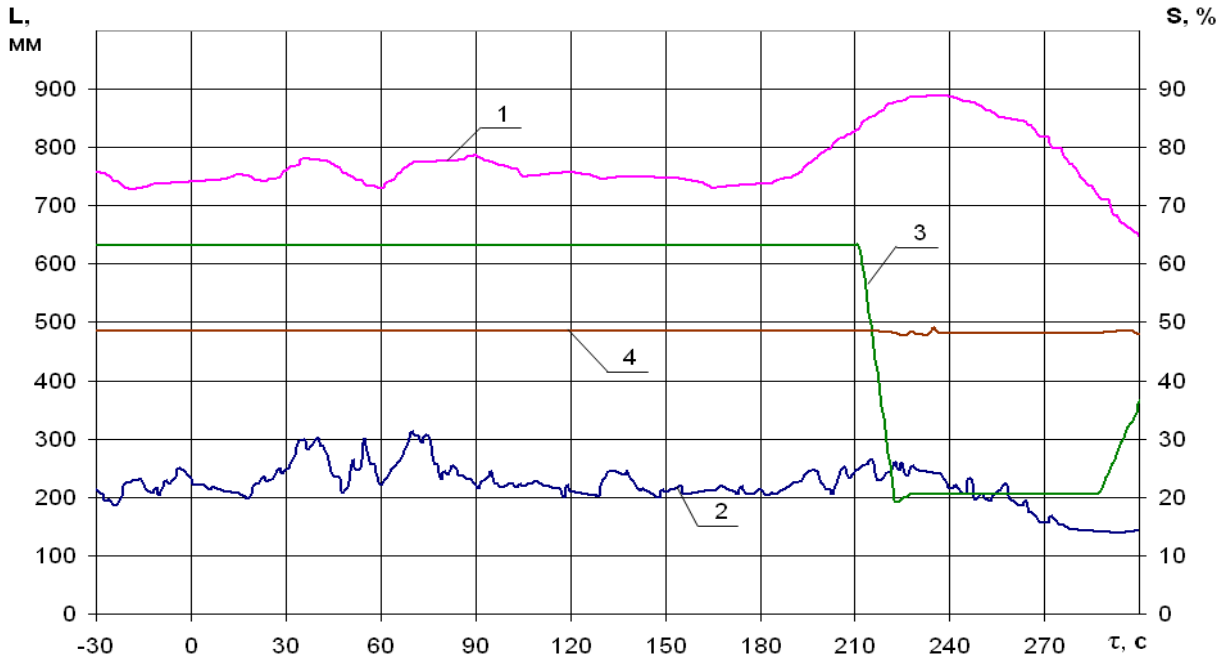

1 – $L_{LP\text{-}PH2\text{-}1000}$; 2 – $L_{LP\text{-}PH2\text{-}1600}$; 3 – $S_{осн}$; 4 – $S_{пуск}$

Fig. 75 – Water level histories (by level measurements based on 1000 and 1600 mm) and the position of the main and starting level control valve of the LP-PH-#2 recorded by the UBLS

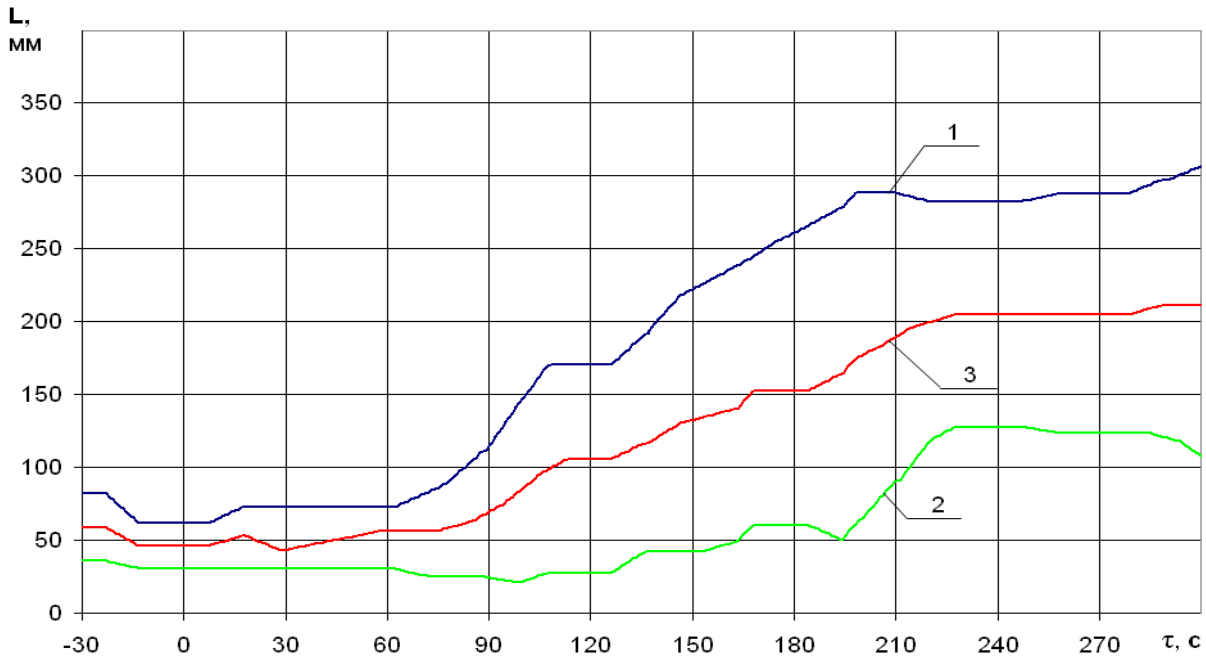

1 – $L_{LP\text{-}PH1\text{-}1}$; 2 – $L_{LP\text{-}PH1\text{-}2}$; 3 – $L_{LP\text{-}PH1}$

Fig. 76 – Water level histories of the LP-PH-1 recorded by the UBLS

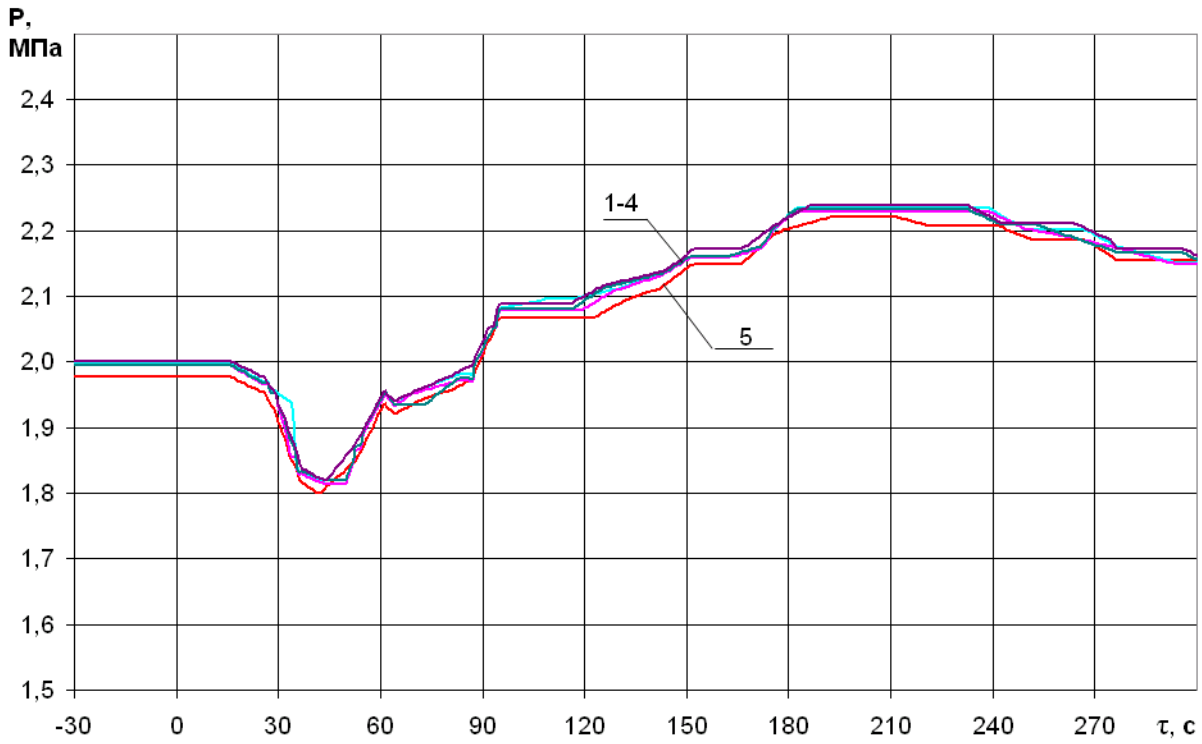

1 – P_{CP2-1}; 2 – P_{CP2-2}; 3 – P_{CP2-3}; 4 – P_{CP2-4}; 5 – P_{CP2}

Fig. 77 – Pressure histories at the pressure side of the CP-#2 1-4 and in the collector of the CP-#2 recorded by the UBLS

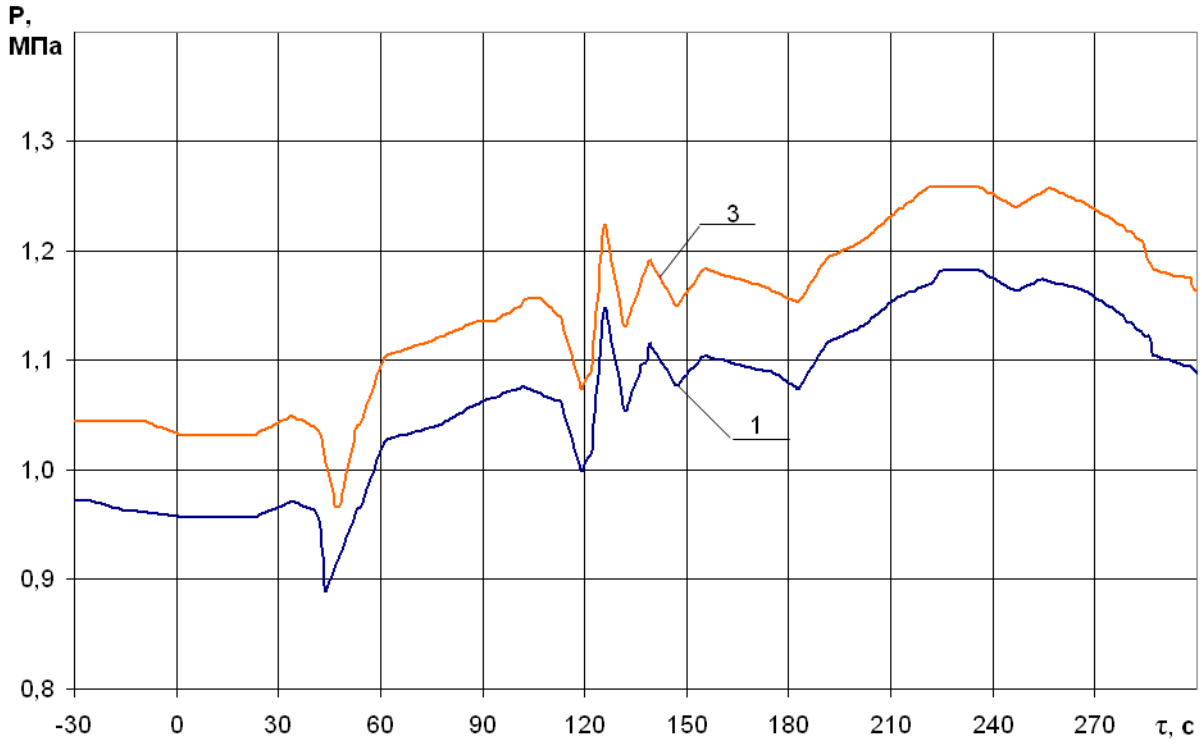

1 – P_{CP1-1}; 3 – P_{CP1-3}

Fig. 78 – Pressure history of CP-#1 1-3 recorded by UBLS

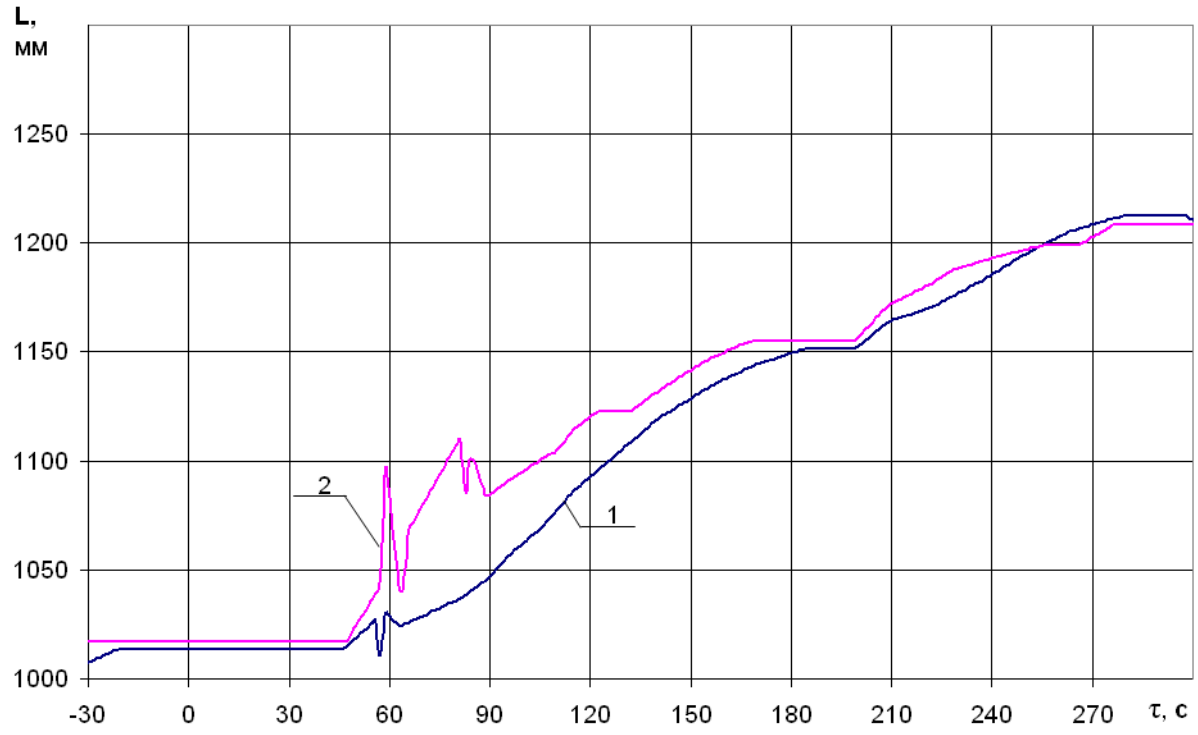

1 – $L_{SD11,12}$; 2 – $L_{SD13,14}$

Fig. 78 – Water level time history of the turbine condensers recorded by the UBLS

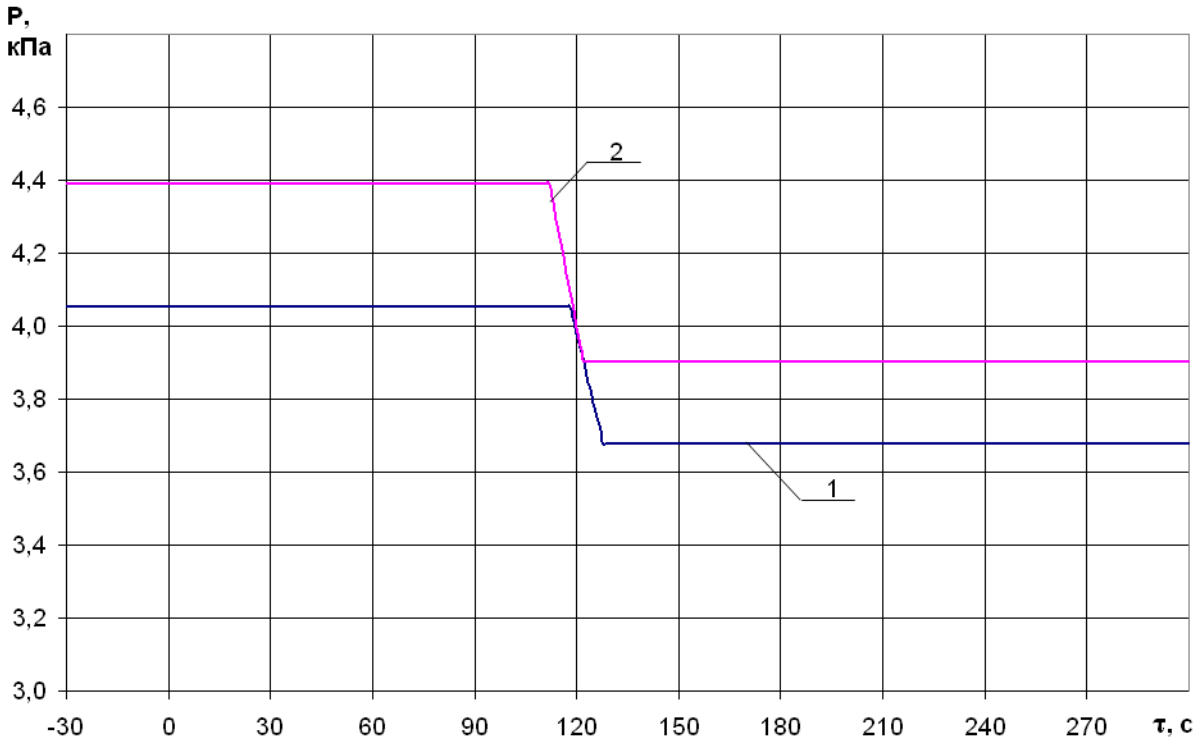

1 – $P_{SD11,12}$; 2 – $P_{SD13,14}$

Fig. 80 –Turbine condensers water level histories recorded by the UBLS

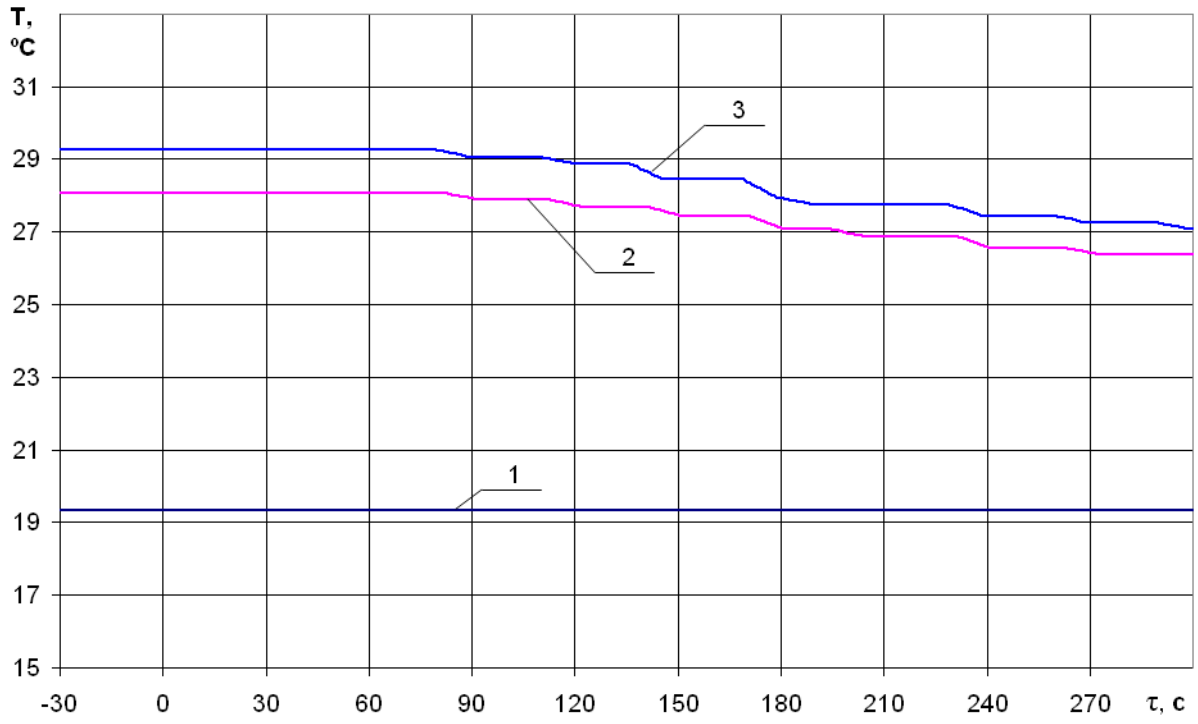

1– $T_{цв}$; 2 – $T_{цв1}$; 3 – $T_{цв2}$

Fig. 81 – Inlet and outlet condenser (group 1 and 2) circulation water temperature histories recorded by UBLS

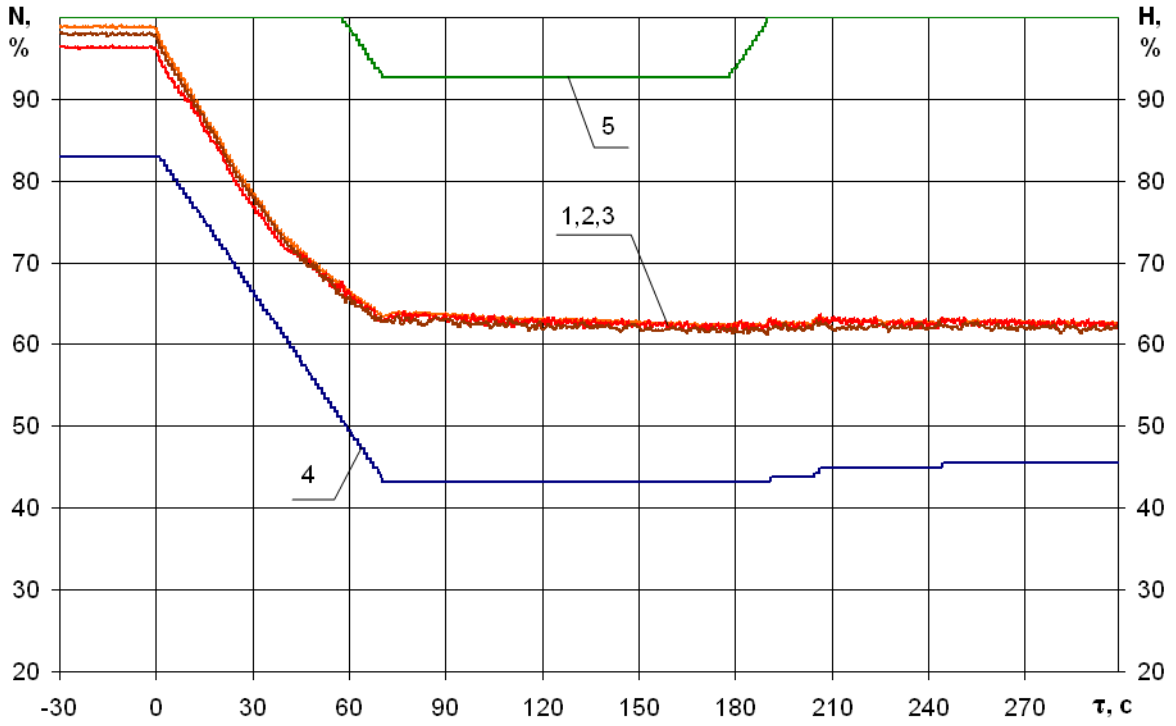

1 – $N_{ик7}$; 2 – $N_{ик17}$; 3 – $N_{ик27}$; 4 – H_{10}; 5 – H_9

Fig. 82 – Reactor power history recorded by NFC and the position change of CPS CR #10 and #9 recorded by MMS

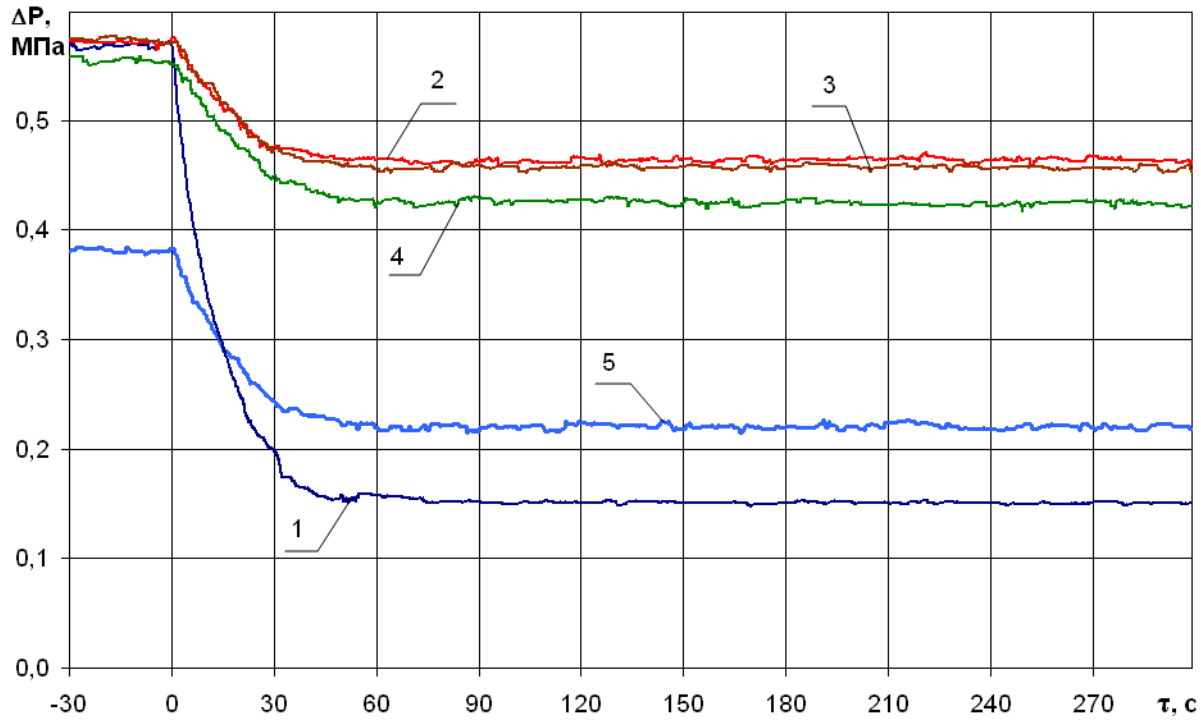

1 – $\Delta P_{МСР1}$; 2 – $\Delta P_{МСР2}$; 3 – $\Delta P_{МСР3}$; 4 – $\Delta P_{МСР4}$; 5 – $\Delta P_{р}$

Fig. 83 – Pressure difference histories of the MCPs and the reactor recorded by MMS

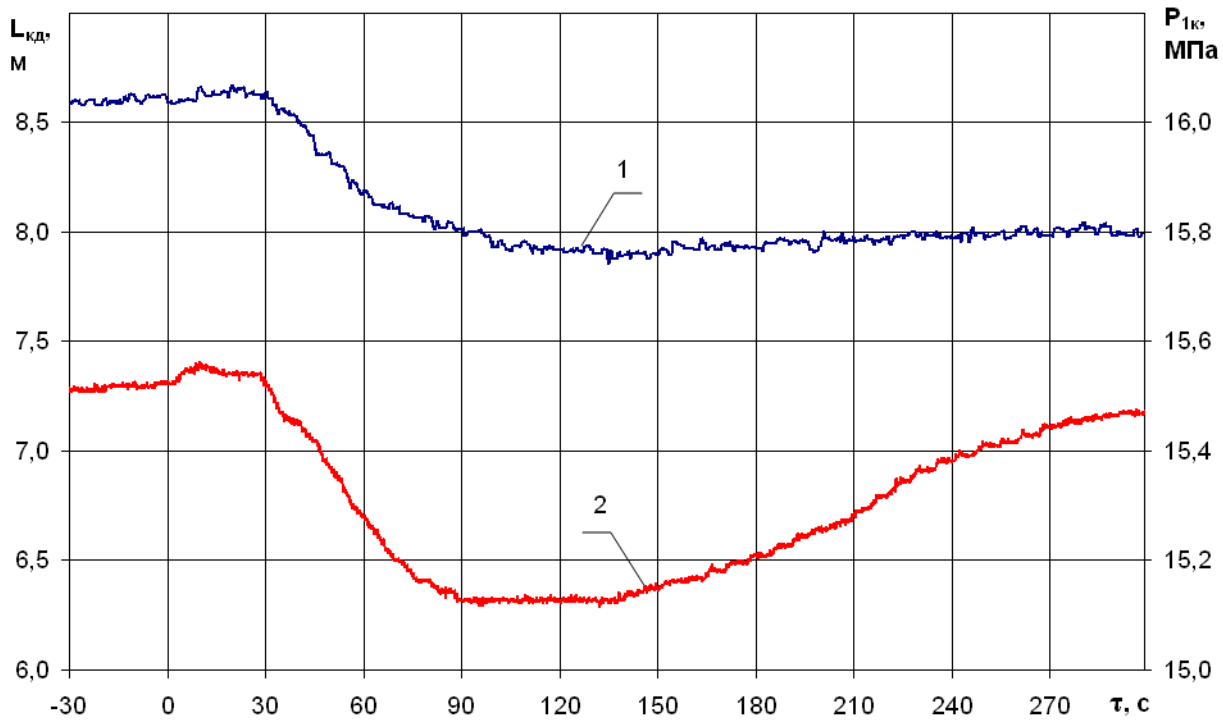

1 – $L_{кд}$; 2 – $P_{1к}$

Fig. 84 – PRZ water level history and the pressure history above the core recorded by MMS

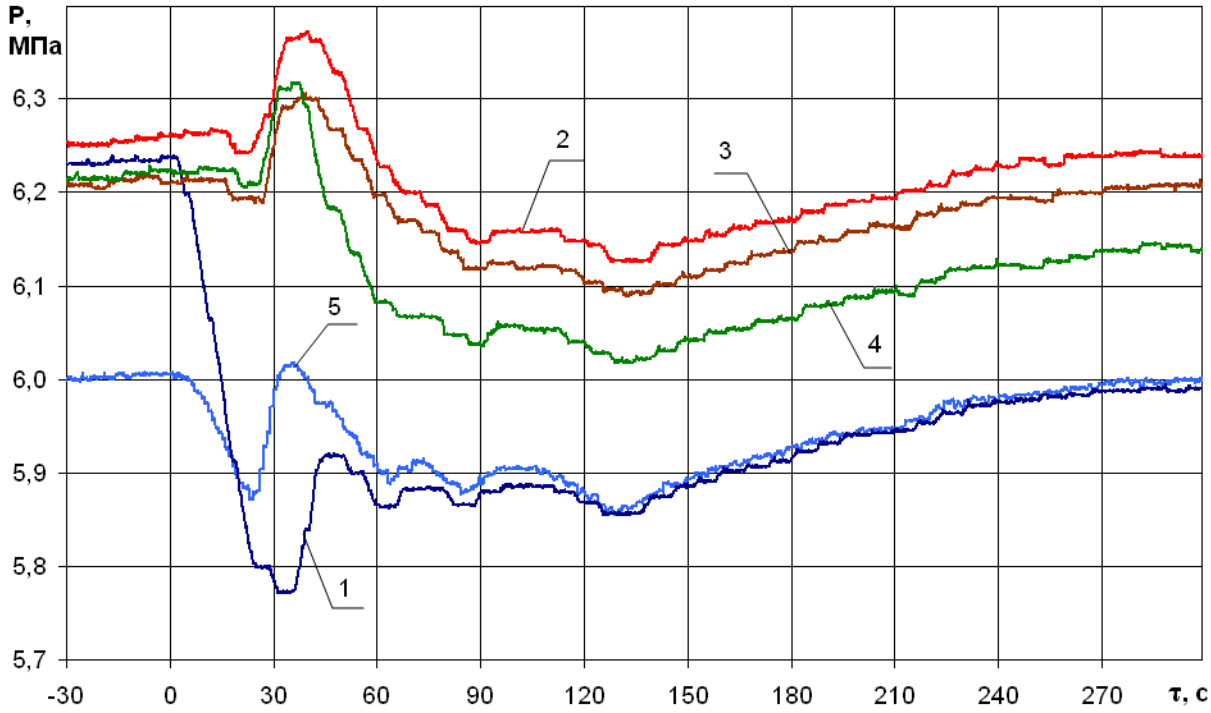

1 – P_{SG1}; 2 – P_{SG2}; 3 – P_{SG3}; 4 – P_{SG4}; 5 – P_{MSH}

Fig. 85 – SG pressure histories and main steam collector pressure history recorded by MMS

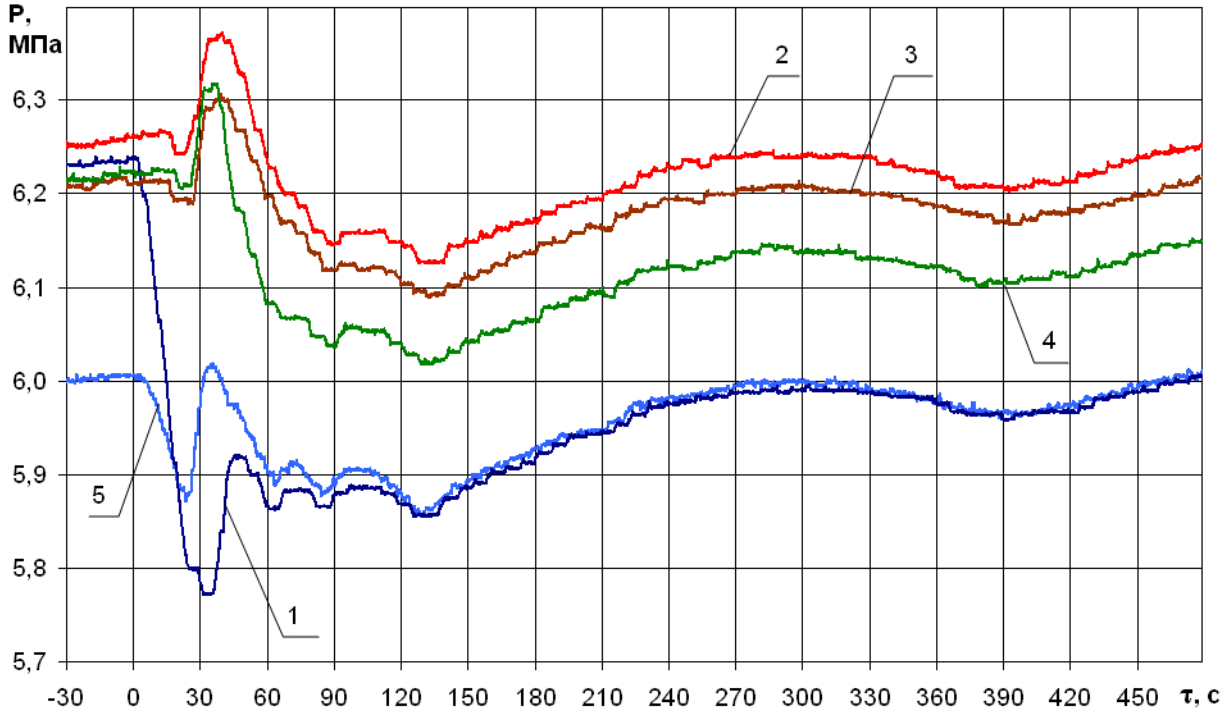

1 – P_{SG1}; 2 – P_{SG2}; 3 – P_{SG3}; 4 – P_{SG4}; 5 – P_{MSH}

Fig. 86 – SG pressure histories and main steam collector pressure history recorded by MMS

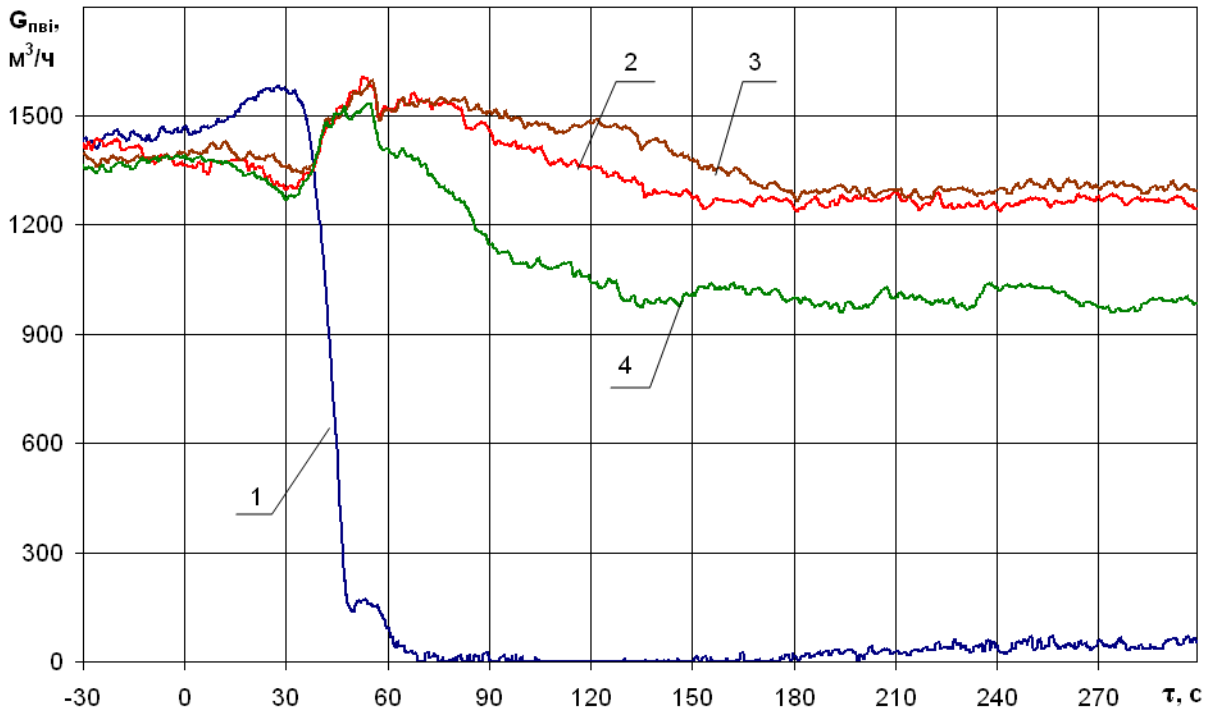

1 – $G_{пв1}$; 2 – $G_{пв2}$; 3 – $G_{пв3}$; 4 – $G_{пв4}$

Fig. 87 – SG inlet feedwater mass flow histories recorded by the MMS

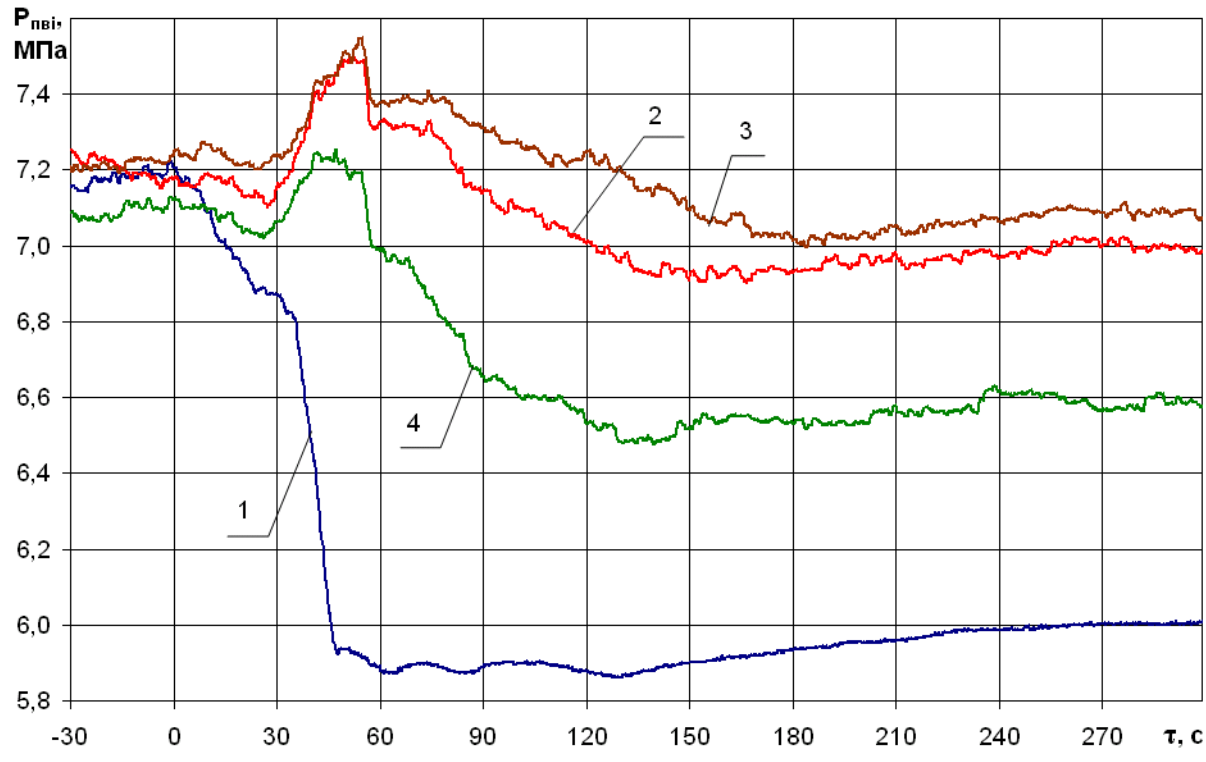

1 – $P_{пв1}$; 2 – $P_{пв2}$; 3 – $P_{пв3}$; 4 – $P_{пв4}$

Fig. 88 – SG inlet feedwater pressure histories recorded by the MMS

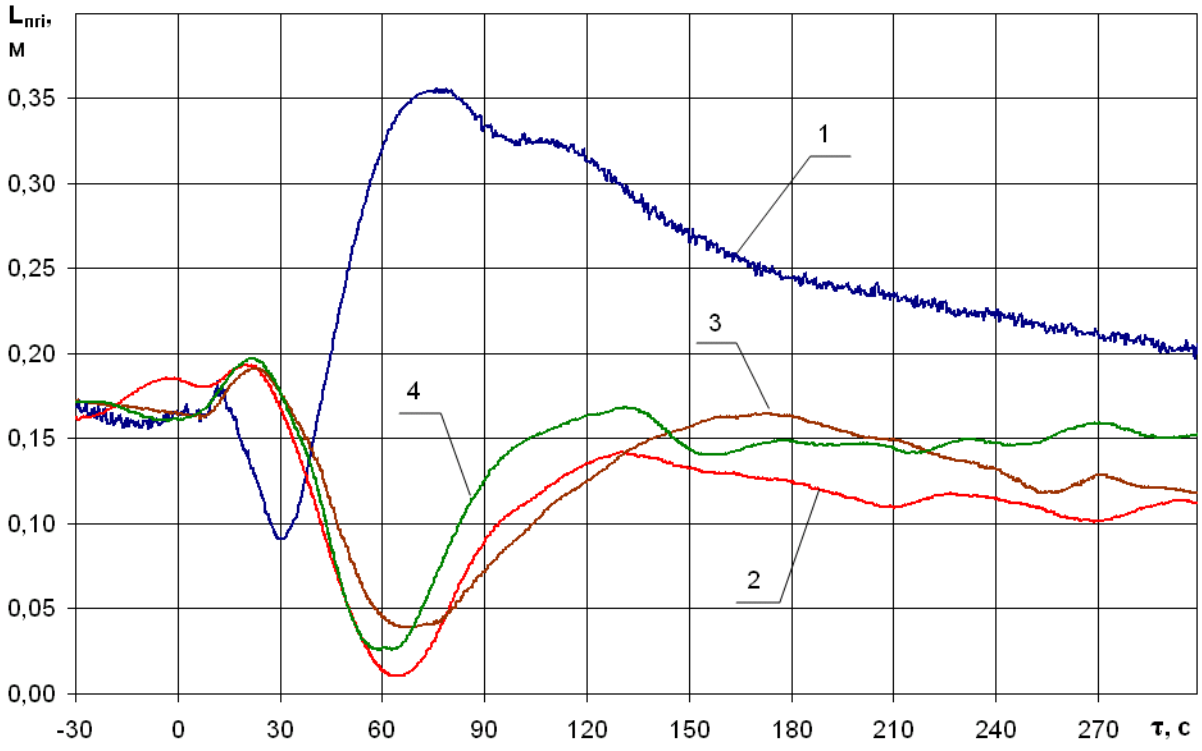

1 – L_{SG1}; 2 – L_{SG2}; 3 – L_{SG3}; 4 – L_{SG4}

Fig. 89 – SG water level histories recorded by the MMS (measurements on “small” basis)

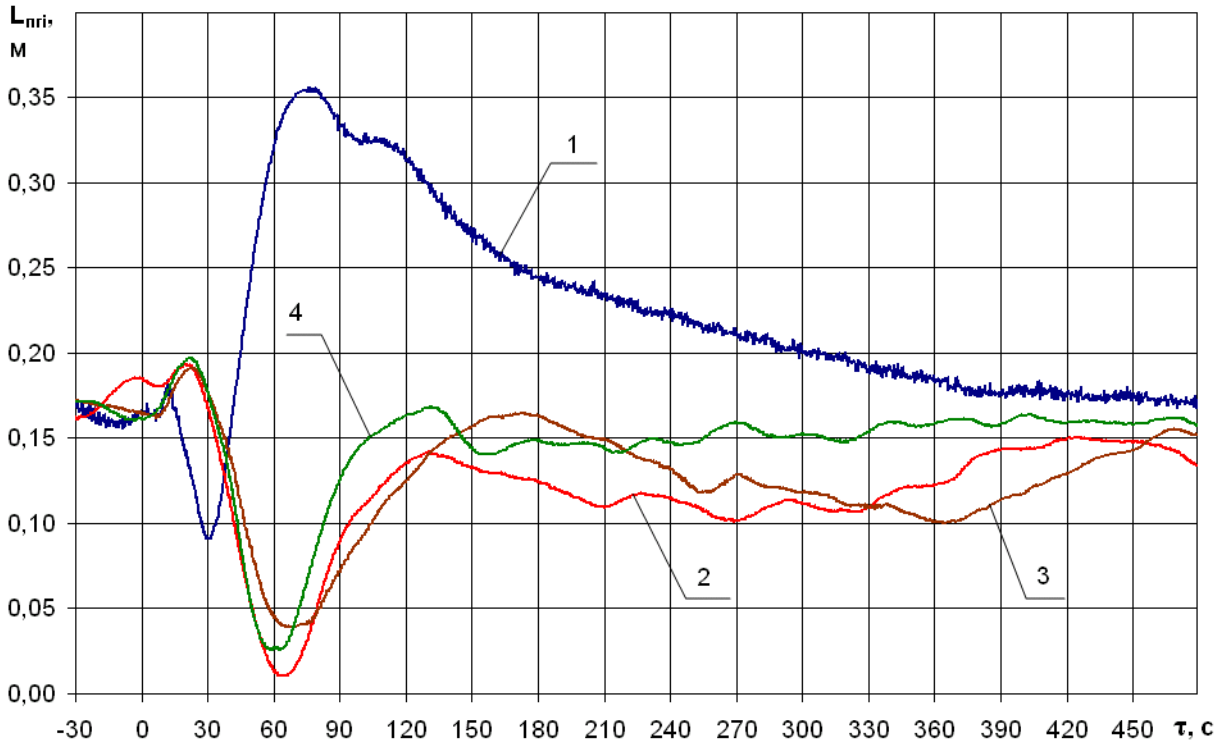

1 – L_{SG1}; 2 – L_{SG2}; 3 – L_{SG3}; 4 – L_{SG4}

Fig. 90 – SG water level histories recorded by the MMS (measurements on “small” basis)

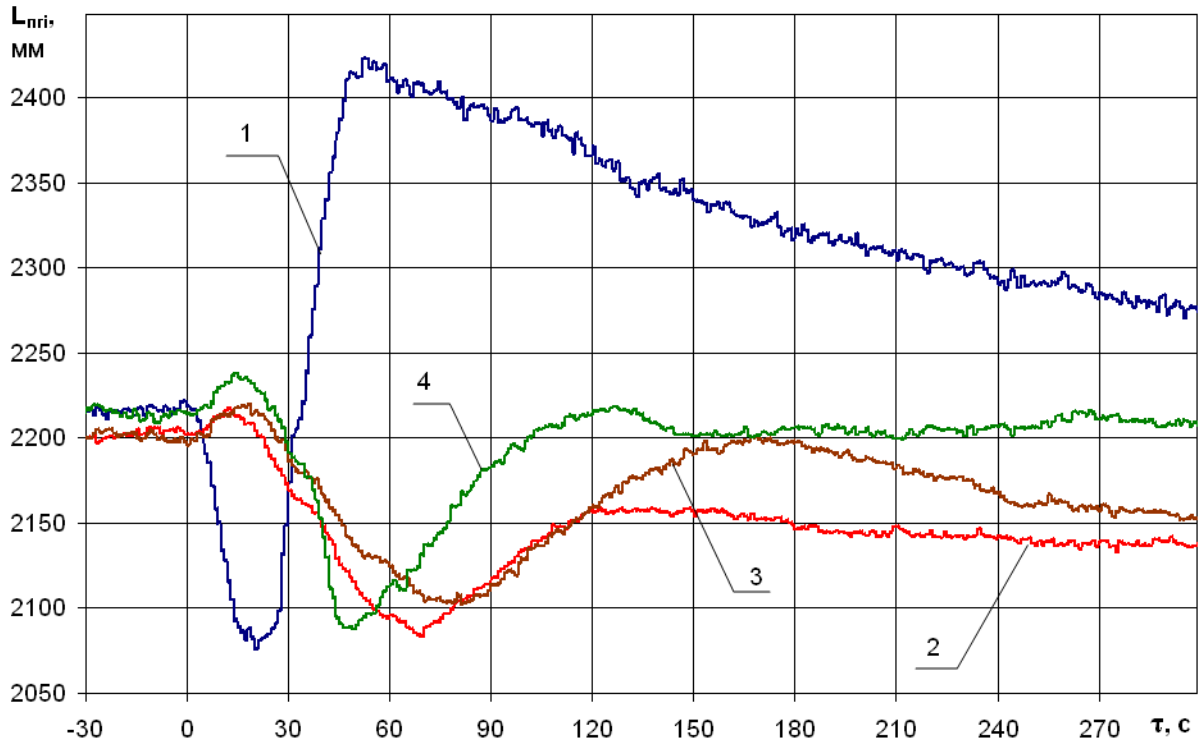

1 – L_{SG1}; 2 – L_{SG2}; 3 – L_{SG3}; 4 – L_{SG4}

Fig. 91 – SG water level histories recorded by the MMS (measurements on “large” basis)

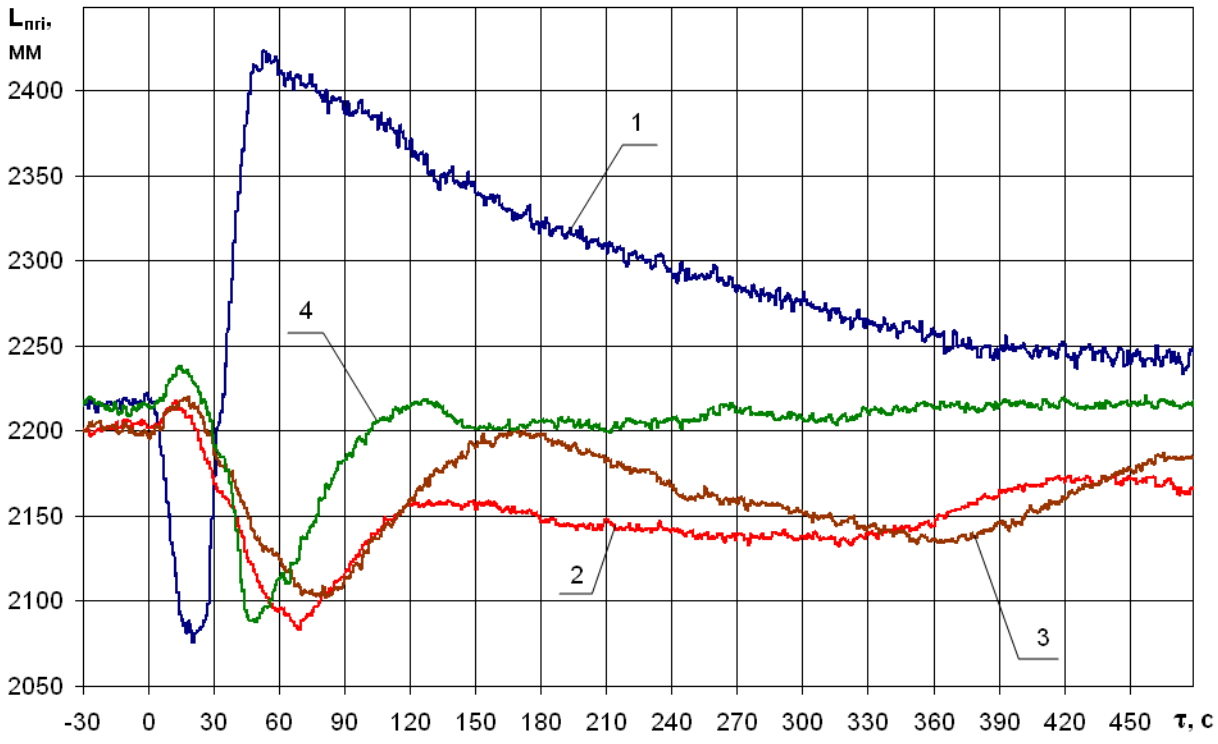

1 – L_{SG1}; 2 – L_{SG2}; 3 – L_{SG3}; 4 – L_{SG4}

Fig. 92 – SG water level histories recorded by the MMS (measurements on “large” basis)

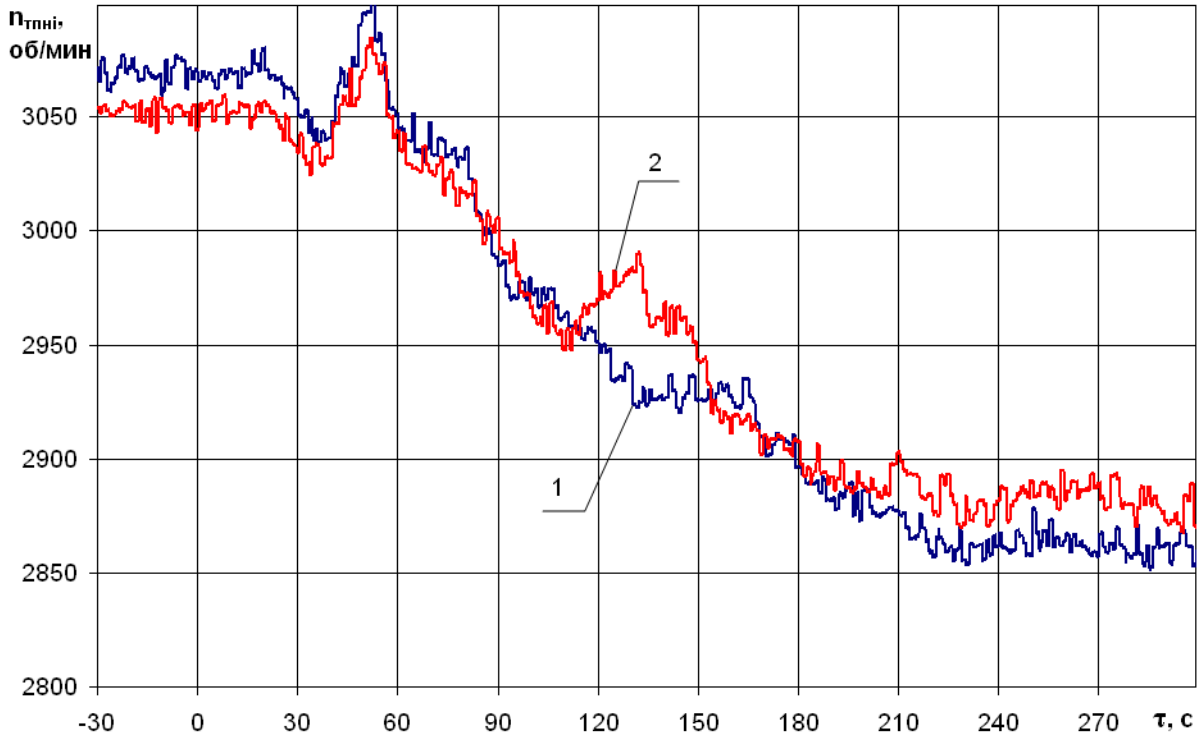

1 – n_{TFWP1}; 2 – n_{TFWP2}

Fig. 93 – Rotation speed of TFWP recorded by MMS

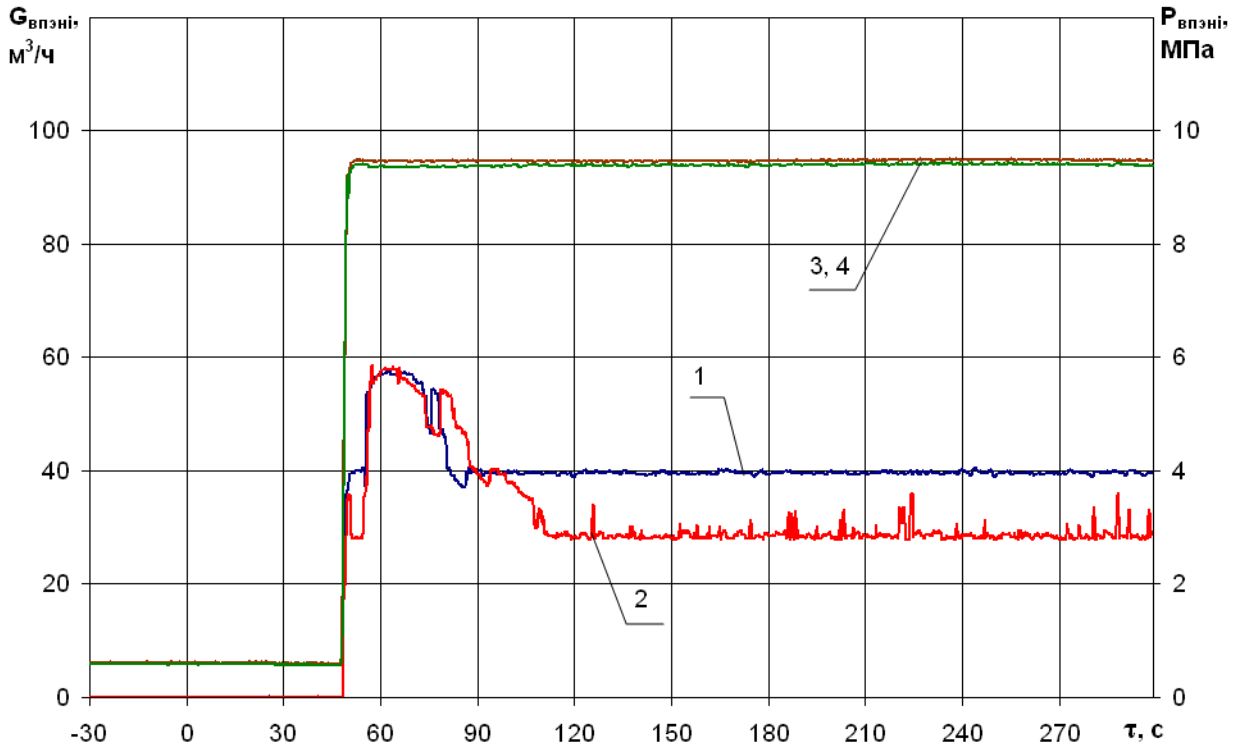

1 – G_{AFWP1}; 2 – G_{AFWP2}; 3 – P_{AFWP1}; 4 – P_{AFWP2}

Fig. 94 – Change in feedwater flow rates and pressure at the pressure side of AFWP recorded by MMS

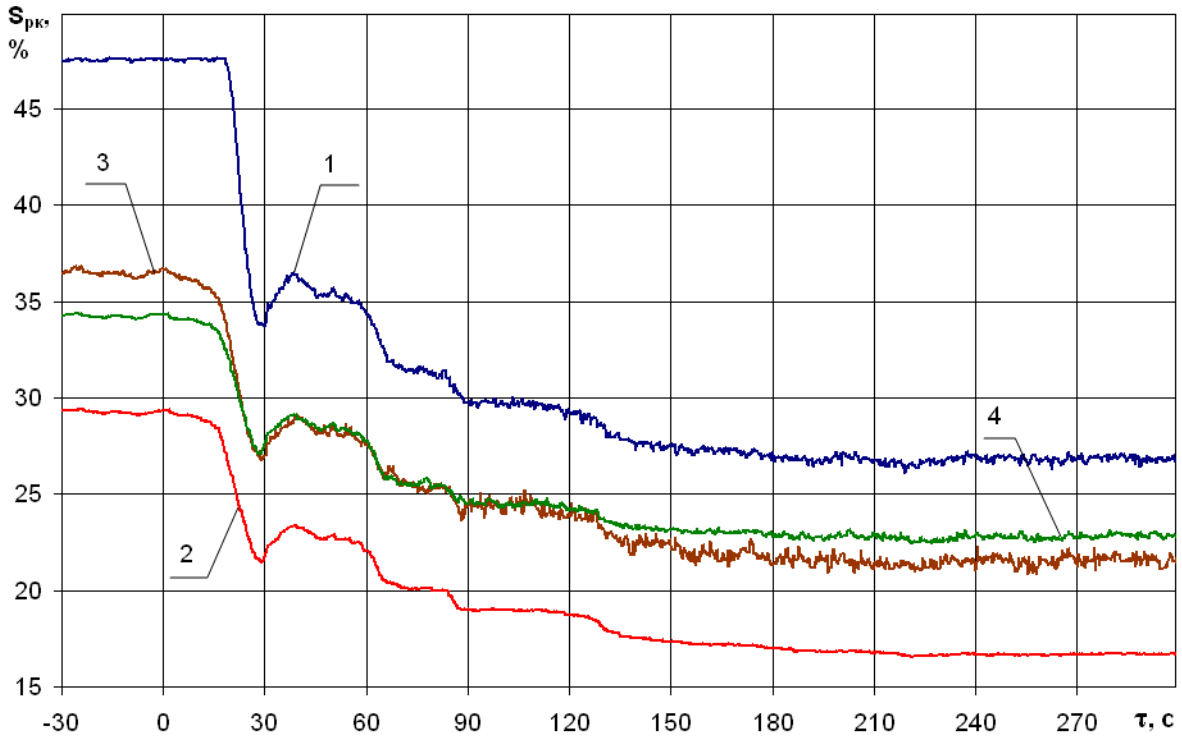

1 – S_{RV1}; 2 – S_{RV2}; 3 – S_{RV3}; 4 – S_{RV4}

Fig. 95 – Change in the position of HP control valves of TG recorded by MMS

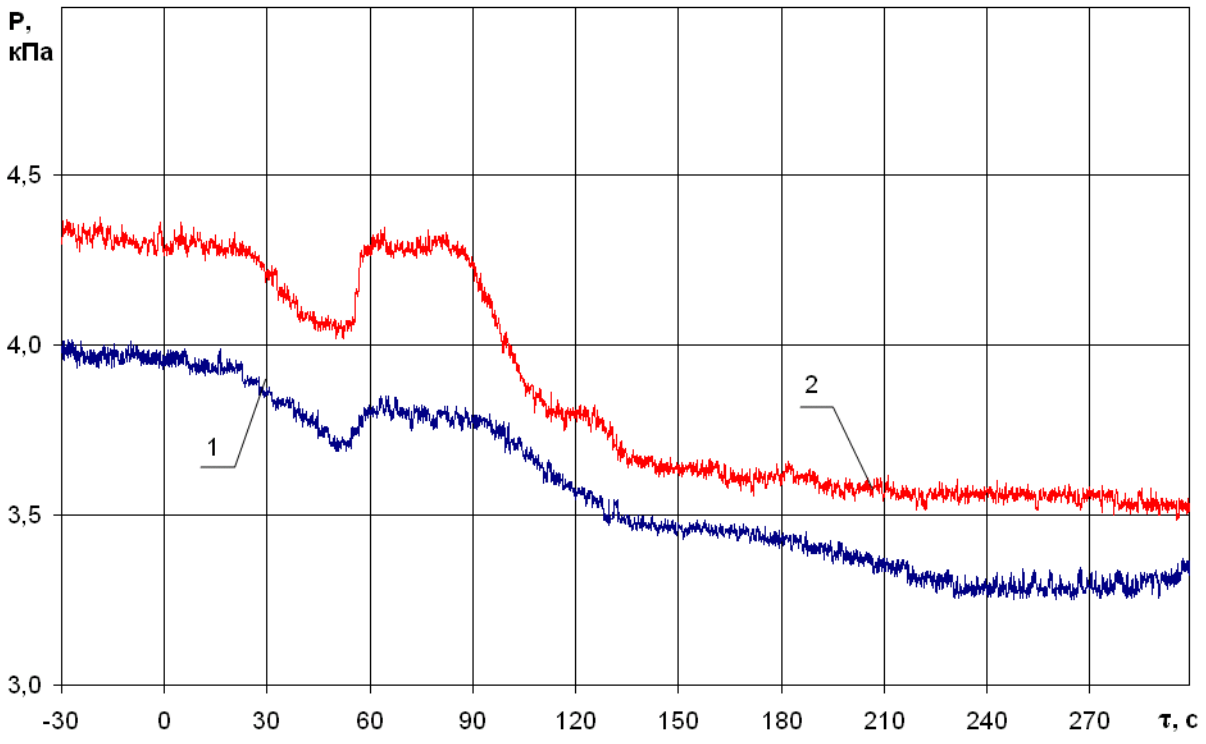

1 – $P_{SD11,12}$; 2 – $P_{SD13,14}$

Fig. 96 – TG condenser pressure histories recorded by MMS

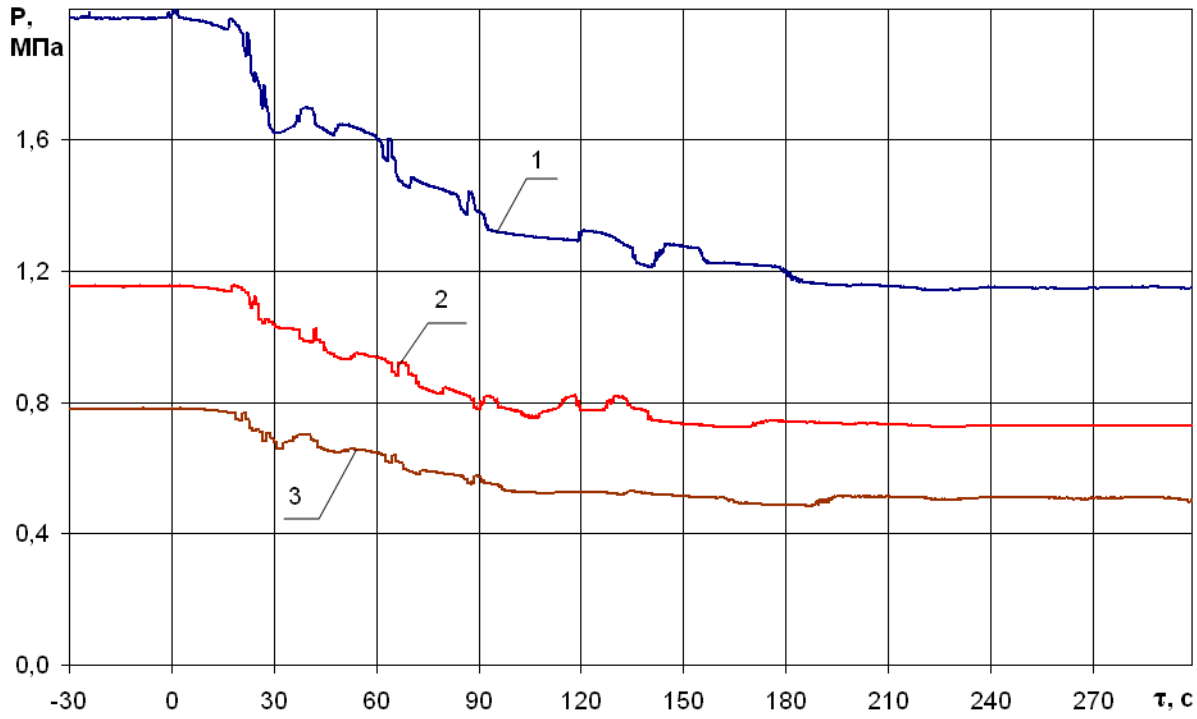

1 – $P_{отб1}$; 2 – $P_{отб2}$; 3 – $P_{отб3}$

Fig. 97 – Steam pressure at the 1th, 2th and 3th intake of the turbine recorded by MMS

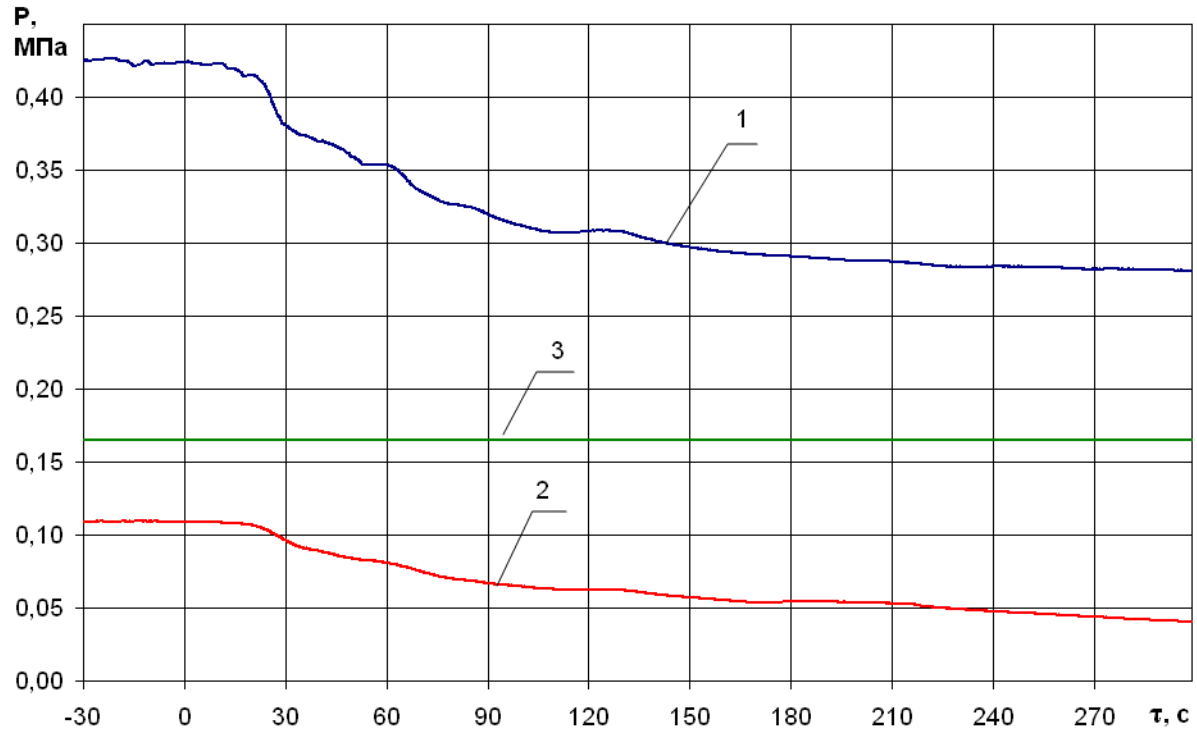

1 – $P_{отб4}$; 2 – $P_{отб5}$; 3 – $P_{отб6}$

Fig. 98 – Steam pressure at the 4th, 5th and 6th intake of the turbine recorded by MMS

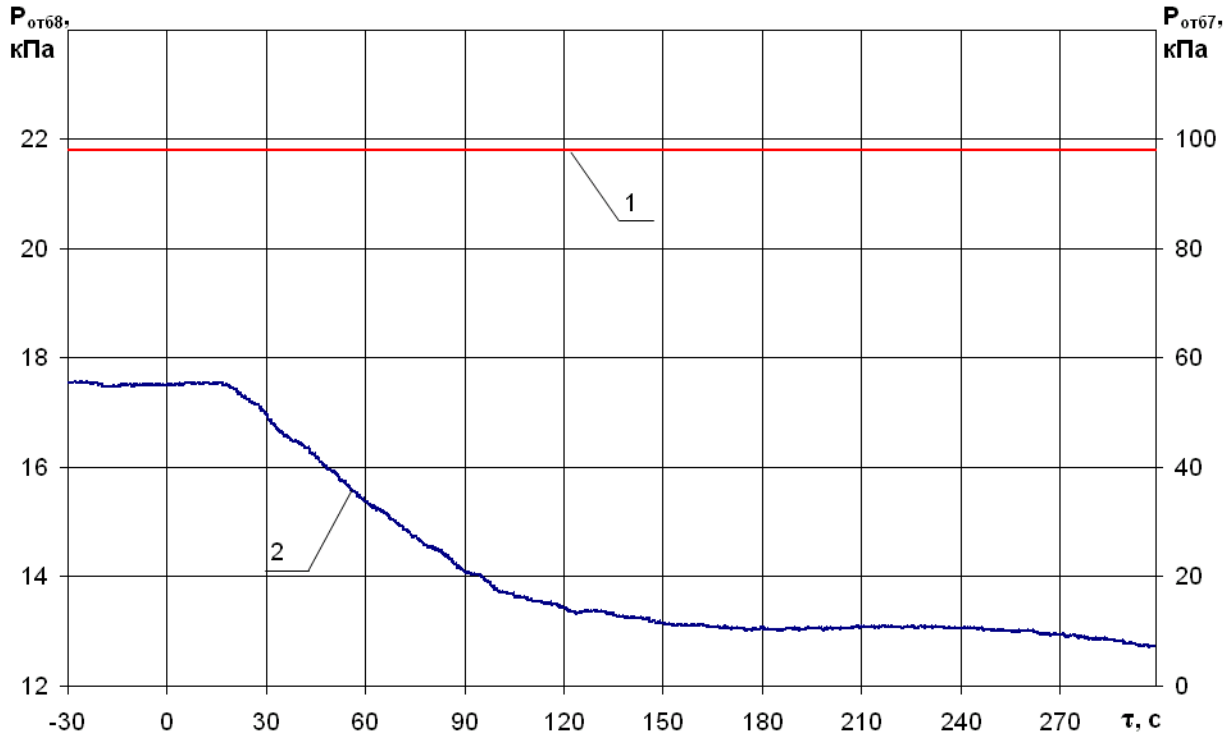

1 – $P_{отб7}$; 2 – $P_{отб8}$

Fig. 99 – Steam pressure at the 7th and 8th intake of the turbine recorded by MMS

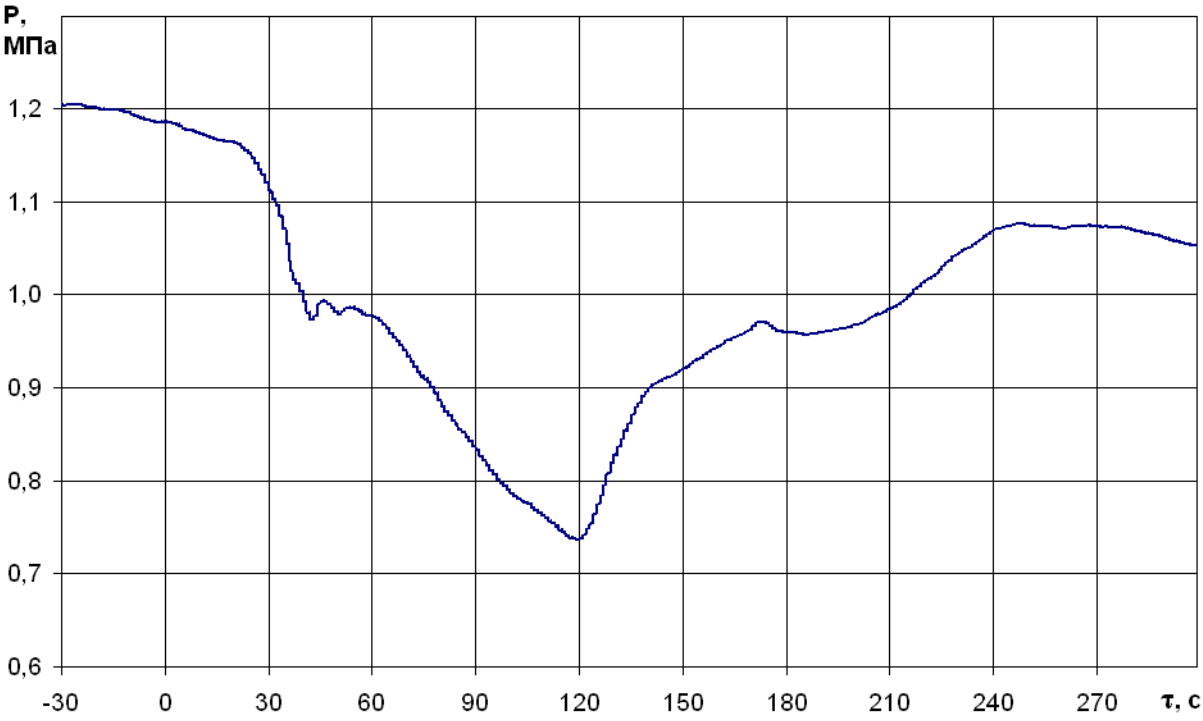

Fig. 100 – ISC steam pressure history recorded by MMS

ANNEX B

FA layout in the reactor core

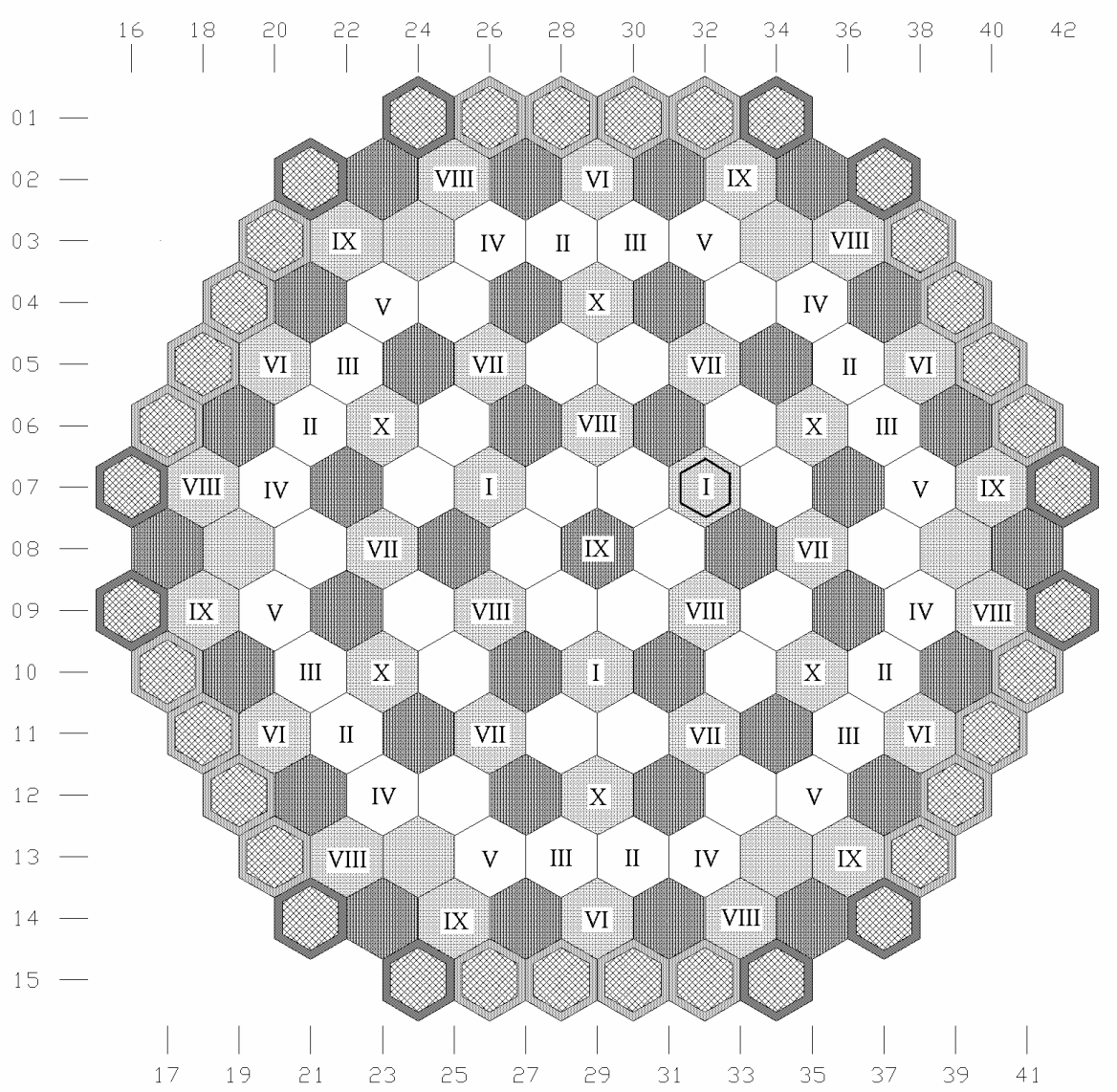

Enrichment of U-235 1.3 % - 48 FA

Enrichment of U-235 2.2 % - 42 FA

Average enrichment of U-235 2.98 % - 37 FA
(303 FA with enrichment 3 %, 9 gad-FA with enrichment 2.4 %

Average enrichment of U-235 3.9 % - 24 „profiled“FA (243 FA with enrichment 4.0 %, 60 FA with enrichment 3.6 %, 9 gad-FA with enrichment 3.3 %)

Average enrichment of U-235 3.9 % - 12 „profiled“ FA (240 FA with enrichment 4.0 %, 66 FA with enrichment 3.6 %, 6 gad-FA with enrichment 3,3 %)

Enrichment of U-235 1,6 (stainless steel)

ANNEX C

Arrangement of the ionization chamber channels; control rods of CPS and their groups' assignment; thermal control sensors at FA outlets and the arrangement of the SPND

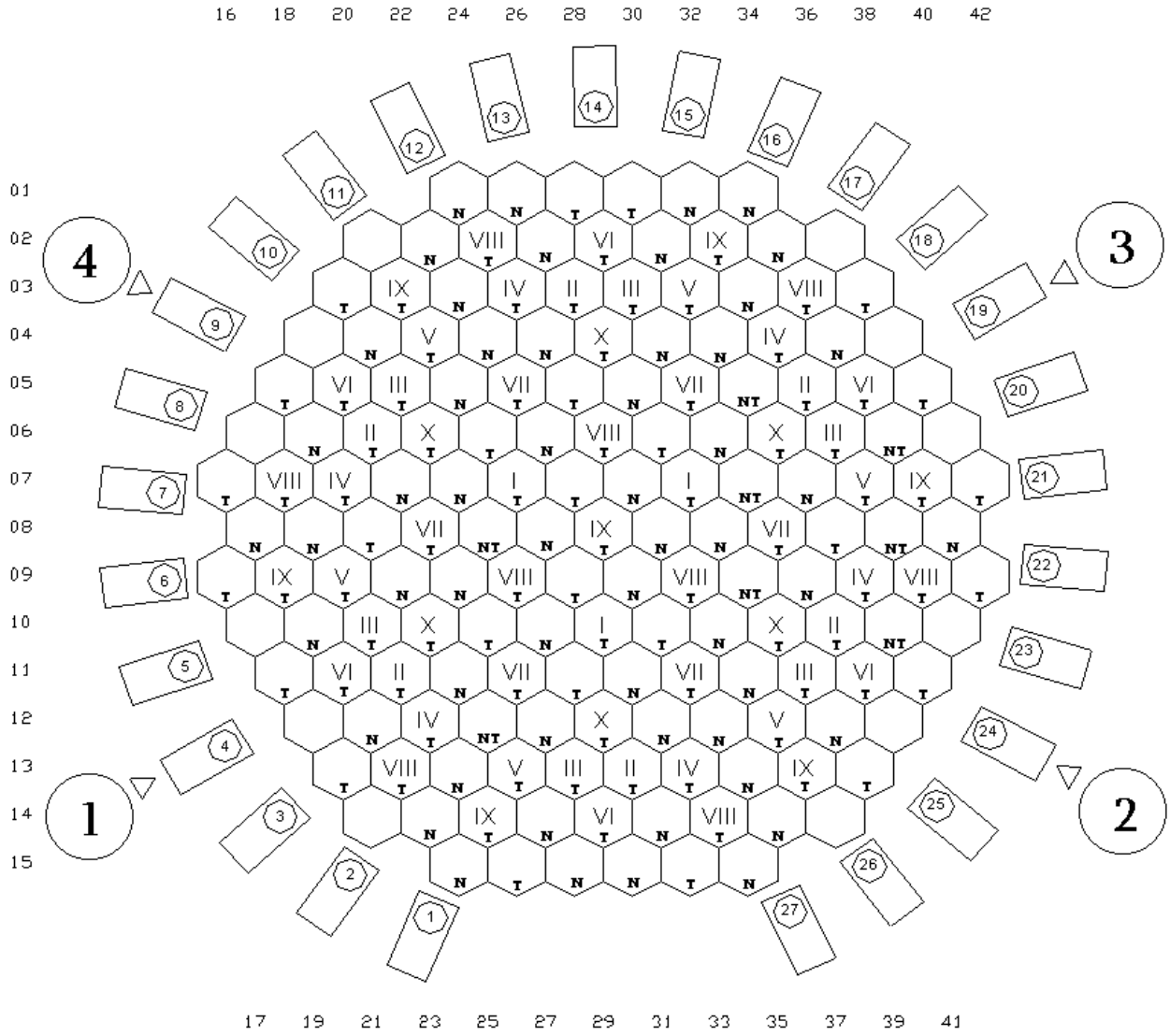

- Number of the ionizing chamber channel

X
N(T)

- Number of the CPS CR group
- Assemblies with SPND (thermal control sensors)

1 - Number of the loop

ANNEX D

Division of the reactor core in 60 °-symmetry sector, layout of FA, CPS control rods and CPS CR group allocation, layout of thermal control sensors at FA outlets and assemblies with SPND

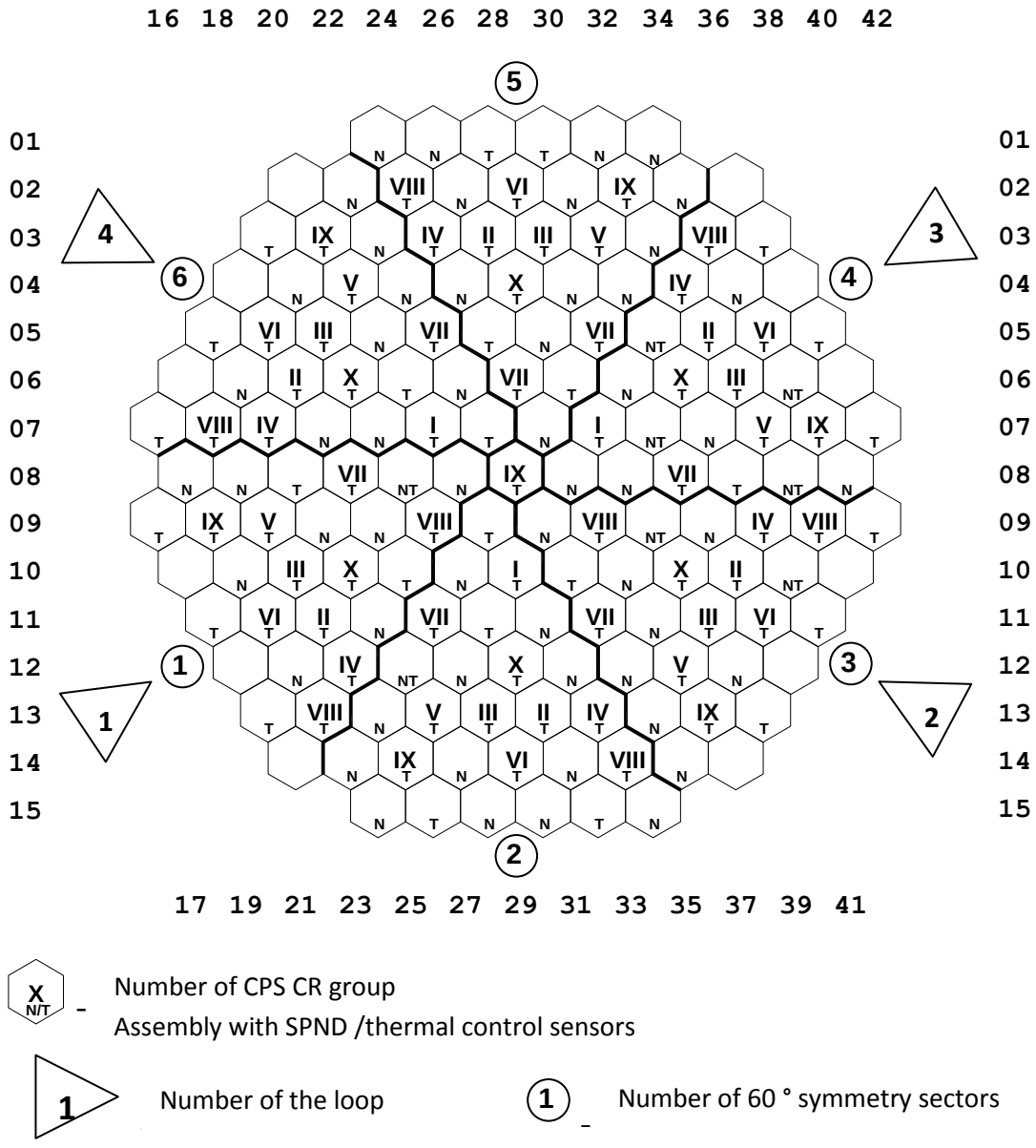

ANNEX E

Location of the temperature monitoring casings in the primary circulation loops

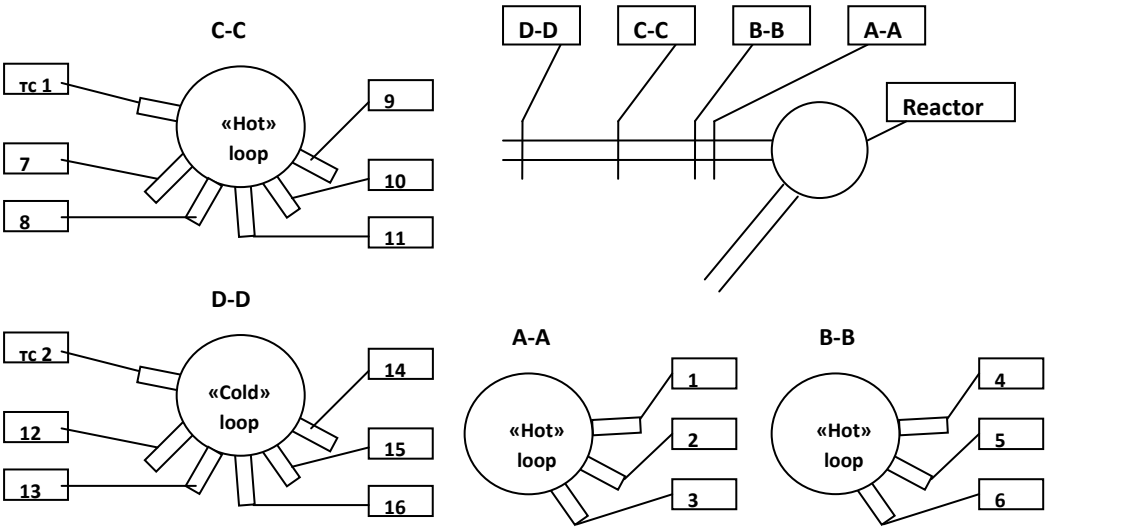

Distance from the center of the reactor:

- cross-section A-A – 6200 mm
- cross-section B-B – 6700 mm
- cross-section C-C – 8200 mm
- cross-section D-D – 10200 mm

1 - casing number